16 State House Station
Augusta, Maine 04333

MaineDOT

Transportation Research Division

Technical Report 14-08

Advanced Bridge Safety Initiative

FRP Flexural Retrofit for Concrete Slab Bridges – Task 4 Deliverables

Final Report – Task 4, June 2014

Technical Report Documentation Page

1. Report No. ME 14-08	2.	3. Recipient's Accession No.	
4. Title and Subtitle Advanced Bridge Safety Initiative: FRP Flexural Retrofit for Concrete Slab Bridges – Task 4 Deliverables		5. Report Date June 2014 6.	
7. Author(s) Hannah Breton Caleb Frederick Bill Davids, Ph.D., P.E.		8. Performing Organization Report No.	
9. Performing Organization Name and Address University of Maine		10. Project/Task/Work Unit No. Project 017666.00 Task 4 11. Contract © or Grant (G) No. Contract # 20100506*5729	
12. Sponsoring Organization Name and Address Maine Department of Transportation 16 State House Station Augusta, Maine 04333		13. Type of Report and Period Covered 14. Sponsoring Agency Code	
15. Supplementary Notes			

16. Abstract (Limit 200 words)

Concrete slab bridges are being examined as part of the MaineDOT Advanced Bridge Safety Initiative. Under Tasks 1 – 3 a finite element analysis program is developed, validated and applied to twenty bridges.

Task 4 investigates and develops a non-proprietary flexural strengthening system for concrete slabs using FRP materials.

This document includes the 5 deliverables under Task 4:

1. FRP Flexural Retrofit Designs
2. FRP Flexural Retrofit Durability Testing Plan
3. Small Beam Bending Tests
4. Environmental Durability Testing and Analysis
5. Additional Environmental Durability and Small Beam Bending Testing and Analysis

17. Document Analysis/Descriptors Concrete slab bridges, flexural strengthening, fiber reinforced polymer (FRP)		18. Availability Statement	
19. Security Class (this report)	20. Security Class (this page)	21. No. of Pages 333	22. Price

Bridge Safety Project

Task 4 (Deliverable 1): FRP Flexural Retrofit Designs

1/3/2012

Hannah Breton, M.S. Candidate
Bill Davids, PhD, PE, John C. Bridge Professor of Civil and Environmental Engineering

University of Maine AEWC Advanced Structures and Composites Center and Department of Civil and Environmental Engineering

Table of Contents

Introduction

This document is an engineering report for the Maine Department of Transportation (MaineDOT) satisfying deliverable 1 from task 4 in the UMaine AEWC Advanced Structures and Composites Center Bridge Safety project funded by the MaineDOT. The report details the design of two non-proprietary fiber-reinforced polymer (FRP) flexural retrofits for an existing flat slab bridge (Levant Bridge #5253) that does not meet the MaineDOT's current load rating criteria. Also included is a detailed literature review on the use of external FRP flexural reinforcing for the retrofitting of concrete structures.

An inventory rating factor of 0.456 for the Levant Bridge (#5253) was determined using a detailed finite-element analysis. The two non-proprietary FRP retrofit systems (denoted herein as system A and system B) were designed to increase this rating factor to a value of 1.0 or higher. System A utilizes FRP strips comprised of woven carbon fiber fabric in an epoxy matrix (AGP370-5h/3501) (p. 379, Daniels & Ishai, 2006) with a thickness and width of 2.03 mm (0.08 in.) and 88.9 mm (3.5 in.), respectively. System B utilizes FRP strips comprised of unidirectional glass fibers in an epoxy matrix (p. 377 Daniel & Ishai, 2006). Two methods of application were considered for the retrofit design: mechanical fastening (MF) and external bonding (EB). Mechanically fastening the retrofit with HILTI, Inc. HVA adhesive anchors (HILTI, Inc., 2006) was selected as the preferred method of application due to the significant amount of labor required in preparing the concrete surface for adhesive bonding of the FRP, and evidence that systems utilizing mechanical fasteners have been used successfully implemented in the field (Whittemore and Durfee 2011).

The project work plan originally called for the development of one non-proprietary FRP flexural retrofit for comparison with a proprietary flexural retrofit. However, the comparison of two non-proprietary systems will provide the MaineDOT with more options and insight than the comparison of one non-proprietary system to a proprietary system.

The body of this report contains a brief project background and project description; a thorough literature review of common FRP materials, FRP durability studies and proprietary FRP systems in today's market; an overview of the process of designing the retrofit systems; and a summary of results and final recommendations. Various appendices contain supporting technical data and load calculations for the design process. Future reports will detail the strength and durability testing and analysis of the performance of the retrofit systems.

Project Background and Description

To develop an understanding of the nature and objectives of this project, the project scope is overviewed and a description of the design bridge (Levant Bridge #5253) used for developing the retrofit system is provided. The intended use and primary objectives of the retrofit systems and technical requirements are also discussed.

Project Scope

The project scope for deliverable 1 from task 4 involves the initial assessment of proprietary FRP retrofit systems and the design of two non-proprietary FRP retrofit systems (A and B). This report does not discuss the performance of systems A and B beyond the design phase. Performance of the systems under durability and strength testing will be reported on at a later date.

Intended Use

The flexural retrofit designs are intended to increase the flexural capacity of a bridge so that the load rating factor of a bridge that was below 1.0 before installation of the retrofit will increase to a value of 1.0 or greater after installation. The development of a non-proprietary FRP retrofit system would allow for the rehabilitation of flat slab bridges as a solution to increase the usable life of the bridge. This rehabilitation would increase the rating factor of the structure preventing replacement, closure or implementation of weight restrictions. Ideally the retrofit system must be durable, light weight and provide a cost effective alternative to current retrofit procedures and bridge replacement solutions. A full discussion on the benefits of using FRP to rehabilitate bridges in comparison to other methods is provided in the Literature Review section of this document.

Technical Requirements

Loads and load rating procedures follow the *Maine Department of Transportation Bridge Design Guide* and the *AASHTO LRFD Bridge Design Specifications*. The design of systems A and B is based on the *ACI 440.2R-08 Guide for the Design and Construction of Externally Bonded FRP Systems for Strengthening Concrete Structures*. Design of the mechanical fastening system follows the technical specifications from the manufacturer of the adhesive anchor, HILTI, Inc., and the *AASHTO LRFD Bridge Design Specifications.*

Design Bridge Description

The Levant Bridge was selected for the retrofit design due to its low load rating factor (0.456) and zero skew. The bridge spans 26ft-7.5in from centerline support to centerline support and is 25ft-8in wide. The design bridge contains 1in diameter reinforcing steel (#8 bar) spaced at 6in on

center at a depth of 17in. Finite-element analysis of the bridge gives an inventory load rating factor of 0.456 based on the HL-93 tandem and lane load. The finite-element load rating was conducted under a separate task of the Bridge Safety project, and details are provided in other project reports to the MaineDOT.

Literature Review of FRP Properties and Proprietary Systems

In order to develop a rehabilitation system for concrete flat slab bridges in Maine, a review of current technologies is required in order to assess their usefulness based on relative cost and expected durability. The process of retrofitting and rehabilitating concrete structures with FRP composites is not a new technology. FRP systems can be used to rehabilitate deteriorated structures to restore their strength, strengthen sound members to increase their resistance to loads due to changes in the use of a structure, mitigate design or construction errors (ACI 2008; Bisby et al. 2010), or increase ductility (Katsuki et al. 2002; Anderson et al. 2010). Various available FRP systems include reinforcing rods and tendons; FRP wraps, sheets or plates for concrete rehabilitation; and pultruded FRP structural sections (Bisby and Fitzwilliam 2008). This review will focus on literature that discusses external FRP reinforcing systems, primarily strips, sheets, plates, and wraps.

There are several causes that can lead to structural deficiencies that require repair or rehabilitation by way of external FRP reinforcement:

- *Environmental effects* - corrosion of conventional reinforcing steel in concrete induced by chloride exposure, freeze-thaw cycling, and dry-wet cycling;

- *Evolution of design loads* - structures cannot safely carry loads specified by updated design codes;
- *Evolution of design guidelines* - from working stress to limit states, structures designed using older procedures are considered inadequate when evaluated under current guidelines;
- *Increased traffic volumes and loads* - more cars and heavier trucks on the roads and highways. (Bisby et al. 2010)

The strengthening and rehabilitation of structures involves FRP plates, strips, sheets, wraps or sometimes bars bonded to the exterior of a structure using high-strength adhesives (Bisby 2006), or mechanical fasteners (Whittemore and Durfee 2011). Attaching FRP sheets to concrete members can increases the flexural and shear capacity of the section, increase the ductility of the section under both service and ultimate loads (Katsuki et al. 2002; Bisby and Fallis 2006), and prevent further deterioration of damaged beams (Bisby 2006). Adhesively bonded external FRP reinforcement is considered *bond critical.* Adequate bonding of the FRP to the concrete is paramount in ensuring that the FRP strengthening system will function as desired; therefore, the bond between the concrete and the FRP is a key factor in the success of the strengthening system (Bisby and Fallis 2006).

The literature reviewed based the success of tested systems on the strength and durability of the FRP-concrete bond interface in both the virgin state and after environmental exposure to freeze-thaw cycles, dry-wet cycles, salt water, alkaline environments, diesel fuels, and ultraviolet (UV) radiation (Subramaniam et al. 2007; Qiao and Xu 2004; Green et al. 2000; Banthia et al. 2009; Dai et al. 2005; Ouyang 2007; Lopez and McSweeny 2005; and Davalos et al. 2010). Mechanical

fasteners, as discussed later, can also be used as an alternative to bonding FRP materials to the structure using adhesives (Whittemore and Durfee 2011).

Background

The extent of bridge deficiencies nationwide as discussed by Ouyang (2007) and Teng et al. (2003), estimated 240,000 (about 40%) of US highway bridges and 14% of bridges rated by the National Bridge Inventory Database in 2001 were deemed structurally deficient or functionally obsolete because service loads and traffic volumes exceed those expected in initial design. Over a 20-year period from 1999-2019 an estimated $5.8 billion per year is required to maintain these bridges. In order to eliminate these deficiencies altogether within the same time period and estimated $10.6 billion per year is required (Ouyang 2007). A cost-of-corrosion study determined that annual cost of damage caused by corrosion to all bridges, including steel bridges, is $8.29 billion (Ouyang 2007). These estimates do not include indirect cost incurred by the traveling public due to bridge closures. Continuing to upgrade and replace existing structures using traditional materials and application methods is no longer affordable for infrastructure owners (Bisby et al. 2010).

The magnitude of the problem in Maine is highlighted in the report titled “Keeping Our Bridges Safe” (MaineDOT 2007). The report concludes that between 30 and 40 bridges need to be replaced each year over the coming decade to reduce additional bridge closures or restrictions. With additional rehabilitation costs, the report concludes that funding for bridge replacement and rehabilitation needs to be increased from $70M/year to $130M/year to ensure bridge safety and minimize bridge restrictions or closures.

Externally bonded (EB) FRP reinforcement systems were developed as alternatives to traditional external reinforcing techniques such as steel plate bonding and steel or concrete column jacketing. FRP reinforcement systems have been used to strengthen and retrofit existing structures around the world since the mid 1980's, and their use has increased significantly over the last few years (ACI 2008; Niemitz et al. 2010). FRP systems have several advantages over traditional reinforcing techniques. FRP materials

- Do not corrode electrochemically;
- Are electromagnetically inert;
- Demonstrate excellent durability in a number of harsh environmental conditions;
- Have extremely high strength-to-weight ratio (up to five times that of steel); and
- Have versatile mechanical properties that can be tailored to best suit a project.

Because of these characteristics, FRP composites can be good candidates for the repair and strengthening of concrete structures. Although the initial material cost for these systems is high, these advantages can prolong the useful service-lives of concrete structures and reduce maintenance and life cycle costs (Bisby et al. 2006; Bisby et al. 2010; Qioa and Xu 2004; ISIS Canada, 2006).

Fiber-Reinforced Polymer (FRP) Constituents and Characteristics

FRP composites are comprised of continuous-length, high-strength fibers encased in a polymer matrix. FRP properties depend on the type of fiber and resin, the individual mechanical properties of the matrix and fibers, the fiber volume fraction, fiber orientation, dimensional effects interaction between the matrix and the fibers, and quality control during and method of manufacturing (ACI 2008; ISIS Canada 2006; Katsuki et al. 2002; Bisby et al. 2010).

Matrix Types

The primary function of the matrix is to transfer loads to the fibers through shear stresses that develop at the fiber-matrix interface. The matrix is also important for environmental protection of the fibers (Bisby et al. 2010). The matrix does not carry any tensile load directly, but rather, it acts as a filler material and holds the fibers together (Katsuki et al 2002). There are three commonly used matrix types used to manufacture FRP composites: (1) polyesters, (2) vinyl esters, and (3) epoxies.

Polyesters are popular for use in FRP systems because they are inexpensive and easily processed (ISIS Canada 2006). Polyesters are available in a varying degree of thermal and chemical stability, moisture absorption, and shrinkage during curing (Bisby and Fitzwilliam 2006).

Vinyl esters are common for rebar because they are strongly resistant to alkalis and acids and exhibit minimal moisture absorption and shrinkage, but are more expensive than polyesters (ISIS Canada 2006; Bisby and Fitzwilliam 2006). When compared to epoxies and polyesters, vinyl esters appear to be more durable and more resistant to microcracking, diffusion, various acids and chemical solutions, and moisture and alkalinity ingress (Bisby 2006).

Epoxies have emerged as the preferred matrix choice for external strengthening applications such as wet-layup and laminate applications despite being the most expensive. Due to their ability to cure well at room temperature and their superior adhesion characteristics, which ensure a strong bond between the FRP components and the concrete substrate, epoxies are ideal for external applications (ISIS Canada 2006; Bisby and Fitzwilliam; Bisby 2006). Additionally, epoxies have high strength, good dimensional stability, relatively good high-temperature properties, strong resistance to chemicals with the exception of acids, and superior toughness (ISIS Canada 2006;

Bisby and Fitzwilliam 2006). It should be noted, however, that epoxies typically contain potentially harmful chemicals, which may be classified as corrosive, flammable, or poisonous (Bisby and Fallis 2006), and rapidly deteriorate when exposed to UV radiation (Katsuki 2002; Yamaguchi 1998).

Fiber types

Fibers provide the tensile strength and stiffness of FRP composite systems. FRP systems are stronger in the direction of the fibers and weaker in the direction perpendicular to the fibers. Like matrixes, there are three commonly used fibers: (1) glass, (2) aramid (Kevlar), and (3) carbon fibers (Bisby 2006; ACI 2008).

Glass is the least expensive of the fibers and available in a variety of grades including alkali resistant. Glass has high strength, moderate modulus, medium density and is used in non-weight or modulus critical applications and can adequately resist fatigue failure (ISIS Canada 2006). Glass fibers deteriorate in alkaline environments and the best protection is ensured with the use of a vinyl ester resin. The rate of deterioration of glass fibers in alkaline environment is highly dependent on the type of fibers (Balázs and Borosnyói, 2007).

Aramid is moderately to highly expensive and is only available in two grades that provide high tensile strength, moderate modulus and low density; however, exhibit low compressive and shear strength. Aramid fibers may be susceptible to UV degradation, moisture absorption, swelling and are sensitive to fatigue (ISIS Canada 2006) and creep (Bisby and Fitzwilliam 2006), and are not extensively used in infrastructure applications in North America (Bisby 2006).

Carbon is the most expensive of the three fibers and available in a variety of grades. Carbon fibers exhibit high strength, high modulus, and low density characteristic and superior durability

and fatigue characteristics (ISIS Canada 2006), and can exhibit a very high ultimate strength and a modulus of elasticity that is comparable to steel and displays more corrosion resistance than steel (Demkowicz 2011). Carbon is typically used in and ideal for weight, modulus, and/or deflection critical applications, and does not show considerable deterioration in any kind of harsh environment. According to Machida (1993) and Tokyo Rope (1993) carbon fiber cannot absorb liquids and is resistant to acid, alkali and organic solvents (as cited by Balázs and Borosnyói, 2007), and also shows resistance to thermal and chemical effects (Bisby 2006).

Aramid and glass fibers show consistency in failure modes regardless of failure load level; however, carbon fibers tend to fail in different modes including fiber pull-out from the matrix and simultaneous failure at the anchorage, fan-type failure, and failure containing components of both of the above (Katsuki et al. 2002).

FRP System Characteristics

It is important when developing FRP systems that the fracture strain of the resins and the compatibility with the fibers are taken into consideration. According to Katsuki et al. (2002), epoxy resins have a low strain capacity and work well in conjunction with carbon fibers, which also have low strain capacity. When epoxy is used with aramid or glass fibers compatibility is less ideal because the fibers' failure strains are higher. The structural properties of a hardened FRP sheet, such as strength and elastic modulus, rely upon the monolithic behavior of all FRP layers. This can only be ensured if the resin completely impregnates the space between the fibers while it hardens. During outdoor applications it is important that the resins are protected from the action of rain, sand, dirt, etc. during the hardening process. To ensure long-term durability, a finishing coat may be applied to the FRP sheets once sufficient hardening has occurred (Katsuki et al. 2002).

All fiber types exhibit a higher tensile strengthen than steel; however, fiber elongation prior to failure of the FRP system is very small, thus warning before failure is reduced due to the reduced ductility of the section (Katsuki et al. 2002; Bisby et al. 2010). Tensile fatigue tests conducted on unidirectional CFRP-epoxy strands have indicated that CFRP can sustain greater average stresses and greater maximum stresses than steel (Bisby and Fitzwilliam 2006). Unlike steel, FRP systems behave linear-elastically to failure resulting in sudden brittle failure modes (Bisby et al. 2006; Bisby et al. 2010; Qioa and Xu 2004; ISIS Canada, 2006). However, this brittle response can be accommodated with proper design methodology such as that prescribed by ACI (2008).

Due to glass fiber's relatively low elastic modulus and tendency to deteriorate by alkali and chloride ions resulting in corrosion-induced failure, carbon FRPs (CFRPs) are beginning to see increased use for structural engineering applications, despite their considerably higher costs. The attraction increase can be attributed to the decreasing cost of carbon, its high elastic moduli, available strengths, low density and weight, and durability (ISIS Canada 2006; Bisby and Fitzwilliam 2006). CFRP materials, however, can contribute to galvanic corrosion if placed in direct contact with aluminum or steel. A thin layer of GFRP is typically applied between the CFRP and metal when necessary (Bisby 2006).

Durability

No widely accepted standards for testing the durability of FRPs were available prior to July 2011, and therefore available research results may not be comparable due to different test methods and exposure times (Demkowicz 2011). ACI Committee 440 released the "Guide to Accelerated Conditioning Protocols for Durability of Internal and External Fiber Reinforced Ploymer (FRP) Reinforcement for Concrete" (2011) to help regulate testing procedures for accelerated conditioning protocols (ACP) and associated standard mechanical test methods that

can be used to assess the durability of FRP reinforcement. It should be noted that these protocols are not necessarily useful in predicting the service life of a particular system; however, they offer a standardized method of testing that allows for direct comparison of the performance of two different FRP systems or products.

According to Bisby (2006), if fabricated properly, FRP materials can achieve outstanding longevity in civil infrastructure applications due to FRP materials' durability and resistance to degradation. ACI 440 (2008) does incorporate reduction factors for strength and modulus for different types of external FRP reinforcement under different environmental exposure regimes and imposes stress limits for ultimate tensile strength and rupture strain design because long-term exposure to various types of environments can reduce the tensile properties and creep-rupture and fatigue endurance of FRP laminates. Environmental reduction factors are based on exposure conditions and fiber types. Carbon, glass, and aramid FRP systems subjected to exterior exposure are reduced by factors of 0.85, 0.65, and 0.75, respectively, to account for degradation caused by thermal effects, alkalinity, acidity, moisture, and humidity. The ACI imposed design stress limits used to mitigate creep-rupture and fatigue failure are covered in length at the conclusion of this section. The following sections discuss different durability exposure studies and their affects on FRP systems.

Thermal Effects

The coefficient of thermal expansion (CTE) for carbon is approximately zero while the CTE for glass is approximately equal to that of concrete. Typical FRPs, however, have a CTE approximately five times greater than that of concrete (ACI 2008).Thermal cycling can cause damage to FRP materials through matrix cracking and fiber fracture which can exacerbate problems due to moisture ingress and/or chemical attack (Bisby and Fitzwilliam 2006). Tensile

strength in the fiber direction typically decreases in temperatures ranging from -10 to -40°C, whereas transverse strength may slightly increase due to matrix hardening. Overall the effects on FRP properties appear to be minor and should not be a serious concern in most infrastructure applications (Bisby 2006). Due to a lack of structured specified testing procedures prior to the release of ACI's guidelines, experimental results vary due to varying procedures. Due to these inconsistencies it is difficult and sometimes impossible to compare results.

Experimental results from Triantaillou and Pelvris (1990), Acevedo (2000) and Subramaniam et al. (2007) found that with increased freeze-thaw cycling, up to 300 cycles, there is a significant decrease in the ultimate load transferring capacity, interfacial fracture energy, critical load, debonding load, and strain in the FRP at full debonding. During the debonding phenomenon, a constant stress transfer length was observed and as the number of freeze-thaw cycles increased the length of this stress transfer zone decreased. No decrease in the elastic modulus of the FRP composite was observed.

Green et al. (2000) also studied the effects of freeze-thaw cycles on the FRP-concrete bond. Beam specimens, in groups of three, were subjected to 0, 50, 150, and 300 freeze-thaw cycles and then tested to failure in four point bending. Contrary to the results discussed above, experimental results from Green et al. (2000) found that the bond between CFRP strips and the concrete was not significantly damaged and after 300 freeze-thaw cycles were able to carry up to 15% more load than any other tested beam. This increase in strength is believed to occur due to a reduction in the shear modulus of the adhesives caused by freeze-thaw cycling, which reduces the magnitude of the shear stresses on the concrete. This reduction in shear stress allows for the FRP composite to take on more load and distribute the shear stresses over a larger bonded surface area. The bond strength did not appear to be significantly affected by the freeze-thaw

cycles in any of the tested specimen. The lowest maximum strain occurred in the control specimen and the highest maximum strain occurred in specimen subjected to 300 freeze-thaw cycles.

When compared to control specimen, the failure mode of freeze-thaw and dry-wet highly cycled (50 to 300 cycles) externally reinforced FRP beams switched from occurring as fracture of the concrete substrate in the control specimen to occurring at the FRP-epoxy interface (Green et al. 2000; Teng et al. 2003; Qiao and Xu 2004). Observations by Qiao and Xu (2004) found the deterioration of the FRP-concrete interface under these conditions was found to be relatively pronounced. As the number of freeze-thaw and dry-wet cycles increased, the bond interface fracture energy and critical loads decreased; decreasing faster in freeze-thaw cycles than in dry-wet cycles.

Green et al. (2006) found that GFRP and CFRP confined concrete columns under extreme conditions saw no significant deterioration of either GFRP or CFRP systems after exposure to freeze-thaw cycles. It was observed that corrosion rates of intermediately corroded reinforcement concrete decreased to levels similar to those measured for specimens wrapped before exposure to severe environmental conditions.

Karbhari et al. (2000) evaluated the short-term effects of freeze-thaw cycling on FRP confined concrete. It was found that the combined effects of freeze-thaw cycling with aqueous solutions, water, or other solutions such as salt water can have a significant effect on mechanical and chemical changes within the FRP composite. Effects included matrix degradation and plasticization, matrix microcracking due to expansion of absorbed moisture, degradation of fiber-

matrix bond, formation of salt concentration profiles through the thickness of the wrap, and damage to the fibers through local notching due to crystal formations on the surface.

Teng et al. (2003) found that confined concrete columns subjected to freeze-thaw cycles and corrosion saw no significant change in failure load for the three types of FRP (carbon, glass, and aramid); however, significant strain loss occurred for GFRP wrapped specimen. CFRP wraps performed best in terms of structural behavior after thermal cycles; however cycling did cause a decrease in the strength and ductility of the wraps and the failure mode was more catastrophic. Minor cycles had no effect on the FRP-wrapped specimens' performance; however, large thermal cycles caused some degradation of ductility in the axial direction. Overall it was found that FRP provides excellent protection against aggressive agents such as salt water or moisture, even when a single layer is used.

Moisture

According to Karbhari et al. (2002), the presence of moisture has a significant effect on both the physical and chemical aging process of FRPs, microcracking, and fiber-matrix bond initiation (as cited by Saenz and Pantelides 2006). The loss of FRP mechanical properties due to moisture penetration depends on the sensitivity the fiber to polymer tensile strength ratio, while bond and/or FRP lap capacity and interlaminar strength are affected by moisture absorption regardless of the fiber to polymer tensile strength ratio (Matthews and Rawlings 1994, Chateuminiois et al. 1993, and Helbling and Karbhari 2002, as cited by Saenz and Pantelides 2006).

Polymers absorb moisture to varying degrees and will absorb moisture until saturation occurs. Moisture absorption typically results in plasticization of the matrix which can cause reductions in the polymer's strength, modulus, strain at failure, and toughness, and can also reduce matrix

properties such as bond, shear, and flexural strength and stiffness. Moisture-induced swelling can cause irreversible matrix cracking and fiber-matrix debonding. (Bisby 2006)

An investigation by Wu and Ton-That (2004) on the effects of water on the properties of epoxy adhesives found that after immersion for 3 months in 113°F (45°C) water, two commonly used adhesive systems had a weight gain of 1.3% and 6.5% (as cited by Pantelides et al. 2006). Chateuminiois et al. (1993, as cited by Saenz and Pantelides 2006) and Gartner et al. (2011) found that water absorbed by polymers can reduce the visco-elastic behavior of the material, weakening the fiber-matrix interface.

The combined effects of moisture and freezing temperatures, frost, can affect the FRP-concrete interface bond behavior. Dai et al. (2005) found frost damage leads to a change of concrete strength and deformability, and affects the bond force capacity transferred from the concrete to the externally bonded CFRP sheets. Non-frost damaged specimen failed by the FRP peeling from the concrete. Failure occurred in all frost damaged specimen due to delamination of a thick layer of substrate that was attached to the CFRP. Substantial frost damage caused an increase in the effective bond length, decreased bonding stiffness, and decreased interfacial fracture energy.

At the time of application temperature, moisture, and humidity can affect the performance of the FRP system. Primers, saturated resins, and adhesives should not be applied to cold or frozen surfaces, which can cause improper curing. Unless formulated for such applications, resins and adhesives should not be applied to damp or wet surfaces. (ACI 2008)

De-Icing Chemicals

Chloride ions from de-icing salts can penetrate into concrete and can accelerate corrosion. In the presence of chloride ions the risk of corrosion of FRP reinforcement may also take place. While

CFRP and AFRP reinforcements are insensitive to chloride ions (Sen et al. 1998a; Sen et al. 1998b), Saadatmanesh and Tannous (1997) found that GFRP reinforcements can be seriously deteriorated in the presence of de-icing salts and lead to corrosion induced failure (as cited by Balázs and Borosnyói, 2007).

Chin et al. (1997) observed no significant changes in CFRP-vinyl ester and GFRP-isopolyester tensile strength after 1300 hours of exposure to saltwater (as cited by Saenz and Pantelides 2006). Similarly, Li and Karbharli (2003) observed no significant changes in tensile strength and interlaminar shear strength of CFRP-T700 (epoxy) based composites after 12 months of exposure to saltwater or alkali solutions (as cited by Saenz and Pantelides 2006).

Hardening of the FRP composite laminate was greater for specimens subjected to exterior exposure compared to those exposed to interior exposure or specimens subjected to severe freeze-thaw cycling in highly concentrated saltwater, where stiffness and ultimate axial strain of the FRP composite laminate exhibited relatively constant values. Environmental degradation can be reduced by applying an additional number of CFRP composite layers to act as a protective shield, and by applying a UV resistant coating. Additional CFRP jackets essentially stopped any corrosion that could seriously reduce structural integrity (Saenz and Pantelides 2006).

The effects of saltwater exposure on CFRPs indicate greater decreases in strength and increases in moisture uptake than that of fresh water exposed CFRPs; however fresh water exposed FRPs show only very slightly less degradation than those exposed to saltwater (Bisby 2006). According to Karbhari et al. (2002) the level of microcracking increases in specimen subjected to freeze-thaw cycles in saltwater compared to specimen subjected to freeze-thaw cycles in deionized water (as cited by Saenz and Pantelides 2006).

Ultra-Violet (UV) Radiation

Glass and carbon fibers are insensitive to UV radiation; however, degradation will occur in exposed aramid fibers. Polymer matrixes experience slight degradation and discoloring when exposed to UV radiation, however protective coatings can be applied to prevent UV radiation damage (ISIS Canada 2006; Bisby and Fitzwilliam 2006).

Panteliedes et al. (2006) found that UV protective coatings enhanced the resistance of the CFRP composite to environmental degradation, whereas unprotected CFRP composites saw adverse effects to the elastic modulus with exposure. Kato et al. (1997) found that UV radiation has limited effects on CFRP composites. After 2500 hours of exposure to direct sunlight, it was found that the tensile strength and Young's modulus decreased by a negligible amount in CFRP but by 10% in GFRP. These effects on the system were attributed to the degradation of the matrix resin (as cited by Balázs and Borosnyói, 2007).

Alkalinity

Behavior under alkaline exposure is dependent on matrix material and fiber type. Bare, unsaturated carbon does not degrade in this environment; however, alkalinity can reduce glass fiber toughness and strength, and cause alkalinity-induced embrittlement. This can be avoided by using an alkali-resistant polymer matrix (ISIS Canada 2006; Bisby and Fitzwilliam 2006; ACI 2008). The effects of alkalinity are a concern primarily for glass FRP systems, since it has been shown in the laboratory that bar glass fibers suffer degradation of mechanical properties under exposure to high pH solutions. Elevated temperature and stress in GFRP increased the rate of degradation when exposed to alkalis. Damage also depends on the protection of the fibers by the matrix, the level of applied stress, and the temperature (Bisby 2006).

Diesel Fuel

In a durability study performed by Cromwell et al. (2011) it was found that diesel fuels had little effect on the FRP systems tested; however, exposure times may not have been long enough, and effects from combination exposure (diesel fuel in conjunction with de-icing chemicals, freeze-thaw cycles, alkaline solutions) were not studied and could adversely affect the FRP systems. In tests performed by Steckel et al. (1999) on a combination of carbon/epoxy systems and E-glass systems with epoxy, polyester, or vinyl ester resins exposed to diesel fuels, with the exception of one E-glass/polymer system and one carbon/epoxy system, the specimens only saw a decrease of about 10% in tensile strength (as cited by Demkowicz 2011).

In a general environmental exposure study it was found that environmental exposures for 100% humidity, saltwater, alkali solution, diesel fuel, ultraviolet light, elevated temperature and freeze-thaw cycling after 3000 h showed no significant changes in tensile properties (Steckel et al. 1998 as cited by Saenz and Pantelides 2006).

Creep Behavior

Creep can result in rupture of FRP materials at sustained load levels that are significantly less than ultimate (Bisby 2006). Fibers are relatively insensitive to creep; carbon is the least susceptible, while glass is the most susceptible. Matrix polymers are visco-elastic and will creep over time (ISIS Canada 2006). In general, creep strain of CFRP at room temperature and humidity under 0.01% after 3000 hours at a tensile stress of even 80% of the tensile strength yields excellent creep behavior (Machida 1993, Saadatmanesh and Tannous 1999, and Tokyo Rope 1993, as cited by Balázs and Borosnyói, 2007), whereas GFRP and AFRP give much higher creep strain under the same conditions (Gerritse 1993, Machida 1993, and Piggott 1980, as cited by Balázs and Borosnyói, 2007) After one million hours, the long-term tensile strength

of CFRP, AFRP, and GFRP can be estimated to be 80-95%, 50-75% and 40-70% of the short-term tensile strength, respectively (Balázs and Borosnyói, 2007).

Creep-rupture occurs when FRP materials are subjected to a constant load over time and suddenly fail after a time period known as the endurance time. The endurance time decreases as the ratio of sustained tensile stress to short-term strength of the FRP laminate increases and also decreases under adverse environmental conditions such as those discussed in previous sections. ACI 440 imposes sustained stress limits to avoid creep-rupture. As long as the sustained stress in the FRP remains below this limit the FRP is available for non-sustained loads (ACI 2008). The imposed stress limit is discussed further following the cyclic loading fatigue behavior section.

Cyclic Loading Fatigue Behavior

Only very limited long term fatigue data are available for FRPs in infrastructure. The matrix resin used appears to play a more significant role in the fatigue performance than the type of fibers. Good fatigue performance in FRPs depends largely on the toughness of the matrix and its ability to resist cracking. In the case of CFRPs, since carbon fibers themselves are resistant to environmental degradation due to most other effects, the fatigue life of CFRPs is essentially unaffected by moisture and temperature unless the resin or fiber/resin interface is degraded by the environment. Other environmental factors do appear to play important roles in determining the fatigue life of GFRPs. Moisture and alkaline and acidic solutions may degrade the fatigue performance of GFRPs due to reductions in the strength and stiffness of the fibers and damage to the matrix and fiber-matrix interface (Bisby 2006).

The typical endurance limit for CFRP is 60-70% of the initial static ultimate strength, even after one million cycles. On a plot of stress vs. the logarithm of number of cycles at failure, the

downward slope for CFRP is approximately 5% of the initial static ultimate strength per decade of logarithmic life and is relatively unaffected by the moisture and temperature exposures of concrete structures unless the fiber-resin interface is substantially degraded by the environment.

In order to prevent creep-rupture and fatigue failure, ACI recommends a check of stress limits under these conditions. The stress levels in a member can be calculated using an elastic analysis and an applied moment due to all sustained loads plus the maximum moment induced in a fatigue loading cycle, because the stress levels will be within the elastic response range of the member. The sustained stress limits are based on a combination of the sustained plus cyclic stress limits. These "safe sustained plus cyclic stress limits" are dependent of fiber type due to differing resistance capacities to creep and fatigue. G-, A-, and CFRP sustained plus cyclic stress limits are calculated as $0.20f_u$, $0.30f_u$, and $0.55f_u$ (ACI 440.2R-8, Table 10-1), respectively, where f_u is the ultimate strength of the FRP reduced by the environmental reduction factor. These values are approximations developed from experimental results by Yamaguchi et al. (1997); Odagiri et al. (1997); and Malvar (1998), and have an imposed factor of safety of 1/0.6 (as cited by ACI 2008).

Application Techniques

Traditional steel plating applications for the rehabilitation of deteriorated structures has the basic drawback that the plate tends to separate or "peel" from the concrete surface and thus may not behave monolithically with the concrete member. It is also difficult to ensure proper adhesion due to the uneven concrete surfaces (Katsuki et al. 2002). FRP sheets have the ability to address both of these issues since the sheets can either be adhered closely to the concrete surface or mechanically fastened to the concrete member (Katsuki et al. 2002; Whittemore and Durfee 2011). According to Bizindavyi and Neale (1999), Chajes et al. (1996), Coronado and Lopez

(2008), Nakaba et al. (2001), Smith and Teng (2002a), Pellegrino et al (2008), Yao et al. (2005), and Yuan et al. (2004), the most successful of the strengthening applications have been those that utilize the FRP sheet's ability to withstand high stresses (as cited by Niemitz et al. 2005).

Externally bonded application processes include wet-layup and pre-cured systems. Wet-layup systems use flexible sheets or fabrics of non-impregnated (raw) or pre-impregnated fibers that are saturated with an epoxy adhesive resin and placed on the concrete surface. Pre-cured systems use rigid FRP strips or plates to the surface of the concrete using an epoxy adhesive, which creates a well-defined bond-line (Bisby et al. 2010). As stated earlier, externally bonded FRP reinforcement is considered *bond critical,* and adequate bonding of the FRP to the concrete is paramount in ensuring that the FRP strengthening system will function as desired (Bisby and Fallis 2006).

The condition of the concrete substrate is one of the most critical aspects to consider prior to strengthening a structure because the concrete must be able to transfer the load from the existing structure to the FRP system through shear stresses that develop in the adhesive and matrix (Bisby et al. 2010). Damaged and spalling concrete should be removed, repaired and smoothed prior to the adhesion of FRP sheets to ensure proper adhesion of the FRP sheets and achieve a satisfactory force transfer from sound concrete to the FRP overlays. Typically application of EB systems requires skilled labor (Bisby et al. 2010; Katsuki et al. 2002; Pantelides et al. 2006; Aldolraimzadeh et al. 2009).

In addition to bonding the FRP systems to the concrete substrate, various anchoring methods have been investigated in order to allow development of higher forces in the FRP sheets beyond those that cause debonding. These anchoring methods include transverse sheets or straps to

prevent debonding due to differential deformation during loading (Niemitz et al. 2003; Coronado and Lopez 2008 as cited by Niemitz et al. 2010; Katsuki et al. 2002), mechanical anchors (Elsayed et al. 2009 as cited by Niemitz et al. 2010), wrapping the end of sheets in rods embedded in grooves formed into the concrete (Eshwar et al. 2008; Khalifa et al. 1999 as cited by Niemitz et al. 2010), or forming and anchoring FRP sheets using FRP anchors (Eshwar et al. 2008; Orton et al. 2008; Ozbakkaloglu and Saatcioglu 2009 (as cited by Niemitz et al. 2010).

Green et al. (2000) found that the critical factor in FRP-concrete anchorage is not necessarily the required length of joint, but the allowable strain in the FRP or possibly, the maximum allowable strain gradient at the loaded end of the joint. Without some form of supplementary anchorage detail, it would be very difficult to use the full strength of the composite. The overall effects of an FRP reinforced beam included increased flexural capacity under both service and ultimate load conditions, finer and more evenly distributed cracks in concrete, increased post-cracking flexural stiffness, and decreased ductility.

McSweeney and Lopez (2005) studied EB-FRP bond behavior through pull-off tests and found that with sufficient bond length, bond failure occurs in stages; and that increased bond length, width, and thickness increased time-to-failure, with bond width being the most influential. Debonding failure occurs when the remaining bonded length is insufficient to transfer stresses between the FRP and the concrete substrate. Longer bonded lengths increased the time-to-failure load, indicating that an increased bond length beyond transfer length can provide some failure warning of the FRP-concrete system without significantly impacting the failure load. Adding extra plies to the FRP system substantially increases the load capacity of the system when increasing bond width is not practical. Concrete compressive strength had limited effects on the bond failure load.

A study performed for the Pennsylvania Department of Transportation performed by Davalos et al. (2010) evaluated transversely anchored (U-anchored) EB-FRP reinforcement. To maximize the total load carrying capacity, U-anchors were placed close to the initiation point of debonding. This debonding location was determined through research and advice referenced by Davalos et al. (2010) from Leung (2006, 2008). According to Lueng (2006, 2008), debonding initiates from a flexural or flexural-shear crack that forms near the load application point and propagates downward at roughly 30° to the vertical (as cited by Davalos et al. 2010). U-wraps were placed at a location slightly beyond where this 30° line met the tension face of the beam so that the U-wraps' resistance was activated before significant debonding had occurred (Davalos et al. 2010). Beam failure occurred by crack-induced debonding and subsequent FRP rupture; however, rupture was contained between anchor strips. For multi-anchored beams, debonding areas were contained between intermediate anchors. Multi-anchored beams saw a reduction in debonding and ductility; however the wrapping scheme did not appear to cause dramatic differences in the overall performance of beams. Davalos et al. (2010) and Qiao and Xu (2004) found the failure mode transformed from crack-induced debonding to weakening of the FRP-concrete interface and tension failure when subjected to cyclic loading.

An alternative application solution was explored by Niemitz et al. (2010) using CFRP anchors adhered into holes predrilled into the concrete substrate. The heads of the anchors were threaded through the CFRP sheet layer, radially splayed, and adhered on the surface of the retrofit CFRP composite layer. Test results showed that higher peak load to rupture load ratios were achieved in specimen attached using a combination of bonded FRP sheets and anchors compared to bond only or anchor only specimen. The force transferred into the anchors was proportional to the anchor splay diameter and sheet thickness. Smaller splay diameters performed better than larger

splay diameters. Larger anchor splay diameters placed higher force demand on individual anchors due to the engagement of a wider sheet region. In addition to anchoring the FRP sheets, bonding the sheets allowed for a fraction of the applied force to be transferred by bond, increased ductility of the anchor system, and provided transverse redistribution capacity.

An experimental program conducted by Yoshitake et al. (2011) looked at the performance of various anchor systems for retrofitting concrete beams. A single layer of CFRP strip and anchorage were adhesively bonded with epoxy to the beams. Anchorage systems studied included steel hooks, mechanical anchor bolts, steel plates, CFRP plates in rectangular and trapezoidal shapes, and near-surface mounted (NSM) CFRP strips.

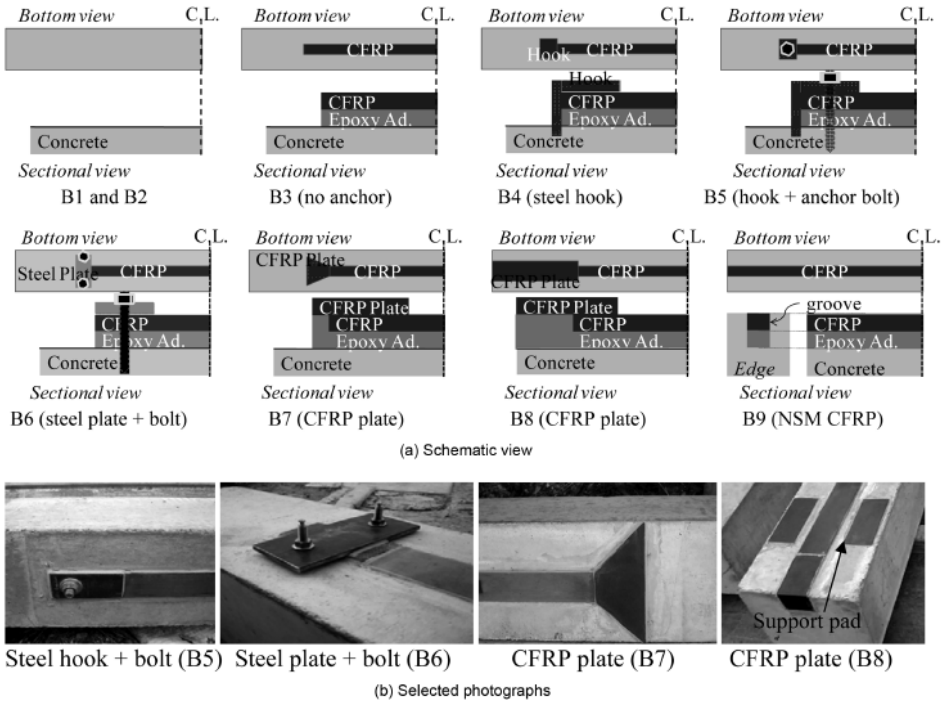

Figure 1: Various anchor systems (Yoshitake et al., 2011)

Figure 1 is from Yoshitake et al. (2011) detailing the various anchor systems tested. Figure 2, from ACI 440, more clearly depicts the difference between laminate and NSM EB-FRP

applications. Laminate applications are bonded to the external face of the structure while NSM applications place bars or strips of FRP into grooves cut into the structure.

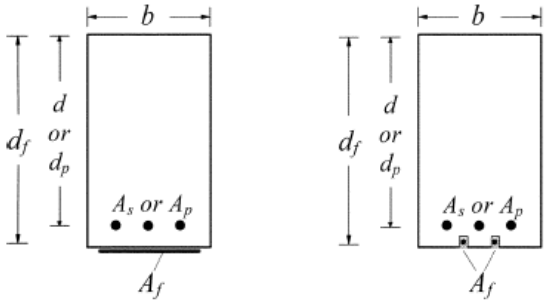

Figure 2: Laminate (left) and NSM (right) EB-FRP reinforcement (ACI 440, 2008)

Beam specimen retrofitted with EB-FRP without anchorage failed due to premature debonding of the CFRP and increased the yield moment by 39.8% compared to a non-retrofitted beam; however ultimate moment capacity was not increased. The performance of the CFRP rectangular and trapezoidal strip anchors were similar, but did not significantly improve the performance of the beam and failed by premature debonding. Steel hooks and anchor bolts performed similarly to the non-anchored retrofitted beam and failed by premature debonding and intermediate-crack induced debonding (IC-debonding), respectively. IC-debonding occurs near the midspan when a crack causes the CFRP strip to debond. The debonding propagates towards the termination points of the strip. Steel plates with anchor bolts increased the yield and ultimate moments by 79.5% and 23.3%, respectively, and significantly enhanced the ductility of the beam. However, the specimens failed by IC-debonding. Lastly, the NSM CFRP strip anchor increased the yield and ultimate moments by 75.0% and 74.4%, respectively. The NSM system produced the largest deflections of all beams tested, failed due to crushing of the concrete and did not produce any noticeable debonding of the CFRP strip (Yoshitake et al. 2011).

A bridge repair performed in Guilford, New Hampshire by Dubois & King Inc. utilized mechanical fasteners to anchor FRP strips to the tension face of a flat slab bridge. Four inch FRP strips placed at 12 inches on center extended the length of the bridge. The 16 foot long strips were fastened to the deck using high strength expansion anchors (wedge bolts) at specified locations along the length of the strip. Because this application process is not bond-critical the preparation of the concrete deck is less than that required if a wet-layup system had been chosen. Due to the simplicity of the construction process, contractors familiar with very basic construction practices should be able to install the strips satisfactorily, unlike wet-layup techniques which require prequalified contractors. The cost of this repair technique was least expensive at $41,000 compared to $85,000 for a wet lay-up repair, $144,000 for a deck replacement, and $420,000 for a complete bridge replacement. It was determined that this method of repair was well suited for flat slab concrete bridges based on both an analytical model and actual field data, and additionally, the construction process can take place exclusively below the bridge causing minimal traffic interruption. (Whittemore and Durfee 2011)

An analysis mechanically fastened FRP (MF-FRP) strips, fastened with steel powder-actuated fasteners and expansion anchors (see Figure 3), by Bank and Arora (2007), found that for MF applications, carbon/epoxy FRPs cannot be used due to inadequate bearing capacity and open-hold capacity. Instead they recommend SAFSTRIP®, a commercially available pultruded FRP system produced by Strongwell (2011a; 2011b) that does not need to be externally bonded to the concrete substrate. The SAFSTRIP® system is composed of carbon tows sandwiched between layers of fiberglass mats and roving bonded together by vinyl ester resin. The combination of glass and carbon fibers provides adequate stiffness from the carbon and bearing strength from the

glass. The SAFSTRIP® system also incorporates a corrosion and UV degradation resistant synthetic veil.

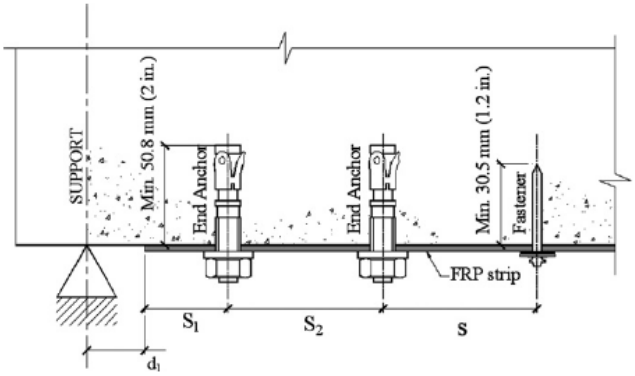

Figure 3: End detail of mechanical fasteners (Bank and Arora, 2007)

Average mechanical properties include a tensile strength of 852 MPa (123.6 ksi), tensile modulus of 62,190 MPa (9.02 x 10^3 ksi), clamped bearing strength of 351 MPa (51 ksi), unclamped bearing strength of 214 MPa (31.0 ksi), and open hole strength of 652 MPa (94.6 ksi) (Strongwell 2011a). After the repair of two bridges in Missouri using the SAFSTRIP® retrofit, a 12-ton load posting was removed from one bridge, and another posting was increased to 20-tons. In another case, the severely deteriorated substrate of another Missouri bridge prevented the use of a bonded FRP system; however, the SAFSTRIP® MF-FRP system was able to adequately repair the bridge (Strongwell 2011a).

A study performed by Ekenel et al. (2005) observed the effects of fatigue loading on flexural performance of (EB-FRP) and MF-FRP. Specimens included glass fiber spike anchored CFRP fabric reinforcement adhered with epoxy and FRP pre-cured laminates attached using mechanical fasteners. The study found that beams reinforced with EB-FRP and spikes saw a 35% increase in strength compared to non-anchored specimen. After performing 2-million fatigue cycles on all specimens it was concluded that mechanical fasteners can be an alternative

to epoxy bonded systems and that MF-FRP systems perform in a more desirable ductile behavior compared to EB-FRP systems.

Summary and Conclusions of Literature Review

Relatively extensive research on the durability of EB-FRP systems have been explored; however results may be inconsistent and incomparable because of differing testing methods due to a lack of testing standards. Extensive research has been conducted on the effects of anchorage systems on the performance of both MF- and EB-FRP systems, while durability studies on these anchorage systems is incomplete.

Carbon/epoxy EB-FRP systems have been researched most extensively and are becoming more popular in infrastructure rehabilitation due to the decreasing cost, low weight, and high strength and durability. However, one major drawback of using a carbon/epoxy EB-FRP system is the amount of substrate preparation and skilled labor required to install the system. MF-FRP systems are gaining popularity due to their ease of installation, minimal substrate preparation requirements, and simple application techniques that do not require skilled labor.

In order to produce a retrofit system that is suitable for application on Maine's deteriorated flat slab bridges, we propose improving on the Yoshitake et al. (2011) steel plate with anchor bolts anchorage system that eliminates IC-debonding failure by creating a strictly MF-FRP retrofit system. The steel plates will be adhered in shop to the FRP strips and adhesive anchor bolts will be used to attach the retrofit to the flexural face of the bridge. A MF-FRP system will reduce concrete preparation, installation time and required skilled labor. The concern of bearing capacity can be eliminated in one of two ways, (1) eliminating the need for predrilled holes in the FRP by extending the width of the steel plate past the width of the FRP, and (2) bond the pre-

drilled steel plate to the FRP, allow the adhesive to dry and drill through the FRP. Option (2) assumes that the adhesive and steel plate will provide enough bearing capacity to mitigate splitting of the FRP.

In addition to the two mechanical fastening options the woven material of system A (carbon) was selected over unidirectional material under the assumption that the non-unidirectional behavior of the material will provide some transverse strength and bearing capacity. Although the glass fibers of system B are potentially problematic due to durability, creep, and fatigue concerns because the retrofit system is aiming for a short-term life cycle increase, due to the low cost of glass FRP systems it is considered reasonable and economical to test this alternative system. Further, system B will utilize unidirectional fiber to minimize weight and provide information on how unidirectional reinforcing performs relative to the woven FRP used in system A.

FRP Retrofit Design Procedure

The design of systems A and B followed the procedures described in ACI 440. A complete summary of the two systems is found at the conclusion of this section and full design calculation packages are provided in the appendix of this document. To design the retrofit the following quantities were initially calculated: existing reduced nominal moment capacity, applied dead and live load moments, existing rating factor, required FRP moment capacity, and strengthening limits. Given these quantities, the retrofit was designed based on ACI 440.2R-08 specifications and the mechanical fastening system was tailored to meet the tensile requirements of the retrofit based on the HILTI, Inc. manufacturer's design guide and the AASHTO LRFD Bridge Design Specifications.

The retrofit design is based on the dimensions and details on the design plans for the Levant Bridge (#5253).

Existing Capacity, Applied Moments and Load Rating Factor

Following ACI 318 design specifications for reinforced concrete structures, an existing reduced nominal moment capacity of 62.14 kip-ft/ft was calculated. The applied moments used for design are based on the finite element analysis results as described in a separate report to the MaineDOT delivered in December 2011. The applied moments are outlined below.

- Moment due to structural components: 23.97 kip-ft/ft
- Moment due to wearing surface: 3.552 kip-ft/ft
- Moment due to live load and impact factor: 34.75 kip-ft/ft

In compliance with section 3.2 of the *MaineDOT Bridge Design Guide* regarding rehabilitation of bridges, these moments do not include a 25% increase to the tandem load that is required for new construction. The ultimate moment, 95.20 kip-ft/ft, was calculated using inventory design load factors of 1.25 for dead and 1.75 for live.

The existing load rating factor was then calculated using the following equation,

$$RF = \frac{\phi * \phi_R * M_n - \gamma_D * M_D}{\gamma_L * M_L}$$

where:

M_D = total dead load moment

M_L = live load moment

M_n = nominal moment capacity

RF = load rating factor

γ_D = inventory dead load factor

γ_L = inventory live load factor

ϕ = greatest of system factor ϕ_s, condition factor ϕ_c, resistance factor ϕ_R

ϕ_R = resistance factor

Strength limits imposed by ACI 440 section 9.2 ensure that the structure being rehabilitated can withstand a reasonable level of load without collapse in the event that the FRP system is damaged. If the existing reduced nominal moment capacity of the structure does not exceed the strengthening limit the system is not a suitable candidate for FRP rehabilitation. The strengthening limit is calculated using the following equation,

$$(\phi R_n)_{existing} \geq (1.1S_{DL} + 0.75S_{LL})_{new}$$

where:

$(\phi R_n)_{existing}$ = existing reduced nominal capacity

S_{DL} = expected dead load of retrofitted system

S_{LL} = expected live load of retrofitted system

The strengthening limit moment for the design was calculated to be 56.33 kip-ft/ft. This is less than the existing reduced nominal capacity of 62.14 kip-ft/ft, making this structure acceptable for FRP retrofitting.

FRP Strip Design

Following the specifications of the ACI 440 guidelines, the width of FRP per foot width of bridge was determined to be 3.5 in and 4.5 in for system A and system B, respectively. The mechanical properties of the two systems are provided in Table 1 below along with supplementary information regarding environmental reduction factors. The environmental reduction factor (ACI 440, section 9.3) accounts for the fiber type and exposure condition of the retrofit system. As discussed previously, different fiber types differ in durability and behavior under long term stresses. The design tensile strength and strain are calculated by multiplying the ultimate tensile strength and strain by the environmental reduction factor (ACI 440, section 9.4). The allowable creep and fatigue tensile stress is then calculated based on ACI 440 section 10.2.9. The allowable creep and fatigue tensile stress reduces the design tensile strength based on fiber type. This allowable tensile stress ensures the stress in the FRP system does not cause the system to fail due to creep and fatigue. To simplify the design process, an FRP thickness was assigned at the beginning of the design and adjusted following the determination of the required area of FRP in order to provide strip width between 3 and 5 in.

Mechanical properties were obtained from Daniel and Ishia (2006). System A is comprised of woven carbon fiber fabric/epoxy (AGP370-5h/3501) (p. 379). System B consists of unidirectional E-glass/epoxy (p. 377).

Table 1: FRP Design Properties

	System A (Carbon)	System B (Glass)
Unit weight (pci)	0.058	0.071
Elastic modulus (ksi)	11200	6000
Ultimate tensile strain	0.013	0.028
Ultimate tensile strength (ksi)	145.6	165
Environmental reduction factor	0.85	0.65
Design tensile strength (ksi)	123.8	107.3
Design tensile strain	0.011	0.018
Allowable creep and fatigue tensile stress (ksi)	68.1	21.5

The required moment capacity of the FRP is determined using the following equation, modified from equation 10-1 of ACI 440.2-R,

$$(M_{FRP})_{required} = \left(\frac{M_u}{\phi_R} - M_n\right)\frac{1}{\psi_f}$$

where:

$(M_{FRP})_{required}$ = required moment capacity of FRP

M_u = ultimate factored moment

M_n = existing nominal moment capacity

ψ_f = FRP uncertainty reduction factor (ACI 440, section 9.1 and 10.2.10)

The FRP uncertainty reduction factor is a recommended reduction of the contribution of strength from the FRP to the capacity of the structure to reflect uncertainties inherent in FRP systems compared to steel reinforced or prestressed concrete. The required moment capacity for both systems was determined to be 42.31 kip-ft/ft. An FRP retrofit system with a moment capacity

greater than or equal to $(M_{FRP})_{required}$ will increase the load rating factor of the Levant Bridge (#5253) to a value greater than or equal to 1.0.

When retrofit systems are installed on a bridge, unless all loads (including dead) are removed from the structure before installation, there is existing service load strain in the section. Because the FRP is installed while these strains exist, the FRP itself does not experience this strain. In order to account for this existing strain ACI 440 section 10.2.3 permits the calculation of the existing strain using cracked section analysis and assuming only dead loads act on the structure at the time of installation. By this procedure an existing flexural tensile strain of 0.0005 was determined.

To determine the required cross-sectional area of FRP to satisfy $(M_{FRP})_{required}$ an iterative approach to satisfy equilibrium was used to determine the following:

- Tensile strain in the FRP (ACI 440 equation 10-3)
- Tensile stress in the FRP (ACI 440 equation 10-9)
- Depth to the neutral axis (ACI 440 equation 10-12)
- Cross-sectional area of FRP

Once equilibrium was satisfied and the required cross-sectional area of FRP determined, the required width of FRP was computed by dividing the required cross-section by the assigned FRP thickness. To account for the eventual loss of cross-sectional area at the mechanical fastener location an additional $^3/_8$ in. (the same measure as the diameter of the selected anchor bolt) was added to the required strip width. If the resulting FRP width was not between 3 and 5 in the FRP thickness was adjusted and the design process was repeated. Once the FRP width was within the desired range of 3 to 5 in, an FRP width was chosen to the closest ¼ in. The tensile strain and

stress and depth to the neutral axis were then again calculated based on the true cross-sectional area of the FRP based on the selected strip width. The effective strain in the FRP (the strain in the FRP due to the anticipated applied loads) and steel were checked against the design strain and yield strain, respectively, to ensure environmental conditions and serviceability requirements were met. The new reduced nominal moment capacity of the retrofit system was then determined using equation 10-13 of ACI 440 and checked against the ultimate moment. Creep and fatigue limit states were checked using equation 10-14 and 10-15 of ACI 440. Following all checks, the new rating factor for the retrofitted system is determined as provided previously with the new reduced nominal moment capacity substituted for the existing nominal moment capacity. Table 2 summarizes the results upon completion of the FRP strip width design process.

Table 2: FRP Strip Width Design Summary

	Existing Structure	System A (Carbon)	System B (Glass)
Strip width (in)	__	3.5	4.5
Strip thickness (in)	__	0.08	0.12
Reduced nominal moment capacity (kip-ft/ft)	62.14	95.41	96.18
Rating factor	0.456	1.004	1.016
Weight of FRP strip (excluding steel) (plf)	__	0.19	0.46

Mechanical Fastening Design

The smallest diameter bolt was selected to minimize the size of the bolt hole in the FRP. Using the HILTI, Inc. technical guide and an HVU capsule with HAS thread rod, ASTM A 325, carbon steel $^{3}/_{8}$ in. anchor, the steel plate for the mechanical fastening system was sized based on the area of adhesive required to carry ultimate tensile stress of the FRP in the adhesive.

Following the HILTI, Inc. technical guide for these anchors the ultimate shear capacity of one anchor bolt was determined. The number of connectors required over the half span was calculated by dividing the ultimate tensile force required to fail the FRP by the shear capacity of

a single anchor. The ultimate tensile force was calculated by multiplying the cross-sectional area of the FRP by the ultimate tensile strength of the FRP. The required spacing between anchor bolts was determined using the following equation,

$$s_b = \frac{L}{2}\frac{1}{(n_{cxn} - 1)}$$

where:

s_b = maximum anchor bolt spacing

L = span length

$n_{cxn=}$ = number of required connections over the half span

Based on this calculation an anchor bolt spacing equal to or less than the s_b was selected. A spacing of 24 in and 10 in for system A and B, respectively, was selected for the design retrofit. The difference in anchor spacing is a consequence of the difference in the ultimate tensile forces required to fail the FRP systems. Because the ultimate strain in system A is approximately half that of system B (0.013 and 0.028, respectively) the resulting ultimate tensile stress of system A is about half that of system B. The additional connectors required for system B results in the decreased spacing between anchors in order to fit the required number of connectors over the half-span of the design bridge.

Adhesive properties from Ashland, Inc. for Pliogrip® epoxy technology (product # 5761B) were used to determine the area of adhesive required to carry the ultimate tensile force of the FRP in the adhesive:

- Shear strength: 3.44 ksi
- Elastic modulus: 645.4 ksi

- Maximum allowable strain: 0.01

For these design calculations the ultimate tensile strength of the FRP is not reduced by the environmental factor. The area of adhesive required to develop the ultimate tensile strength of the FRP was determined by dividing the ultimate tensile force in the FRP by the shear strength of the adhesive. The required surface area of the steel plate, therefore, must be equal to or greater than the required area of the adhesive plus the area of the bolt hole.

The dimensions of the plate parallel to the tensile force of the FRP and plate thickness were determined using section 6.13.2.9 equation 6.13.2.9-1 of the AASHTO Bridge Design Specifications.

$$\phi_b R_n = \phi_b 2.4 d t F_u$$

where:

R_n = bearing strength

L_c = clear distance, in the direction of the force, between the edge of the hole and the edge of the adjacent hole or edge of the material

F_u = specified minimum tensile strength of the connected material

d = nominal bolt diameter

t = thickness of connected material

ϕ_b = bearing strength reduction factor, 1.0

The use of equation 6.13.2.9-1 requires a clear end distance (L_c) greater than two times the bolt diameter. Based on this constraint the required length of the steel plate is calculated using the following equation:

$$L_c = \frac{1}{2}(w_{PL} - d) > 2.0d$$

where:

L_c = clear end distance

w_{PL} = plate dimension parallel to FRP tensile force

The length of the plate was selected to satisfy the condition of equation 6.13.2.9. The width of the steel plate was then determined by dividing the required area of the steel plate by w_{PL} and rounding to the nearest ¼ in. The required plate thickness *t* was found by substituting the ultimate tensile strength of the FRP for the bearing strength in equation 6.13.2.9 and solving for *t*.

The ultimate strain in the adhesive was calculated by dividing the strain in the adhesive at the ultimate strength of the FRP by the area of adhesive used. This ultimate strain cannot exceed the maximum allowable strain of the adhesive.

Based on these calculations, both system A and system B require a 2.0 in. x 1.0 in x $\frac{1}{8}$ in plate. The total weight of the retrofit was determined to be 0.23 plf for system A and 0.50 plf for system B. This implies that for a 25 ft slab bridge (a typical simple span), one FRP and steel plate strip for system A and B would weigh approximately 5.77 lbs and 12.40 lbs, respectively.

Summary of Results

In order to increase the usable life-cycle of underrated flat slab concrete bridges in Maine it was proposed to develop an FRP flexural retrofit system that is easy to install, lightweight, durable and provides an alternative to conventional rehabilitation. Based on a thorough literature review and the external reinforcement design guides, two FRP retrofit systems, one utilizing woven carbon fiber, the other unidirectional glass were designed and theoretically analyzed. The details of these systems are summarized below.

System A: Woven carbon fiber fabric/epoxy consisting of a 3.5 in wide by 0.08 in thick strip with 3/8in HILTI, Inc. HVU adhesive anchors spaced at 24 in on center with 2.0 in x 1.0 in x $\frac{1}{8}$ in steel plates adhered to the FRP strip.

System B: Unidirectional E-glass/epoxy in a 4.5 in wide by 0.12 in thick strip with 3/8 in HILTI, Inc. HVU adhesive anchors spaced 10 in on center with 2.0 in x 1.0 in x $\frac{1}{8}$ in steel plates adhered to the FRP strip.

Figure 4(a) details the dimensions and spacing of a section of systems A and Figure 4(b) details the dimensions and spacing of a section of system B.

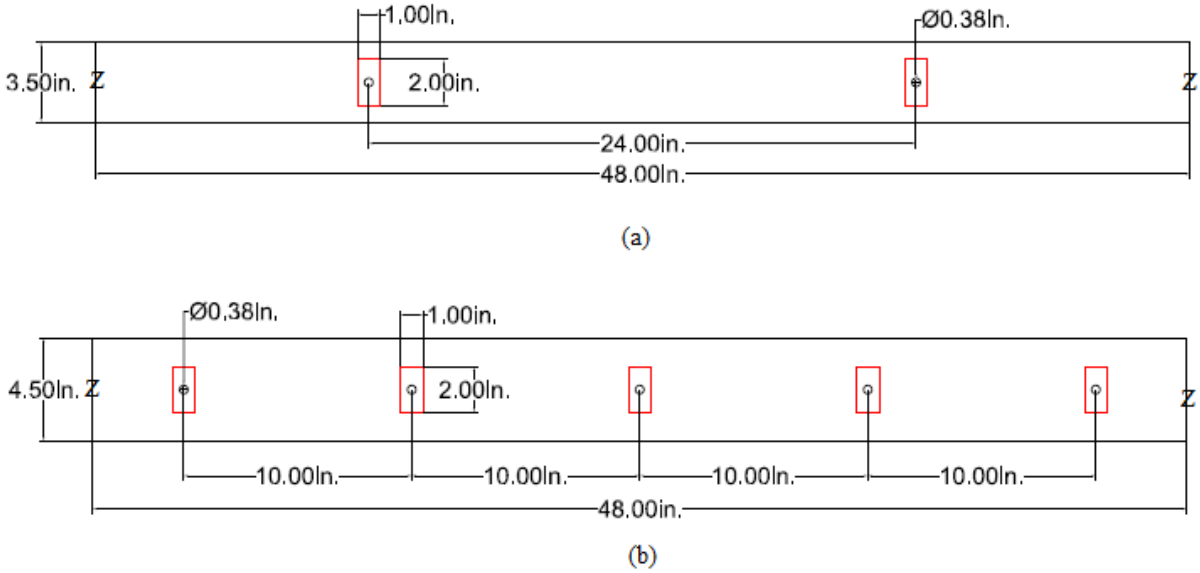

Figure 4: Detailed drawings of a section of FRP strip, (a) System A; (b) System B

Upon installation of the flexural retrofit, system A would increase the flexural capacity of the existing structure by 53.6%. System B would increase the flexural capacity of the existing structure by 54.7%. System A is relatively lightweight, 0.23 plf, while System B weighs 0.50 plf. However, System B could provide a feasible low cost alternative.

In order to determine the best system for MaineDOT to use, the remainder of the deliverables must be carried out. The remaining deliverables include developing a durability testing plan (estimated delivery 03/31/2012), performing small beam bend tests (estimated delivery 06/20/2012), and performing durability tests (estimated delivery 07/31/2013). Based on the results from these tests a final conclusion regarding the best non-proprietary flexural retrofit for rehabilitating flat slab bridges in Maine can be determined.

References

American Association of State Highway and Transportation Officials (AASHTO). (2007). *AASHTYO LRFD bridge design specifications: Customary US units* (4th ed.). Washington DC, USA.

American Association of State Highway and Transportation Officials (AASHTO). (2009). *AASHTO LRFD guide for design of externally bonded FRP systems for strengthening concrete bridges (DRAFT #2)*. Washington DC, USA: Paul Liles.

American Concrete Institute (ACI), Committee 318. (2008). *Building code requirements for structural concrete (ACI 318-08) and commentary*. American Concrete Institute.

American Concrete Institute (ACI), Committee 440. (2008). *Guide for the design and construction of externally bonded FRP systems for strengthening concrete structures*. Farmington Hills, MI, USA.

Anderson, M., Chen, A., Davalos, J.F., Justice, A., and Ray, I. (2010). *District 3-0 investigation of fiber wrap technology for bridge repair and rehabilitation – phase III* (Contract No. 510401). Morgantown, WV: West Virginia University.

ASCE report card for America's infrastructure. Available from: http://www.asce.org/reportcdard/2005/. Accessed by Bisby, Fam, et al. 2006 23 January 2003.

Ashland, Inc. (2010). *Pliogrip® structural adhesives, Pliogrip® 5761B epoxy adhesive system.* Available from: http://www.ashland.com/Ashland/Static/Documents/APM/PLIOGRIP%205761B%20%202524%20v1%20EN-1%20F2.pdf. Accessed 07 December 2011.

Balázs, C.L., and Borosnyói, A. (2001). Long-term behavior of FRP. *Composites in Construction: A Reality*. Reston, VA: ASCE, 84-91.

Bank, L.C., and Arora, D. (2007). Analysis of RC beams strengthened with mechanically fastened FRP (MF-FRP) strips. *Composite Structures, Vol. 79* (No. 2), 180-191.

Banthia, N., Abdolrahimzadeh, A., and Boulfiza, M. (2009). Proceedings from SBEIDCO '09: *1st International Conference on sustainable built Environment Infrastructures in Developing Countries*. Oran, Algeria: ENSET.

Bisby, L.A. (2006). *ISIS educational module 8: Durability of FRP composites for construction.* Retrieved from www.isiscanada.com/education/download.asp.

Bisby, L.A., and Fallis, G. (2006). *ISIS educational module 6: Application and handling of FRP reinforcements for concrete.* Retrieved from www.isiscanada.com/education/download.asp.

Bisby, L.A., and Fitzwilliam, J. (2006). *ISIS educational module 2: An introduction to FRP composites for construction.* Retrieved from www.isiscanada.com/education/download.asp.

Bisby, L.A., and Ranger, M. (2006). *ISIS educational module 1: Mechanics examples incorporating FRP materials.* Retrieved from www.isiscanada.com/education/download.asp.

Bisby, L.A., Noel, M., and Wahab, N. (2010). *ISIS educational module 4: An introduction to FRP strengthening of concrete structures.* Retrieved from www.isiscanada.com/education/download.asp.

Bisby, L.A., Ranger, M., and Williams B.K. (2006). *ISIS educational module 3: An introduction to FRP-reinforced concrete*. Retrieved from www.isiscanada.com/education/download.asp.

Bizindavyi, L., and Neale, K. W. (1999). Transfer lengths and bond strengths for composites bonded to concrete. *Journal of Composites for Construction, Vol. 3* (No.4), 153-160.

Chajes, M. J., Finch, W. W., Jr., Januszka, T. F., and Thomson, T.A., Jr. (1996). Bond and force transfer of composite material plates bonded to concrete. *ACI Structural Journal, Vol. 93* (No. 2), 209-217.

Chateauminiois, A., Chabert, B., Soulier, J.P., and Vincent, L. (1993). "Hygrothermal aging effects on the static fatigue of glass/epoxy composites." *Composites, Vol. 24* (No. 7), 547-255.

Chin, J.W., Aouadi, K., and Nguyen, T. (1997). Effects of environmental exposure on fiber-reinforced plastic (FRP) materials used in construction. *Journal of Composite Technologies and Research, Vol. 19* (No. 4), 205-213.

Coronado, C.A., and Lopez, M. M. (2008). Experimental characterization of concrete-epoxy interfaces. *Journal for Materials in Civil Engineering, Vol. 20* (No. 4), 303-312.

Cromwell, J.R., Harries, K.A., and Shahrooz, B.M. (2011). Environmental durability of externally bonded FRP materials intended for repair of concrete structures. *Construction and Building Materials, Vol. 25* (No. 5), 2528-2539.

Dai, J.G., Saito, Y., Ueda, T., and Sato, Y. (2005). Static and fatigue bond characteristics of interfaces between CFRP sheets and frost damage experienced concrete. *Proc. 7th Int. Symp. on Fiber Reinforced Polymer Reinforcement for Reinforced Concrete Structures,* 1515-1530. Kansas City, Missouri, November 6-10.

Daniel, I.M., and Ishai, O. (2006). *Engineering mechanics of composite materials* (2nd ed.). New York, NY: Oxford University Press, Inc.

Davalos, J.F., Chen, A., Ray, I., Justic, A., and Matthew, A. (2010). *District 3-0 investigation of fiber wrap technology for bridge repair and rehabilitation – phase III* (Contract No. 510401). Morgantown, WV: West Virginia University.

Desiderio, P., and Feo, L. (2005). Durability evaluation of EBR CFRP strengthened masonry structure. *Proc. of the Int. Symp. on Bond Behaviour of FRP in Structures (BBFS 2005).*

Ekenel, M., Rizzo, A., Myers, J.J., and Nanni, A. (2005) Effect of fatigue loading on flexural performance of reinforced concrete beams strengthened with FRP fabric and pre-cured laminate systems. *Composites in Construction 2005 – Third International Conference*. Lyon, France, July 11-13.

Elsayed, W. E., Ebead, U. A., and Neale, K. W. (2009). Studies on mechanically fastened fiber-reinforced polymer strengthening systems. *ACI Structural. Journal, Vol. 106* (No. 1), 49-59.

Eshwar, N., Nanni, A., and Ibell, T.J. (2008). Performance of two anchor systems of externally bonded fiber-reinforced polymer laminates. *ACI Materials Journal, Vol. 105* (No. 1), 72-80.

Gartner, A., Douglas, E.P., Dolan, C.W., and Hamilton, H.R. (2011). Small beam bond test method for CFRP composites applied to concrete. *Journal of Composites for Construction, Vol. 15* (No.1), 52-61.

Gerritse, A. (1993). Aramid-based prestressing tendons. *Alternative Materials for the Reinforcement and Prestressing of Concrete*, ed. Clarke, Chapman & Hall, London, 1993, 172-199.

Green, M.F., Bisby, L.A., Beaudoin, Y., and Labossiere, P. (2000). Effect of freeze-thaw cycles on the bond durability between fibre reinforced polymer plate reinforcement and concrete. *Canadian Journal of Civil Engineering, Vol. 27*(No. 5), 949-959.

Green, M.F., Bisby, L.A., Fam, A.Z., and Kodur, V.K.R. (2006). FRP confined concrete columns: Behaviour under extreme conditions. *Cement and Concrete Composites, Vol. 28* (No. 10), 928-937.

Helbling, C.S., and Karbhari, V.M. (2002). Environmental durability of E-glass/vinyl ester composites under the combined effect of moisture, temperature, and stress. *Proc., 2nd Int. Conf. on Durability of Fiber Reinforced Polymer Composites for Construction*, B. Benmokrane and E. El-Salakawy eds. Montreal, 247-255.

HILTI, Inc. (2006). *North American product technical guide.* Tulsa, OK: Hilti, Inc.

Intelligent Sensing for Innovative Structures (ISIS) Canada. (2006). *ISIS educational module 2: An introduction to FRP composites for construction* [Powerpoint slides]. Retrieved from www.isiscanada.com/education/download.asp.

Karbhari, V.M., Rivera, J., and Dutta, P.K. (2000). Effect of short-term freeze-thaw cycling on composite confined concrete. *Journal of Composites for Construction, Vol. 4* (No. 4), 191-197.

Kato, Y., Yamaguchi, T., Nishimura, T., and Uomoto, T. (1997). Computational model for deterioration of aramid fiber by ultraviolet rays. *Proc. 3rd Int. Symp. on Fiber Reinforced Polymer Reinforcement for Reinforced Concrete Structures,* JCI, 1997, *Vol. 2*, 163-170.

Khalifa, A., Alkhradji, T., Nanni, A., and Lansburg, S. (1999). Anchorage of surface mounted FRP reinforcement. *Concrete International, Vol. 21* (No. 10), 49-54.

Li, Y., and Karbhari, V.M. (2003). Durability characterization of T700 based composites for use in civil infrastructure. *Proc. for Society for the Advancement of Material and Process Engineering* 2003 (SAMPE 2003), Long Beach, CA.

Machida, A. (1993). State-of-the-art report on continuous fiber reinforcing materials. JSCE, Tokyo, 1993.

MaineDOT (2007). *Keeping our Bridges Safe*. Available at http://www.maine.gov/mdot/pdf/Keeping%20Our%20Bridges%20Safe.1107.pdf (accessed 7/27/2011).

Matthews, F.L., and Rawlings, R.D. (1994). *Composite materials: Engineering and science.* Chapman and Hall: New York.

McSweeney, B.M., and Lopez, M.M. (2005). FRP-concrete bond behavior: A parametric study through pull-off testing. *Proc. 7th Int. Symp. on Fiber Reinforced Polymer Reinforcement for Reinforced Concrete Structures,* 441-460. Kansas City, Missouri, November 6-10.

Nakaba, K., Kanakubo, T., Furuta, T., and Yoshizawa, H. (2001). Bond behavior between fiber-reinforced polymer laminates and concrete. *ACI Structural Journal, Vol. 98* (No. 3), 359-367.

Niemitz, C.A., James, R., and Breña, S.B. (2010). Experimental behavior of carbon fiber-reinforced polymer (CFRP) sheets attached to concrete surfaces using CFRP anchors. *ASCE Journal of Composites for Construction, Vol. 14* (No.2), 185-194.

Orton, S. L., Jirsa, J. PO., and Bayrak, O. (2008). Design considerations of carbon fiber anchors. *Journal for Composites in Construction, Vol. 12* (No. 6), 608-616.

Ouyang, Z. (2007). Durability of bond between FRP and concrete in moist environments: experimental, numerical and analytical study. (Doctoral dissertation). Marquette University, Milwaukee, Wisconsin. Retrieved from UMI Microform. (3275946).

Ozbakkaloglu, T., and Saatcioglu, M. (2009). Tensile behavior of FRP anchors in concrete. *Journal for Composites in Construction, Vol. 13* (No. 2), 83-92.

Pantelides, C.P., Reay, J.T., and Reaveley, L.D. (2006). *Time dependent effects from monitoring of State Street Bridge FRP composite retrofit* (Report No. UT-07.01). Salt Lake City, Utah: University of Utah.

Pellegrino, C., Tinazzi, D., and Modena, C. (2008). Experimental study on bond behavior between concrete and FRP reinforcement. *Journal for Composites in Construction, Vol. 12* (No. 2), 180-189.

Piggott, M.R. (1980). *Load bearing fibre composites*. Pergamon Press, Oxford, 1980.

Qiao, P., and Xu, Y. (2004). Effects of freeze-thaw and dry-wet conditioning on the mode-I fracture of FRP-concrete interface bonds. *Proc. of Conf. for Engineering, Construction, and Operations in Challenging Environments: Earth & Space 2004*, 601-608.

Saadatmanesh, H., and Tannous, F.E. (1997). Durability of FRP rebars and tendons. *Proc. 3rd Int. Symp. on Fiber Reinforced Polymer Reinforcement for Reinforced Concrete Structures*, JCI: Vol 2.,147-154.

Saadatmanesh, H., and Tannous, F.E. (1999). Relaxation, creep, and fatigue behavior of carbon fiber reinforced plastic tendons. *ACI Materials Journal, Vol. 96* (No. 2), 143-153.

Saenz, N., and Pantelides, C.P. (2006). Short and medium term durability evaluation of FRP-confined circular concrete. *Journal of Composites for Construction, Vol. 10* (No. 3), 244-253.

Sen, R., Shahawy, M., Rosas, J., and Sukumar, S. (1998a). Durability of aramid pretensioned elements in a marine environment. *ACI Structural Journal, Vol. 95* (No. 5), 578-587.

Sen, R., Shahawy, M., Rosas, J., and Sukumar, S. (1998b). Durability of carbon pretensioned elements in a marine environment. *ACI Structural Journal, Vol. 95* (No. 6), 578-587.

Smith, S. T., and Teng, J. C. (2002a). FRP-strengthened RC Beams-I: Review of debonding strength models. *Engineering Structures, Vol. 24* (No. 4), 385-395.

Steckel, G.L., Hawkins, G.F., and Bauer, J.L. (1998). Environmental durability of composites for seismic retrofit of bridge columns. *Proc., 2nd Int. Conf. on Composites in Infrastructure,* Tucson, Ariz., H. Saadatrmanesh and M.R. Ehsani, eds., 460-475.

Strongwell (2011a). *SAFSTRIP® fiber reinforced strengthening strip.* Retrieved from www.alton.com.sg/pdf/strongwell/strongwell14.pdf, July 26, 2011.

Strongwell (2011b). *Pultruded products: Structural reinforcement and strengthening.* Retrieved from www.strongwell.com/products/pultruded_prod/struc_reinforcement_and_strength/, July 26, 2011.

Subramaniam, K.V., Ghosn, M., and Ali-Ahmad, M. (2007). Impact of freeze-thaw degradation on FRP-concrete interface fracture. *Advances in Construction Materials 2007, Part V* (419-426). New York, New York: Springer.

Teng, M. Sotelino, E.D., and Chen, W. (2003). Performance evaluation of reinforced concrete bridge columns wrapped with fiber reinforced polymers. *Journal of Composites for Construction, Vol. 7* (No. 2), 83-92.

Tokyo Rope. (1993). Technical data on CFCC. Tokyo Rope Mft. Co., Ltd. *Manual,* Tokyo, October 1993.

Triantatillou, T. C., and Pelvris N., (1990). Strengthening of RCbeams with epoxy-bonded fiber-composite materials. *Materials and Structures, Vol. 25* (No. 249), 201-211.

Uomoto, T. Mutsuyoshi, H., Katsuki, F., and Misra, S. (2002). Use of fiber reinforced polymer composites as reinforcing material for concrete. *Journal of Materials in Civil Engineering, Vol. 14* (No. 3), 191-209.

Whittemore, M.D., and Durfee, R.H. (2011). Low-cost rehabilitation with FRP strips. *International Bridge Conference 2011*. Pittsburg, Pennsylvania, June 5-8.

Yoshitake, I., Yumikura, K., Mimura, Y., Kim, Y.J. (2011). Composite strips with various anchor systems for retrofitting concrete beams. *International Journal of Computing Science and Mathematics, Vol. 5* (No. 1), 43-48.

Appendix A: Bridge Properties, Loads, and Existing Rating Factor

Bridge and Reinforcing Steel Dimensions and Properties

Concrete Slab

Span Length	$L := 319.5in = 26.62 \cdot ft$
Slab thickness	$h := 18.5in$
Slab width	$W := 308in = 308 \cdot in$
Strip width	$b_w := 12in$
Compressive strength	$f'c := 2.5ksi$
Elastic Modulus	$E_c := 57000\sqrt{f'c \cdot psi} = 2850 \cdot ksi$
Ultimate stress	$\varepsilon_{cu} := 0.003$
Poisson's Ratio	$\nu_c := 0.19$
Unit weight	$\gamma_c := 150pcf$

Curb

Top curb height	$h_{curb\_top} := 12in$
Top curb width	$b_{curb\_top} := 22in$
Bottom curb height	$h_{curb\_bot} := 12in$
Bottom curb width	$b_{curb\_bot} := 22in$

Wearing Surface

Surface thickness	$t_{wear} := 4in$
Unit Weight	$\gamma_{wear} := 144pcf$
Surface width	$b_{wear} := W - 2 \cdot b_{curb\_bot} = 22 \cdot ft$

Reinforcing Steel

Reinforcing bar diameter	$d_b := 1in$
Bar spacing	$s_b := 6in$
Area of steel (per foot)	$As_{ft} := d_b^2 \cdot \frac{\pi}{4} \cdot \frac{1}{s_b} = 1.57 \cdot \frac{in^2}{ft}$
Area of steel	$As := As_{ft} \cdot b_w = 1.57 \cdot in^2$
Steel yielding strength	$fy := 33ksi$
Depth to steel	$d := 17in$
Steel elastic modulus	$Es := 29000ksi$
Steel yielding strain	$\varepsilon_y := \frac{fy}{Es} = 0.00114$
Modular Ratio	

Existing Reduced Nominal Moment Capacity

Stress block β_1 factor (Section 2.8.2.5):

$$\beta_1 := \begin{cases} 0.85 \text{ if } f'c \le 4ksi \\ \left(1.05 - 0.05 \cdot \frac{f'c}{ksi}\right) \text{ if } f'c > 4ksi \wedge f'c > 8ksi \\ 0.65 \text{ if } f'c \ge 8ksi \end{cases} = 0.85$$

Distance from extreme compression fiber to N.A. (LRFD Design eqn 5.7.3.1.1-4):

$$c := \frac{As \cdot fy}{0.85 \cdot f'c \cdot b_w \cdot \beta_1} = 2.39 \cdot in$$

Compression block height (LFRD Design eqn 5.7.3.2.3):

$$a_1 := \beta_1 \cdot c = 2.03 \cdot in$$

Existing nominal moment capacity:

$$Mn_{existing} := As_{ft} \cdot fy \cdot \left(d - \frac{a_1}{2}\right) = 69.04 \frac{kip \cdot ft}{ft}$$

Existing net tensile strain in reinforcing steel:

$$\varepsilon_t := \varepsilon_{cu} \cdot \left(\frac{d - c}{c}\right) = 0.02$$

Existing net tensile stress in the reinforcing steel:

$$f_s := \begin{cases} fy \text{ if } \varepsilon_t \ge \varepsilon_y \\ Es \cdot \varepsilon_t \text{ if } \varepsilon_t < \varepsilon_y \end{cases} = 33 \cdot ksi$$

Resistance factor (Eqn. 2-6)

$$\phi_R := \begin{cases} 0.90 \text{ if } \varepsilon_t \ge 0.005 \\ \left[0.65 + \frac{0.25 \cdot (\varepsilon_t - \varepsilon_y)}{0.005 - \varepsilon_y}\right] \text{ if } \varepsilon_t > \varepsilon_y \wedge \varepsilon_t < 0.005 \\ 0.65 \text{ if } \varepsilon_t \le \varepsilon_y \end{cases} = 0.9$$

Reduced nominal capacity:

$$\phi Mn_{existing} := \phi_R \cdot Mn_{existing} = 62.14 \frac{kip \cdot ft}{ft}$$

$$n_s := \frac{Es}{E_c} = 10.18$$

Applied Loads
Loads based on the loads determined through finite element analysis and reported in the Slab Rate report

Dead Load Moments

Moment due to structural component:

$$M_{DC} := 23.972\frac{kip\cdot in}{in}$$

Moment due to wearing surface:

$$M_{DW} := 3.552\frac{kip\cdot in}{in}$$

Moment due to permanent loads other than dead loads

Permanent load:

$$P := 0\frac{kip}{ft}$$

Moment due to permanent load:

$$M_P := 0kip\cdot ft$$

Live Load Moments

Impact factor:

$$IM := 1.33$$

Moment due to live load and impact factor:

$$M_{LL\_IM} := 34.739\frac{kip\cdot in}{in}$$

Ultimate Moment

Load Factors (Inventory Design Loads)

LRFD load factor for structural components and attachments $\gamma\_DC := 1.25$

LRFD load factor for wearing surface and utilities $\gamma\_DW := 1.25$

LRFD load factor for permanent loads other than dead loads $\gamma\_P := 1.0$

Evaluation live load factor $\gamma\_LL := 1.75$

Ultimate Factored Moment:

$$M_u := \gamma\_DC\cdot\left(M_{DC} + M_{DW}\right) + \gamma\_LL\cdot\left(M_{LL\_IM}\right) = 95.20\frac{kip\cdot ft}{ft}$$

Existing Load Rating Factor

System factor: $\phi_s := 1.0$

Condition Factor:
(Provided by MDOT bridge inspection 9/29/09) $\phi_c := 1.0$

$$\phi := \max\left(\phi_R, \phi_s, \phi_c\right) = 1.0$$

Existing load rating factor:

$$RF_{existing} := \frac{\phi \cdot \phi Mn_{existing} - \gamma\_DC \cdot M_{DC} - \gamma\_DW \cdot M_{DW} - \gamma\_P \cdot M_P}{\gamma\_LL \cdot M_{LL\_IM}} = 0.4562$$

Strengthening Limits (Section 2.5.1)
Strengthening limits are imposed to ensure that in the event that the FRP system is damaged, the structure will still be capable of resisting a reasonable level of load without collapse.

$$M_{limit} := 1.1 \cdot \left(M_{DC} + M_{DW}\right) + 0.75 \cdot \left(M_{LL\_IM}\right) = 56.33 \frac{kip \cdot ft}{ft}$$

Check that the existing reduced nominal moment is less than the strengthening limit moment:

$$\begin{cases} \text{"OK"} & \text{if } \phi Mn_{existing} \geq M_{limit} \\ \text{"NG"} & \text{if } \phi Mn_{existing} < M_{limit} \end{cases} = \text{"OK"}$$

Appendix B: Design of System A

FRP Dimensions and Properties

Carbon Fabric/Epoxy AGP370-5H/3501-6S Ef = 11200ksi ultimate strain = 0.013; pg 379 Daniel & Ishai Eng. Mech. of Comp. Mat.

Fiber type	$Fiber_{type} := "Carbon"$
Exposure Conditions (Bridge or Aggressive)	$Condition := "Bridge"$
Unit weight	$\gamma_f := 0.058\,pci$
Strip thickness	$t_f := 0.04\,in$
Number of plies	$n := 2$
Strip spacing	$s_f := 6\,in$
Strip length	$l_f := L = 319.5\,in$
Dist. from extreme compression fiber to FRP CG	$d_f := h + \frac{n \cdot t_f}{2} = 18.54\,in$
Elastic modulus	$E_f := 11200\,ksi$
Manufacturer's tensile strain	$\varepsilon_{fu} := 0.013$
Manufacturer's tensile strength	$f_{fu} := E_f \cdot \varepsilon_{fu} = 145.6\,ksi$
Modular ratio	$n_f := \frac{E_f}{E_c} = 3.93$
FRP reduction factor	$\psi_f := 0.85$

FRP Design Tensile Strength and Strain & Allowable Stress

Environmental reduction factor (Table 2.4-1)

$$C_E := \begin{cases} 0.85 \text{ if } (Condition = "Bridge" \vee Condition = "Aggressive") \wedge Fiber_{type} = "Carbon" = 0.85 \\ 0.65 \text{ if } Condition = "Bridge" \wedge Fiber_{type} = "Glass" \\ 0.75 \text{ if } Condition = "Bridge" \wedge Fiber_{type} = "Aramid" \\ 0.50 \text{ if } Condition = "Aggressive" \wedge Fiber_{type} = "Glass" \\ 0.70 \text{ if } Condition = "Aggressive" \wedge Fiber_{type} = "Aramid" \end{cases}$$

Design tensile strength:

$$f_{fd} := f_{fu} \cdot C_E = 123.76\,ksi$$

Design tensile strain:

$$\varepsilon_{fd} := \varepsilon_{fu} \cdot C_E = 0.0111$$

Allowable creep & fatigue tensile stress:

$$f_{fs\_allow} := \begin{cases} (0.55 \cdot f_{fd}) \text{ if } Fiber_{type} = "Carbon" = 68.07\,ksi \\ (0.20 \cdot f_{fd}) \text{ if } Fiber_{type} = "Glass" \\ (0.30 \cdot f_{fd}) \text{ if } Fiber_{type} = "Aramid" \end{cases}$$

Required FRP Moment Capacity

$$M_{FRP\_required} := \left(\frac{M_u}{\phi_R} - Mn_{existing}\right)\cdot\frac{1}{\psi_f} = 43.21\cdot\frac{kip\cdot ft}{ft}$$

Existing Strain of Section at Service Conditions

Service moment (service, loads on bridge during time of installation of FRP system):

$$M_{service} := b_w\cdot\left(M_{DC} + M_{DW}\right) = 27.52\cdot kip\cdot ft$$

Location of N.A. for a cracked section from extreme compression fiber:

Given $\quad kd_s := 1in$

$$\left(kd_s\right)\cdot\left(\frac{kd_s}{2}\right) = As_{ft}\cdot n_s\cdot\left(d - kd_s\right)$$

$$kd_s := Find\left(kd_s\right) = 5.53\cdot in$$

Cracked moment of inertia:

$$I_{CR} := \frac{b_w\cdot kd_s^{\,3}}{12} + kd_s\cdot b_w\cdot\left(\frac{kd_s}{2}\right)^2 + As\cdot n_s\cdot\left(d - kd_s\right)^2 = 2779.26in^4$$

Existing (initial) strain in the section:

$$\varepsilon_{bi} := \frac{\left(M_{DC} + M_{DW}\right)\cdot\left(d_f - kd_s\right)}{I_{CR}\cdot E_c}\cdot b_w = 0.00054$$

Required Width of FRP per Foot Width of Bridge

Derivation of M_{FRP} and A_f as a function c, the depth to the neutral axis:

Tensile strain in the FRP:

$$\varepsilon_f = \varepsilon_{cu}\cdot\left(\frac{d_f - c}{c}\right) - \varepsilon_{bi} \qquad \text{(Eqn 1)}$$

Tensile stress in the FRP:

$$f_f = E_f\cdot\varepsilon_f \qquad \text{(Eqn 2)}$$

Depth to the neutral axis:

$$c = \frac{As\cdot f_s + A_f\cdot f_f}{0.85\cdot f'c\cdot\beta_1} \qquad \text{(Eqn 3)}$$

Depth of compression block:

$$a = c\cdot\beta_1 \qquad \text{(Eqn 4)}$$

Substituting equation 2 into equation 3 and solving for A_f yields:

$$A_f = \frac{0.85 \cdot f'c \cdot \beta_1 \cdot c - As \cdot f_s}{E_f \cdot \varepsilon_f} \qquad \text{(Eqn 5)}$$

Moment capacity of FRP:

$$M_{FRP} = A_f \cdot f_f \cdot \left(d_f - \frac{a}{2} \right) \qquad \text{(Eqn 6)}$$

Substitute equations 2, 4 and 5 into equation 6:

$$M_{FRP} = \frac{0.85 \cdot f'c \cdot \beta_1 \cdot c - As \cdot f_s}{E_f \cdot \varepsilon_f} \cdot E_f \cdot \varepsilon_f \cdot \left(d_f - \frac{c \cdot \beta_1}{2} \right) \qquad \text{(Eqn 7)}$$

Simplify equation 7:

$$M_{FRP} = \left(0.85 \cdot f'c \cdot \beta_1 \cdot c - As \cdot f_s\right) \cdot \left(d_f - \frac{c \cdot \beta_1}{2} \right) \qquad \text{(Eqn 8)}$$

Substitute M_{FRP} as determined previously into equation 8 and solve for c, depth of neutral axis, assume fs = fy:

Given $\quad c := 0.2 \cdot d$

$$M_{FRP\_required} = \left(0.85 \cdot f'c \cdot \beta_1 \cdot c - As_{ft} \cdot fy\right) \cdot \left(d_f - \frac{c \cdot \beta_1}{2} \right)$$

$$c := \text{Find}(c) = 3.81 \cdot \text{in}$$

This depth of neutral axis represents the required depth of the neutral axis that corresponds to the minimum required FRP moment capacity to satisfy $\phi M_n \geq M_u$.

Stress and Strain in FRP at Minimum M_{FRP} Requirement

Strain in FRP:

$$\varepsilon_f := \varepsilon_{cu} \cdot \left(\frac{d_f - c}{c} \right) - \varepsilon_{bi} = 0.01107$$

Note: Although $\varepsilon_f > \varepsilon_{fd}$ is not allowed due to environmental strength limits, this value is only used to determine the required width of FRP. ε_f must be checked after the used width of FRP is selected.

Effective stress in FRP:

$$f_f := E_f \cdot \varepsilon_f = 124.03 \text{ksi}$$

Check steel yielded assumption:

$$\varepsilon_s := \left(\varepsilon_f + \varepsilon_{bi}\right) \cdot \left(\frac{d - c}{d_f - c} \right) = 0.0104$$

$$\begin{cases} \text{"OK"} & \text{if } \varepsilon_s \geq \varepsilon_y \\ \text{"NG"} & \text{otherwise} \end{cases} = \text{"OK"}$$

Required area of FRP:

$$A_{f\_required} := \frac{0.85 f'c \cdot \beta_1 \cdot c - As_{ft} \cdot fy}{E_f \cdot \varepsilon_{fd}} = 0.25 \frac{in^2}{ft}$$

Required width of FRP per foot:

$$b_{f\_required} := \frac{A_{f\_required}}{n \cdot t_f} = 3.1 \frac{in}{ft}$$

Required width of FRP per foot accounting for anchor bolt hole:

$$b_{f\_required} := \frac{A_{f\_required}}{n \cdot t_f} + \frac{3}{8}\frac{in}{ft} = 3.47 \frac{in}{ft}$$

Selected width of FRP per foot

$$b_f := 3.5 \frac{in}{ft}$$

Area of FRP:

$$A_f := b_f \cdot n \cdot t_f = 0.28 \frac{in^2}{ft}$$

Effective Stress and Strain in FRP at Nominal Resistance

Determine depth of compression block:

Effective strain in FRP:

$$\varepsilon_f(c) := \varepsilon_{cu} \cdot \left(\frac{d_f - c}{c} \right) - \varepsilon_{bi}$$

Effective stress in FRP:

$$f_f\left(\varepsilon_f, c\right) := E_f \cdot \varepsilon_f(c)$$

Effective strain in steel reinforcement:

$$\varepsilon_s\left(\varepsilon_f, c\right) := \left(\varepsilon_f(c) + \varepsilon_{bi}\right) \cdot \left(\frac{d - c}{d_f - c} \right)$$

Effective stress in steel reinforcement:

$$f_s\left(\varepsilon_f, c\right) := \min\left(fy, Es \cdot \varepsilon_s\left(\varepsilon_f, c\right)\right)$$

Determine depth of neutral axis, c:

Given $\quad c := 0.2 \cdot d$

$$c = \frac{As_{ft} \cdot f_s\left(\varepsilon_f, c\right) + A_f \cdot f_f\left(\varepsilon_f, c\right)}{0.85 f'c \cdot \beta_1}$$

$$c := \text{Find}(c) = 3.93 in$$

Effective strain in FRP:

$$\varepsilon_{fe} := \varepsilon_f(c) = 0.01062$$

Effective stress in FRP:

$$f_{fe} := f_f\left(\varepsilon_f, c\right) = 118.92\,\text{ksi}$$

Effective strain in steel reinforcement:

$$\varepsilon s := \varepsilon_s\left(\varepsilon_f, c\right) = 0.0100$$

Effective stress in steel reinforcement:

$$fs := f_s\left(\varepsilon_f, c\right) = 33\cdot\text{ksi}$$

Check that effective FRP strain is less than allowable FRP strain:

$$\begin{cases} \text{"OK"} & \text{if } \varepsilon_{fe} \le \varepsilon_{fd} \\ \text{"NG"} & \text{otherwise} \end{cases} = \text{"OK"}$$

Check that reinforcing steel yields:

$$\begin{cases} \text{"OK"} & \text{if } \varepsilon s \ge \varepsilon_y \\ \text{"NG"} & \text{otherwise} \end{cases} = \text{"OK"}$$

New Reduced Nominal Moment Capacity

Depth to neutral axis:

$$c = 3.93\,\text{in}$$

Depth of compression block:

$$a := c\cdot\beta_1 = 3.34\,\text{in}$$

Steel reinforcement contribution to moment capacity:

$$Mn_s := As_{ft}\cdot fs\cdot\left(d - \frac{a}{2}\right) = 66.22\,\frac{\text{kip}\cdot\text{ft}}{\text{ft}}$$

FRP retrofit contribution of moment capacity:

$$Mn_{FRP} := A_f\cdot f_{fe}\cdot\left(d_f - \frac{a}{2}\right) = 46.81\,\frac{\text{kip}\cdot\text{ft}}{\text{ft}}$$

Nominal and reduced nominal moment capacity:

$$Mn_{new} := Mn_s + \psi_f\cdot Mn_{FRP} = 106.02\,\frac{\text{kip}\cdot\text{ft}}{\text{ft}}$$

$$\phi Mn_{new} := \phi_R\cdot Mn_{new} = 95.41\,\frac{\text{kip}\cdot\text{ft}}{\text{ft}}$$

Check that the reduced nominal moment capacity is greater than the ultimate moment:

$$\begin{cases} \text{"OK"} & \text{if } \phi Mn_{new} \ge M_u \\ \text{"NG"} & \text{otherwise} \end{cases} = \text{"OK"}$$

Check Fatigue and Creep Rupture Limit States

Steel reinforcement ratio:

$$\rho_s := \frac{As_{ft}}{d} = 0.0077$$

FRP reinforcement ratio:

$$\rho_f := \frac{A_f}{d} = 0.00137$$

Compression block factor:

$$k := \sqrt{\left(\rho_s \cdot n_s + \rho_f \cdot n_f\right)^2 + 2 \cdot \left(\rho_s \cdot n_s + \rho_f \cdot n_f \cdot \frac{d_f}{d}\right)} - \left(\rho_s \cdot n_s + \rho_f \cdot n_f\right) = 0.34$$

Stress level in reinforcement steel:

$$f_{ss} := \frac{\left[\frac{M_{service}}{b_w} + \varepsilon_{bi} \cdot A_f \cdot E_f \cdot \left(d_f - \frac{k \cdot d}{3}\right)\right] \cdot (d - k \cdot d) \cdot Es}{As_{ft} \cdot Es \cdot \left(d - \frac{k \cdot d}{3}\right) \cdot (d - k \cdot d) + A_f \cdot E_f \cdot \left(d_f - \frac{k \cdot d}{3}\right) \cdot \left(d_f - k \cdot d\right)} = 13.92 \cdot ksi$$

Stress level in FRP system:

$$f_{fs} := f_{ss} \cdot \frac{E_f}{Es} \cdot \frac{d_f - kd_s}{d - kd_s} - \varepsilon_{bi} \cdot E_f = 0.02 \cdot ksi$$

Check that stress level in FRP system is below allowable stress level:

$$\begin{cases} \text{"OK"} & \text{if } f_{fs} \le f_{fs\_allow} \\ \text{"NG"} & \text{if } f_{fs} > f_{fs\_allow} \end{cases} = \text{"OK"}$$

Retrofitted System Properties

New Rating Factor

$$RF_{new} := \frac{\phi \cdot \phi Mn_{new} - \gamma\_DC \cdot M_{DC} - \gamma\_DW \cdot M_{DW} - \gamma\_P \cdot M_P}{\gamma\_LL \cdot M_{LL\_IM}} = 1.0035$$

Increase in Moment Capacity

$$Increase := \frac{Mn_{new} - Mn_{existing}}{Mn_{existing}} = 53.55\,\%$$

Weight of FRP Retrofit

$$W_{FRP} := \gamma_f \cdot A_f \cdot b_w = 0.19 \cdot plf$$

Mechanical Fastening Connection Design

Tension in the FRP at ultimate capacity:

$$T_{FRP} := A_f \cdot ft \cdot f_{fu} = 40.77 \cdot kip$$

Anchor Bolt Dimensions and Properties
HILTI, Inc. HVU capsule with HAS thread rod, ASTM A 325, Carbon steel

Bolt diameter:

$$\phi_{bolt} := \frac{3}{8} in$$

Nominal bolt area:

$$A_{bolt} := \frac{\pi \cdot \phi_{bolt}^2}{4} = 0.11 in^2$$

Standard depth of embedment:

$$h_{ef} := 3.5 in$$

Maximum thickness fastened:

$$t := 1 in$$

Maximum tightening torque:

$$t_{max} := 18 ft \cdot lbf$$

Minimum base material thickness:

$$h_{base} := 5.5 in$$

HVU Ultimate bond/concrete capacity:

$$bond_{capacity} := 12.715 kip$$

Embedment depth:

$$d_e := h_{ef} + t = 4.5 in$$

Bolt yield strength:

$$fy_{bolt} := 92 ksi$$

Bolt ultimate strength:

$$fu_{bolt} := 120 ksi$$

Ultimate tensile strength:

$$T_{u\_bolt} := 0.75 \cdot fu_{bolt} \cdot A_{bolt} = 9.94 \cdot kip$$

Ultimate shear strength:

$$V_{u\_bolt} := 0.45 \cdot fu_{bolt} \cdot A_{bolt} = 5.96 \cdot kip$$

Required Number of Connectors Over the Half Span

$$n_{cxn} := ceil\left(\frac{T_{FRP}}{V_{u\_bolt}}\right) = 7$$

Maximum connection spacing:

$$s_{bolt} := \frac{L}{2\left(n_{cxn} - 1\right)} = 26.63in$$

Selected connection spacing:

$$s_{bolt} := 24in$$

Force per bolt:

$$T_b := \frac{T_{FRP}}{n_{cxn}} = 5.82kip$$

Adhesive Properties

Ashland, Inc. Pliogrip® Epoxy Technology adhesive (Product # 5761B)

Adhesive shear strength:

$$f_{adv} := 23.7MPa = 3.44ksi$$

Adhesive elastic modulus:

$$E_{adv} := 4450MPa = 645.42ksi$$

Adhesive maximum allowable shear strain:

$$\varepsilon_{adv\_max} := \frac{f_{adv}}{E_{adv}} = 0.00533$$

Area of adhesive required to develop T_b:

$$A_{adv} := \frac{T_b}{f_{adv}} = 1.69in^2$$

Area of steel plate required equals area of adhesive required:

$$A_{PL} := A_{adv} + \frac{\pi \cdot \phi_{bolt}^2}{4}$$

Required length of plate to satisfy Lc > 2.0ϕ_{bolt} of section 6.13.2.9 of AASHTO LRFD Bridge Specs:

$$L_c\left(w_{PL}\right) := \frac{1}{2}\cdot\left(w_{PL} - \phi_{bolt}\right)$$

Given $\quad w_{PL} := 1in$

$$L_c\left(w_{PL}\right) > 2.0\cdot\phi_{bolt}$$

$$w_{PL} := \left(find\left(w_{PL}\right)\right) = 1.87in$$

Used plate length:

$$w_{PL} := 2.0in$$

Required width of plate:

$$b_{PL} := \frac{A_{PL}}{w_{PL}} = 0.9in$$

Used plate width:

$$b_{PL} := 1.0\,in$$

Used area of steel plate:

$$A_{PL} := b_{PL} \cdot w_{PL} = 2\,in^2$$

Check Strain in Adhesive:

Area of adhesive equals the area of the steel plate:

$$A_{adv} := A_{PL} - \frac{\pi \cdot \phi_{bolt}^2}{4}$$

Stress in the adhesive:

$$\sigma_{adv1} := \frac{T_b}{A_{adv}} = 3.08\,ksi$$

Strain in the adhesive:

$$\varepsilon_{adv} := \frac{\sigma_{adv1}}{E_{adv}} = 0.0048$$

Steel Plate Thickness

Clear distance, in the direction of the force, between the edge of the hole and the edge of the adjacent hold or edge of material:

$$L_c(w_{PL}) = 0.81\,in$$

Specified minimum tensile strength of the connected material, assumed A36 steel:

$$fu_{PL} := 58\,ksi$$

Determine plate thickness to the clothes 16th of an inch:

$$t_{PL} := \frac{T_b}{2.4 \cdot \phi_{bolt} \cdot t \cdot fu_{PL}}$$

$$t_{PL} := \frac{ceil(t_{PL} \cdot 16)}{16} \cdot in = \frac{1}{8}\,in$$

Weight of the Steel Plate:

Unit weight of steel:

$$\gamma_{stl} := 495\,pcf$$

Volume of steel plate:

$$V_{PL} := b_{PL} \cdot w_{PL} \cdot t_{PL} = 0.25\,in^3$$

Weight of steel plate:

$$W_{PL} := \gamma_{stl} \cdot V_{PL} = 0.07\,lbf$$

Total weight of retrofit:

$$W := W_{FRP} + W_{PL} \cdot \frac{1}{s_{bolt}} = 0.23\,plf$$

Appendix C: Design of System B

FRP Dimensions and Properties
E-Glass/Epoxy unidirectional composite; pg. 377 Daniel & Ishai Eng. Mech. of Comp. Mat.

Fiber type	$Fiber_{type} := "Glass"$
Exposure Conditions (Bridge or Aggressive)	$Condition := "Bridge"$
Unit weight	$\gamma_f := 0.071 pci$
Strip thickness	$t_f := 0.04 in$
Number of plies	$n := 3$
Strip spacing	$s_f := 12 in$
Strip length	$l_f := L = 319.5 in$
Dist. from extreme compression fiber to FRP CG	$d_f := h + \frac{n \cdot t_f}{2} = 18.56 in$
Elastic modulus	$E_f := 6000 ksi$
Manufacturer's tensile strength	$f_{fu} := 165 ksi$
Manufacturer's tensile strain	$\varepsilon_{fu} := \frac{f_{fu}}{E_f} = 0.028$
Modular ratio	$n_f := \frac{E_f}{E_c} = 2.105$
FRP reduction factor	$\psi_f := 0.85$

FRP Design Tensile Strength and Strain & Allowable Stress

Environmental reduction factor (Table 2.4-1)

$$C_E := \begin{cases} 0.85 \text{ if } (Condition = "Bridge" \vee Condition = "Aggressive") \wedge Fiber_{type} = "Carbon" \\ 0.65 \text{ if } Condition = "Bridge" \wedge Fiber_{type} = "Glass" \\ 0.75 \text{ if } Condition = "Bridge" \wedge Fiber_{type} = "Aramid" \\ 0.50 \text{ if } Condition = "Aggressive" \wedge Fiber_{type} = "Glass" \\ 0.70 \text{ if } Condition = "Aggressive" \wedge Fiber_{type} = "Aramid" \end{cases} = 0.65$$

Design tensile strength:

$$f_{fd} := f_{fu} \cdot C_E = 107.25 ksi$$

Design tensile strain:

$$\varepsilon_{fd} := \varepsilon_{fu} \cdot C_E = 0.0179$$

Allowable creep & fatigue tensile stress:

$$f_{fs\_allow} := \begin{cases} (0.55 \cdot f_{fd}) \text{ if } Fiber_{type} = "Carbon" \\ (0.20 \cdot f_{fd}) \text{ if } Fiber_{type} = "Glass" \\ (0.30 \cdot f_{fd}) \text{ if } Fiber_{type} = "Aramid" \end{cases} = 21.45 ksi$$

Required FRP Moment Capacity

$$M_{FRP\_required} := \left(\frac{M_u}{\phi_R} - Mn_{existing}\right)\cdot\frac{1}{\psi_f} = 43.214\frac{kip\cdot ft}{ft}$$

Existing Strain of Section at Service Conditions

Service moment (service, loads on bridge during time of installation of FRP system):

$$M_{service} := b_w\cdot\left(M_{DC} + M_{DW}\right) = 27.524 kip\cdot ft$$

Location of N.A. for a cracked section from extreme compression fiber:

Given $kd_s := 1in$

$$\left(kd_s\right)\cdot\left(\frac{kd_s}{2}\right) = As_{ft}\cdot n_s\cdot\left(d - kd_s\right)$$

$$kd_s := Find\left(kd_s\right) = 5.528 in$$

Cracked moment of inertia:

$$I_{CR} := \frac{b_w\cdot kd_s^{\,3}}{12} + kd_s\cdot b_w\cdot\left(\frac{kd_s}{2}\right)^2 + As\cdot n_s\cdot\left(d - kd_s\right)^2 = 2779.258 in^4$$

Existing (initial) strain in the section:

$$\varepsilon_{bi} := \frac{\left(M_{DC} + M_{DW}\right)\cdot\left(d_f - kd_s\right)}{I_{CR}\cdot E_c}\cdot b_w = 0.00054$$

Required Width of FRP per Foot Width of Bridge

Derivation of M_{FRP} and A_f as a function c, the depth to the neutral axis:

Tensile strain in the FRP:

$$\varepsilon_f = \varepsilon_{cu}\cdot\left(\frac{d_f - c}{c}\right) - \varepsilon_{bi} \qquad \text{(Eqn 1)}$$

Tensile stress in the FRP:

$$f_f = E_f\cdot\varepsilon_f \qquad \text{(Eqn 2)}$$

Depth to the neutral axis:

$$c = \frac{As\cdot f_s + A_f\cdot f_f}{0.85 f'c\cdot\beta_1} \qquad \text{(Eqn 3)}$$

Depth of compression block:

$$a = c\cdot\beta_1 \qquad \text{(Eqn 4)}$$

Substituting equation 2 into equation 3 and solving for A_f yields:

$$A_f = \frac{0.85 \cdot f'c \cdot \beta_1 \cdot c - As \cdot f_s}{E_f \cdot \varepsilon_f} \qquad \text{(Eqn 5)}$$

Moment capacity of FRP:

$$M_{FRP} = A_f \cdot f_f \cdot \left(d_f - \frac{a}{2} \right) \qquad \text{(Eqn 6)}$$

Substitute equations 2, 4 and 5 into equation 6:

$$M_{FRP} = \frac{0.85 \cdot f'c \cdot \beta_1 \cdot c - As \cdot f_s}{E_f \cdot \varepsilon_f} \cdot E_f \cdot \varepsilon_f \cdot \left(d_f - \frac{c \cdot \beta_1}{2} \right) \qquad \text{(Eqn 7)}$$

Simplify equation 7:

$$M_{FRP} = \left(0.85 \cdot f'c \cdot \beta_1 \cdot c - As \cdot f_s \right) \cdot \left(d_f - \frac{c \cdot \beta_1}{2} \right) \qquad \text{(Eqn 8)}$$

Substitute M_{FRP} as determined previously into equation 8 and solve for c, depth of neutral axis, assume fs = fy:

Given $\quad c := 0.2 \cdot d$

$$M_{FRP\_required} = \left(0.85 \cdot f'c \cdot \beta_1 \cdot c - As_{ft} \cdot fy \right) \cdot \left(d_f - \frac{c \cdot \beta_1}{2} \right)$$

$$c := \text{Find}(c) = 3.804\,\text{in}$$

This depth of neutral axis represents the required depth of the neutral axis that corresponds to the minimum required FRP moment capacity to satisfy $\phi M_n \geq M_u$.

Stress and Strain in FRP at Minimum M_{FRP} Requirement

Strain in FRP:

$$\varepsilon_{fe} := \varepsilon_{cu} \cdot \left(\frac{d_f - c}{c} \right) - \varepsilon_{bi} = 0.0111$$

Note: Although $\varepsilon_{fe} > \varepsilon_{fd}$ is not allowed due to environmental strength limits, this value is only used to determine the required width of FRP. ε_{fe} must be checked after the used width of FRP is selected.

Effective stress in FRP:

$$f_{fe} := E_f \cdot \varepsilon_{fe} = 66.573\,\text{ksi}$$

Check steel yielded assumption:

$$\varepsilon_s := \left(\varepsilon_{fe} + \varepsilon_{bi} \right) \cdot \left(\frac{d - c}{d_f - c} \right) = 0.0104$$

$$\begin{cases} \text{"OK"} & \text{if } \varepsilon_s \geq \varepsilon_y \\ \text{"NG"} & \text{otherwise} \end{cases} = \text{"OK"}$$

Required area of FRP:

$$A_{f\_required} := \frac{0.85 f'c \cdot \beta_1 \cdot c - As_{ft} \cdot fy}{E_f \cdot \varepsilon_{fe}} = 0.46 \frac{in^2}{ft}$$

Required width of FRP per foot:

$$b_{f\_required} := \frac{A_{f\_required}}{n \cdot t_f} = 3.831 \frac{in}{ft}$$

Required width of FRP per foot accounting for anchor bolt hole:

$$b_{f\_required} := \frac{A_{f\_required}}{n \cdot t_f} + \frac{3}{8}\frac{in}{ft} = 4.206 \frac{in}{ft}$$

Selected width of FRP per foot

$$b_f := 4.5 \frac{in}{ft}$$

Area of FRP:

$$A_f := b_f \cdot n \cdot t_f = 0.54 \frac{in^2}{ft}$$

Effective Stress and Strain in FRP at Nominal Resistance:

Determine depth of compression block:

Effective strain in FRP:

$$\varepsilon_f(c) := \varepsilon_{cu} \cdot \left(\frac{d_f - c}{c} \right) - \varepsilon_{bi}$$

Effective stress in FRP:

$$f_f\left(\varepsilon_f, c\right) := E_f \cdot \varepsilon_f(c)$$

Effective strain in steel reinforcement:

$$\varepsilon_s\left(\varepsilon_f, c\right) := \left(\varepsilon_f(c) + \varepsilon_{bi}\right) \cdot \left(\frac{d - c}{d_f - c} \right)$$

Effective stress in steel reinforcement:

$$f_s\left(\varepsilon_f, c\right) := \min\left(fy, Es \cdot \varepsilon_s\left(\varepsilon_f, c\right)\right)$$

Determine depth of neutral axis, c:

Given $c := c$

$$c = \frac{As_{ft} \cdot f_s\left(\varepsilon_f, c\right) + A_f \cdot f_f\left(\varepsilon_f, c\right)}{0.85 f'c \cdot \beta_1}$$

$$c := \text{Find}(c) = 3.962 in$$

Effective strain in FRP:

$$\varepsilon_{fe} := \varepsilon_f(c) = 0.01051$$

Effective stress in FRP:

$$f_{fe} := f_f\left(\varepsilon_f, c\right) = 63.052\,\text{ksi}$$

Effective strain in steel reinforcement:

$$\varepsilon s := \varepsilon_s\left(\varepsilon_f, c\right) = 0.0099$$

Effective stress in steel reinforcement:

$$fs := f_s\left(\varepsilon_f, c\right) = 33\cdot\text{ksi}$$

Check that effective FRP strain is less than allowable FRP strain:

$$\begin{cases} \text{"OK"} & \text{if } \varepsilon_{fe} \le \varepsilon_{fd} \\ \text{"NG"} & \text{otherwise} \end{cases} = \text{"OK"}$$

Check that reinforcing steel yields:

$$\begin{cases} \text{"OK"} & \text{if } fs \ge fy \\ \text{"NG"} & \text{otherwise} \end{cases} = \text{"OK"}$$

New Reduced Nominal Moment Capacity

Depth to neutral axis:

$$c = 3.962\,\text{in}$$

Depth of compression block:

$$a := c\cdot\beta_1 = 3.368\,\text{in}$$

Steel reinforcement contribution to moment capacity:

$$Mn_s := As_{ft}\cdot fs\cdot\left(d - \frac{a}{2}\right) = 793.924\,\frac{\text{kip}\cdot\text{in}}{\text{ft}}$$

FRP retrofit contribution of moment capacity:

$$Mn_{FRP} := A_f\cdot f_{fe}\cdot\left(d_f - \frac{a}{2}\right) = 574.599\,\frac{\text{kip}\cdot\text{in}}{\text{ft}}$$

Nominal and reduced nominal moment capacity:

$$Mn_{new} := Mn_s + \psi_f\cdot Mn_{FRP} = 1282.333\,\frac{\text{kip}\cdot\text{in}}{\text{ft}}$$

$$\phi Mn_{new} := \phi_R\cdot Mn_{new} = 1154.1\,\frac{\text{kip}\cdot\text{in}}{\text{ft}}$$

Check that the reduced nominal moment capacity is greater than the ultimate moment:

$$\begin{cases} \text{"OK"} & \text{if } \phi Mn_{new} \ge M_u \\ \text{"NG"} & \text{otherwise} \end{cases} = \text{"OK"}$$

Check Fatigue and Creep Rupture Limit States

Steel reinforcement ratio:

$$\rho_s := \frac{As_{ft}}{d} = 0.0077$$

FRP reinforcement ratio:

$$\rho_f := \frac{A_f}{d} = 0.00265$$

Compression block factor:

$$k := \sqrt{\left(\rho_s \cdot n_s + \rho_f \cdot n_f\right)^2 + 2 \cdot \left(\rho_s \cdot n_s + \rho_f \cdot n_f \cdot \frac{d_f}{d}\right)} - \left(\rho_s \cdot n_s + \rho_f \cdot n_f\right) = 0.335$$

Stress level in reinforcement steel:

$$f_{ss} := \frac{\left[\frac{M_{service}}{b_w} + \varepsilon_{bi} \cdot A_f \cdot E_f \cdot \left(d_f - \frac{k \cdot d}{3}\right)\right] \cdot (d - k \cdot d) \cdot Es}{As_{ft} \cdot Es \cdot \left(d - \frac{k \cdot d}{3}\right) \cdot (d - k \cdot d) + A_f \cdot E_f \cdot \left(d_f - \frac{k \cdot d}{3}\right) \cdot \left(d_f - k \cdot d\right)} = 13.92 \cdot ksi$$

Stress level in FRP system:

$$f_{fs} := f_{ss} \cdot \frac{E_f}{Es} \cdot \frac{d_f - kd_s}{d - kd_s} - \varepsilon_{bi} \cdot E_f = 0.011 \cdot ksi$$

Check that stress level in FRP system is below allowable stress level:

$$\begin{cases} \text{"OK"} & \text{if } f_{fs} \le f_{fs\_allow} \\ \text{"NG"} & \text{if } f_{fs} > f_{fs\_allow} \end{cases} = \text{"OK"}$$

New Rating Factor

$$RF_{new} := \frac{\phi \cdot \phi Mn_{new} - \gamma\_DC \cdot M_{DC} - \gamma\_DW \cdot M_{DW} - \gamma\_P \cdot M_P}{\gamma\_LL \cdot M_{LL\_IM}} = 1.0161$$

Increase in Moment Capacity

$$Increase := \frac{Mn_{new} - Mn_{existing}}{Mn_{existing}} = 54.772\%$$

Weight of FRP Retrofit

$$W_{FRP} := \gamma_f \cdot A_f \cdot b_w = 0.46 \cdot plf$$

Mechanical Fastening Connection Design

Tension in the FRP at ultimate capacity:

$$T_{FRP} := A_f \cdot ft \cdot f_{fu} = 89.1 \cdot kip$$

Anchor Bolt Dimensions and Properties
HILTI, Inc. HVU capsule with HAS thread rod, ASTM A 325, Carbon steel

Bolt diameter:

$$\phi_{bolt} := \frac{3}{8} in$$

Nominal bolt area:

$$A_{bolt} := \frac{\pi \cdot \phi_{bolt}^2}{4} = 0.11 in^2$$

Standard depth of embedment:

$$h_{ef} := 3.5 in$$

Maximum thickness fastened:

$$t := 1 in$$

Maximum tightening torque:

$$t_{max} := 18 ft \cdot lbf$$

Minimum base material thickness:

$$h_{base} := 5.5 in$$

HVU Ultimate bond/concrete capacity:

$$bond_{capacity} := 12.715 kip$$

Embedment depth:

$$d_e := h_{ef} + t = 4.5 in$$

Bolt yield strength:

$$fy_{bolt} := 92 ksi$$

Bolt ultimate strength:

$$fu_{bolt} := 120 ksi$$

Ultimate tensile strength:

$$T_{u\_bolt} := 0.75 \cdot fu_{bolt} \cdot A_{bolt} = 9.94 \cdot kip$$

Ultimate shear strength:

$$V_{u\_bolt} := 0.45 \cdot fu_{bolt} \cdot A_{bolt} = 5.964 \cdot kip$$

Required Number of Connectors Over the Half Span

$$n_{cxn} := \text{ceil}\left(\frac{T_{FRP}}{V_{u\_bolt}}\right) = 15$$

Maximum connection spacing:

$$s_{bolt} := \frac{L}{2\left(n_{cxn} - 1\right)} = 11.411\,\text{in}$$

Selected connection spacing:

$$s_{bolt} := 10\,\text{in}$$

Force per bolt:

$$T_b := \frac{T_{FRP}}{n_{cxn}} = 5.94\,\text{kip}$$

Adhesive Properties

Ashland, Inc. Pliogrip® Epoxy Technology adhesive (Product # 5761B)

Adhesive shear strength:

$$f_{adv} := 23.7\,\text{MPa} = 3.437\,\text{ksi}$$

Adhesive elastic modulus:

$$E_{adv} := 4450\,\text{MPa} = 645.418\,\text{ksi}$$

Adhesive maximum allowable shear strain:

$$\varepsilon_{adv\_max} := \frac{f_{adv}}{E_{adv}} = 0.00533$$

Area of adhesive required to develop T_b:

$$A_{adv} := \frac{T_b}{f_{adv}} = 1.728\,\text{in}^2$$

Area of steel plate required equals area of adhesive required:

$$A_{PL} := A_{adv} + \frac{\pi \cdot \phi_{bolt}^{\,2}}{4}$$

Required length of plate to satisfy Lc > 2.0ϕ_{bolt} of section 6.13.2.9 of AASHTO LRFD Bridge Specs:

$$L_c\left(w_{PL}\right) := \frac{1}{2}\cdot\left(w_{PL} - \phi_{bolt}\right)$$

Given $\quad w_{PL} := 1\,\text{in}$

$$L_c\left(w_{PL}\right) > 2.0\cdot\phi_{bolt}$$

$$w_{PL} := \left(\text{Find}\left(w_{PL}\right)\right) = 1.875\,\text{in}$$

Used plate length:

$$w_{PL} := 2.0\,\text{in}$$

Required width of plate:

$$b_{PL} := \frac{A_{PL}}{w_{PL}} = 0.919\,\text{in}$$

Used plate width:

$$b_{PL} := 1.0\,in$$

Used area of steel plate:

$$A_{PL} := b_{PL} \cdot w_{PL} = 2\,in^2$$

Check Strain in Adhesive:

Area of adhesive equals the area of the steel plate:

$$A_{adv} := A_{PL} - \frac{\pi \cdot \phi_{bolt}^2}{4}$$

Stress in the adhesive:

$$\sigma_{adv1} := \frac{T_b}{A_{adv}} = 3.144\,ksi$$

Strain in the adhesive:

$$\varepsilon_{adv} := \frac{\sigma_{adv1}}{E_{adv}} = 0.0049$$

Steel Plate Thickness

Clear distance, in the direction of the force, between the edge of the hole and the edge of the adjacent hold or edge of material:

$$L_c(w_{PL}) = 0.813\,in$$

Specified minimum tensile strength of the connected material, assumed A36 steel:

$$fu_{PL} := 58\,ksi$$

Determine plate thickness to the clothes 16th of an inch:

$$t_{PL} := \frac{T_b}{2.4 \cdot \phi_{bolt} \cdot t \cdot fu_{PL}}$$

$$t_{PL} := \frac{ceil(t_{PL} \cdot 16)}{16} \cdot in = \frac{1}{8}\,in$$

Weight of the Steel Plate:

Unit weight of steel:

$$\gamma_{stl} := 495\,pcf$$

Volume of steel plate:

$$V_{PL} := b_{PL} \cdot w_{PL} \cdot t_{PL} = 0.25\,in^3$$

Weight of steel plate:

$$W_{PL} := \gamma_{stl} \cdot V_{PL} = 0.072\,lbf$$

Total weight of retrofit:

$$W := W_{FRP} + W_{PL} \cdot \frac{1}{s_{bolt}} = 0.496\,plf$$

Bridge Safety Project

Task 4 (Deliverable 2): FRP Flexural Retrofit Durability Testing Plan

3/26/2012

Hannah Breton, M.S. Candidate
Bill Davids, PhD, PE, John C. Bridge Professor of Civil and Environmental Engineering

University of Maine AEWC Advanced Structures and Composites Center and Department of Civil and Environmental Engineering

Table of Contents

Introduction

This document is an engineering report for the Maine Department of Transportation (MaineDOT) satisfying deliverable 2 from Task 4 in the UMaine AEWC Advanced Structures and Composites Center Bridge Safety project funded by the MaineDOT. This report details the plan for testing the durability of two proposed mechanically-fastened (MF) fiber-reinforced polymer (FRP) flexural retrofits. In accordance with the Bridge Safety Proposal, durability testing of the FRP retrofits will include freeze-thaw cycling and exposure to de-icing chemicals.

Test specimens will be subjected to either 1000, 3000, and 10000 hours of submersion in saltwater or 20 freeze-thaw cycles and then destructively tested to determine the failure strength of the specimen for comparison to the failure strength of unconditioned specimen. Acceptable performance will be based on a percent retention of failure strength following conditioning.

The retrofit design proposed in deliverable 1 of Task 4 in (delivered January 2012) describes an FRP flexural retrofit with woven carbon fiber reinforcement and an alternative FRP flexural retrofit with unidirectional glass fiber reinforcement. Both options require the adhesion of steel plates at connection locations for adequate bearing capacity and pre-drilling of the concrete flexural face at the adhesive anchor bolt locations. Based on further evaluation of the design and professional guidance it was determined to be in the projects best interest to adapt the FRP and connection design in three ways:

1. Include only unidirectional glass reinforcement
2. Eliminate the need for steel plates by incorporating glass or carbon woven fabric in the strip design at 90° or ±45°
3. Reduce installation preparation and time by using powder actuated anchors.

Details pertaining to these changes are discussed within this report.

It should be noted that the environmental conditions covered in this durability plan do not cover all possible environmental conditions that the FRP retrofits could experience in service. It is recommended that the MaineDOT consider conducting additional durability testing pending the results of the proposed tests.

Project Background and Description

As reported in Deliverable 1 of Task 4 the proposed FRP retrofit designs (system A and system B) incorporate strips of FRP attached to the flexural face of a flat slab concrete bridge using adhesive anchor bolts. System A incorporated woven carbon fiber fabric reinforcement and system B incorporated unidirectional glass reinforcement for tensile strength. Three alterations have been made to these systems regarding reinforcing fibers, anchor bolts and bearing strength reinforcement.

Design Alterations

Based on literature regarding the durability of various FRPs discussed in Deliverable 1 of Task 4 it was determined that since the performance of carbon FRPs exceed that of glass FRPs both retrofit systems will be reinforced with glass fibers under the assumption that carbon fibers will perform better in durability tests in the event glass systems are unsatisfactory. This approach will reduce the cost of the proposed systems since glass fibers are less expensive than carbon fibers.

An additional alteration to the retrofit design was made regarding the bearing strength of the system. Following a discussion with Jake Marquis from Kenway Corporation of Augusta, Maine (February 10, 2012), it was determined that it would be beneficial to eliminate the need for steel

plates by incorporating off-axis material within the FRP strips. This change to the strip design provides three benefits:

1. Elimination of adhered steel plates for bearing capacity and thus elimination of potential issues arising from rust or bond line inadequacies;
2. Simplification of the manufacturing process by eliminating the work required to adhere steel plates to the strip;
3. Added versatility of the strip by allowing for connections to be placed at any location along the length of the strip.

This alteration satisfies two FRP system requirements stated in the proposal. System A will utilize carbon fiber and system B will use glass fiber to provide bearing strength at connection locations. Systems A and B will be tested and compared following environmental conditioning to determine their relative performance.

Finally, the proposed HILTI, Inc. HVU capsule with HAS thread rod, ASTM A 325, carbon steel 3/8 in. anchor will be replaced with the HILTI, Inc. X-CR powder actuated, corrosion resistant, stainless steel nail that will be embedded in the concrete 1 ¼ in. The use of powder actuated anchors provides two benefits:

1. Reduction in preparation and installation time by eliminating the need for pre-drilling of the concrete for adhesive anchors;
2. Simplified installation of the strip flush to the concrete eliminating unnecessary slack that could result in inefficient use of the FRP.

Project Scope

The scope of deliverable 2 from Task 4 includes the development and explanation of a finalized durability testing plan. A minimum of nine concrete-FRP specimens of each system will be fabricated for standardized tests to assess the durability of each system and connection strength. One third of the specimens will be subjected to freeze-thaw cycles and another third will be exposed to de-icing chemicals. The remaining third of the specimens will be control specimens. Upon completion of environmental conditioning, specimens will be visually inspected and destructively tested to determine the reduction in strength following environmental conditioning compared to control specimen. An exact test specimen design is yet to be determined; however, potential designs are discussed within this report.

Technical Requirements

The durability and strength tests conducted will follow the test procedures, standards, and literature sources as outlined below unless otherwise noted:

- ASTM C1645 Standard Test Method for Freeze-thaw and De-icing Salt Durability of Solid Concrete Interlocking Paving Units (ASTM 2011)
- Using Composites in Seismic Retrofit Applications (Karbhari 2005)
- Acceptability Criteria for Concrete and Reinforced and Unreinforced Masonry Strengthening Using Externally Bonded Fiber-Reinforced Polymer (FRP) Composite Systems (ICC-ES 2010).

Intended Use

The results from durability testing are intended to be a means of comparing the performance of the two proposed flexural retrofit systems in order to assist in determining which retrofit system will be the most cost effective for use in rehabilitating flat-slab concrete bridges in Maine.

Durability Testing Plan

As stated in the Bridge Safety Proposal, durability testing of the two proposed systems will include freeze-thaw cycling and exposure to de-icing chemicals. Details pertaining to the conditioning of specimen to simulate prolonged exposure to these conditions are discussed in the following sections.

Test Specimen

To adequately evaluate the durability of the entire flexural retrofit system, test specimens will consist of concrete blocks of set dimensions with an FRP retrofit strip anchored into the concrete using the proposed X-CR powder actuated nails. Examples of potential specimen and descriptions of how they will be tested are provided below.

Test Specimen 1

The first proposed test specimen, shown in Figure 1 below, will consist of a concrete block of set dimensions with a portion of FRP strip (dark grey strip, shown on the left of the specimen) attached using the proposed powder actuated nail anchoring system. Following the conditioning of the test specimen, a reusable steel plate (blue strip, shown on the right of the specimen) will be anchored into the concrete, opposite the FRP strip. The steel plate and anchor bolts will be designed to have a strength of three to four times the anticipated strength of the FRP.

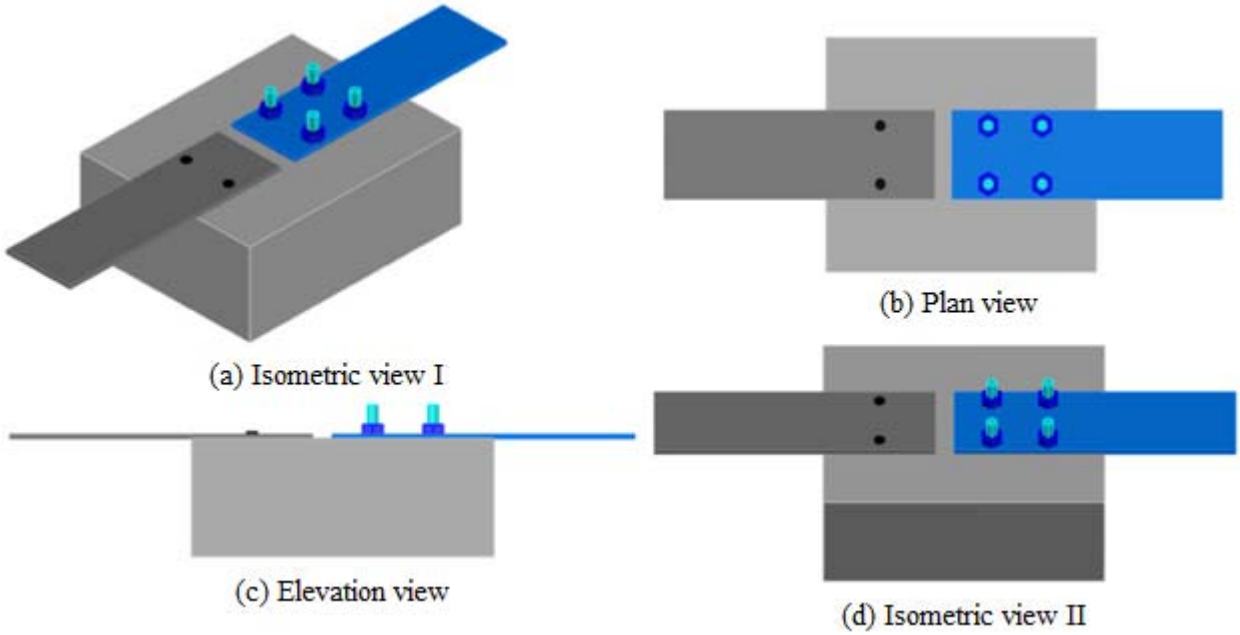

Figure 1: Test specimen 1

Both the FRP strip and steel plate will be gripped and pulled during the direct shear test. This specimen design allows for the load to be applied concentrically between the two strips, which is ideal; however, during loading the concrete block will be placed in tension. This can be mitigated with internal reinforcing or externally anchored unbounded reinforcing.

Test Specimen 2

The second proposed test specimen, shown in Figure 2 below, will consist of a concrete block of set dimensions with a portion of FRP strip attached using the proposed powder actuated nail anchoring system. Using plastic tubing a hole will be cast in the concrete to allow for a threaded rod to be placed through the concrete following conditioning. During salt water conditioning the hole through the concrete will be sealed with silicone caulk to prevent excessive deterioration of the concrete block interior. Following conditioning and the insertion of the threaded rod, a steel plate will be placed onto the threaded rod and tightened against the concrete face beneath the FRP strip (plate 1, shown on the left, vertical concrete face) and another steel plate (plate 2,

shown to the right of the test specimen) will be placed on the threaded rod at the opposite end (as shown in Figure 2).

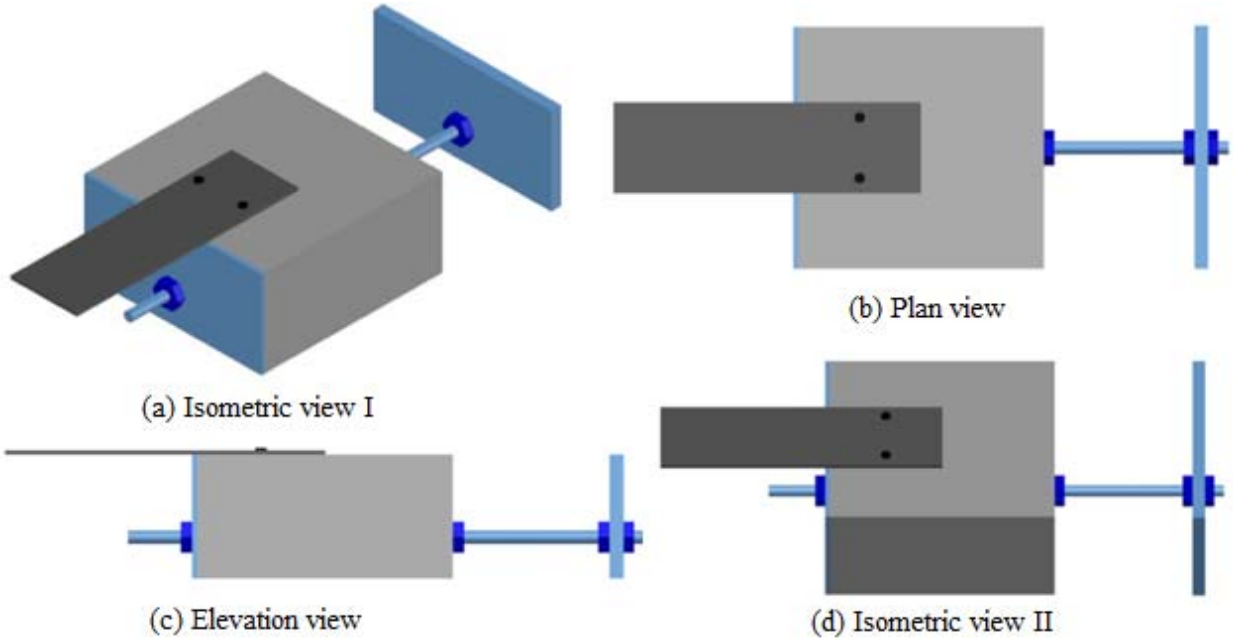

Figure 2: Test specimen 2

The plate 2 will be used to anchor the test specimen in the T-slot of an actuator. Once anchored in the actuator, the FRP strip will then be gripped and pulled in direct shear until failure. By anchoring the test specimen in this manner, as load is applied to the FRP strip, the concrete block is put into compression. This helps prevent the undesirable failure of concrete in tension during testing. One downside to this specimen design is the eccentric load path which will cause bending of the rod.

It should be noted that test specimen designs are not yet finalized. Exact dimensions, strengths and material requirements are still to be determined.

Tabbing Specimen

If acceptable development length can be incorporated into the specimen design, it will be unnecessary to tab specimens for testing. According to ASTM D3039: Standard Test Method for Tensile Properties of Polymer Matrix Composite Materials (ASTM 2008b), the minimum required tab length for test specimen is calculated as follows,

$$L_{min} = \frac{F^{tu} * h}{2 * F^{su}}$$

where:

L_{min} = minimum required bond length

F^{tu} = coupon ultimate tensile strength

h = coupon thickness

F^{su} = ultimate shear strength of adhesive, coupon material or tab material (whichever is lowest)

However, prior experience shows that it is likely tabbing the ends of FRP strips will be required following conditioning to prevent damage to the FRP caused by the grips of the testing apparatus, to help the apparatus securely grip the specimen, and to center the applied load. Similar to the work performed by Demkowicz (2011) for the durability testing of the bridge-in-a-backpack technology, tabs will be manufactured by DESS Machine and consist of 0, 90° glass laminate. Tabs will be bonded using high shear strength adhesive Pliogrip 7779 (Ashland).

Environmental Durability Tests

To quantify the durability of the FRP retrofit designs, an environmental durability test matrix is referenced that builds on the work of prior FRP durability research performed at the AEWC Center by Demkowicz (2011) regarding the durability of the composite arches for the bridge-in-a-backpack technology. In addition, the *AASHTO LRFD Guide Specifications for the Design of Externally Bonded FRP Systems for Strengthening Concrete Bridges* (AASHTO 2009) provides an environmental durability test matrix "for the purpose of manufacturer's quality control and for the purchaser's quality assurance" and specifies a minimum of five samples of sufficient length for testing. The conditioning matrix was developed through collaboration between the California Department of Transportation (Caltrans) and the Aerospace Corporation (Karbhari 2005). The testing matrix provides guidelines for water, saltwater, alkali, dry heat, fuel, ultraviolet light and freeze-that environmental exposure. The testing conditions environments pertinent to this research (freeze-thaw and saltwater) are summarized in Table 1.

Table 1: Partial Environmental Durability Test Matrix (AASHTO 2009)

Environmental Durability Test	Test Conditions	Test Duration
Salt Water Resistance	Immersion at 70±2°F	1000, 3000, 10000hr
Freeze/Thaw Resistance	Cycle between 100% humidity at 100°F and freezer at 0°F	24hr cycle for 20 cycles

In addition to general environmental conditions and test duration, Karbhari (2005) references applicable ASTM standards, provides additional conditioning protocols specific to environmental condition and provides performance acceptability criteria based on environmental condition and exposure duration.

Saltwater Exposure

It is necessary to test the durability of the retrofit design when exposed to saltwater due to the use of de-icing salts on roads during Maine winters. Specifications regarding saltwater exposure from Karbhari (2005) are intended for testing the durability of composites with prolonged marine exposure and references ASTM D1141 Standard Practice for the Preparation of Substitute Ocean Water (ASTM 2008a). To better represent the effects of de-icing salt exposure the saltwater test solution will be made according to ASTM C1645 Standard Test Method for Freeze-thaw and De-icing Salt Durability of Solid Concrete Interlocking Paving Units (ASTM 2011). Although this standard is not specifically for FRP materials, it provides a standardized method for creating a de-icing salt solution representative of that which may be used on paved roads. The standard requires a 3 ±0.1% (by weight) NaCl solution.

De-icing chemicals will be obtained from a supplier who currently provides the state with de-icing chemicals. Current suppliers and their materials listed on the Maine government website (www.maine.govmdot/winterdrivingt/sim.htm) include:

- Harcros – rock salt (sodium chloride, NaCl)
- Eastern Salt Company – rock salt
- Cargill – rock salt
- Innovative – Ice-B-Gone (corrosion-inhibited magnesium chloride liquid blend)

Conditioning will occur in polyethylene storage bins of adequate size to allow for the immersion of specimens, with sealable lids to minimize evaporation of the solution in order to maintain a constant salt concentration. Test specimen will be fully submerged in the solution at the same time and allowed to condition for 1000, 3000, and 10,000 hours. We will explore the use of

heaters to maintain a temperature of 70±2°F as specified by the durability testing matrix, but may need to conduct the tests at ambient temperatures. We do not expect that this will significantly affect results. A small aquarium pump will be used to circulate the saltwater. Specimens will be placed in containers such that the concrete supports the FRP strip(s). The free ends of the FRP strip(s) will be supported by wood blocks or foam. Due to the anticipated size of the test specimen one container per specimen will be required.

Following specified conditioning durations specimens will be removed from their conditioning containers, rinsed with tap water, wiped with a dry cloth, and left to air dry at room temperature. Specimens will be tested in direct shear within four days of removal from conditioning or otherwise noted.

The assessment of durability will follow the acceptance criteria AC125 (ICC-ES 2010) referenced by Karbhari (2005).. AC125 (ICC-ES 2010) requires as a criterion of acceptance that all specimen not show less than 90% retention of unexposed tensile properties after 1000 hours of exposure and not less than 85% retention after 3000 hours of exposure. AC125 (ICC-ES 2010) and Karbhari (2005) specify determining tensile properties based on ASTM standards (e.g. ASTM D3039: Standard Test Method for Tensile Properties of Polymer Matrix Composite Materials (ASTM 2008b)) for determining the properties of FRP laminates. Since the primary concern lies with the performance of the system as a whole, failure strength of the conditioned test specimen will be compared to the failure strength of unexposed control specimen. Acceptable performance of the conditioned test specimen will then be based on the requirements of AC125 (ICC-ES 2010). AC125 does not provide any acceptance criteria for the performance of test specimens following 10000 hours of exposure.

Freeze-thaw Cycling

Bridges in Maine commonly undergo freeze-thaw cycling. It is necessary to assess the effects of freeze-thaw cycling of the retrofit system to determine if the cycling is detrimental to the performance of the retrofit. When water seeps into concrete and freezes it expands causing the concrete to crack. When the water thaws it is able to seep further into the concrete through the expanded cracks causing more cracking during the following freeze period. A similar form of freeze-thaw damage can be observed in composites, where the matrix can experience micro-cracking due to infiltrating water freezing and thawing gradually degrading the composite's material properties (Demkowicz 2011).

Specifications provided by Karbhari (2005) were developed to simulate the effects of freezing following significant water absorption. Karbhari (2005) requires specimen to be preconditioned at 100% relative humidity and 100°F for 3 weeks followed by 20 cycles of 0°F for a minimum of 4 hours and in a humidity chamber for a minimum of 12 hours at 100% relative humidity and 100°F.

Freeze-thaw conditioning will occur either in a walk-in-freezer and humidity chamber or an ESPEC environmental chamber, pending the finalized design and size of test specimen. Large specimens will not fit within the ESPEC chamber and will be required to be moved between a walk-in-freezer and a humidity chamber until the desired 20 cycles are completed. The freezer and humidity chamber are not specific to individual projects and it is likely that the environmental conditions experienced within the chambers would not directly match those specified above. Additionally, although it is not expected to affect results, inconsistencies in exposure duration may arise due to the inability to monitor and move specimen between freeze and thaw conditions throughout a 24 hour period during the 20 exposure cycles.

Use of the ESPEC chamber is preferred over the walk-in-freeze and humidity chamber because the ESPEC chamber allows for programming of the desired environmental conditions (temperature and relative humidity), desired exposure durations and specified number of cycles. The ESPEC chamber is used for one project at a time and therefore allows for complete control over the environmental conditions throughout the conditioning duration. Additionally, the ability to program the conditioning cycles allows for consistent environmental conditions. In order to use the ESPEC chamber, however, specimen must be small enough to fit within the chamber.

Following conditioning specimens will be removed from the conditioning chamber and allowed to reach ambient conditions before being subjected to direct shear tests. Direct shear tests will occur within four days of removal from conditioning or otherwise noted.

The assessment of durability following freeze-thaw exposure will follow the same criteria as saltwater exposure after 1000 hours, requiring specimen to retain 90% of their unconditioned failure strength.

Summary

Assessing the durability of the FRP retrofit design provides a quantitative means for measuring the relative performance of the alternative designs and provides insight into their behavior due to extreme environmental conditions. The results acquired from the durability testing will be used in conjunction with the small beam bend tests (deliverable 3) to determine the most cost effective FRP retrofit solution for increasing the capacity of degrading flat slab bridges in Maine. It is recommended that MaineDOT consider conducting additional durability testing pending the

results of the proposed tests in order to evaluate the effects of additional potential environmental conditions that could affect the performance of the retrofit in service.

A report containing the results of durability testing (or all results with the exception of the 10000 hour saltwater exposure) will tentatively be delivered to the MaineDOT by July 2013. Deliverable 3 of task 4 containing the results and analysis of the small beam bend tests will tentatively be delivered to the MaineDOT by October 2012.

References

AASTHO (2009). “AASHTO LRFD Guide for Design of Externally Bonded FRP Systems for Strengthening Concrete Bridges (DRAFT #2).” Washinton DC, USA: Paul Liles

ASTM (2008a). “ASTM D1141: Standard Practice for the Preparation of Substitue Ocean Water.” ASTM International, West Conshohocken, PA.

ASTM (2008b). “ASTM D3039: Standard Test Method for Tensile Properties of Polymer Matrix Composite Materials.” ASTM International, West Conshohocken, PA.

ASTM (2011). “ASTM C1645 Standard Test Method for Freeze-thaw and De-icing Salt Durability of Solid Concrete Interlocking Paving Units.” ASTM International, West Conshohocken, PA.

Breton, H. and Davids, W. (2012). “Bridge Safety Project, Task 4 (Deliverable 1): FRP Flexural Retrofit Designs”, University of Maine, Orono.

Demkowicz, M. (2011). “Environmental Durability of Hybrid Braided Polymer Matrix composites for Infrastructure Applications.” University of Maine, Orono.

International Code Council Evaluation Service (ICC-ES) (2010). “Acceptance Criteria for Concrete and Reinforced and Unreinforced Masonry Strengthening Using Externally Bonded Fiber-Reinforced Polymer (FRP) Composite Systems.”

Karbhari, V.M. (2005). “Using Composites in Seismic Retrofit Applications.” State of California Department of Transportation, El Segundo, California.

Bridge Safety Project

Task 4 (Deliverable 3): Small Beam Bend Tests

8/9/2013

Hannah Breton, M.S. Candidate in Civil and Environmental Engineering
Bill Davids, PhD, PE, John C. Bridge Professor and Chair of Civil and Environmental Engineering

University of Maine Advanced Structures and Composites Center and Department of Civil and Environmental Engineering

Contents

Introduction

This document is an engineering report for the Maine Department of Transportation (MaineDOT) satisfying deliverable 3 from Task 4 in the UMaine Advanced Structures and Composites Center Bridge Safety project funded by the MaineDOT. This report details the procedures and analysis of flexural strength testing performed on FRP-strengthened reinforced concrete beams.

Steel reinforced concrete beams were strengthened with strips of FRP mechanically fastened to the flexural face to increase the capacity of the beam relative to a non-FRP strengthened beam. Beams were designed to have similar characteristics to the Levant Bridge. Following the analysis of the environmental durability specimen (see Breton & Davids, Bridge Safety Project, Task 4 (Deliverable 4): FRP Flexural Retrofit Environmental Durability Testing Analysis, 2013)) the GC45 and GC90 systems were selected for further testing based on their durability performance.

Under four-point bending, beam specimens were subjected to an initial loading regimen to generate flexural cracks and induce strain into the reinforcing steel similar to what would be caused by service live loads. Specimen were then reinforced with an MF-FRP strip and tested to failure. All specimens failed due to concrete crushing within the moment span. GC45 specimen exhibited an average increase in yield and ultimate moment of 41% and 47%, respectively, and decreased center span deflection by 31%. GC90 specimens exhibited an average increase in yield and ultimate moment of 46% and 49%, respectively, and decreased center span deflection by 36%. The following sections detail the test specimen design, reinforcing steel tension tests and results, and flexural test protocols, results and conclusions.

Project Scope

The scope of deliverable 3 of Task 4 includes the presentation and discussion of the results of small beam four-point bend flexural tests.

Intended Use

The results from flexural strength tests are intended to be used as a means to suggest a single FRP flexural strengthening system for continued study or potential use by the MaineDOT for strengthening understrength flat-slab concrete bridges.

Flexural Strength Tests

Reinforced concrete beams were subjected to two-phase loading to initially generate flexural cracks in the concrete and induce service level strains into the reinforcing steel, allow for installation of FRP strengthening strips into crack concrete, destructively test FRP-strengthened concrete beams to failure under four-point loading. The following sections detail the test

specimen design, loading procedures, reinforcing steel tensile strength tests, FRP installation procedures, and test results

Test Specimen

To evaluate the effectiveness of the GC45 and GC90 MF-FRP systems for increasing the flexural capacity of flat-slab concrete bridges, reinforced concrete beam specimens were designed, constructed, and cured at the University's testing facility following design specifications provided by ACI – Committee 318 (2008). The beam specimens maintained the same span-to-depth and reinforcement ratios of the Levant Bridge, described in Deliverable 4 (Breton & Davids, 2013) and chosen as the design bridge, such that the test specimen would mimic the behavior of a flat-slab concrete bridge. One discrepancy between the design bridge and the as-built specimen is the grade of the reinforcing steel – the test specimens used Grade 60 reinforcing vs. the Grade 33 reinforcing likely used in the design bridge. Further, the concrete compressive strength of the test specimens was higher than that of the design bridge.

The following sections outline the beam design, bridge details, and tensile strength testing of the steel reinforcement used in the construction of the specimen. Specimens were labeled according to the strip they were strengthened with and their sequential number. For example, a beam reinforced with the GC45 specimen and tested second out of the three GC45 strengthened beams would be labeled 'GC45 2'.

Design of Beam Specimen

Flexural strength test specimens were designed to mimic a unit width of flat-slab concrete bridge and in accordance with ACI – Committee 318 (2008). The Levant Bridge #5253 has a span-to-depth ratio of 16.2 and a reinforcement ratio of 7.7×10^{-3}. According to construction details, the steel reinforcement use in building the bridge had a yield strength of 225MPa (33ksi). This is common for structures built during this era. As-built beam dimensions are provided in Table 1.

Table 1: As-built flexural test beam specimen dimensions

Width, mm (in)	Depth, mm (in)	Length, mm (in)	Span, mm (in)
305 (12)	203 (8)	3962 (156)	3353 (132)

The steel reinforced concrete beams were designed assuming Grade 60 (415MPa (60ksi)) tension and shear reinforcing steel and 20.7MPa (3000psi) compressive strength concrete. A 3353mm (132in) centerline span was used during testing to maintain the span-to-depth ratio of the design bridge. Two (2) No. 5 tension reinforcing bars were spaced 152mm (6in) on center at a depth of 165mm (6.5in). Stirrups constructed of No. 3 steel reinforcing bars were placed 25.4mm (1in) below the surface of the concrete and spaced (12in) apart through the centerline span to prevent shear failure and ensure a flexural failure. Two (2) No. 3 steel reinforcing bars were placed (1.375in) from the top of the beam and were used for hanging the stirrups, but not considered compression reinforcement. Figure 1 depicts the typical cross section for a beam specimen. The

nominal shear and flexural capacity of the beams with assumed steel and concrete properties was determined to be 69.8kN (15.7kip) and 24.5kN-m (18.1kip-ft), respectively.
As-built flexural test specimens were cast at the same time as the environmental durability specimen and therefore had an average 28-day concrete compressive strength of 28.3MPa (4100psi). The average yield strength of the reinforcing steel (see Section 0) was determined to be 511MPa (74.2ksi). Following tensile strength testing of the steel reinforcing steel (see Section 5.1.2) a more representative shear and flexural capacity of the as-built beams was determined. Nominal shear and flexural capacity was determined to be 83.6kN (18.8kip) and 28.0kN-m (20.5kip-ft), respectively. Full calculations for the design beam specimens for both assumed and as-built properties are provided in APPENDIX A.

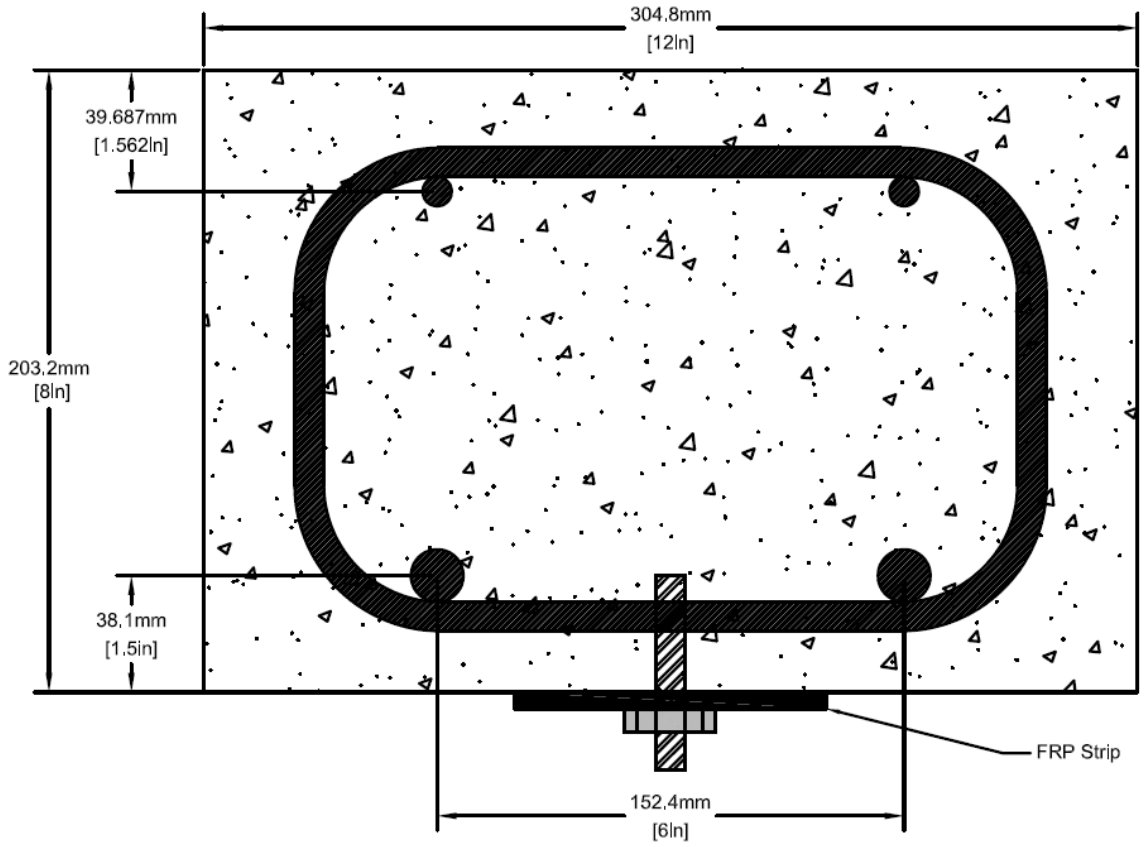

Figure 1: Flexural beam specimen cross-sectional view

MF-FRP Dimensions and Details

FRP panels of GC45 and GC90 were manufactured by Kenway Corp. according to the specifications outlined in Deliverable 4 (Breton & Davids, 2013) and were delivered to the University. Based on the average peak sustained load (APSL) determined in Deliverable 4 of 15.3kN (3.44kip) and 13.7kN (3.08kip) for the GC45 and GC90 environmental control specimen, respectively, an assumed maximum bearing capacity of 13.3kN (3.0kip) per anchor was used to determine the spacing of mechanical fasteners. Assuming each fastener can sustain a

maximum of bearing load of 13.3kN (3.0kip), an end distance of 76.2mm (3in), and a (10ft) strip length, a maximum anchor spacing of 139.7mm (5.5in) of 11anchors over the half-span was determined according to Equation 1.

$$n_b = \frac{T_{FRP}}{P_b} \qquad \text{Equation 1}$$

where:

n_b = required number of connections over the half-span

T_{FRP} = tension in FRP at nominal bending capacity of the FRP- and steel-reinforced specimen, kN (kip)

P_b = maximum bearing capacity of the FRP, kN (kip)

The true FRP strip length used for strengthening specimen was 3.042m (9.979ft). This allowed for easy installation of the FRP strips between the beam supports. Holes 12.7mm (0.5in) in diameter were drilled into the FRP strips at an end distance of 73.0mm (2.875in) and spaced at 127mm (5in) over the half-span. This spacing allowed for 12 anchors over the half-span. Strips were 101.6mm (4in) in width with an average thickness of 5.46mm (0.215in) and 5.41mm (0.213in) for the GC45 and GC90 strips, respectively.

Reinforcing Steel Tensile Strength Tests

Tensile strength tests were performed on pieces of tensile reinforcing steel extracted from the untested ends of failed flexural strength beam specimens. These tests were performed to obtain the true yield strength of the steel used in constructing the specimens. The reinforcement was determined to have an average yield strength of 511MPa (74.2ksi). This experimental yield strength is approximately 24% higher than the minimum specified design yield strength and is used to better approximate the theoretical capacity of both FRP strengthened and non-strengthened beam specimen.

Test Specimen and Test Method

Following the flexural testing of concrete beam specimens to failure, beams were removed from the test setup and turned over to expose the flexural face of the beam. The concrete at the ends of a beam was scored using a masonry saw and knocked off of the beam to expose the underlying steel rebar. One rebar per beam specimen was extracted for tensile strength testing using a grinding wheel. Rebar lengths varied between 390mm and 492mm (15.375in and 19.375in) depending on the ease of cutting the rebar within the concrete. These cut lengths allowed for a 203mm (8in) testing length and adequate grip length (see Figure 2 and Figure 5.3). The diameter

of each specimen was measured in three locations to determine the average cross-sectional area. The average cross-sectional area for all specimens was determined to be 177.5mm^2 (0.275in^2) (see Table 2). It should be noted that this cross-sectional area is lower than the nominally reported cross-sectional area for a No. 5 bar, (0.31in^2).

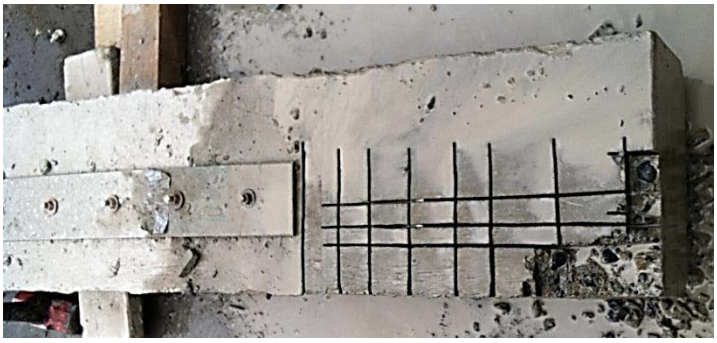

Figure 2: Rebar extraction –Scored concrete

Figure 3: Rebar extraction – Extracted bar

Specimen were pulled in tension to failure according to ASTM A370 specifications (ASTM, 2012) in a 450kN (100kip) capacity Baldwin actuator at a load rate of 12.7mm/min (0.5in/min). Load and position were recorded during testing and used to determine the stress and strain of each specimen. Specimens were labeled according to the beam from which they were extracted.

Results and Conclusions

All specimens failed by rupture following extensive necking of the steel bar within the testing length with the exception of ‘GC45 2’. During testing of the ‘GC45 2’ specimen, the actuator

malfunctioned and shut down. The results from this specimen were kept and used in the determination of the yield strength of the steel since the yield point of the specimen can be observed in the data collected from the test (see Figure 4).

The yield point of each test was determined graphically based on the autographic diagram method or "top of knee" method. As defined in ASTM A370 (ASTM, 2012), this method defines the yield point as the load or stress corresponding to the top of the knee of an autographic recording; the load or stress at which the curve drops creating a sharp-knee in the graph. The yield point for each specimen is provided in Table 2. Figure 5 contains a graphical overlay of all rebar specimen load-displacement plots.

Based on the average cross-sectional area and average yield force, an average yield stress of 511MPa (74.2ksi) was determined for the steel reinforcement used to construct the concrete beam specimen for flexural evaluation. Assuming the steel's elastic modulus of 200,000MPa (29,000ksi), the average yield strain of the steel rebar specimen is 0.0026. The nominal yield force and yield strain of Grade 60, No. 5 reinforcing steel is 82.7kN (18.6kip) and .00207. As demonstrated above, the actual force required to yield the bars used to construct the beam specimen is 9.85% larger than the nominal value.

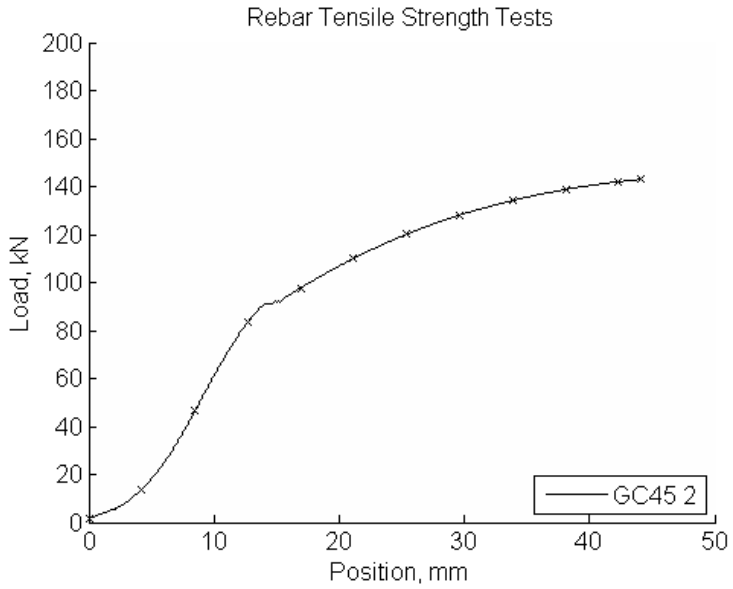

Figure 4: 'GC45 2' load-deformation plot without rupture

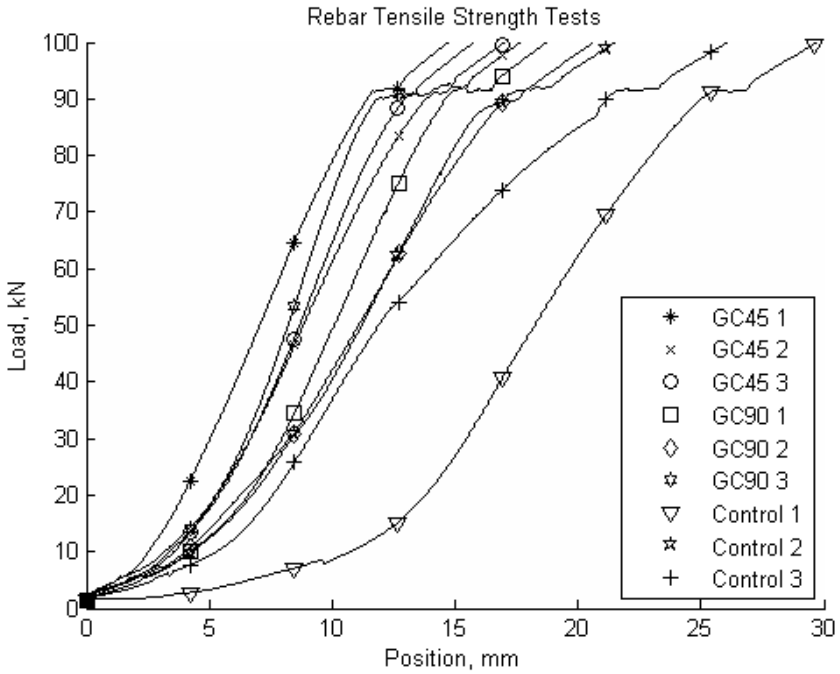

Figure 5: Rebar tensile strength test load-deformation overlay

Table 2: Reinforcing steel cross-sectional area and yield force by "top of knee" method

Specimen Label	Cross-sectional Area, mm^2 (in^2)	Yield Force, kN (kip)
'Ctrl 1'	174 (0.270)	91.5 (20.6)
'Ctrl 2'	176 (0.273)	91.0 (20.5)
'Ctrl 3'	175 (0.271)	91.4 (20.5)
'GC45 1'	181 (0.280)	91.4 (20.4)
'GC45 2'	181 (0.280)	91.2 (20.5)
'GC45 3'	182 (0.282)	90.5 (20.3)
'GC90 1'	176 (0.273)	91.6 (20.6)
'GC90 2'	181 (0.280)	89.3 (20.1)
'GC90 3'	174 (0.270)	90.1 (20.3)
Average	177.5 (0.275)	90.9 (20.4)
Std. Dev.	3.01 (0.0047)	0.73 (0.16)
Cov (%)	1.7	0.8

Flexural Capacity Test Method and Instrumentation

Beam specimens were subjected to two loading regimens: initial loading and failure loading. Specimens were loaded with a 490kN (110kip) capacity Instron actuator. The purpose of the initial loading was to generate a concrete surface on the flexural face that was more representative of a surface that had been in service. The failure loading was used to determine the increase in yield and ultimate capacities of a MF-FRP strengthened specimen. Using the ACI design guidelines (ACI - Committee 440, 2008), anticipated nominal flexural capacities for beam specimen were calculated using both assumed and real concrete and steel strength values (see

APPENDIX A). The resulting expected FRP-strengthened beam moment capacities and resulting FRP stress are outlined in Table 3.

Table 3: Expected FRP-strengthened beam moment capacities and corresponding FRP stresses

Concrete and Steel Strength	Assumed Strengths f'c = 28.3MPa (4100psi) fy = 415MPa (60ksi)		As-built Strengths f'c = 28.3MPa (4100psi) fy = 511MPa (74.2ksi)	
	Nominal Moment Capacity kN-m (kip-ft)	FRP Stress at Capacity MPa (ksi)	Nominal Moment Capacity kN-m (kip-ft)	FRP Stress at Capacity MPa (ksi)
GC45	43.4 (32.0)	203.4 (29.5)	39.6 (29.3)	163.6 (22.7)
GC90	48.4 (35.7)	262.7 (38.1)	43.8 (32.3)	206.2 (29.9)

Loading Procedures

Beams were loaded in four-point bending with load heads located at the third-points of the centerline span, 1117.6mm (44in) from the support center line (see Figure 6), under simply supported conditions. Supports measured 304mm (12in) in length, giving a 3048mm (120in) clear span.

Each beam specimen was subjected to an initial loading to produce flexural cracks in the tension face of the beam and condition the specimen such that the MF-FRP system would be anchored into a cracked concrete face. The loading regimen consisted of four steps: (1) ramp up load, (2) hold position, (3) ramp down load, (4) hold position.

(1) The load was ramped up under load control over a period of 6.75min to an absolute load of 21.8kN (4.9kip), at a load rate of approximately 3.25kN/min (0.73kip/min). The absolute load applied by the actuator generates a service level moment of 14.2kN-m (10.5kip-ft) resulting in a computed maximum compressive stress of 45% of the concrete compressive strength (see APPENDIX A).

(2) Under position control, the actuator position corresponding to the position at which the absolute load of 21.8kN (4.9kip) occurs was held for 10s.

(3) The load was ramped down under load control over a period of 6.75min to an absolute load of 0.89kN (0.2kip) to maintain a load on the beam while under load control.

(4) Similar to step (2), under position control, the actuator position corresponding to the position at which the absolute load of 0.89kN (0.2kip) occurs was held for 10s.

Steps 1 – 4 were repeated once and then the load was entirely removed from the beam specimen.

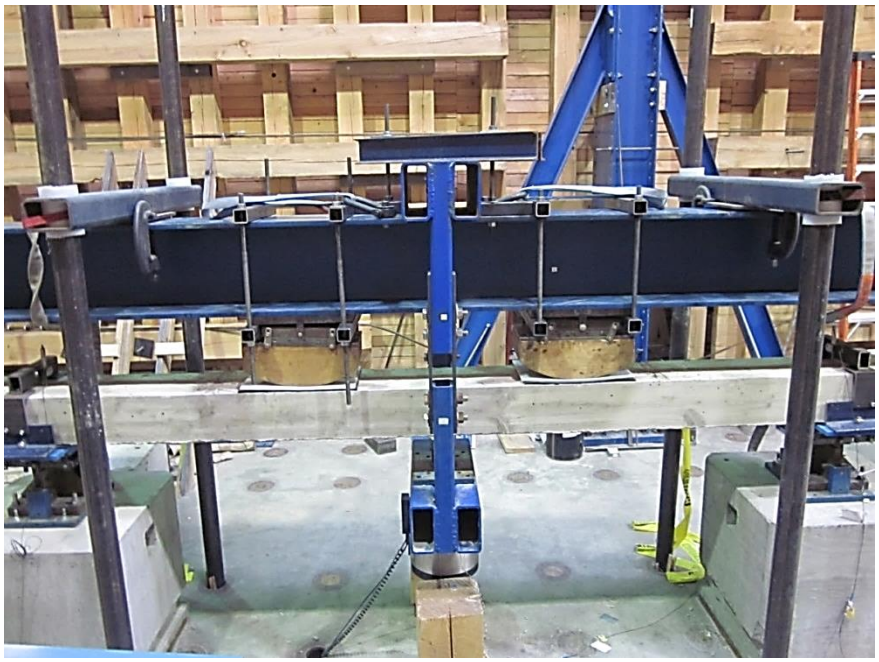

Figure 6: Flexural capacity test setup with specimen in place

After the initial loading, an FRP strip was installed (see Section 0) on the flexural face of the beam specimen. Beam specimens were loaded in four-point bending to failure at a position controlled rate of 12.7mm/min (0.5in/min).

Beam Specimen Instrumentation

Beams were instrumented with two string pots located at the center span, one LVDT at each support end to measure support compression, a strain gage on one of the tension steel reinforcing bars embedded in the concrete, and eight strain gages at redundant locations on the FRP strips over the half-span.

Instrumentation labels for string pots and LVDTs were determined based on their relative cardinal locations. As shown in Figure 6, from left to right the test setup runs from North to South. LVDTs were labeled ‘N LVDT’ and ‘S LVDT’ for their respective locations. The foreground of Figure 6 is located in the west, and therefore the string pot attached to the western edge of the beam is labeled ‘West’ and the string pot attached to the edge in the background, towards the East, is labeled ‘East’.

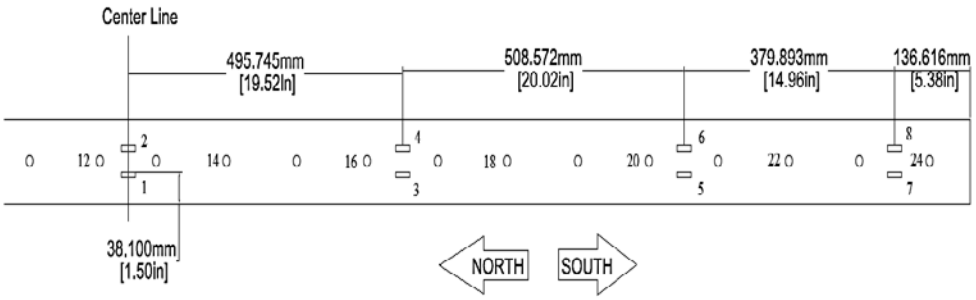

Figure 7: FRP strain gage and hole labeling

As shown in Figure 7, eight strain gages (numbered 1 through 8) were applied to the FRP strips prior to their installation on the beam specimen. Odd numbered gages were located on the western side of the beam and even numbered gages were located on the eastern side of the beam. Gage locations were selected such that the variation in strain over the strip could be measured. Additionally, for easy identification, holes in the FRP were labeled with numbers 1 through 24 from North to South (even numbered holes 12 through 24 are shown in Figure 7). Figure 8 shows a portion of an actual strip with connection holes drilled and strain gages attached (arrow shows longitudinal fiber direction).

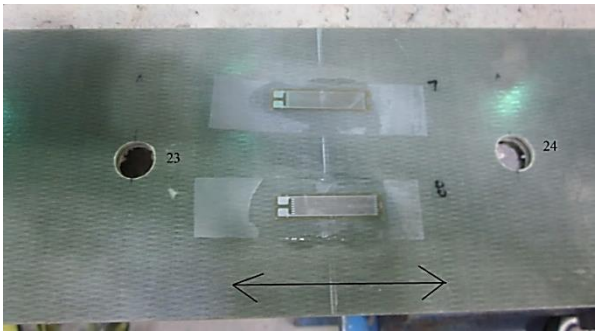

Figure 8: FRP strip portion with strain gages and anchor holes

Care was taken prior to casting the beam specimen to protect the strain gage on the tension reinforcing steel from incurring damage. Plastic piping was placed around the gage and filled with expansive foam to prevent concrete from infiltrating the pipe and damaging the gage (see Figure 9 and Figure 10).

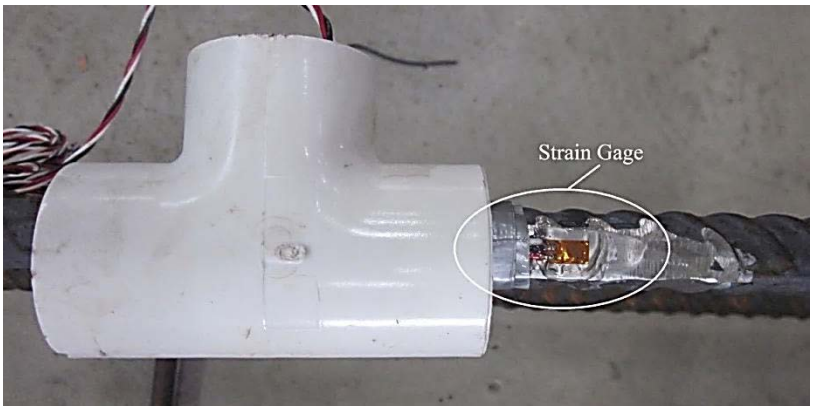

Figure 9: Strain gage on tension reinforcing steel

Figure 10: Foam filled pipe protecting strain gage on tension reinforcing steel

MF-FRP Installation

Following the initial loading of a beam, an FRP strip was adhered to the tension face of a beam specimen using 3M™ VHB™ 5952 (3M, 2011) industrial double-sided, visco-elastic foam tape. The FRP strip was then used as a template for drilling anchor holes into the beam. Using a hammer drill and an 11.1mm (0.438in) diameter drill bit, holes were drilled 38.1mm (1.5in) into the concrete. Following the epoxy adhesive cure time, nuts and washers were applied to the anchors and torqued to 16.9kN-m (12.5kip-ft). The time required to install a strip with a two-person team is approximately 90min; however, this time assumes that the curing of the epoxy adhesive does not begin until the last anchor is installed.

Problems encountered while installing the MF-FRP strip included failure of the adhesive tape during drilling or injection of the epoxy adhesive for the anchors. It was found that allowing the adhesive tape to remain undisturbed following the adhesion of the FRP to the concrete substrate, the tape was able to establish a better bond and was less likely to detach during the installation process. According to 3M (2011), VHB tapes achieve 50% bond strength after 20min at room temperature, 90% bond strength after 24hr, and 100% bond strength after 72hr. The FRP on ‘GC45 2’ separated from the concrete substrate while epoxy adhesive for the anchors was being installed. Epoxy flowed into the gap between the FRP and concrete and hardened. FRP shims

were wedged into the gap (see Figure 11). Analysis of the test results showed no noticeable effect to the beams performance due to this mishap.

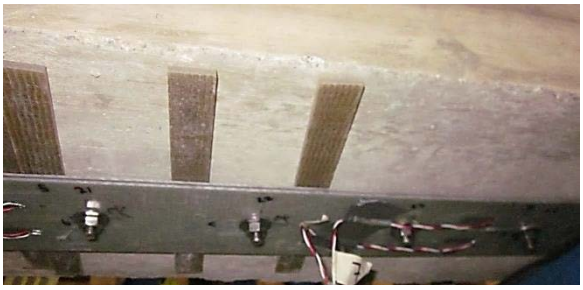

Figure 11: FRP shims placed in gap between FRP strip and concrete substrate

Flexural Behavior

The initial loading of the specimens produced small flexural cracks in the moment span of all beams and, for the rebar strain data collected, strains remained well below the yield strain (0.0026). Figure 12 shows the typical rebar strain response during initial loading. The onset of concrete cracking is clearly depicted in the figure below. Based on the as-built beam properties, the force required to generate the cracking moment is 7.1kN (1.6kip). The approximate onset of cracking appears to occur at 13kN (2.9kip). Plots of rebar strain under initial loading are provided in APPENDIX B.

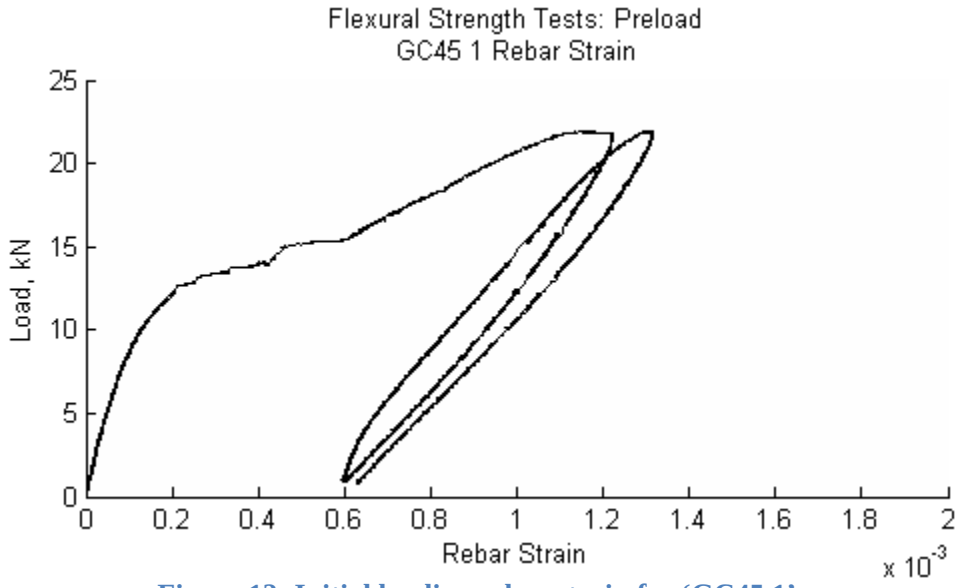

Figure 12: Initial loading rebar strain for 'GC45 1'

Under the failure loading, all specimens failed due to concrete crushing within the moment span, exhibited permanent deformation, and yielding of the tension steel was achieved. Plots of load-deflection display a bi-linear behavior of strengthened beams. Figure 13 shows the load-deflection curve of all beam specimens. The graph clearly displays a 'knee' in the FRP strengthened specimen curves where the steel reinforcement begins to yield, the FRP reinforcement begins to carry more load and the stiffness of the beam changes. Figure 14, Figure

15, and Figure 16 show the load-strain plots of all beams with working strain gages on the embedded tension reinforcement. A dotted vertical line on each plot corresponds to the experimentally determined yield strain of 0.0026. A dotted horizontal line on each plot corresponds to the yield load determined by the 'top of knee' method.

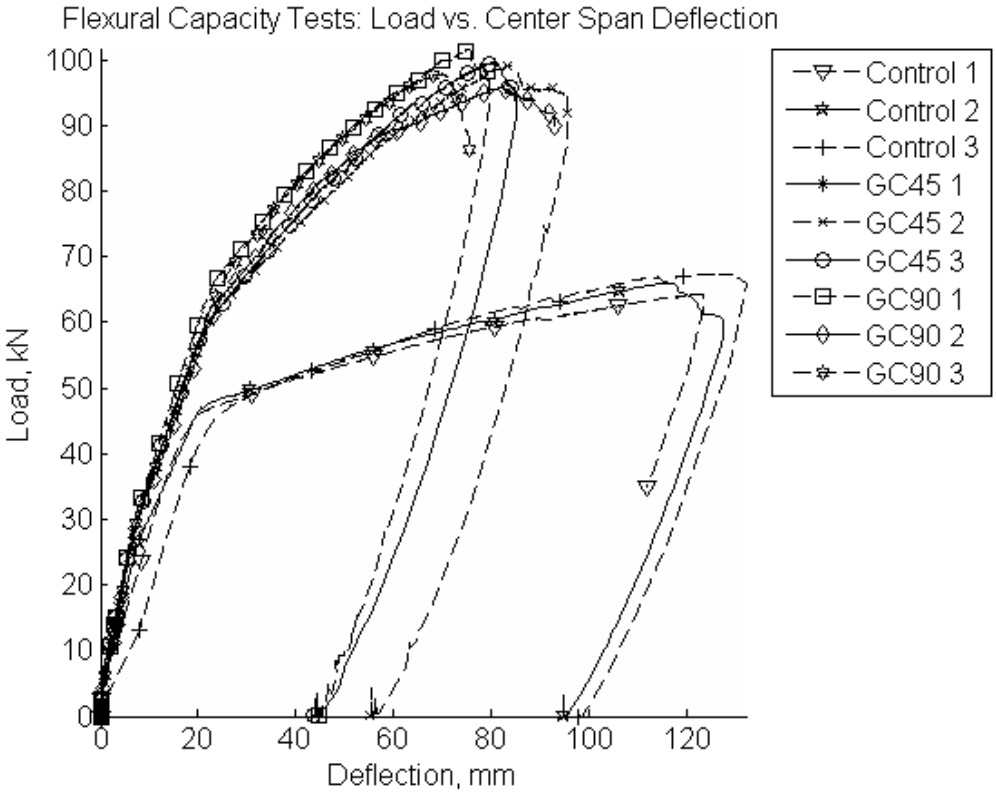

Figure 13: Actuator load vs. center span deflection of all beam specimen tests

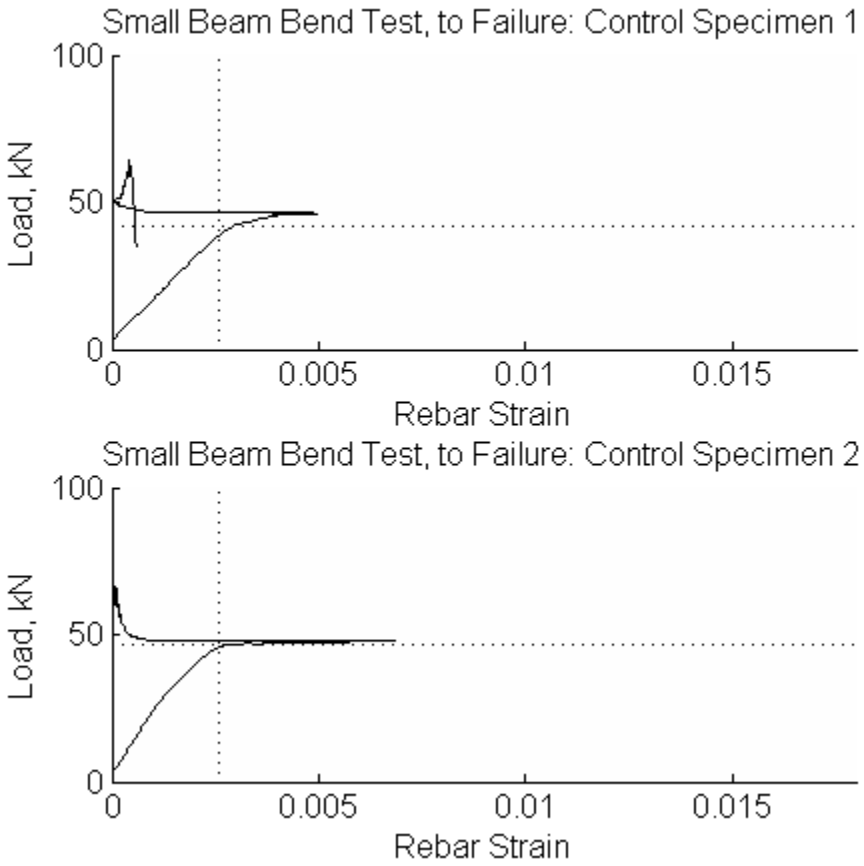

Figure 14: Actuator load-strain plots of embedded tension reinforcing steel in control beam specimens

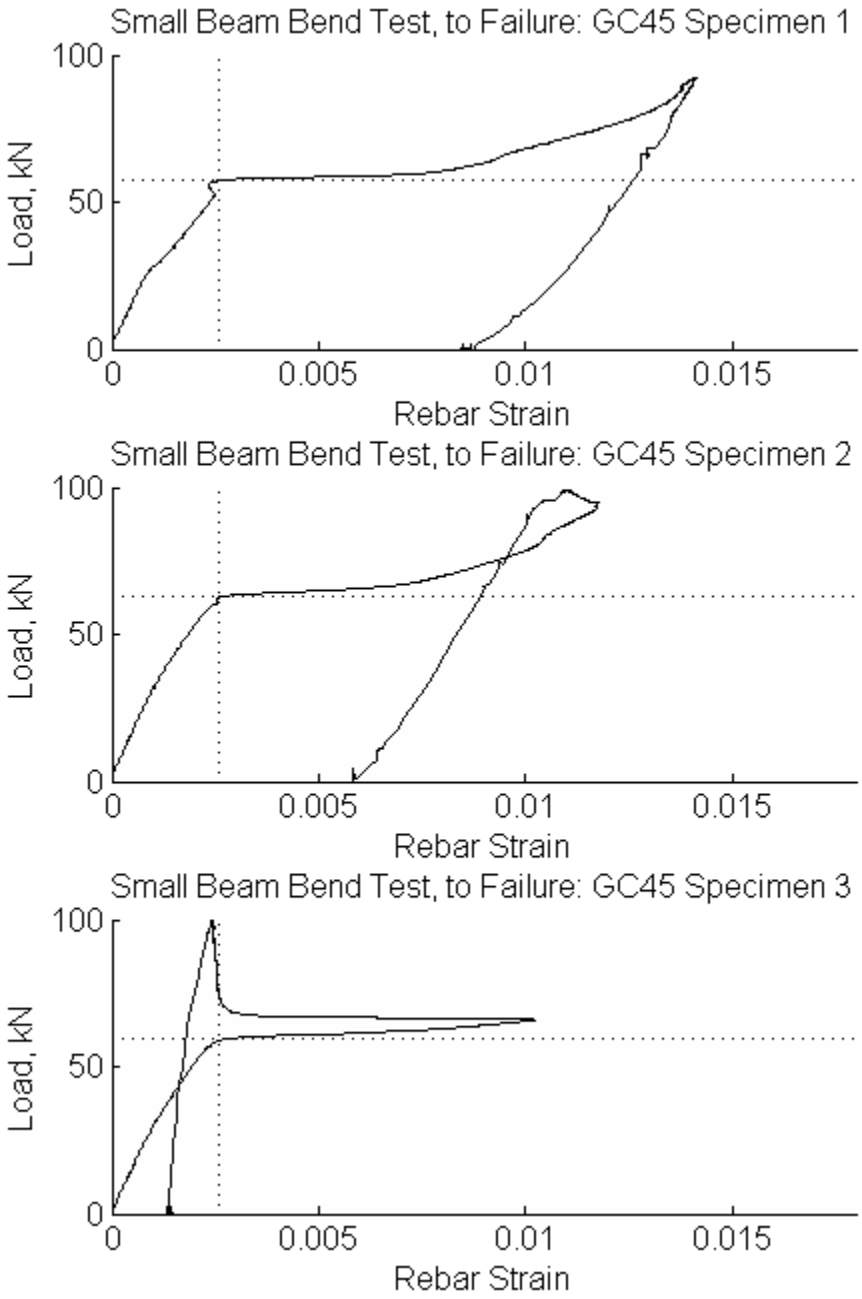

Figure 15: Actuator load-strain plots of embedded tension reinforcing steel in GC45 beam specimens

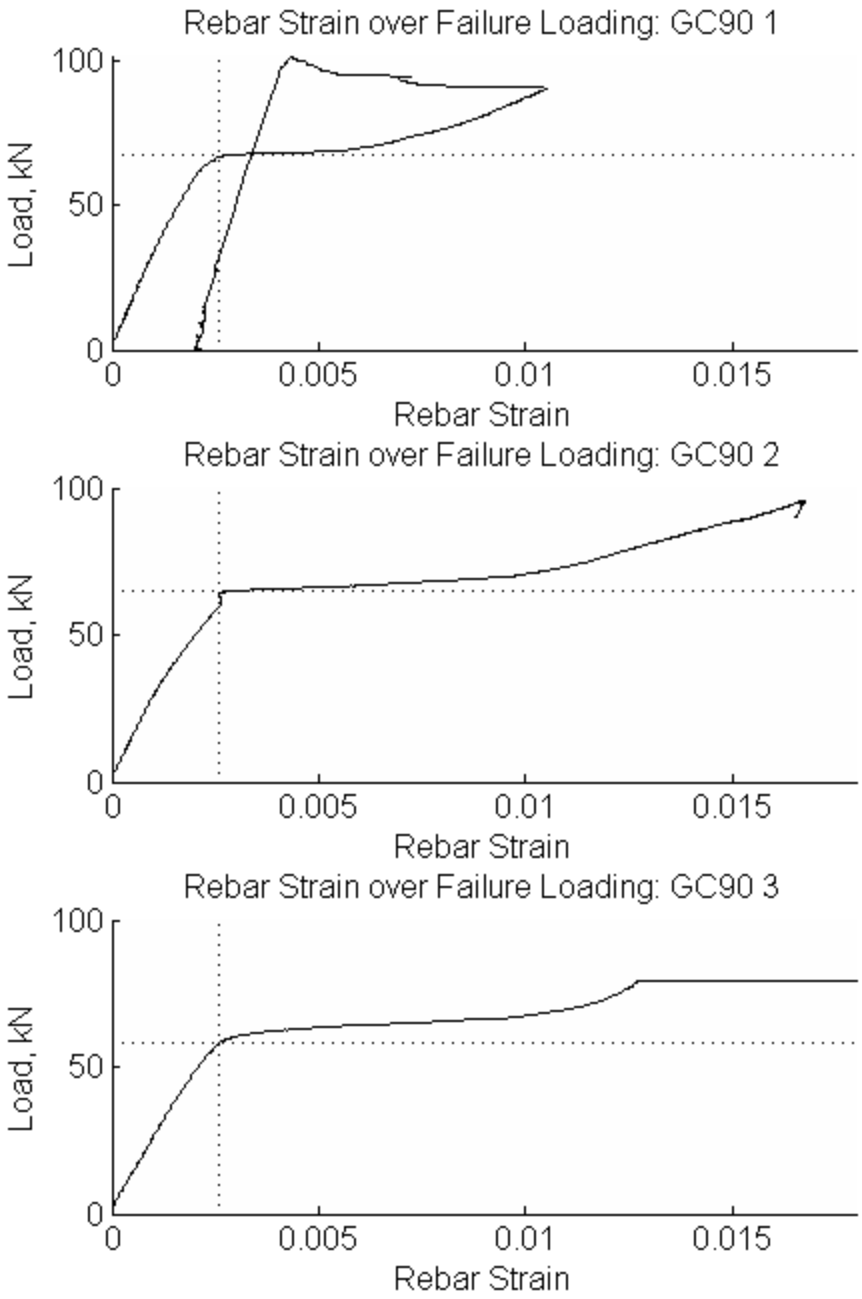

Figure 16: Actuator load-strain plots of embedded tension reinforcing steel in GC90 beam specimens

Several instrumentation and program difficulties were encountered during testing. During the initial loading of 'Ctrl 1', the loading program did not run correctly and the beam was loaded to 24.0kN (5.4kip) during the initial ramp phase. The load program was terminated before irreversible damage was caused to the beam that would render it unusable for flexural strengthening. The rebar strain gage for 'Ctrl 3' failed to provide data; therefore rebar strain plots for this specimen are unavailable. The string pots for 'GC45 1' failed to provide data during the failure loading; therefore load-deflection plots for this specimen are not available. Strain gage issues are discussed later in this report.

The GC45 system was able to increase yield and moment capacity by 41% and 47%, respectively, and decreased beam center span deflection by 31%. The GC90 system was able to increase the yield and moment capacity by 46% and 49%, respectively, and decreased beam center span deflection by 36%. Ultimate capacity was defined as the highest load resisted by the beam specimen. Yield capacity was determined by evaluating the rebar strain gage data gathered during the failure loading. The yield load was determined by the 'top of knee' method on load-strain graphs and compared to the load at which 0.0026 strain (the yield strain determined from rebar tension tests); the resulting yield moments are provided in Table 4 - Table 6. Ultimate moments and recorded deflections are provided in Table 7 – Table 9. When compared to the as-built expected moment capacities, the achieved capacities are 36.9% and 25.6% greater than expected for GC45 and GC90 systems, respectively.

Table 4: Comparison of yield response for control beam specimens

	Strain by 'Top of Knee' Method	Yield Moment by 'Top of Knee' Method kN-m (kip-ft)	Yield Moment by 0.0026 strain kN-m (kip-ft)
Ctrl 1	0.003	23.51 (17.34)	21.63 (15.95)
Ctrl 2	0.0028	26.05 (19.21)	25.53 (18.83)
Ctrl 3	--	--	--
Avg.	0.0029	24.78 (18.28)	23.58 (17.39)
Std.	0.0001	1.27 (0.94)	1.95 (1.44)
COV (%)	3.45	5.13	8.27
Difference (%)*			**4.96**

*% difference between the average yield moments

Table 5: Comparison of yield response for GC45 beam specimens

	Strain by 'Top of Knee' Method	Yield Moment by 'Top of Knee' Method kN-m (kip-ft)	Yield Moment by 0.0026 strain kN-m (kip-ft)
GC45 1	0.00255	32.02 (23.62)	32.05 (23.64)
GC45 2	0.0026	35.09 (25.88)	35.03 (25.83)
GC45 3	0.0027	33.20 (24.49)	32.85 (24.23)
Avg.	0.026	33.44 (24.66)	33.31 (24.57)
Std.	0.00008	1.27 (0.93)	1.26 (0.93)
COV (%)	2.94	3.79	3.78
Difference (%)*			**0.39**

*% difference between the average yield moments

Table 6: Comparison of yield response for GC90 beam specimens

	Strain by 'Top of Knee' Method	Yield Moment by 'Top of Knee' Method kN-m (kip-ft)	Yield Moment by 0.0026 strain kN-m (kip-ft)
GC90 1	0.0030	37.70 (27.81)	37.22 (27.45)
GC90 2	0.0028	36.23 (26.72)	33.45 (24.67)
GC90 3	0.0029	33.35 (24.73)	32.43 (23.92)
Avg.	0.0029	35.82 (26.42)	34.36 (25.35)
Std.	0.00007	1.73 (1.27)	2.06 (1.52)
COV (%)	2.55	4.83	5.99
Difference (%)*			**4.15**

*% difference between the average yield moments

Table 7: Maximum response of control beam specimens

	Max. Moment kN-m (kip-ft)	Max. Shear kN (kip)	Max. Mid-span Deflection, West mm (in)	Max. Mid-span Deflection, East mm(in)
Ctrl 1	35.97 (26.53)	32.18 (7.24)	122.78 (4.83)	121.75 (4.79)
Ctrl 2	36.90 (27.22)	33.02 (7.42)	116.15 (4.57)	115.41 (4.54)
Ctrl 3	37.69 (27.80)	33.72 (7.58)	126.33 (4.97)	126.15 (4.97)
Avg.	36.85 (27.18)	32.97 (7.41)	121.75 (4.79)	121.10 (4.77)
Std.	0.702 (0.518)	0.629 (0.141)	4.220 (0.166)	4.410 (0.174)
COV (%)	1.91	1.91	3.47	3.64

Table 8: Maximum response of GC45 beam specimens

	Max. Moment kN-m (kip-ft)	Max. Shear kN (kip)	Max. Mid-span Deflection, West mm (in)	Max. Mid-span Deflection, East mm(in)
GC45 1	51.29 (38.05)	46.17 (10.38)	--	--
GC45 2	55.40 (40.86)	49.57 (11.14)	83.77 (3.30)	85.17 (3.35)
GC45 3	55.66 (41.05)	49.80 (11.20)	80.16 (3.16)	84.80 (3.34)
Avg.	54.22 (39.99)	48.51 (10.91)	81.96 (3.23)	84.98 (3.35)
Std.	1.86 (1.37)	1.66 (0.37)	1.81 (0.19)	0.07 (0.01)
COV (%)	3.43	3.43	2.20	0.22

Table 9: Maximum response of GC90 beam specimens

	Max. Moment kN-m (kip-ft)	Max. Shear kN (kip)	Max. Mid-span Deflection, West mm (in)	Max. Mid-span Deflection, East mm(in)
GC90 1	56.83 (41.91)	50.85 (11.43)	75.30 (2.96)	77.84 (3.06)
GC90 2	53.33 (39.48)	74.90 (10.77)	82.70 (3.26)	88.42 (3.48)
GC90 3	54.71 (40.35)	48.96 (11.01)	69.80 (2.75)	73.31 (2.89)
Avg.	55.02 (40.58)	49.23 (11.07)	75.93 (2.99)	79.86 (3.14)
Std.	1.36 (1.01)	1.22 (0.27)	5.28 (0.21)	6.33 (0.25)
COV (%)	2.48	2.48	6.96	7.93

All concrete beams failed in flexure within the moment span. Control beams failed due to concrete crushing at the mid-span and exhibited permanent deflection, yielded tension reinforcement, and flexural cracks. All GC45 and GC90 FRP strengthened beams failed in concrete crushing underneath a load head. Beams exhibited permanent deflection, yielded tension reinforcement, and flexural cracks. During failure loading, it was observed that flexural cracks would propagate from mechanical fastener locations. As shown in Figure 17, the large crack to the left of the image is located over 'hole 7' and travels up the beam to the section of crushed concrete. These cracks measured approximately 3.175mm (0.125in) across (see Figure 18). Figure 19 shows the extensive cracking caused following failure loading.

Figure 17: Concrete crushing and flexural cracks of a failed FRP strengthened beam specimen

Figure 18: Flexural cracks on FRP strengthened load while still under load

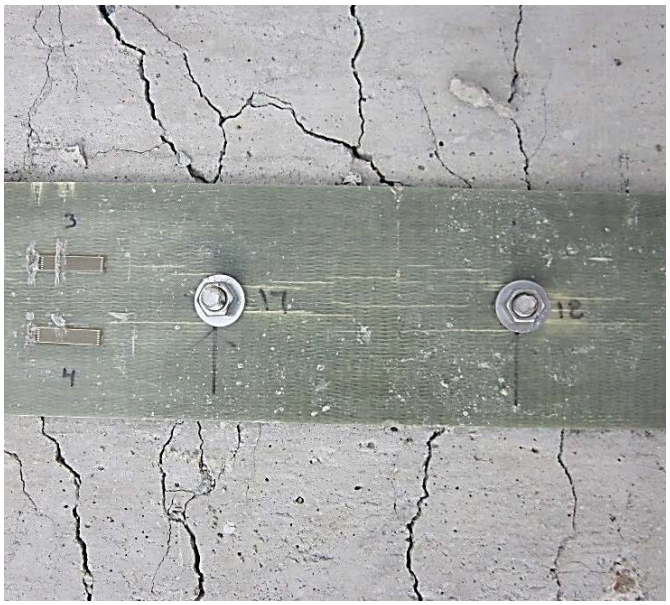

Figure 19: Extensive concrete cracking following failure loading of FRP strengthened beam specimen

Mechanical anchors within the shear span were observed to bend towards the center-span under increased loading (see Figure 20), due the engagement of the anchors in bearing on the FRP. This behavior was also observed during the single fastener, environmental durability tests. The vertical reference line in Figure 20 shows the approximate alignment of the anchor prior to testing provides.

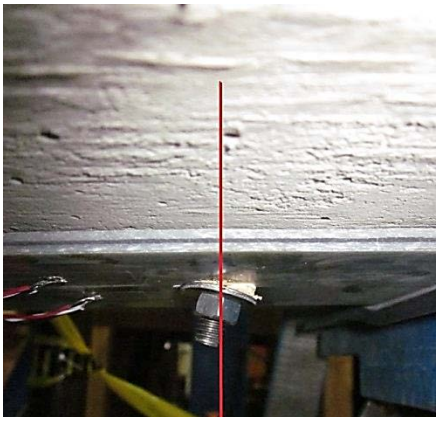

Figure 20: End anchor bent toward the center-span following failure loading

FRP Strains

Various strain gages on the FRP strips failed; however, due to the redundant placement of strain gages adequate data was collected to generate plots of the strain variation in the FRP over the strip length along at least one side of the FRP strip (East or West). With the exception of 'GC45 1', at least one gage at each longitudinal position along an FRP strip provided strain data. Gages

‘5’ and ‘6’ both failed to provide data for ‘GC45 1’. Figure 21 - Figure 26 show the variation in strain in the FRP over the half-span of beam specimens. Strain in the FRP is shown at three distinct loadings: half of the load required to generate steel yielding; the load that results in steel yielding; ultimate loading. The location of load application is shown with a solid vertical line at 0.55m from the mid-span. Strain in the FRP decreased as distance from the center-span increased. There is a significant increase in FRP strain as the tensile stress demand on the FRP increases following the yielding of the steel reinforcement. The average difference between redundant longitudinal gages at ultimate load, when data from two gages at the same longitudinal location was available, is provided in Table 10.

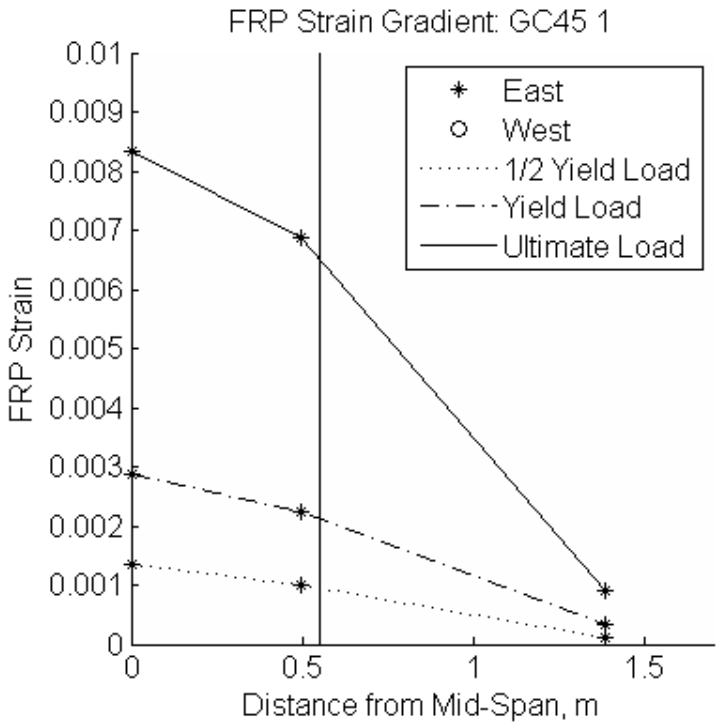

Figure 21: Variation of FRP strain for GC45 specimen 1

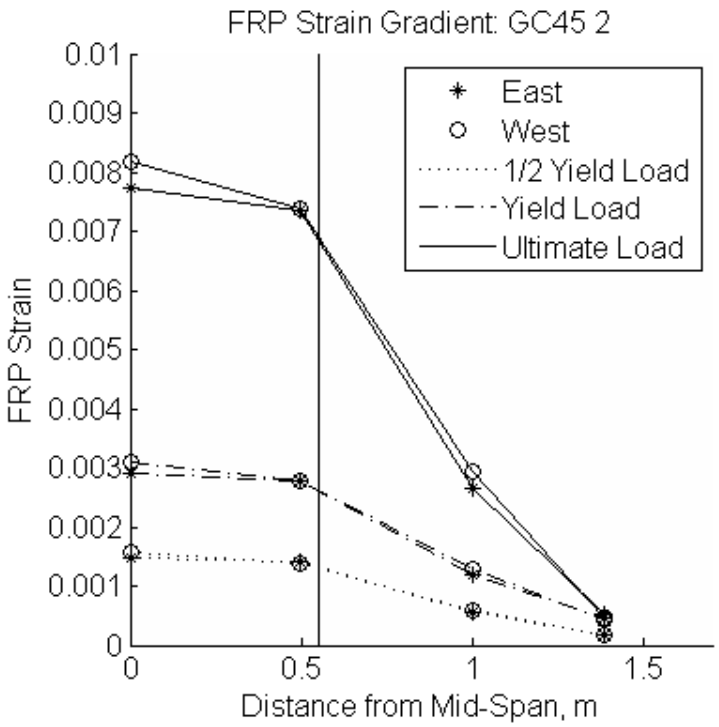

Figure 22: Variation of FRP strain for GC45 specimen 2

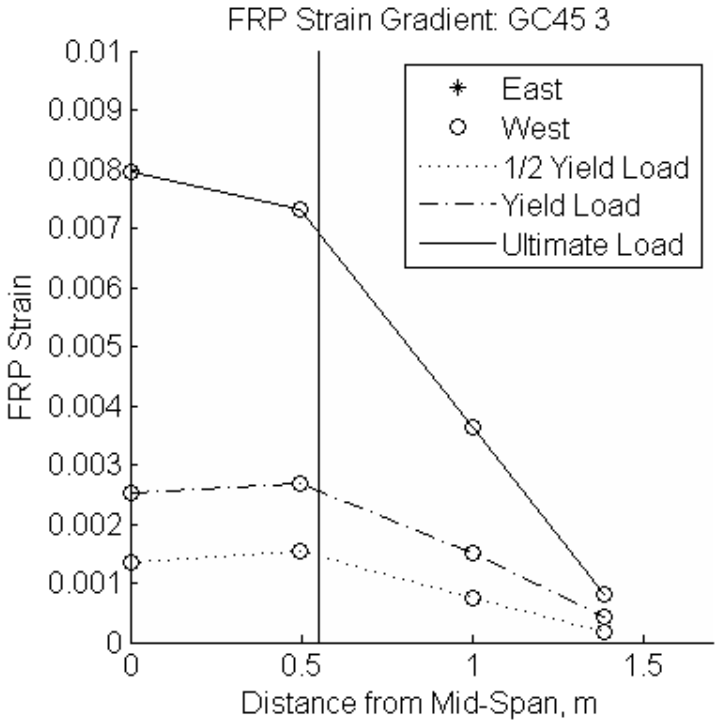

Figure 23: Variation of FRP strain for GC45 specimen 3

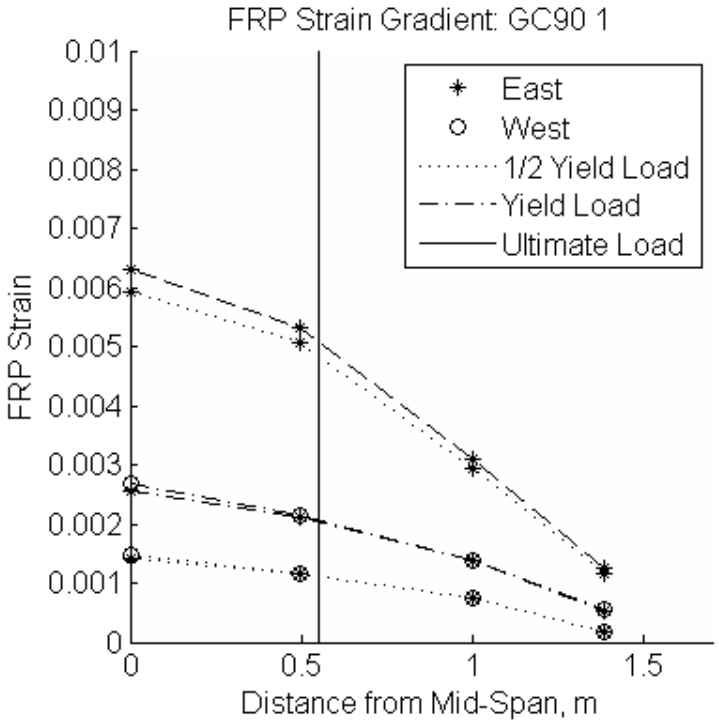

Figure 24: Variation of FRP strain for GC90 specimen 1

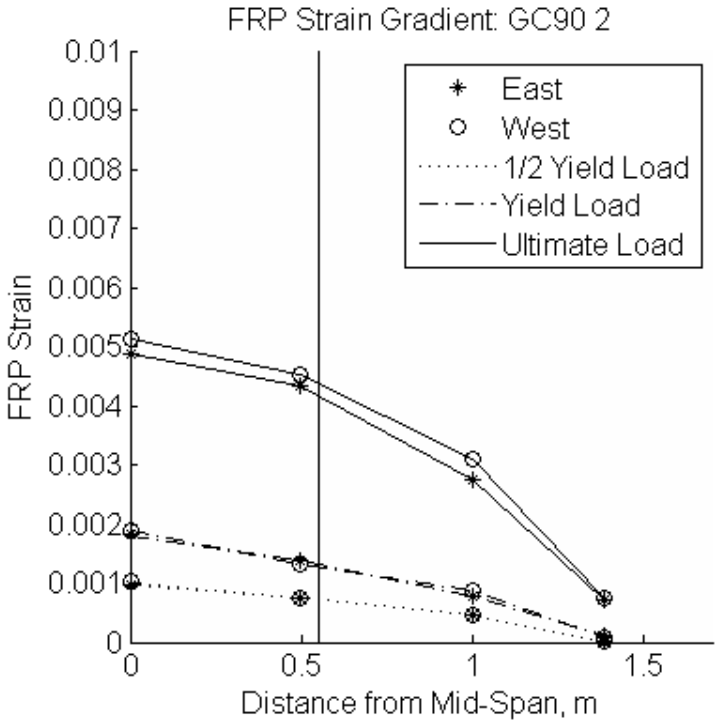

Figure 25: Variation of FRP strain for GC90 specimen 2

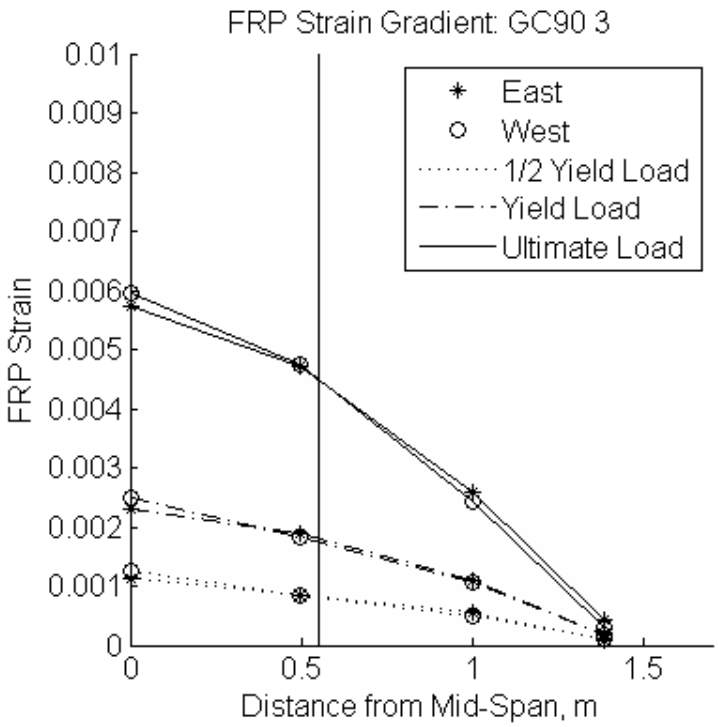

Figure 26: Variation of FRP strain for GC90 specimen 3

Table 10: Average difference in strain readings between longitudinally redundant gages at ultimate load

	Gage 1 & 2*	Gage 3 & 4*	Gage 5 & 6*	Gage 7 & 8*
GC45 1	--	--	--	0.040
GC45 2	0.249	0.011	0.143	0.046
GC45 3	0.039	--	--	0.029
GC90 1	0.171	0.086	0.058	0.052
GC90 2	0.141	0.069	0.183	0.024
GC90 3	0.167	0.026	0.072	0.059

*Strain × 10^{-3} reported

Figure 27 and Figure 28 show the variation of FRP strain by gage location for 'GC45 2' and 'GC90 1'. APPENDIX C contains plots of FRP strains for each strengthened specimen over the duration of the failure loading. From these plots it can be seen that for gages 1 through 4, which are located within the load span, the strain in the FRP is relatively constant. Gages 5 through 8, which are located outside the load span, show a greater variation in strain. As the load and bearing of the fasteners on the FRP increases, a greater tensile demand is placed on the FRP where stresses are largest within the load span (gage 1 – 4), while greater bearing demand is placed on the FRP outside of the load span. Additionally, referring back to Figure 21 – Figure 26, following the yielding of the steel reinforcement, is it observed that there is a drastic difference between the change in strain of the FRP between gages within the load span and those

outside of the load span. The difference in these gages is not as pronounced for loads below yielding.

Using the strain data collected over the duration of the failure loadings, the average bearing force per fastener at the maximum applied load was calculated. The average strain recorded at each longitudinal gage location was determined and the resulting tensile force in the FRP determined using the experimentally derived elastic moduli (see Deliverable 4 (Breton & Davids, 2013)) and average measured cross-sectional areas. The average bearing force per fastener between each pair of gages was determined by dividing the difference in FRP forces by the number of anchors within the gage span. Table 11 – Table 14 summarize the calculated FRP tension and anchor bearing forces, respectively. Tensile forces in Table 11 and Table 12 are listed beneath the gages corresponding to the average strain from which the force was calculated. Average bearing forces are listed in Table 13 and Table 14 beneath the respective gage span in which the anchors are located. With the exception of fasteners near the mid-span, anchors in bearing withstood forces greater than the assumed maximum bearing capacity per fastener location of 13.3kN (3kip).

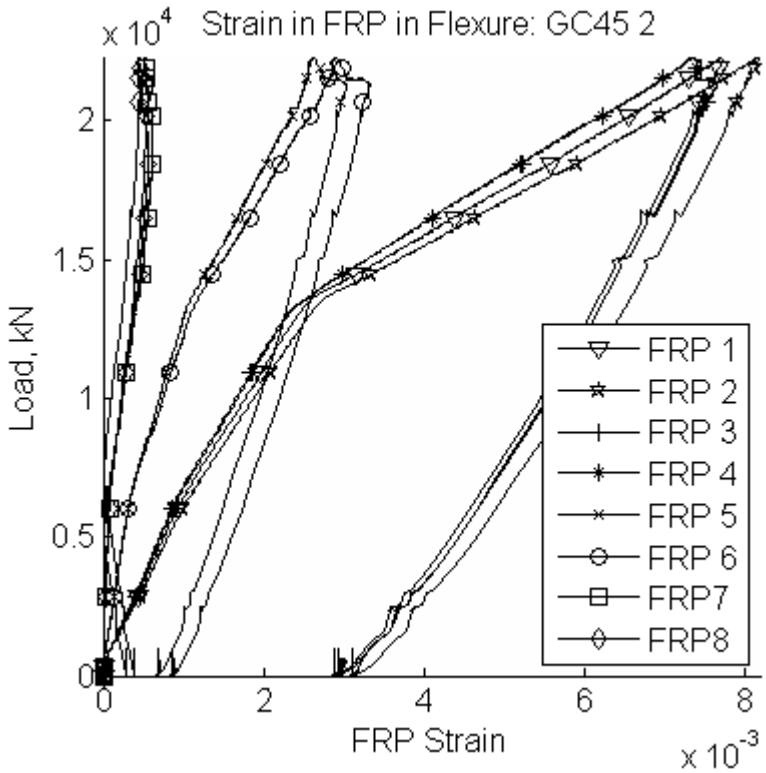

Figure 27: Strain in GC45 2 over loading duration

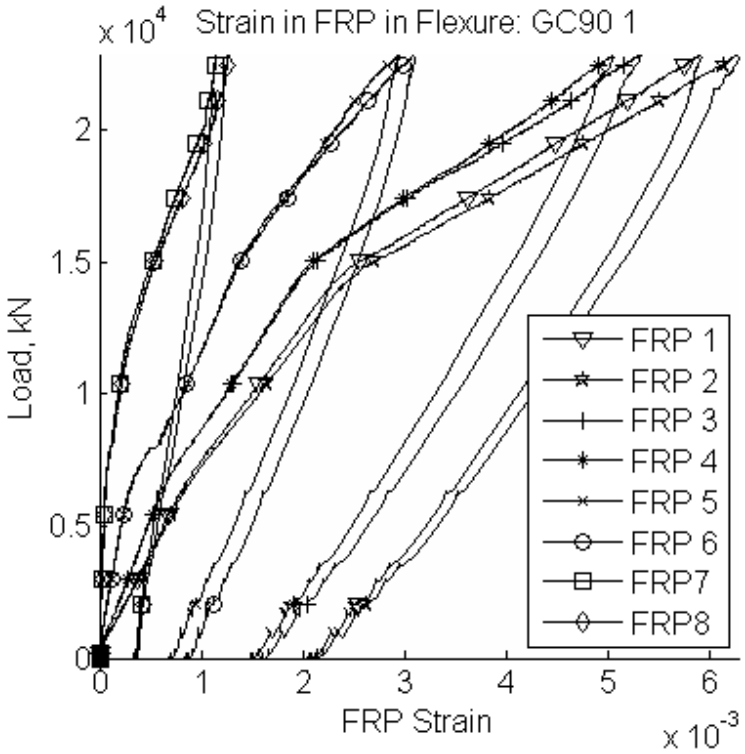

Figure 28: Strain in GC90 1 over loading duration

Table 11: Tension force in GC45-reinforcement between strain gages

	Gage 1&2 kN (kip)	Gage 3&4 kN (kip)	Gage 5&6 kN (kip)	Gage 7&8 kN (kip)
½ Yield Load				
GC45 1	38.4 (8.6)	28.2 (6.3)	--	3.0 (0.7)
GC45 2	43.7 (9.8)	39.8 (9.0)	16.6 (3.7)	5.1 (1.1)
GC45 3	38.4 (8.6)	43.5 (9.8)	21.1 (4.7)	5.0 (1.1)
Avg.	40.2 (9.0)	37.2 (8.4)	18.8 (4.2)	4.4 (1.0)
Std.	2.5 (0.6)	6.5 (1.5)	2.3 (0.5)	1.0 (0.2)
COV (%)	6.3	17.6	12.0	21.9
Yield Load				
GC45 1	82.2 (18.5)	64.0 (14.4)	--	9.7 (2.2)
GC45 2	85.7 (79.3)	79.3 (17.8)	35.2 (7.9)	12.9 (2.9)
GC45 3	72.4 (16.3)	76.7 (17.2)	42.8 (9.6)	11.8 (2.6)
Avg.	80.1 (18.0)	73.3 (16.5)	39.0 (8.8)	11.5 (2.6)
Std.	5.6 (1.3)	6.7 (1.5)	3.8 (0.9)	1.3 (0.3)
COV (%)	7.0	9.1	9.8	11.6
Ultimate Load				
GC45 1	237.5 (53.4)	196.1 (44.1)	--	26.7 (6.0)
GC45 2	226.6 (50.9)	209.8 (47.2)	79.2 (17.8)	14.0 (3.1)
GC45 3	227.7 (51.2)	207.2 (46.6)	103.4 (23.3)	23.6 (5.3)
Avg.	230.6 (51.8)	204.4 (45.6)	91.3 (20.5)	21.4 (4.8)
Std.	4.9 (1.1)	6.0 (1.3)	12.1 (2.7)	5.4 (1.2)
COV (%)	2.1	2.9	13.2	25.3

Table 12: Tension force in GC90-reinforcement between strain gages

	Gage 1&2 kN (kip)	Gage 3&4 kN (kip)	Gage 5&6 kN (kip)	Gage 7&8 kN (kip)
½ Yield Load				
GC90 1	53.1 (11.9)	42.7 (9.6)	27.5 (6.2)	6.3 (1.4)
GC90 2	36.7 (8.3)	27.8 (6.3)	17.0 (3.8)	0.7 (0.2)
GC90 3	44.0 (9.9)	31.3 (7.0)	19.6 (4.4)	3.7 (0.8)
Avg.	44.6 (10.0)	33.9 (7.6)	21.4 (4.8)	3.6 (0.8)
Std.	6.7 (1.5)	6.4 (1.4)	4.5 (1.0)	2.3 (0.5)
COV (%)	15.0	18.7	20.9	63.4
Yield Load				
GC90 1	96.7 (21.7)	78.2 (17.6)	50.9 (11.5)	19.6 (4.4)
GC90 2	68.6 (15.4)	49.9 (11.2)	30.4 (6.8)	3.7 (0.8)
GC90 3	88.7 (19.9)	68.8 (15.5)	40.0 (9.0)	6.4 (1.4)
Avg.	84.7 (19.0)	65.5 (14.8)	40.4 (9.1)	9.9 (2.2)
Std.	11.8 (2.7)	11.8 (2.6)	8.4 (1.9)	6.9 (1.6)
COV (%)	13.9	17.9	20.7	70.1
Ultimate Load				
GC90 1	225.7 (50.7)	191.9 (43.1)	111.7 (25.1)	44.5 (10.0)
GC90 2	185.1 (41.6)	163.3 (36.7)	108.0 (24.3)	27.1 (6.1)
GC90 3	216.2 (48.6)	174.8 (39.9)	92.8 (20.9)	13.7 (3.1)
Avg.	209.0 (47.0)	176.7 (39.7)	104.2 (23.4)	28.4 (6.4)
Std.	17.4 (3.9)	11.7 (2.6)	8.2 (1.8)	12.6 (2.8)
COV (%)	8.3	6.6	7.8	44.4

Table 13: GC45 average bearing force per anchor between strain gages

	Gage 1&2 to 3&4 kN (kip)	Gage 3&4 to 5&6 kN (kip)	Gage 5&6 to 7&8 kN (kip)
½ Yield Load			
GC45 1	2.6 (0.6)	3.96 (0.8)*	--
GC45 2	1.0 (0.2)	5.8 (1.3)	3.8 (0.9)
GC45 3	-1.3 (-0.3)**	5.6 (1.3)	5.4 (1.2)
Avg.	1.8 (0.4)	5.0 (1.1)	4.6 (1.0)
Std.	0.8 (0.2)	1.0 (0.2)	0.8 (0.2)
COV (%)	44.5	20.0	16.6
Yield Load			
GC45 1	4.6 (1.0)	7.8 (1.7)*	--
GC45 2	1.6 (0.4)	11.0 (2.5)	7.4 (1.7)
GC45 3	-1.1 (-0.2)**	8.5 (1.9)	10.4 (2.3)
Avg.	3.1 (0.7)	9.1 (2.0)	8.9 (2.0)
Std.	1.5 (0.3)	1.4 (0.3)	1.5 (0.3)
COV (%)	48.3	15.5	16.4
Ultimate Load			
GC45 1	10.4 (2.3)	24.2 (5.4)*	--
GC45 2	4.2 (0.9)	32.6 (7.3)	21.8 (4.9)
GC45 3	5.1 (1.2)	25.9 (5.8)	26.6 (6.0)
Avg.	6.6 (1.5)	27.6 (6.2)	24.2 (5.4)
Std.	2.7 (0.6)	3.6 (0.8)	2.4 (0.5)
COV (%)	41.1	13.2	10.0

*Average bearing force for the seven anchors between gage 3&4 and gage 7&8 due to missing strain data for gage 5&6

** Negative difference between FRP strain is assumed to result in zero bearing force at the anchor. Value excluded from avg., std. and COV calculations

Table 14: GC90 average bearing force per anchor between strain gages

	Gage 1&2 to 3&4 kN (kip)	Gage 3&4 to 5&6 kN (kip)	Gage 5&6 to 7&8 kN (kip)
½ Yield Load			
GC90 1	2.6 (0.6)	3.8 (0.9)	7.1 (1.6)
GC90 2	2.2 (0.5)	2.7 (0.6)	5.4 (1.2)
GC90 3	3.2 (0.7)	2.9 (0.7)	5.3 (1.2)
Avg.	2.7 (0.6)	2.9 (0.7)	5.9 (1.3)
Std.	0.4 (0.09)	0.5 (0.1)	0.8 (0.2)
COV (%)	14.6	15.1	13.6
Yield Load			
GC90 1	4.6 (1.0)	6.8 (1.5)	10.5 (2.4)
GC90 2	4.7 (1.1)	4.9 (1.1)	8.9 (2.0)
GC90 3	5.0 (1.1)	7.2 (1.6)	11.2 (2.5)
Avg.	4.8 (1.1)	6..3 (1.4)	10.2 (2.3)
Std.	0.2 (0.04)	1.0 (0.2)	1.0 (0.2)
COV (%)	3.4	16.1	9.3
Ultimate Load			
GC90 1	8.4 (1.9)	20.0 (4.5)	22.4 (5.0)
GC90 2	5.4 (1.2)	13.8 (3.1)	27.0 (6.1)
GC90 3	10.3 (2.3)	20.5 (4.6)	26.4 (5.9)
Avg.	8.1 (1.8)	18.1 (4.1)	25.3 (5.7)
Std.	2.0 (0.5)	3.0 (0.7)	2.0 (0.5)
COV (%)	25.0	16.8	8.0

Bearing failure of the FRP, observed as elongation at connection locations, was recorded for both GC45 and GC90 specimen. As shown in Figure 29 and Figure 30, hole elongation occurred at connection locations within both the shear and moment span, suggesting that including the connections in the moment span helps to utilize the FRP strip more. However, hole elongation was significantly greater within the shear span, which is where beam theory predicts that shear stress transfer between the FRP and concrete will occur, and where the calculated average bearing forces per anchor are the greatest (see Table 13 and Table 14). Further, the elongation of the holes in the load span could be due primarily to the large deflections and tension-face strains occurring as the beam reached its ultimate capacity.

Figure 29: Elongation of hole 19 on a GC45 FRP strip within the shear span, after beam failure

Figure 30: Elongation of hole 13 on a GC90 FRP strip within the load span, after beam failure

The maximum recorded strain and the resulting stress (calculated by multiplying the recorded strain by the elastic modulus determined from ASTM D3039 testing) for each strengthened specimen are provided in Table 15 and Table 16. Compared to the ultimate capacities determined in Deliverable 4, on average 47.9% of the GC45 system's strength was utilized at beam failure while 37.4% of the GC90 system's strength was utilized at beam failure.

Table 15: Maximum GC45 FRP strain, stress and capacity utilization

	Max. Strain ($\times 10^{-3}$)	Max. Stress, MPa (ksi)	FRP Capacity Utilization (%)
GC45 1	8.33	248.3 (36.1)	48.8
GC45 2	8.18	243.8 (35.4)	47.9
GC45 3	8.05	239.9 (34.8)	47.1
Avg.	8.19	244.0 (35.4)	47.9
Std.	0.12	3.45 (0.50)	0.68
COV (%)	1.41	1.41	1.41

Table 16: Maximum GC90 FRP strain, stress, and capacity utilization

	Max. Strain ($\times 10^{-3}$)	Max. Stress, MPa (ksi)	FRP Capacity Utilization (%)
GC90 1	6.12	245.8 (35.7)	40.6
GC90 2	5.01	200.2 (29.0)	33.1
GC90 3	5.85	232.5 (33.7)	38.4
Avg.	5.80	226.1 (32.8)	37.4
Std.	0.49	19.15 (2.78)	3.17
COV (%)	8.47	8.47	8.47

Conclusions

To assess the capability of the two MF-FRP systems selected for further studying following environmental durability testing, steel-reinforced concrete bridges designed to mimic flat-slab concrete bridges were strengthened with FRP strips and loaded to failure. The beam specimens were designed such that they maintained a span-to-depth ratio and reinforcement ration similar to that of the Levant Bride (#5253).

To obtain a true yield strength of the steel rebar used in constructing the beam specimen, tension tests were performed on portions of rebar extracted from specimens following their failure testing. Rebar portions were taken from the ends of beams. Following analysis of the collected data, using the 'top of knee' method, a yield stress of 511MPa (74.2ksi) and corresponding 0.0026 yield strain were determined. This value allows for a more accurate evaluation of the true and strengthened capacities of the beam specimens. Based on assumed properties the control beam moment capacity was predicted to be 24.5kN-m (18.1kip-ft) where the as-built properties predicted a capacity of 28.0kN-m (20.5kip-ft). The assumed properties conservatively predicted the strength of the beam specimens by approximately 50% under the actual average failure capacity, and the as-built properties conservatively predicted the strength of the beam specimens by only 20%. Although beam specimen tests provided very good results, future work should be conducted on beams with steel and concrete strengths closer to those of existing flat-slab concrete bridges.

FRP composite panels for GC45 and GC90 systems were manufactured by Kenway Corp. following the same material specifications outlined in Deliverable 4. Mechanical fasteners were installed into the tension face of concrete beams that had undergone an initial loading routine to generate flexural cracks and induce service level strains in the rebar. MF-FRP strengthened beams were loaded to failure and compared to the yield and ultimate capacities and maximum deflection values of failed control beams. Beams strengthened with GC45 increased beam yield and ultimate capacities by 41% and 47%, respectively, and decreased beam center span deflection by 31%. Beams strengthened with GC90 increased beam yield and ultimate capacities by 46% and 49%, respectively, and decreased center span deflection by 36%. All beam specimens failed due to concrete crushing within the moment span, exhibited permanent deformation, yielded steel, and flexural cracks. Strain data collected from various points on the FRP strips strain in the FRP is greatest at the center span and decreases as distance from the center span increases. On average, at ultimate capacity, beams strengthened with GC45 strips utilized 47.9% of the FRP's tensile capacity; beams strengthened with GC90 strips utilized 37.4% of the FRP's tensile capacity. In general, stress in the FRP was greatest within the load span, where bearing of the fasteners was at a minimum. The majority of bearing forces occurred in the eight anchors towards the ends of the FRP strips, where stress in the FRP was at a minimum.

Based on the data and observations collected in this study it was concluded that both the GC45 and GC90 systems are capable of increasing flexural capacity while providing adequate deflection warning prior to failure. The GC90 system is recommended for further evaluation or use due to its slight economical advantage in manufacturing and performance in durability and flexural strengthening. Both mechanical fasteners and FRP composites withstood forces necessary to successfully implement an MF-FRP system.

Works Cited

3M. (2011, June). *3M VHB(TM) Tapes.* Retrieved 2012, from 3M in the United States: solution.3m.com

ACI - Committee 318. (2008). *Building code requirements for structural concrete (ACI 318-08) and commentary.* American Concrete Institute.

ACI - Committee 440. (2008). *Guide for the design and construction of externally bonded FRP systems for strengthening concrete structures.* Farmington Hills, MI, USA: American Concrete Institute.

ASTM. (2012). ASTM A370 Standard Test Methods and Definitions for Mechanical Testing of Steel Products. West Conshohocken, Pa: ASTM International.

Breton, H., & Davids, W. (2013). *Bridge Safety Project, Task 4 (Deliverable 4): FRP Flexural Retrofit Environmental Durability Testing Analysis.* Engineering Report, University of Maine, Civil and Environmental Engineering, Orono.

APPENDIX A.

FLEXURAL STRENGTH TEST BEAM SPECIMEN DESIGN CALCULATIONS

The following sections provide the calculations for the nominal and as-built capacities of the flexural strength tests specimens and for the anticipated capacities of FRP-strengthened beams.

A.1 Nominal Flexural Strength Test Specimen Design Calculations

The following design calculations are for the theoretical design of steel reinforced concrete beam specimen for use in four-point flexural tests. The design follows guidelines provided by ACI-318 and characteristics of the design bridge (Levant Bridge, MDOT #5253) as outlined in Chapter 3 and Chapter 5.

Levant Bridge Details

Span Length $L := 25ft$

Slab thickness $h := 18.5in$

Slab width $W := 308in = 25.667 \cdot ft$

Strip width $b_w := 12in$

Compressive strength $f'c := 2.5ksi$

Elastic Modulus $E_c := 57000\sqrt{f'c \cdot psi} = 2850 \cdot ksi$

Ultimate stress $\varepsilon_{cu} := 0.003$

Reinforcing bar diameter $d_b := 1in$

Bar spacing $s_b := 6in$

Area of steel $As := d_b^{\,2} \cdot \frac{\pi}{4} \cdot \frac{b_w}{s_b} = 1.571 \cdot in^2$

Steel yielding strength $fy := 33ksi$

Depth to steel $d := 17in$

Steel elastic modulus $Es := 29000ksi$

Steel yielding strain $\varepsilon_y := \frac{fy}{Es} = 0.00114$

Modular Ratio $n_s := \frac{Es}{E_c} = 10.175$

Span-to-depth ratio $ld := \frac{L}{h} = 16.216$

Reinforcement ratio $\rho_s := \frac{As}{d \cdot b_w} = 0.0077$

The small beam specimen are designed such that they maintain the characteristics of a flat-slab bridge in terms of the span-to-depth and reinforcement ratios. This is achieved using an 11ft span, 1ft width, 8in deep beam with two #5 steel rebar.

Small Beam Flexural Specimen

Span Length	$L := 11ft$
Beam thickness	$h := 8in$
Strip width	$b_w := 12in$
Unit weight	$\gamma_c := 150pcf$
Compressive strength	$f'c := 3.0ksi$
Concrete rupture stress	$fr := 7.5\sqrt{f'c \cdot psi} = 410.792\ psi$
Elastic Modulus	$E_c := 57000\sqrt{f'c \cdot psi} = 3122.019 \cdot ksi$
Ultimate stress	$\varepsilon_{cu} := 0.003$
Reinforcing bar diameter	$d_b := \frac{5}{8}in$
Bar spacing	$s_b := 6in$
Area of steel	$As := d_b^{2} \cdot \frac{\pi}{4} \cdot \frac{b_w}{s_b} = 0.614 \cdot in^2$
Steel yielding strength	$fy := 60ksi$
Depth to steel	$d := 6.5in$
Steel elastic modulus	$Es := 29000ksi$
Steel yielding strain	$\varepsilon_y := \frac{fy}{Es} = 0.00207$
Modular Ratio	$n_s := \frac{Es}{E_c} = 9.289$
Stirrup: Area of steel	$A_{stirrup} := 0.11in^2$
Stirrup: Spacing	$s_s := 12in$
Span-to-depth ratio	$ld := \frac{L}{h} = 16.5$
Reinforcement ratio	$\rho_s := \frac{As}{d \cdot b_w} = 0.0079$

Beam self-weight $w_D := \gamma_c \cdot b_w \cdot h = 100 \cdot plf$

Stress $\beta_1 := \begin{cases} 0.85 & \text{if } f'c \le 4ksi \\ \left(1.05 - 0.05 \cdot \frac{f'c}{ksi}\right) & \text{if } f'c > 4ksi \wedge f'c < 8ksi \\ 0.65 & \text{if } f'c \ge 8ksi \end{cases}$

$\beta_1 = 0.85$

Distance from extreme compression fiber to N.A.:

$$c := \frac{As \cdot fy}{0.85 \cdot f'c \cdot b_w \cdot \beta_1} \qquad c = 1.415\,in$$

Nominal Moment Capacity:

$$Mn := As \cdot fy \cdot \left(d - \frac{\beta_1 \cdot c}{2}\right) \qquad Mn = 18.1 \cdot kip \cdot ft$$

Nominal Shear Capacity

$$Vn := 2\sqrt{f'c \cdot psi} \cdot b_w \cdot (d) + \frac{2 \cdot A_{stirrup} \cdot fy \cdot d}{s_s} \qquad Vn = 15.694 \cdot kip$$

Third-Point load required to generate nominal moment:

$$Pm := \left(Mn - \frac{w_D \cdot L^2}{8}\right) \cdot \frac{3}{L} \qquad Pm = 4.523 \cdot kip$$

Actuator load: $P_{m\_act} := 2 \cdot Pm$ $\qquad P_{m\_act} = 9.046 \cdot kip$

Third-Point load required to generate nominal shear:

$$Pv := Vn - \frac{w_D \cdot L}{2} \qquad Pv = 15.144 \cdot kip$$

Actuator load: $P_{v\_act} := 2 \cdot Pv$ $\qquad P_{v\_act} = 30.289 \cdot kip$

A.2 As-Built Flexural Strength test Specimen Design Calculations

Small beam specimen were built to the dimensions specified in the theoretical small beam design calculations. Based on the results on concrete compression and reinforcement tension tests, the strengths of these materials were used to calculate the anticipated capacity of the small beams.

Small Beam Flexural Specimen

Span Length	$L := 11ft$
Beam thickness	$h := 8in$
Strip width	$b_w := 12in$
Unit weight	$\gamma_c := 150pcf$
Compressive strength	$f'c := 4.1ksi$
Concrete rupture stress	$fr := 7.5\sqrt{f'c \cdot psi} = 480.234psi$
Elastic Modulus	$E_c := 57000\sqrt{f'c \cdot psi} = 3649.781ksi$
Ultimate stress	$\varepsilon_{cu} := 0.003$
Reinforcing bar diameter	$d_b := \frac{5}{8}in$
Bar spacing	$s_b := 6in$
Area of steel	$As := 2 \cdot 0.275in^2 = 0.55 \cdot in^2$
Steel yielding strength	$fy := 74.2ksi$
Depth to steel	$d := 6.5in$
Steel elastic modulus	$Es := 29000ksi$
Steel yielding strain	$\varepsilon_y := \frac{fy}{Es} = 0.00256$
Modular Ratio	$n_s := \frac{Es}{E_c} = 7.946$
Stirrup: Area of steel	$A_{stirrup} := 0.11in^2$
Stirrup: Spacing	$s_s := 12in$
Span-to-depth ratio	$ld := \frac{L}{h} = 16.5$
Reinforcement ratio	$\rho_s := \frac{As}{d \cdot b_w} = 0.0071$

Beam self-weight $w_D := \gamma_c \cdot b_w \cdot h = 100 \cdot plf$

Stress block β_1 factor:

$$\beta_1 := \begin{cases} 0.85 & \text{if } f'c \le 4ksi \\ \left(1.05 - 0.05 \cdot \frac{f'c}{ksi}\right) & \text{if } f'c > 4ksi \wedge f'c < 8ksi \\ 0.65 & \text{if } f'c \ge 8ksi \end{cases} \qquad \beta_1 = 0.845$$

Distance from extreme compression fiber to N.A.:

$$c := \frac{As \cdot fy}{0.85 \cdot f'c \cdot b_w \cdot \beta_1} \qquad c = 1.155\,in$$

Nominal Moment Capacity:

$$Mn := As \cdot fy \cdot \left(d - \frac{\beta_1 \cdot c}{2}\right) \qquad Mn = 20.45 \cdot kip \cdot ft$$

Nominal Shear Capacity

$$Vn := 2\sqrt{f'c \cdot psi} \cdot b_w \cdot (d) + \frac{2 \cdot A_{stirrup} \cdot fy \cdot d}{s_s} \qquad Vn = 18.831 \cdot kip$$

Third-Point load required to generate nominal moment:

$$Pm := \left(Mn - \frac{w_D \cdot L^2}{8}\right) \cdot \frac{3}{L} \qquad Pm = 5.164 \cdot kip$$

Actuator load: $P_{m\_act} := 2 \cdot Pm \qquad P_{m\_act} = 10.327 \cdot kip$

Third-Point load required to generate nominal shear:

$$Pv := Vn - \frac{w_D \cdot L}{2} \qquad Pv = 18.281 \cdot kip$$

Actuator load: $P_{v\_act} := 2 \cdot Pv \qquad P_{v\_act} = 36.562 \cdot kip$

A.3 Service Load and Anticipated Capacity of non-Strengthened Flexural Strength Test Specimen Design Calculations

Beam span (center-line to center-line of support) $L := 11ft$

Beam width $b := 12in$

Beam depth $h := 8in$

Concrete compressive strength $f'c := 4100psi$

$$\beta_1 := 1.05 - 0.05 \cdot \frac{f'c}{1000psi} = 0.85$$

Concrete MoE $$Ec := 57000psi \sqrt{\frac{f'c}{psi}} = 3650 \cdot ksi$$

Steel yield strength $fy := 60ksi$

Steel MoE $Es := 29000ksi$

Reinforcement clear cover $clr := 1.5in$

Depth to reinforcement $d := h - clr = 6.5 \cdot in$

Area of reinforcemening steel (2 #5 bars) $As := 0.62in^2$

Distributed dead weight of beam $w_D := 150pcf \cdot b \cdot h = 100 \cdot plf$

Dead load moment $$M_D := \frac{w_D \cdot L^2}{8} = 1.5 \cdot kip \cdot ft$$

Cracking Moment Load:

Rupture stress $$fr := 6psi \cdot \sqrt{\frac{f'c}{psi}} = 384\,psi$$

Modular ratio $$n_s := \frac{Es}{Ec} = 7.946$$

Transformed steel area $As_n := (n_s - 1) \cdot As = 4.3 \cdot in^2$

Neutral axis $$y := \frac{b \cdot h \cdot \frac{h}{2} + As_n \cdot clr}{b \cdot h + As_n} = 3.9 \cdot in$$

Moment of Inertia $$I := \frac{b \cdot h^3}{12} + b \cdot h \cdot \left(\frac{h}{2} - y\right)^2 + As_n \cdot (y - clr)^2 = 538 \cdot in^4$$

Cracking moment $$Mcr := \frac{fr \cdot I}{y} = 4.4 \cdot kip \cdot ft$$

Actuator load required in 4-point bend to produce Mcr (less the amount of moment caused by dead weight of the beam)

$$Pcr := 2\cdot\left(Mcr - M_D\right)\cdot\frac{3}{L} = 1.6\cdot kip$$

Service Load:

Given

$$y_{cr} := 1in$$

$$0 = b\cdot\left(d - y_{cr}\right)\cdot\frac{\left(d - y_{cr}\right)}{2} - n_s\cdot As\cdot y_{cr}$$

$$y_{cr} := \text{Find}\left(y_{cr}\right) = 4.564\cdot in$$

Depth of uncracked concrete

$$c := d - y_{cr} = 1.936\cdot in$$

Cracked moment of inertia

$$I_{cr} := \frac{b\cdot c^3}{12} + b\cdot c\cdot\left(\frac{c}{2}\right)^2 + n_s\cdot As\cdot y_{cr}^{\ 2} = 131.6\cdot in^4$$

Concrete elastic limit

$$fc := 0.45\cdot f'c = 1845\,psi$$

Service Moment

$$Ms := \frac{fc\cdot I_{cr}}{c} = 10.5\cdot kip\cdot ft$$

Actuator load required in 4-point bend to produce Ms (less the amount of moment caused by dead weight of the beam)

$$Ps := 2\cdot\left(Ms - M_D\right)\frac{3}{L} = 4.9\cdot kip$$

Failure Load:

Depth of stress block

$$a := \frac{As\cdot fy}{0.85\cdot f'c\cdot b} = 0.89\cdot in$$

Nominal moment capacity

$$Mn := As\cdot fy\cdot\left(d - \frac{a}{2}\right) = 18.8\cdot kip\cdot ft$$

Actuator load required in 4-point bend test

$$P := 2\cdot\left(Mn - M_D\right)\cdot\frac{3}{L} = 9.4\cdot kip$$

Service modulus of rupture

$$fr := 7.5\cdot\sqrt{\frac{f'c}{psi}}\cdot psi = 480.2\,psi$$

Service cracking moment

$$Mcr_s := \frac{fr\cdot b\cdot h^3}{12}\cdot\frac{2}{h} = 5.1\cdot kip\cdot ft$$

Effective moment of inertia

$$Ie := \min\left[\left(\frac{Mcr_s}{Mn}\right)^3\cdot\frac{b\cdot h^3}{12} + \left[1 - \left(\frac{Mcr_s}{Mn}\right)^3\right]\cdot I_{cr}, \frac{b\cdot h^3}{12}\right] = 139.4\cdot in^4$$

A.4 Anticipated Capacity of GC45-Strengthened Flexural Strength Test Specimen Calculations

Assumed Beam Properties: fy = 60ksi, As = 0.62in^2

FRP width $b_f := 4in$

FRP depth $t_f := 0.22in$

FRP area $Af := b_f \cdot t_f = 0.88 \cdot in^2$

Depth to FRP $d_f := h + \frac{t_f}{2} = 8.11 \cdot in$

FRP MoE $Ef := 4500ksi$

FRP ultimate stress $f_{fu} := 71ksi$

Strain in concrete under dead load $\varepsilon_{bi} := \frac{M_D \cdot y}{I \cdot Ec} = 3.6 \times 10^{-5}$

Stress & Strain equations

$$\varepsilon_f(c) := 0.003 \cdot \left(\frac{d_f - c}{c} \right)$$

$$f_f(c) := Ef \cdot \varepsilon_f(c)$$

$$\varepsilon_s(c) := \min\left[\frac{fy}{Es}, \left(\varepsilon_f(c) + \varepsilon_{bi}\right) \cdot \left(\frac{d - c}{d_f - c} \right) \right]$$

$$f_s(c) := Es \cdot \varepsilon_s(c)$$

Determine depth to N.A Given $c := 1in$

Depth to neutral axis

$$c = \frac{As \cdot f_s(c) + Af \cdot f_s(c)}{0.85 \cdot f'c \cdot b \cdot \beta_1}$$

$c_{45} := Find(c) = 2.5 \cdot in$

Depth of compression block $a_{45} := c_{45} \cdot \beta_1 = 2.2 \cdot in$

Stress in steel at failure $f_s(c_{45}) = 60 \cdot ksi$

Stress in FRP at failure $f_f(c_{45}) = 29.49 \cdot ksi$

Moment Capacity $M_{45} := As \cdot f_s(c_{45}) \cdot \left(d - \frac{a_{45}}{2} \right) + Af \cdot f_f(c_{45}) \cdot \left(d_f - \frac{a_{45}}{2} \right) = 32.0 \cdot kip \cdot ft$

Actuator load required in 4-point bend test $P_{45} := 2 \cdot \left(M_{45} - M_D\right) \cdot \frac{3}{L} = 16.6 \cdot kip$

As-Built Beam Properties:

$fy := 74.2ksi \qquad As := 2 \cdot 0.275in^2$

FRP width $b_f := 4in$

FRP depth $t_f := 0.22in$

FRP area $Af := b_f \cdot t_f = 0.88 \cdot in^2$

Depth to FRP $d_f := h + \frac{t_f}{2} = 8.11 \cdot in$

FRP MoE $Ef := 4500ksi$

FRP ultimate stress $f_{fu} := 71ksi$

Strain in concrete under dead load $\varepsilon_{bi} := \frac{M_D \cdot y}{I \cdot Ec} = 3.6 \times 10^{-5}$

Stress & Strain equations

$$\varepsilon_f(c) := 0.003 \cdot \left(\frac{d_f - c}{c} \right)$$

$$f_f(c) := Ef \cdot \varepsilon_f(c)$$

$$\varepsilon_s(c) := \min\left[\frac{fy}{Es}, \left(\varepsilon_f(c) + \varepsilon_{bi}\right) \cdot \left(\frac{d - c}{d_f - c} \right) \right]$$

$$f_s(c) := Es \cdot \varepsilon_s(c)$$

Determine depth to N.A

Given

$c := 1in$

Depth to neutral axis

$$c = \frac{As \cdot f_s(c) + Af \cdot f_s(c)}{0.85 \cdot f'c \cdot b \cdot \beta_1}$$

$c_{45} := Find(c) = 3 \cdot in$

Depth of compression block $a_{45} := c_{45} \cdot \beta_1 = 2.5 \cdot in$

Stress in steel at failure $f_s(c_{45}) = 74.2 \cdot ksi$

Stress in FRP at failure $f_f(c_{45}) = 22.96 \cdot ksi$

Moment Capacity $M_{45} := As \cdot f_s(c_{45}) \cdot \left(d - \frac{a_{45}}{2} \right) + Af \cdot f_f(c_{45}) \cdot \left(d_f - \frac{a_{45}}{2} \right) = 29.3 \cdot kip \cdot ft$

Actuator load required in 4-point bend test $P_{45} := 2 \cdot \left(M_{45} - M_D\right) \cdot \frac{3}{L} = 15.2 \cdot kip$

A.5 Anticipated Capacity of GC90-Strengthened Flexural Strength Test Specimen Calculations

Assumed Beam Properties: fy = 60ksi, As = 0.62in^2

FRP width		$b_f := 4in$
FRP depth		$t_f := 0.21in$
FRP area		$Af := b_f \cdot t_f = 0.84 \cdot in^2$
Depth to FRP		$d_f := h + \frac{t_f}{2} = 8.105 \cdot in$
FRP MoE		$Ef := 5600ksi$
FRP ultimate stress		$f_{fu} := 87ksi$
Strain in concrete under dead load		$\varepsilon_{bi} := \frac{M_D \cdot y}{I \cdot Ec} = 3.6 \times 10^{-5}$
Stress & Strain equations		$\varepsilon_f(c) := 0.003 \cdot \left(\frac{d_f - c}{c} \right)$
		$f_f(c) := Ef \cdot \varepsilon_f(c)$
		$\varepsilon_s(c) := \min\left[\frac{fy}{Es}, \left(\varepsilon_f(c) + \varepsilon_{bi}\right) \cdot \left(\frac{d - c}{d_f - c} \right) \right]$
		$f_s(c) := Es \cdot \varepsilon_s(c)$
Determine depth to N.A	Given	$c := 1in$
Depth to neutral axis		$c = \frac{As \cdot f_s(c) + Af \cdot f_s(c)}{0.85 \cdot f'c \cdot b \cdot \beta_1}$
		$c_{90} := Find(c) = 2.5 \cdot in$
Depth of compression block		$a_{90} := c_{90} \cdot \beta_1 = 2.1 \cdot in$
Stress in steel at failure		$f_s(c_{90}) = 60 \cdot ksi$
Stress in FRP at failure		$f_f(c_{90}) = 38.13 \cdot ksi$
Moment Capacity		$M_{90} := As \cdot f_s(c_{90}) \cdot \left(d - \frac{a_{90}}{2} \right) + Af \cdot f_f(c_{90}) \cdot \left(d_f - \frac{a_{90}}{2} \right) = 35.7 \cdot kip \cdot ft$
Actuator load required in 4-point bend test		$P_{90} := 2 \cdot \left(M_{90} - M_D\right) \cdot \frac{3}{L} = 18.7 \cdot kip$

As-Built Beam Properties: $fy := 74.2ksi$ $As := 2 \cdot 0.275in^2$

FRP width $b_f := 4in$

FRP depth $t_f := 0.21in$

FRP area $Af := b_f \cdot t_f = 0.84 \cdot in^2$

Depth to FRP $d_f := h + \frac{t_f}{2} = 8.105 \cdot in$

FRP MoE $Ef := 5600ksi$

FRP ultimate stress $f_{fu} := 87ksi$

Strain in concrete under dead load $\varepsilon_{bi} := \frac{M_D \cdot y}{I \cdot Ec} = 3.6 \times 10^{-5}$

Stress & Strain equations

$$\varepsilon_f(c) := 0.003 \cdot \left(\frac{d_f - c}{c} \right)$$

$$f_f(c) := Ef \cdot \varepsilon_f(c)$$

$$\varepsilon_s(c) := \min\left[\frac{fy}{Es}, \left(\varepsilon_f(c) + \varepsilon_{bi}\right) \cdot \left(\frac{d - c}{d_f - c} \right) \right]$$

$$f_s(c) := Es \cdot \varepsilon_s(c)$$

Determine depth to N.A Given $c := 1in$

$$c = \frac{As \cdot f_s(c) + Af \cdot f_s(c)}{0.85 \cdot f'c \cdot b \cdot \beta_1}$$

Depth to neutral axis $c_{90} := Find(c) = 2.9 \cdot in$

Depth of compression block $a_{90} := c_{90} \cdot \beta_1 = 2.5 \cdot in$

Stress in steel at failure $f_s(c_{90}) = 74.2 \cdot ksi$

Stress in FRP at failure $f_f(c_{90}) = 29.85 \cdot ksi$

Moment Capacity $M_{90} := As \cdot f_s(c_{90}) \cdot \left(d - \frac{a_{90}}{2} \right) + Af \cdot f_f(c_{90}) \cdot \left(d_f - \frac{a_{90}}{2} \right) = 32.3 \cdot kip \cdot ft$

Actuator load required in 4-point bend test $P_{90} := 2 \cdot \left(M_{90} - M_D\right) \cdot \frac{3}{L} = 16.8 \cdot kip$

APPENDIX B.

REBAR STRAINS UNDER INITIAL LOADING OF FLEXURAL STRENGTH TEST SPECIMEN

Flexural strength test specimens were subjected to an initial loading regimen to produce flexural cracks and introduce service level strains into the steel rebar. The following figures are load-strain plots for the instrumented internal longitudinal reinforcement as detailed in Chapter 5.

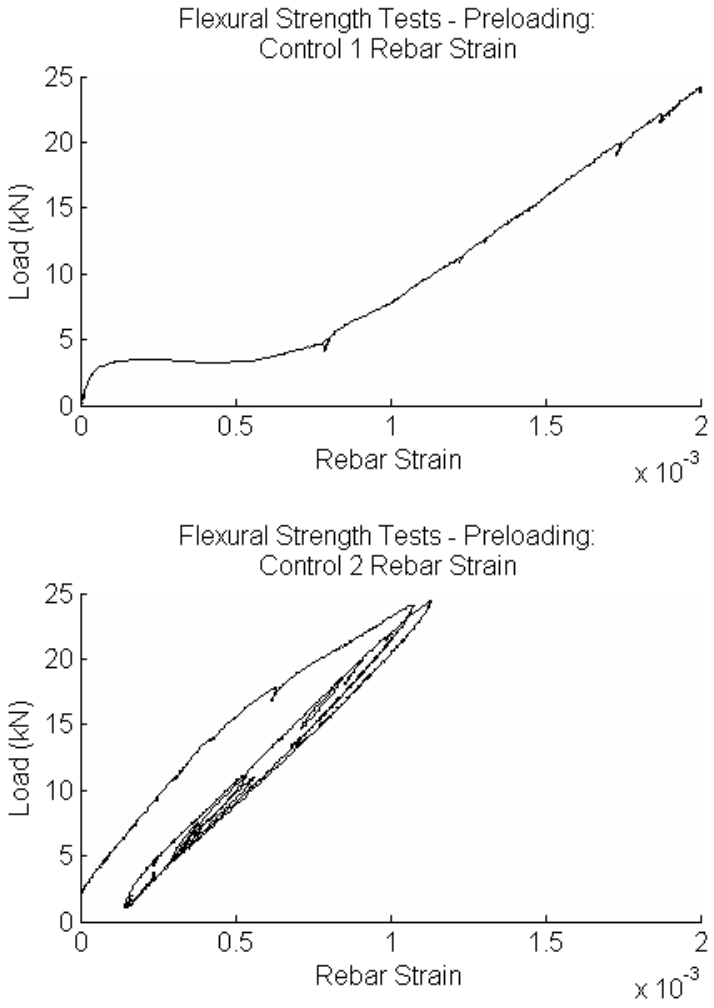

Figure B.1: Control specimen rebar strains under flexural strength test preloading

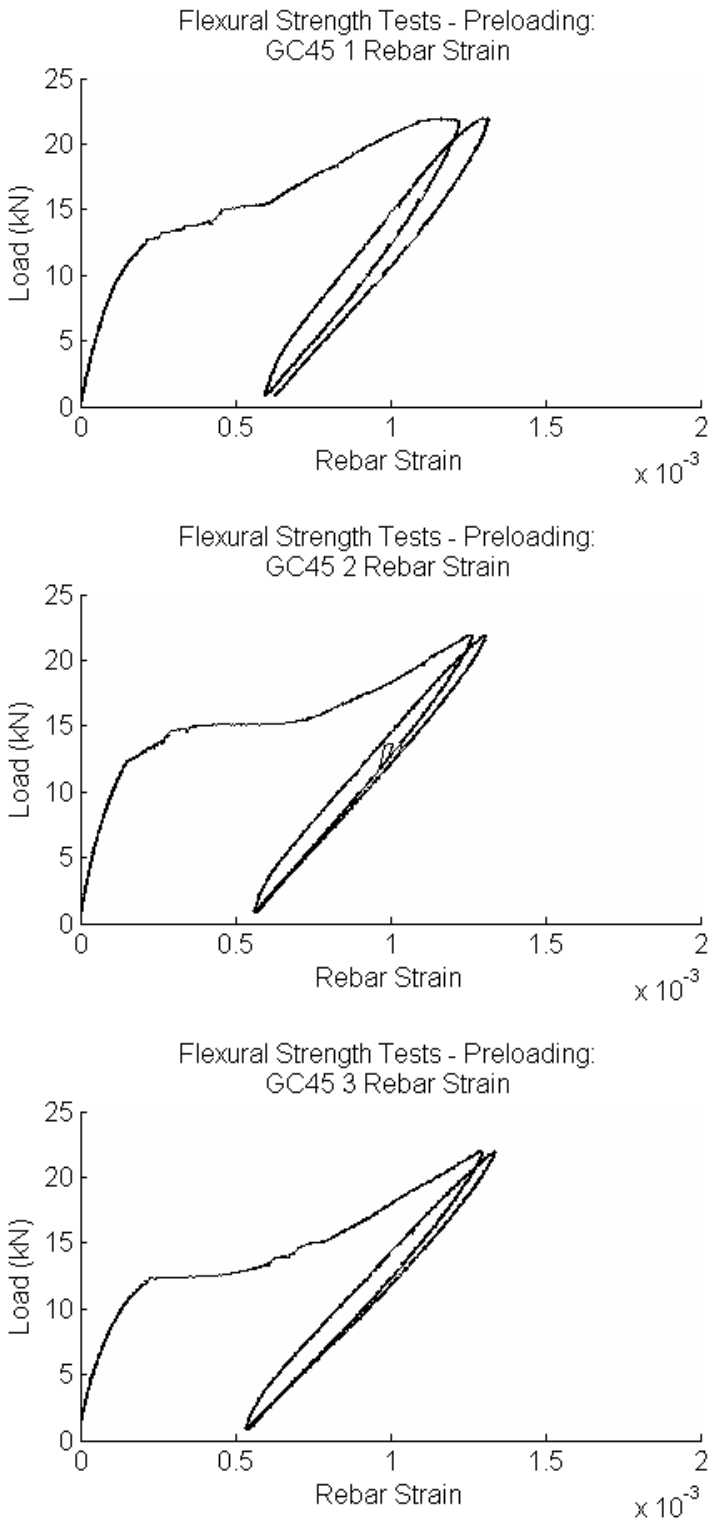

Figure B.2: Control specimen rebar strains under flexural strength test preloading

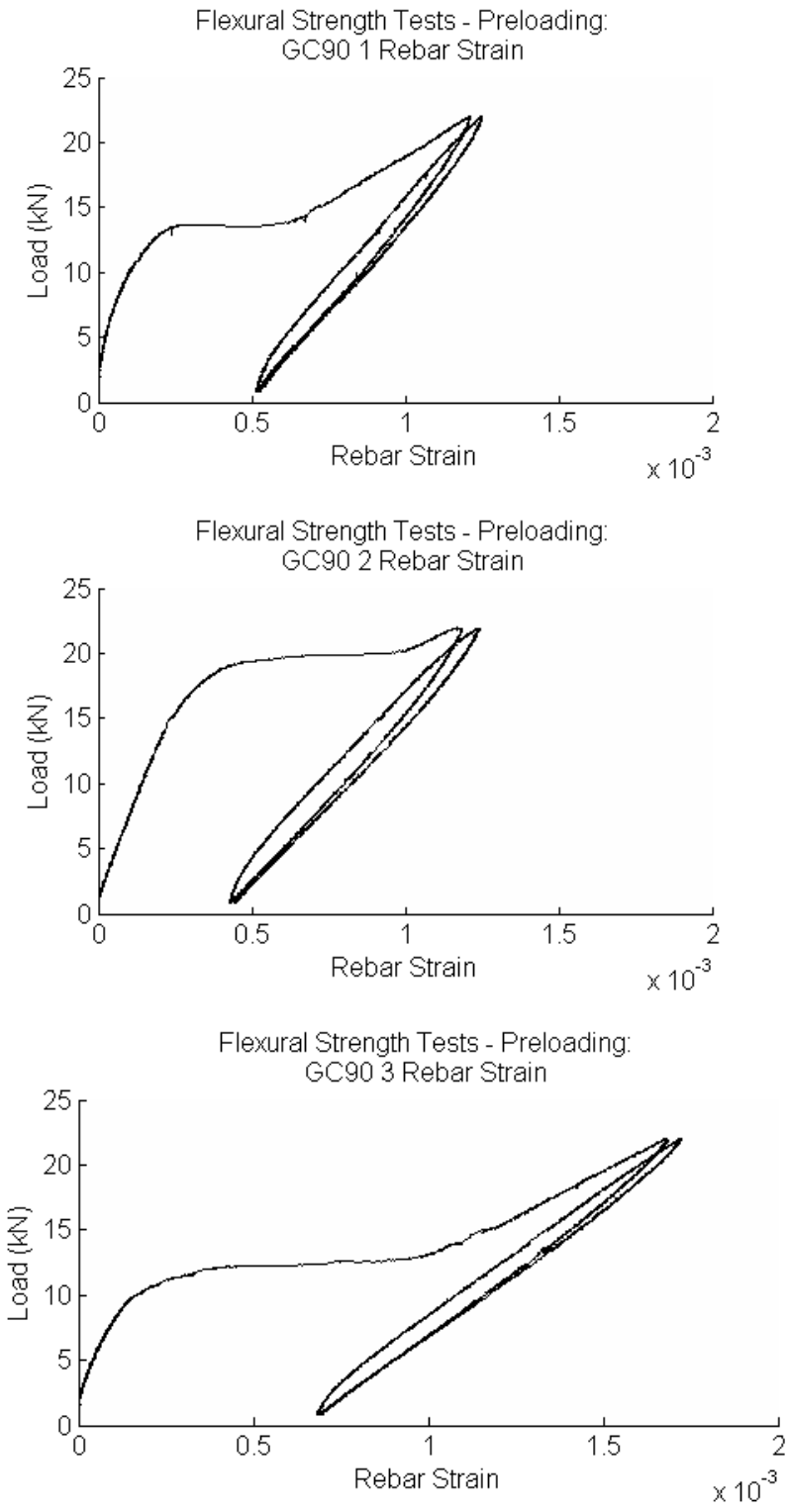

Figure B.3: Control specimen rebar strains under flexural strength test preloading

APPENDIX C.

FRP LOAD-STRAIN PLOTS FOR FLEXURAL STRENGTH TESTS

The following plots show the strain recorded by the eight strain gages attached to each FRP strip used to strengthen a steel-reinforced concrete beam over the loading duration to failure. Details pertaining to the position of each gage can be found in Chapter 5. It should be noted in tests of GC90 2 and GC90 3, data collection was terminated prior to the unloading of the beam specimen; therefore, the load-strain graphs for these specimens do not show the unloading portion of the test (see Figure I.2).

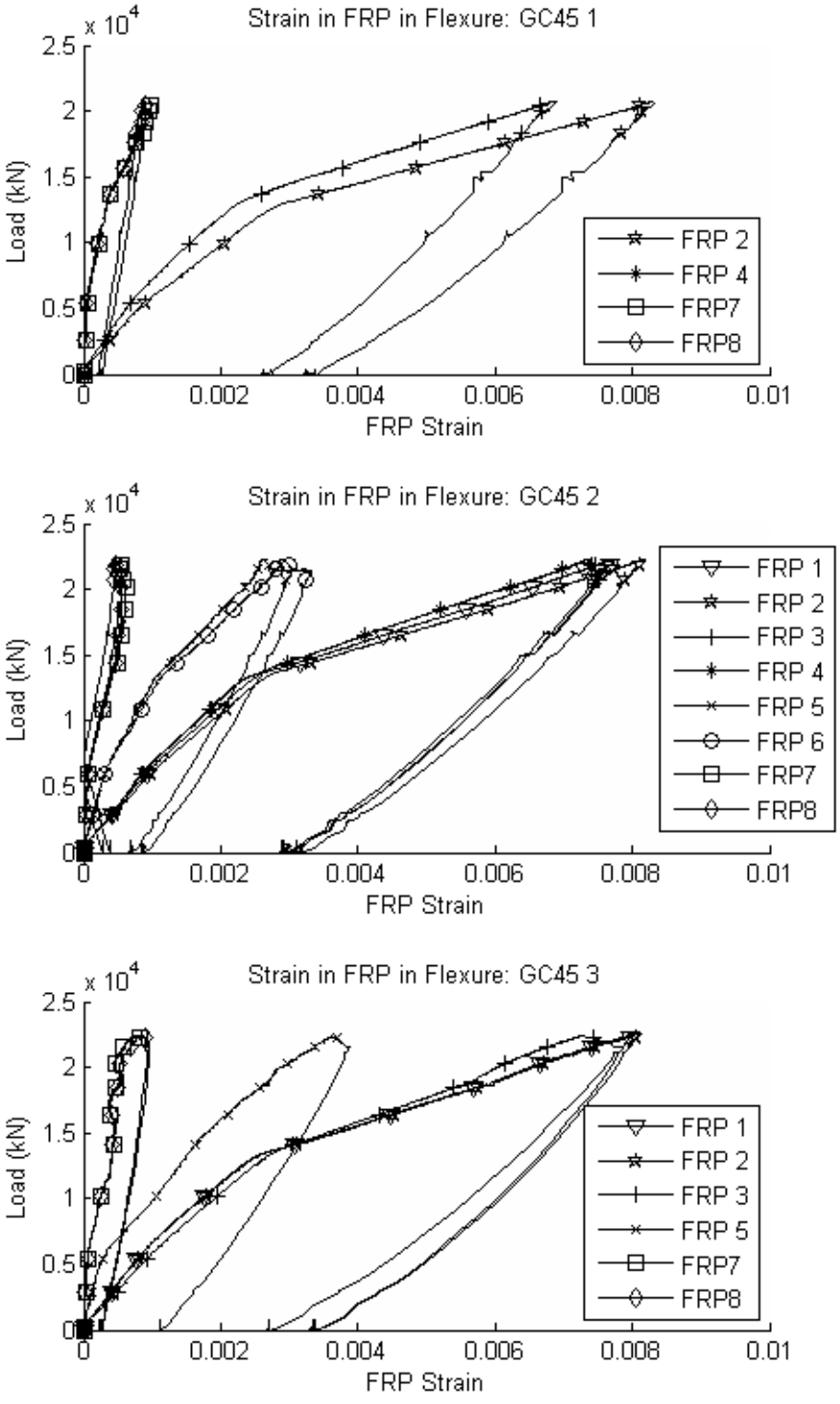

Figure C.1: Strain GC45-FRP during flexural testing failure loading

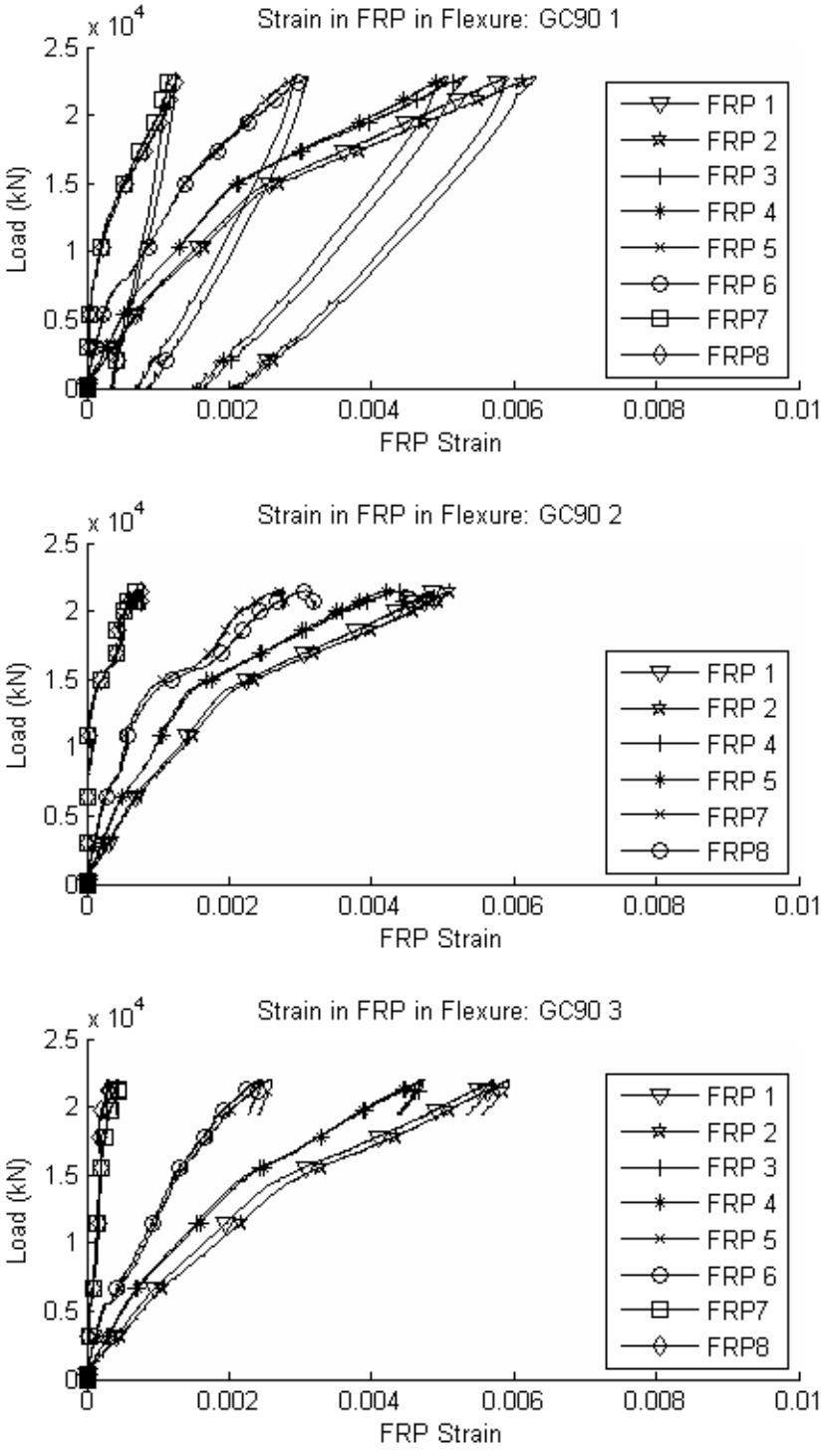

Figure C.2: Strain in GC90-FRP during flexural testing failure loading

Bridge Safety Project

Task 4 (Deliverable 4): FRP Flexural Retrofit Environmental Durability Testing and Analysis

5/17/2013

Hannah Breton, M.S. Candidate in Civil and Environmental Engineering
Bill Davids, PhD, PE, John C. Bridge Professor and Chair of Civil and Environmental Engineering

University of Maine Advanced Structures and Composites Center and Department of Civil and Environmental Engineering

Table of Contents

Introduction

This document is an engineering report for the Maine Department of Transportation (MaineDOT) satisfying deliverable 4 from Task 4 for the UMaine Advanced Structures and Composites Center Bridge Safety project funded by MaineDOT. This report details the fiber-reinforced polymer (FRP) systems manufactured for use in this study:

- The design of post-tensioned concrete test specimens for use in durability analysis;
- The exposure protocols for extreme environmental durability simulation;
- The test method and data analysis of durability specimen in tension-bearing loading; and
- Conclusions of durability results; and

The four FRP systems proposed in Deliverable 2 (Breton & Davids, 2012) and used in this study were manufactured by Kenway Corp. and delivered to the Advanced Structures and Composites Center. These systems included two all-glass systems with unidirectional glass fiber outer layers and a twill woven glass-fabric core layer oriented at 0°/90° or ±45° to the longitudinal axis (denoted as GG90 and GG45, respectively) and two glass-carbon hybrid systems with unidirectional glass outer layers and plain woven carbon-fabric core layers oriented at 0°/90° or ±45° to the longitudinal axis (denoted as GC90, GC45, respectively). The FRP panels were cut into test specimen coupons for use in mechanical strength tensile tests or environmental durability tension-bearing tests.

Environmental durability test specimens were subjected to 1000 and 3700 hours of submersion in saltwater or 20 freeze-thaw cycles and then destructively tested to determine the maximum sustained load and average peak sustained load. Results from environmentally conditioned specimens were compared to those of control specimens to determine the percent strength retention following exposure. The GG90 and GG45 systems did not pass the acceptability criteria as outlined in the durability plan provided in Deliverable 2 (Breton & Davids, 2012). Acceptability criterion state that 1000 hour saltwater and freeze-thaw exposed test specimens must retain 90% of the control specimens' strength and 3000 hour saltwater exposed test specimens must retain 85% of the control specimens' strength. Based on the results of the 1000 hour saltwater and freeze-thaw exposure condition testing and the outlined acceptability criteria, the GC90 and GC45 systems were selected for use in forthcoming small beam four-point bend tests.

Project Background

As reported in deliverable 2 of Task 4, the proposed FRP retrofit systems are to be subjected to environmental durability regimens to assess their ability to withstand extreme exposure to deicing salt and freeze-thaw cycling.

Deliverable 2 of Task 4 (Breton & Davids, 2012) contained proposed design alterations to the original FRP flexural rehabilitation design detailed in Deliverable 1 of Task 4 (Breton & Davids,

2012). The two systems consisted of (1) a woven carbon-fiber fabric reinforced system and (2) a unidirectional glass fiber reinforced system. Bearing capacity of the original design was to be established with the use of steel plates adhered to the FRP. Systems were to be attached using powder actuated fasteners at each steel plate location. Deliverable 2 altered these original designs by proposing unidirectional glass be used tensile strength in the longitudinal direction for all systems and the use of woven fiber material (either glass or carbon) as a core layer for bearing capacity and eliminating the need for steel plates. Further design alterations in addition to those discussed in Deliverable 2 were incorporated into the final design. These additional alterations include substituting stainless steel, epoxy adhered, threaded rod mechanical fasteners for the powder-actuated fasteners and manufacturing the core of each system in two distinct orientations: 0°/90° or ±45° to the longitudinal axis. This section contains details on design alterations and the manufacture, testing, and analysis of the four FRP systems.

Design Alterations

Although not stated within the scope of the proposal, it was determined that the effect of the core fiber orientation on the bearing strength for each system should be evaluated. During the layup of the fibers in the manufacturing process core fibers were oriented at either 0°/90° or ±45° to the longitudinal axis.

It was determined that fatigue of the powder actuated anchors should be evaluated considering their use in a high cyclic fatigue application. After research of literature and a discussion with HILTI, Inc. representatives (July 2012) it was determined that powder actuated nails would not perform well under high cycle fatigue applications. Literature for fatigue of powder actuated nails in concrete could not be found and a HILTI, Inc. representative confirmed that they do not test the fatigue of these anchors due to the small shank diameter of the anchor and the limited anchor embedment depth controlled by the location of steel reinforced in the concrete.

HILTI, Inc. products were again reviewed for a post-installed anchor capable of withstanding high cyclic fatigue in cracked concrete. The HIT-HY 150 MAX-SD fast cure (30 minutes) adhesive anchoring system with stainless steel threaded rod inserts, washers and nuts was selected as the new proposed anchoring system. This anchoring system requires more preparation than the powder actuated nail application due to the need to pre-drill holes in the concrete to insert the adhesive and anchor rod; however, it is applicable in high cyclic fatigue applications and suitable in cracked concrete applications. Additionally, a single adhesive anchor has a higher shear capacity than a single powder actuated nail. This increase in capacity per anchor allows for fewer anchors to be installed in order to develop and transfer the ultimate tensile capacity of the concrete to the FRP. Installation of fewer anchors also reduces the number of holes drilled into the FRP strips and localized stress regions at the holes. Although preparation and installation of the adhesive anchors requires more time and effort than the powder actuated fasteners, fatigue performance was considered more critical to the performance of the systems than reduced installation time.

Project Scope

The scope of deliverable 4 of Task 4 includes the presentation of and discussion on the results of tension-bearing testing of specimen following the execution of the durability plan outlined in deliverable 2.

Intended Use

The results from durability testing are intended to be a means of comparing the performance of the four proposed flexural retrofit systems in order to assist in determining which retrofit systems will be the most effective for us in rehabilitating flat-slab concrete bridges.

FRP Composite Systems

Kenway Corp. of Augusta was provided with a general outline of each FRP systems' material types, layup order and desired layer thicknesses. These outline details were based on assumed material properties and thicknesses used in the preliminary design of the systems. Through collaboration with Kenway Corp. representative Jake Marquis, readily available off-the-shelf materials were located for use in manufacturing. Following the production of FRP systems, mechanical strength testing following ASTMD3039 (ASTM, A.S.f.T.M., 2008) was performed on each system to determine the actual maximum tensile strength, stress, and chord modulus of elasticity The following sections provide details on the materials and procedures used for manufacturing the FRP systems and the test methods and results of mechanical strength testing.

Manufacturing Materials and Procedure

Fiberglass Industries (FGI) SW1900 18oz./yd^2 stitched, chopped core, unidirectional glass fiber layers were used for the outer unidirectional laminate layers for all systems (Figure 1 and Figure 2: layers 1-2, 10-11; Figure 3 and Figure 4: layers 1-4, 6-9). Vectorply E-LR 1208 12oz./yd^2 stitched, unidirectional E-glass fibers were used for the inner unidirectional laminate layers for the carbon core systems, GC90 and GC45 (Figure 1 and Figure 2: layers 3-4, 8-9). FGI ROVCLOTH® CPS-409 twill woven, 27 oz./yd^2 glass fiber fabric was for the core of the glass core systems, GG90 and GG45 (Figure 3 and Figure 4: layer 5). JB Martin TC-12-P plain woven, 12 oz./yd^2 carbon fiber fabric was used for the core of GC90 and GC45 (Figure 1 and Figure 2: layers 5-7). All systems were infused using EPOVIA® KAYAK KF3202l-00 toughened epoxy vinyl ester infusion resin. Panel layup schedules are illustrated in Figure 1-Figure 4. Technical data sheets for all fabrics and resin, panel layup schedules, and panel infusion layups are included in APPENDIX A.

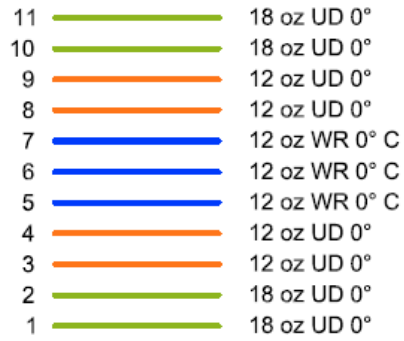

Figure 1: GC90 Layup Schedule

Figure 2: GC45 Layup Schedule

Figure 3: GG90 Layup Schedule

Figure 4: GG45 Layup Schedule

Difficulties were encountered during the infusion process involving the carbon core panels that resulted in portions of the panel not fully wetting out. Kenway Corp. cut out these dry portions of the panels prior to delivery, and panel area sufficient for the testing program was still available.

Mechanical Strength Property Testing

Specimen coupons for all FRP layups were put through tensile testing according to ASTM D3039 (ASTM, A.S.f.T.M., 2008) to determine ultimate tensile strengths and tensile chord moduli of elasticity. These mechanical properties are used to more accurately characterize the behavior of a retrofitted reinforced concrete beam based on the true properties of the composite.

Test Specimen

Coupons measuring 25.4 × 254mm (1 × 10in) were machine cut using a Flow, Inc. waterjet cutter. A number of coupons were damaged during the machine cutting process due to the programmed cut path. Cutting was initiated at the mid-point of the long edge of the specimen. The puncture force of the waterjet stream when making the first cut through the face of the FRP caused the delamination of lamina layers. Figure 5 depicts an acceptable coupon and a coupon damaged from cutting. Specimens damaged in this manner were deemed unacceptable for use in tensile testing. The programmed cut path was altered to prevent further damage of specimen in this manner by initiating cutting at an outer, sacrificial edge of the FRP panel.

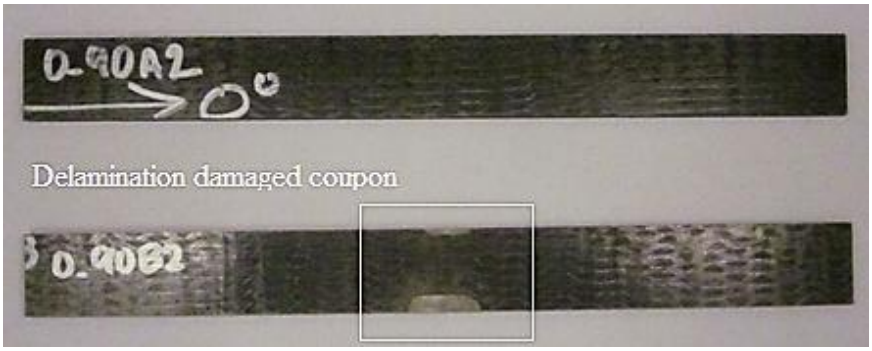

Figure 5: Undamaged FRP Tensile Test Coupon (top); Cutting Damaged FRP Tensile Test Coupon (bottom)

To distinguish the core fiber orientation of specimen, immediately following cutting, coupons were labeled "0_90" for 0°/90° oriented core fibers or "0_45" for ±45° oriented core fibers. Labeling coupons with their core fiber material type was forgone due to the distinct color differences between the systems. The black carbon fibers gave the carbon core systems dark gray color, while the glass core systems were opaque beige in color.

In accordance with ASTM D3039 (2008), the width and thickness of each test specimen was measured at three locations prior to testing. The average, standard deviation and coefficient of variation for the width, thickness, and cross-sectional area of specimen that failed by an acceptable failure more are reported in Table 1. For individual measurements, see APPENDIX B.

Table 1: ASTM D3039 Test Specimen Dimensions

	FRP System	GG90	GG45	GC90	GC45
Width mm (in)	*Avg.*	25.1 (0.992)	25.4 (1.00)	24.8 (0.978)	25.3 (0.995)
	STD	0.073 (0.0029)	0.089 (0.0035)	0.053 (0.0021)	0.097 (0.0038)
	COV (%)	0.3	0.4	2.1	0.4
Thickness mm (in)	*Avg.*	5.20 (0.205)	5.59 (0.220)	4.90 (0.193)	5.08 (0.200)
	STD	0.122 (0.0048)	0.064 (0.0025)	0.076 (0.0030)	0.224 (0.0045)
	COV (%)	2.3	1.1	1.5	2.3
Area mm^2 (in^2)	*Avg.*	5.17 (0.204)	5.35 (0.216)	4.89 (0.188)	4.97 (0.196)
	STD	0.139 (0.0055)	0.069 (0.0027)	0.109 (0.0043)	0.118 (0.0047)
	COV (%)	2.7	1.3	2.3	2.4

Test Method

Specimens were placed in the actuator grips and vertically aligned. The grips were closed and the grip pressure recorded. If a tested specimen failed by an undesirable grip failure, the grip pressure was adjusted accordingly for the next test. A 50.8mm (2in) gauge length extensometer was clipped to the specimen to digitally measure strain (Figure 6). Tape was adhered to the specimen to provide a gripping surface for the extensometer clips. Specimens were monotonically loaded in tension to failure at a displacement rate of 1.27mm/min (0.05 in/min) under a 100kN (22 kip) load cell. Ultimate load, actuator position, and extensometer strain were collected during testing.

Figure 6: ASTM D3039 FRP coupon tensile strength testing setup

Initially, grip tabs were adhered to the coupons using Pliogrip 7779 adhesive from Ashland, Inc. During initial testing, it was found the adhesive was not able to transfer the load from the actuator grips to the specimen. This was observed through the slip of the grip tabs. It was later determined that the adhesive used had expired. Tabs were removed from all coupons and testing proceeded with untabbed specimens.

Results

Due to the hybrid nature of the composite systems, the failure modes identified in ASTM D3039 were not fully applicable to the failure modes exhibited during testing. Acceptable primary failure modes include fiber rupture and matrix cracking (

Figure 7) or longitudinal splitting within the gauge length (

Figure 8). The presence of delamination between layers in accompaniment with any of these primary failures was also an acceptable failure mode (Figure 9). The combination of primary failure modes was also accepted. Unacceptable failure modes include grip slip (Figure 10), lateral failure at the grip (

Figure 11), specimen splitting within the grips (Figure 12), fiber rupture and matrix cracking within the grips (Figure 13), and delamination of the outer glass layer from the core layer without the presence of other failure modes (not pictured).

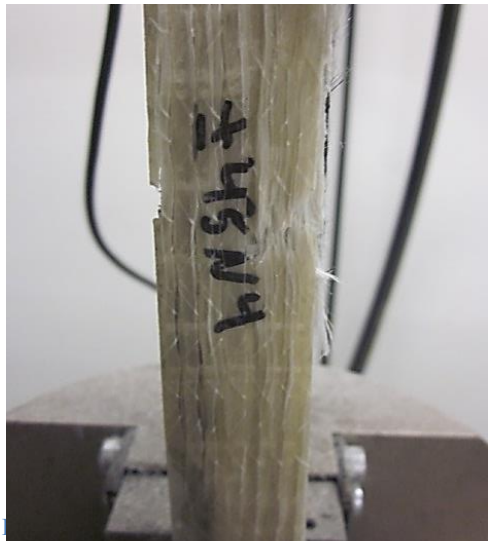

Figure 9: Lateral splitting at grips resulting in longitudinal splitting

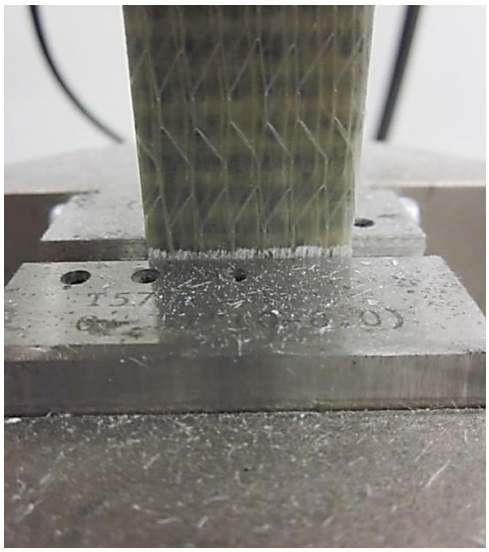

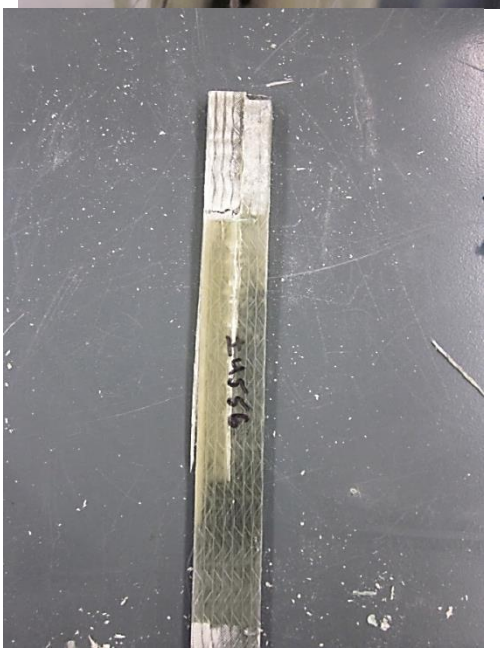

Figure 11: Lateral splitting at grips resulting in longitudinal splitting

Figure 13: Fiber rupture within grips

The failure modes of each coupon and the acceptability of the failure for use of the data in strength calculations are provided in APPENDIX C. Acceptable failures are denoted with an 'A' in the tables, while not accepted failures are denoted with an 'N'. In several instances, the data collected from the extensometer provided noisy results (see Figure 14) due to slippage of the extensometer clips. This occurred in both the GG090 and GC45 data sets. Data exhibiting this behavior was excluded from the average strength calculations in favor of smoother stress-strain curves (see Figure 15). All stress-strain plots are provided in APPENDIX D

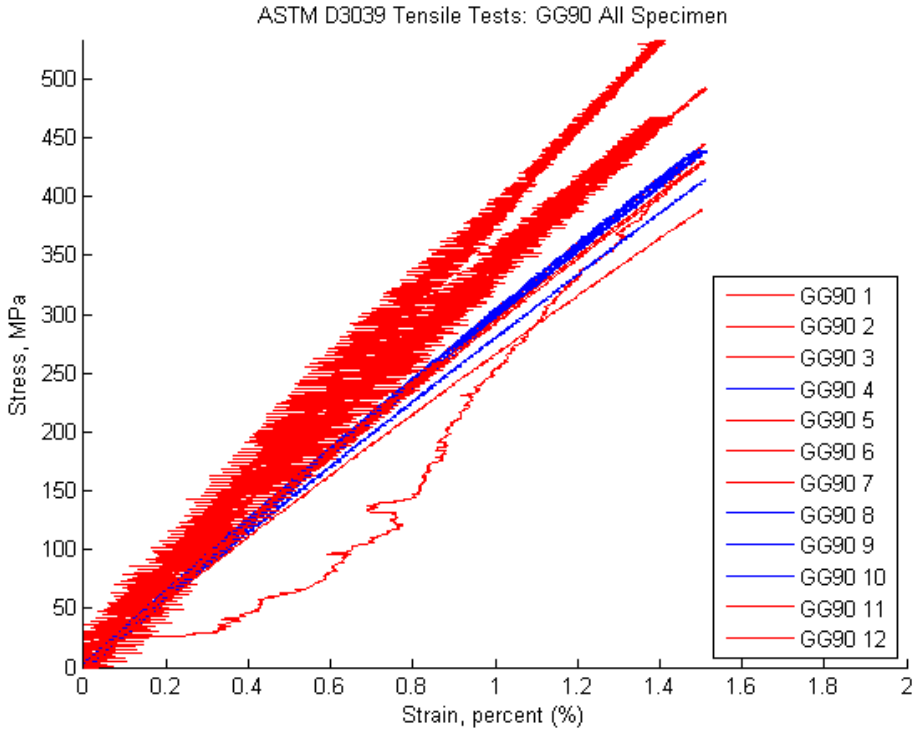

Figure 14: GG90 stress vs. strain plot with noisy strain data

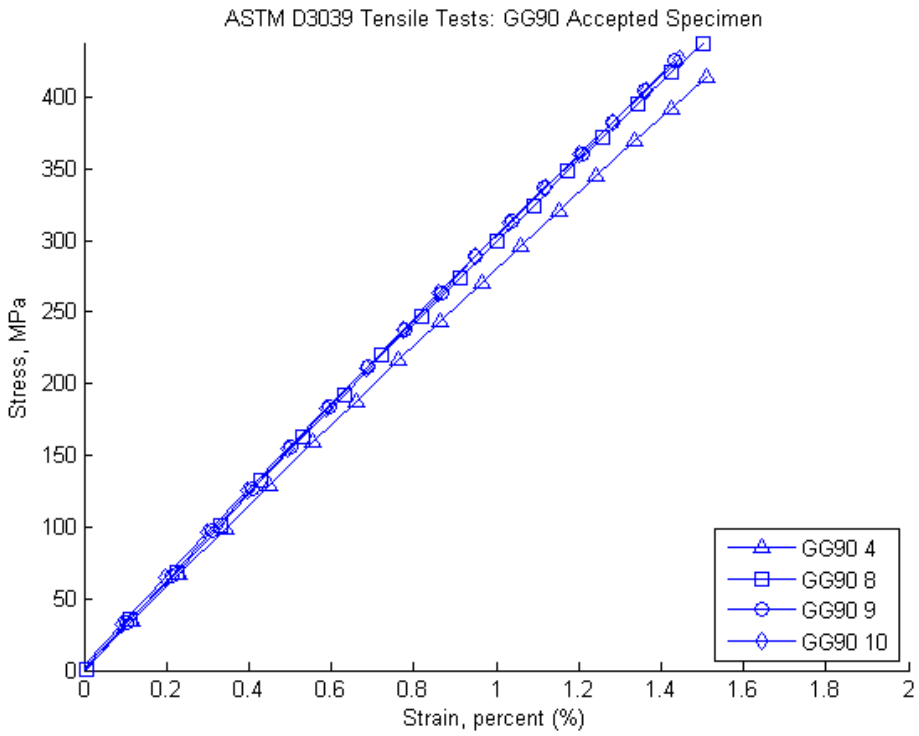

Figure 15: GG90 stress vs. strain plot of accepted specimens only

Following testing, the tensile chord modulus of elasticity, maximum load, and maximum tensile strength for each specimen was determined. Maximum tensile strength is defined by ASTM D3039 (2008) as the maximum force before failure divided by the cross-sectional area of the test specimen (see (Equation **1**).

$$F^{tu} = P^{max}/A \qquad \text{(Equation 1)}$$

Where:

F^{tu} = ultimate tensile strength, MPa (psi);

P^{max} = maximum force before failure, N (lbf);

A = average cross-sectional area, mm^2 ($in.^2$)

The tensile chord modulus of elasticity is defined by ASTM D3039 (2008) as the slope of the stress-strain data calculated between the points of 1000με and 3000με $E^{chord} = \Delta\sigma/\Delta\varepsilon$ (Equation **2**). Since strain data was collected digitally using an extensometer, the data points closest to the range end points were used in the calculation:

$$E^{chord} = \Delta\sigma/\Delta\varepsilon \qquad \text{(Equation 2)}$$

Where:

E^{chord} = tensile chord modulus of elasticity, MPa (psi);

$\Delta\sigma$ = difference in applied tensile stress between the two strain range end points;

$\Delta\varepsilon$ = difference between the two strain range end points (nominally 0.002).

The maximum load, maximum tensile strength and tensile chord modulus of elasticity for each accepted specimen are provided in Table 2. Calculated values for individual tests and stress-strain plots are provided in APPENDIX E

Table 2: FRP System Mechanical Properties

FRP System		GG90 (4)*	GG45 (9)*	GC90 (8)*	GC45 (8)*
Max. Load kN (kip)	*Avg.*	74.7 (16.8)	70.3 (15.8)	73.4 (16.5)	64.1 (14.4)
	STD	4.11 (0.924)	1.37 (0.307)	3.15 (0.707)	4.47 (1.01)
	COV (%)	5.5	1.9	4.3	7.0
Max. Tensile Stress MPa (ksi)	*Avg.*	568 (82.4)	507 (73.5)	605 (87.7)	509 (73.8)
	STD	28.1 (4080)	14.7 (2130)	27.1 (3930)	35.2 (5100)
	COV (%)	5.0	2.9	4.5	6.9
Elastic Modulus MPa (ksi)	*Avg.*	30400 (4408)	30200 (4384)	39000 (5660)	29800 (4329)
	STD	2359 (341)	3500 (507.1)	3720 (539)	2220 (322)
	COV (%)	7.7	12	9.5	7.4

*Number of specimens used in calculations

Conclusions

The existing flexural capacity per unit width of the design bridge is 307 kN-m/m (69.0 kip-ft/ft). Based on the mechanical strength properties determined through tensile testing in accordance with ASTM D3039 (2008) and flexural capacity equations provided by ACI (2008)

$\boldsymbol{M_n = A_s f_s \left(d - \frac{\beta_1 c}{2}\right) + \psi_f A_f f_{fe} \left(d_f - \frac{\beta_1 c}{2}\right)}$ (Equation **3**) the idealized anticipated increase in flexural capacity % $\boldsymbol{Capacity\ Increase = \frac{M_n - M_{n,existing}}{M_{n,existing}} \times 100\%}$ (Equation **4**) of the design bridge was determined for each system type (see Table 3).

$$\boldsymbol{M_n = A_s f_s \left(d - \frac{\beta_1 c}{2}\right) + \psi_f A_f f_{fe} \left(d_f - \frac{\beta_1 c}{2}\right)} \quad \text{(Equation 3)}$$

Where:

M_n = flexural capacity of FRP reinforced section, kN-m/m (lbf-in/in)

A_s = area of nonprestressed steel reinforcement, mm^2 (in^2)

f_s = stress in nonprestressed steel reinforcement, MPa (psi)

d = distance from extreme compression fiber to centroid of tension reinforcement, mm (in)

β_1 = ratio of depth of equivalent rectangular stress block to depth of the neutral axis

c = distance from extreme compression fiber to the neutral axis, mm (in)

ψ_f = FRP strength reduction factor; 0.85 for flexure

A_f = area ofFRP external reinforcement, mm^2 (in^2)

f_{fe} = effective stress in the FRP; stress level attained at section failure, MPa (psi)

d_f = effective depth of FRP flexural reinforcement, mm (in)

$$\%\ \boldsymbol{Capacity\ Increase} = \frac{\boldsymbol{M_n - M_{n,existing}}}{\boldsymbol{M_{n,existing}}} \times \mathbf{100}\% \qquad \text{(Equation 4)}$$

Where:

$M_{n,\ existing}$ = flexural capacity of non-FRP reinforced concrete section, kN-m/m (lbf-in/in)

Table 3: Anticipated Levant Bridge Flexural Capacity Increased

FRP System	FRP Reinforced Section Flexural Capacity kN-m/m (kip-ft/ft)	Anticipated Flexural Capacity Increase
GG90	488 (110)	59 %
GG45	495 (111)	61 %
GC90	510 (115)	66 %
GC45	483 (109)	57 %

These anticipated increases in flexural capacity do not consider the strength of the mechanical fastening system and assume perfect bond between the FRP and concrete. Small beam bend testing of retrofitted reinforced concrete beams will provide a quantitative increase in flexural capacity.

Environmental Durability Analysis

As noted earlier, the four retrofit systems are denoted as follows: (1) GC45; unidirectional glass outer laminates with a woven carbon fiber core oriented at ±45°, (2) GC90; unidirectional glass outer laminates with a woven carbon fiber core oriented at 90°, (3) GG45; unidirectional glass outer laminates with twill woven glass fiber core oriented at ±45°, and (4) GG90; unidirectional glass outer laminates with twill woven glass fiber core oriented at 90°. Specimens were fabricated by attaching a FRP coupon to a concrete prism with stainless steel epoxy anchors. To assess the effects of severe environmental exposure to the strength of fiber reinforced polymer (FRP) flexural retrofit systems, four (4) FRP systems were exposed to two durations of saltwater submersion or 20 freeze-thaw cycles.

Test Specimen

Exposure to the elements can affect all facets of the retrofit system. To evaluate the environmental durability of the rehabilitation systems, it is necessary to study the system as a whole: concrete prism section, FRP coupon, epoxy adhesive, and stainless steel, threaded rod

anchors. Each specimen tested consists of all the parts listed previously assembled into a single unit. Details pertaining to each part of the system can be found in the following sections.

Epoxy Adhesive and Mechanical-fasteners

HILTI, Inc. products were reviewed for a post-installed anchor capable of withstanding high cyclic fatigue in cracked concrete. The HIT-HY 150 MAX-SD (HILTI, 2012) fast cure (30 minutes) adhesive anchoring system with stainless steel threaded rod inserts (Figure 16), washers and nuts was selected as the new proposed anchoring system.

Figure 16: Stainless steel epoxy adhesive anchor

Post-Tensioned Concrete Prism

Concrete prism sections dimensioned 127 × 127 × 546.1mm (5 × 5 × 21.5in) were designed to accommodate powder actuated fasteners. Formwork for these specimen was already constructed when it was determined that these fasteners would be inadequate for their intended applications as noted earlier in this report. As shown in Figure 17, 9.53mm (3/8in) threaded rods cast into the prism were used to attach a steel plate that served as grip location in the test setup. Two rods, spaced at 38.1mm (1.5in) o.c. and located at 152.4mm (6in) from one end of the prism, pass through the specimen, with washers and nuts on both sides of the prism. A PVC pipe with a 19.05mm (¾in) inner diameter was placed longitudinally in the center of the prism to create a conduit for a third threaded rod to pass through for post-tensioning of the prism prior to tension-bearing testing for confining the concrete (Figure 18).

Figure 17: Concrete formwork for environmental durability specimen

Figure 18: Cross-sectional view of post-tensioning conduit cast in environmental specimen

FRP System Coupons

Dimensions: a 101.6mm (4in) width was required based on design calculations for retrofit systems; 533.4mm (21in) length to allow for material behind connection, material over concrete cover, and sufficient length for grips and extensometer clips. The saltwater specimen coupon lengths were reduced by 76.2mm (3in) in order to fit the specimens into the submersion bins.

One 12.7mm (½in) in diameter hole was drilled into each coupon at the center line of the longitudinal direction and 152.4mm (6in) from the coupon end. This hole served as the connection point of the coupon to the concrete prism.

During the cutting process, some GG90 and GG45 specimen were left unlabeled. Without labels it is essentially impossible to determine the core orientation of the fibers by nondestructive visual observation. To determine the core orientation, 12.7mm (½in) wide strips of composite was cut from each unidentified specimen. Each specimen and its respective identification sample were labeled using a letter and number designation system. The letter “U” for “Unidentified core” was written on each coupon so that these coupons could be tracked throughout the testing process. Each coupon was then designated a number (1-32) representing the 32 specimen that required core identification. Using a chisel, the specimen’s core was revealed and then labeled with its correct core orientation to prevent further confusion.

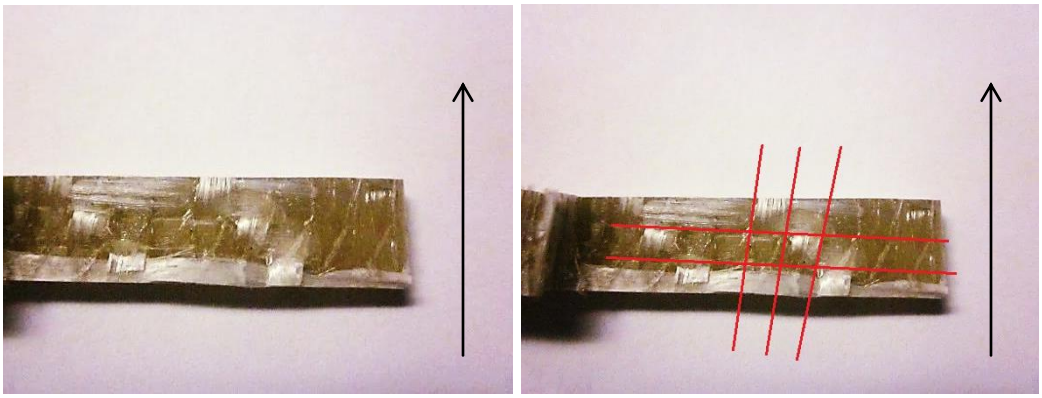

Figure 19: GG90 core identification sample

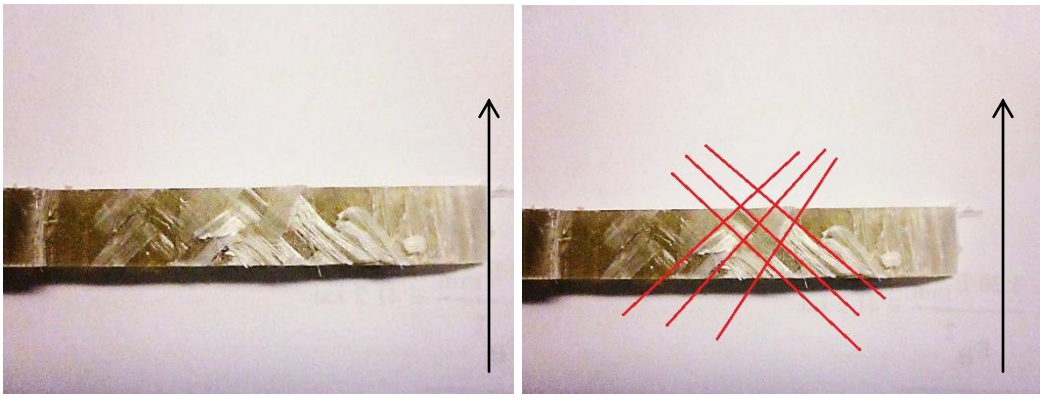

Figure 20: GG45 core identification sample

It can be seen when comparing Figure 19 to Figure 20 that the orientation of the core fibers in the first figure is 0°/90° (orientation further accentuated by the lines drawn in the images to the right in each figure). The arrow in each image depicts the longitudinal direction of the unidirectional outer layer fiber orientation.

Testing Plan

To quantify the durability of the FRP retrofit designs, an environmental durability test matrix is developed that builds on the work of prior hybrid FRP composite durability research performed at UMaine by Demkowicz (2011). In addition, the AASHTO (2012) design specification references an environmental durability test matrix "for the purpose of manufacturer's quality control and for the purchaser's quality assurance" and specifies a minimum of five samples of sufficient length for testing. The conditioning matrix was developed through collaboration between the California Department of Transportation (Caltrans) and the Aerospace Corporation (Karbhari, 2005). The testing matrix provides guidelines for water, saltwater, alkali, dry heat, fuel, ultraviolet light, and freeze-thaw environmental exposure.

The scope of Task 4 states that the effects of freeze-thaw cycling and exposure to de-icing salts would be evaluated and used in the selection of a non-proprietary FRP system for the MaineDoT. To assess the durability of each FRP composite system, the durability matrix referenced in the

AASHTO design guide (2012) was used for establishing exposure durations and acceptability criteria for each selected environmental condition. Descriptions of the exposure protocols used are detailed in the following sections.

Saltwater (De-icing Salt) Exposure

According to ASTM C1645 (ASTM, A.S.f.t.M., 2011) 3% sodium chloride (NaCl), by weight, in solution is used for simulating de-icing salt exposure of solid concrete paving units. This specification was used for determining the amount of de-icing salt to use in solution for exposing single-fastener FRP and concrete durability test specimen. Since the FRP retrofit systems will be used on roadway infrastructure, the saltwater exposure protocol outlined in this standard was used due to its focus on a concrete roadway application.

The original testing plan outlined in deliverable 2 (Breton & Davids, 2012) stated that the specimen would be exposed to saltwater for durations of 1000 and 3000 hours. The actual exposure times of specimen Specimens of each type were submerged in approximately 3% NaCl solution for 1000 hours and 3700 hours. Road salt used for creating the solution was obtained from the UMaine Division of Facilities Management. Buckets of water were filled, weighed, and then emptied into submersion bins until the specimen were completely submerged (see Figure 21). Based on the amount of water required to fill each bin, road salt was weighed and added to the respective bin to create a solution that was 3% NaCl by weight.

Aquarium pumps (Petco Animal Supplies: Petco air pump for freshwater & marine aquariums, Model: AC-9904 (2012)) rated for 98.4L to 802L (26-212 gal.) tanks were used for circulating the water and keeping the salt in solution (see Figure 22). Four air outlets lead from each pump. Two leads were used per bin. Leads were taped to the bottom of the bins to ensure the greatest amount of airflow and circulation within in the bins (see Figure 23).

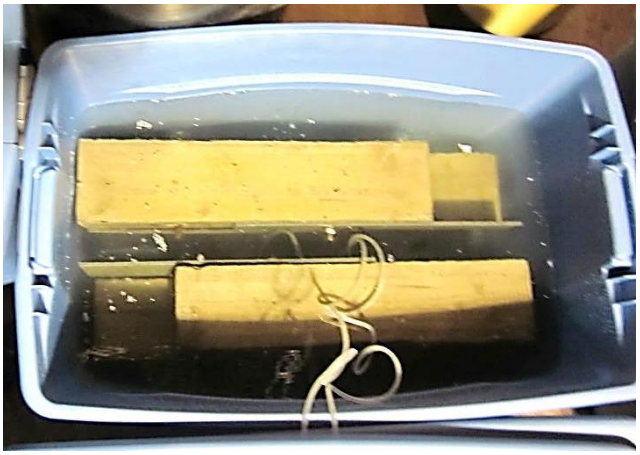

Figure 21: Saltwater durability specimen submerged in solution

Figure 22: Aquarium Pump

Figure 23: Aquarium pump leads at the bottom of submersion bin

Freeze-Thaw Exposure

Specimens of each type were placed in an ESPEC environmental chamber and exposed to 20 freeze-thaw cycles as specified by the testing matrix (Figure 24). The testing matrix calls for each cycle to last 24hr. For testing convenience, each cycle was reduced to last only 22hr. Each cycle consisted of 6 hours at -17.8°C (0°F) then 14 hours at 37.8°C (100°F) and 100% relative humidity. One hour ramping time was allotted between temperature extremes.

Figure 24: Freeze-thaw durability specimen in an ESPEC environmental chamber

Test Method

Following environmental conditioning, the specimens were tested by a combined tension and anchor bearing loading. Data collected during testing included load, cross-head position, and the displacement of the FRP due to loading and connection slip. Strain in the FRP was collected if the FRP coupon had adequate length to accommodate a clip-on type strain gage in addition to the other instrumentation. Per the proposal, based on the test data analysis of the freeze-thaw and 1000 hour specimens, two of the four FRP systems were be selected for use in retrofitting small beam bend specimen.

Concrete specimens were post-tensioned using a threaded rod and end plates. A medium strength alloy steel 15.875mm (5/8in.) threaded rod (ASTM A193 Grade B7 steel) was passed through the cast-in conduit and end plates. Using heavy-hex nuts, the section was post-tensioned to 122 N-m (90 ft-lb) torque generating a compression force of approximately 34.9kN (7850lbf). Larger post-tensioning loads could not be applied due to the tendency for the threaded rod to strip or heavy hex nuts to lock up, preventing the disassembly of the specimen after testing.

A steel plate was attached to the cast-through threaded rods opposite the FRP coupon (Figure 25 right). A small plate was attached to the underside of the concrete using the cast-through threaded rods (Figure 25 left). All nuts were torqued to 16.9N-m (12.5 ft-lb). Specimens were lifted into the actuator grips and secured at a grip pressure of 6.9MPa (1000 psi). Wood clamps, as pictured in Figure 25, were secured to the specimen. The top clamp was located at the center of the FRP anchor connection and the bottom clamp was abutted to the concrete face. These

camps secured an LVDT for measuring the displacement of the FRP coupon relative to the concrete prism. Displacement during testing occurred due to slip at specimen connection, elongation of the FRP coupon, and crushing of the FRP at the anchor connection due to bearing. An extensometer clip gage was attached to the coupon if enough space existed between the actuator grips and the bottom wood clamps (Figure 26). Specimens were loaded at a rate of 2.54mm/min (0.10in/min) under a 250kN (55kip) load cell until concrete cracking occurred or until it was evident the FRP coupon could no long sustain increased loading.

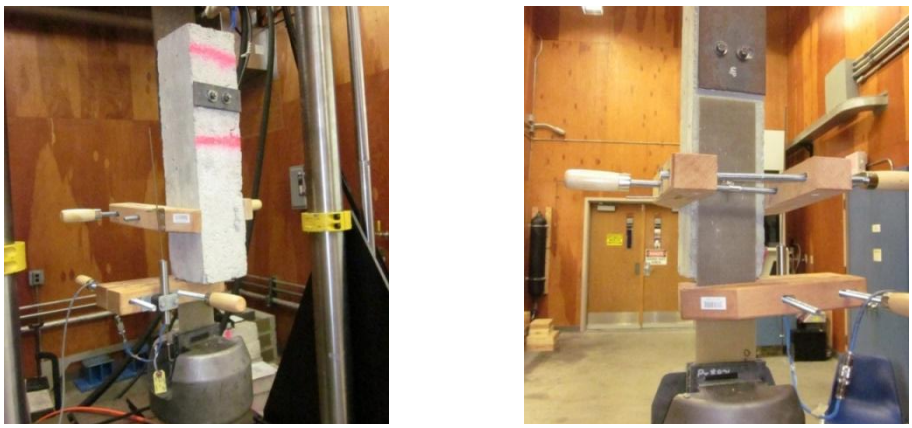

Figure 25: Tension-bearing environmental durability specimen in test setup

Figure 26: Clip-on extensometer strain gage on FRP of environmental durability test specimen

Results

Bearing failures at the FRP connection location were typical for all system types. With increased loading, bending of the adhesive anchors was observed. Loading was allowed to continue until the FRP was clearly unable to sustain higher tension loads, or cracking of the concrete occurred at either the FRP anchor or steel plate anchors. The specimen depicted in Figure 27 first failed in bearing at the FRP anchor location. Following increased loading the anchor began to bend and bear on the concrete, causing the concrete section to crack. The maximum load for each specimen was determined based on the collected test data and the mean maximum load per system and exposure type was calculated. The results are summarized in
Table 4.

Figure 27: Failed GG environmental durability specimen

One specimen exhibited a sudden failure of the concrete around the anchorage connection. As shown in Figure 28, bearing of the epoxy anchor on the concrete caused a failure of the aggregate-cement interface in the concrete. This failure was determined to have occurred due to the amount of smooth, clean aggregate located at the concrete failure plane. Results from this test were not used in strength calculations.

Figure 28: Failure anomaly: Sudden failure of concrete around epoxy anchor

Table 4: Average Maximum Load by System and Exposure Type

Exposure Type	Mean, kN (kip)	Coefficient of Variation	Percent Retention
GG90			
Control (5)	22.5 (5.06)	4.5%	--
Freeze-Thaw (5)	20.6 (4.63)	5.4%	91.5%
1000hr Saltwater (5)	19.2 (4.32)	6.4%	85.4%$^{+}$
3000hr Saltwater (4)	17.9 (4.04)	4.4%	79.7%$^{+}$
GG45			
Control (5)	21.6 (4.85)	7.8%	--
Freeze-Thaw (4)	17.9 (4.03)	3.7%	83.0%$^{+}$
1000hr Saltwater (4)	20.3 (4.56)	2.0%	94.0%
3000hr Saltwater (1)	17.1 (3.85)	--*	79.3%$^{+}$
GC90			

Control (4)	20.3 (4.57)	2.7%	--
Freeze-Thaw (5)	18.9 (4.25)	4.4%	93.1%
1000hr Saltwater (3)	20.9 (4.71)	5.5%	103.0%
3000hr Saltwater (2)	17.2 (3.86)	4.6%	84.5%
GC45			
Control (5)	19.1 (4.30)	10.7%	--
Freeze-Thaw (4)	17.7 (3.99)	7.0%	92.7%
1000hr Saltwater (4)	19.0 (4.27)	17.9%	99.2%
3000hr Saltwater (4)	15.8 (3.55)	11.3%	82.5%

Numbers in parentheses following exposure type represent the number of specimens used in calculations
*****Coefficient of variation not available for this test; only one specimen produced acceptable results
[+]Specimen do not pass acceptability criteria

The adopted performance acceptance criteria requires conditioned specimens to retain 90% strength relative to control specimen following both freeze-thaw and 1000 hour saltwater exposure and 85% strength relative to control specimen following 3000 hour saltwater exposure. Provided the longer exposure time endured by the 3000 hour specimen and assuming a linear trend in the outlined acceptability criteria, it was determined through linear extrapolation that 80% strength retention would be considered acceptable for the saltwater specimen that were exposed for approximately 3700 hours. Based on this criterion, the GG45 specimens failed to meet acceptability requirements for freeze-thaw exposure and the GG90 specimens failed to meet the acceptability requirements for 1000 hour saltwater exposure. Since the orientation of the glass core is the only difference between the two glass core systems, it is expected that the larger strength reduction would occur due to the same exposure type. As shown in Table 4, however, this is not the case. The 0°/±45° oriented core saw the largest strength reduction due to freeze-thaw exposure, while the 0°/90° core saw the largest strength reduction due to saltwater exposure. Due to this inconsistency, it was determined that further evaluation of the test data should be performed before determining which two FRP systems will be used in future testing.

The test data was reanalyzed based on averaged sustained peak load. Initially, the average sustained peak load was defined as averaging the load sustained by a specimen between a defined deformation range. Based on load-deformation plots of the freeze-thaw and 1000 hour saltwater exposure specimen data, it was determined that a deformation range of 7.62mm-12.7mm (0.3in.-0.5in.) captured the typical behavior of a system after the linear range of loading. It was found that due to the inherent slip in the anchor connection that secured the FRP to the concrete specimen it was necessary to correct the test data and eliminate the deformation that occurred due to slip. This was done by extrapolating the linear portion of the load-deformation curve for specimens with slip back to zero load and finding the corresponding deformation at this location (denoted as Δ_i). The average sustained peak load was then determined by averaging measured load between the corrected deformation range: $7.62+\Delta_i$ to $12.7+\Delta_i$ (mm) ($0.3+\Delta_i$ to $0.5+\Delta_i$ (inch)). This average peak sustained load range is shown load-displacement plot for a

GG90 environmental control specimen in Figure 29 as the region between the dotted vertical lines.

Following the testing of the 3000 hour saltwater exposure specimen, review of the data showed that the displacement range would not suffice due to the low amount to displacement measured in these tests (typically less than 7.62mm (0.3in.)) (see Figure 30). Although the displacement of the 3000 hour exposed specimen was less than the 1000 hour and freeze-thaw specimen, test data shows that sustained loads achieved were still within a similar range. It was determined that in order to analyze all data by a universal system, the average peak sustained load range needed to be redefined.

Based on the original acceptability criteria and the load-displacement plots for tested specimen the average peak sustained load range was defined using the two following points:

- Initial point – the first recorded occurrence of 85% of peak load prior to the occurrence of peak load
- Final point – the first recorded occurrence of 85% peak load following the occurrence of peak load

The dashed, horizontal line in Figure 29 and Figure 30 shows the location of 85% peak load. The redefined average sustained peak load value begins averaging values when the horizontal line first intersects the data line. The last data point used in calculating the averaged sustained peak load occurs at the first intersection of the horizontal line and the data set, post-peak load. Load-displacement curves for each specimen are provided in Appendix F. The average sustained peak loads, coefficient of variation and percent strength retention for each system and exposure time are provided in

Figure 30: Load-displacement plot for average peak sustained load (2)

.

Table 5: Averaged Sustained Peak Load by System and Exposure Type

Exposure Type	Mean, kN (kip)	Coefficient of Variation	Percent Retention
GG90			
Control (5)	18.3 (4.12)	9.0%	--
Freeze-Thaw (5)	16.0 (3.59)	18.2%	87.2%$^{+}$
1000hr Saltwater (5)	18.9 (3.80)	5.0%	92.2%
3000hr Saltwater (4)	15.1 (3.40)	8.4%	82.6%
GG45			
Control (5)	18.2 (4.10)	12.5%	--
Freeze-Thaw (4)	14.0 (3.14)	14.4%	76.5%$^{+}$
1000hr Saltwater (4)	17.4 (3.91)	7.4%	95.4%
3000hr Saltwater (1)	12.5 (2.90)	--*	68.7%$^{+}$

GC90			
Control (4)	13.7 (3.08)	15.0%	--
Freeze-Thaw (5)	15.9 (3.57)	6.1%	116.1%
1000hr Saltwater (3)	18.6 (4.18)	6.9%	135.9%
3000hr Saltwater (2)	15.3 (3.44)	8.1%	111.9%
GC45			
Control (5)	15.3 (3.44)	17.5%	--
Freeze-Thaw (4)	14.4 (3.23)	12.3%	94.0%
1000hr Saltwater (4)	14.9 (3.36)	16.0%	97.7%
3000hr Saltwater (4)	13.8 (3.10)	13.5%	90.1%

*Coefficient of variation not available for this test; only one specimen produced acceptable results

[+]Specimen do not pass acceptability criteria

Following the same acceptance criteria as mentioned previously, the two glass core systems still do not meet requirements; however, from this analysis, the two systems see the most reduction in strength due to the same environmental exposure: freeze-thaw.

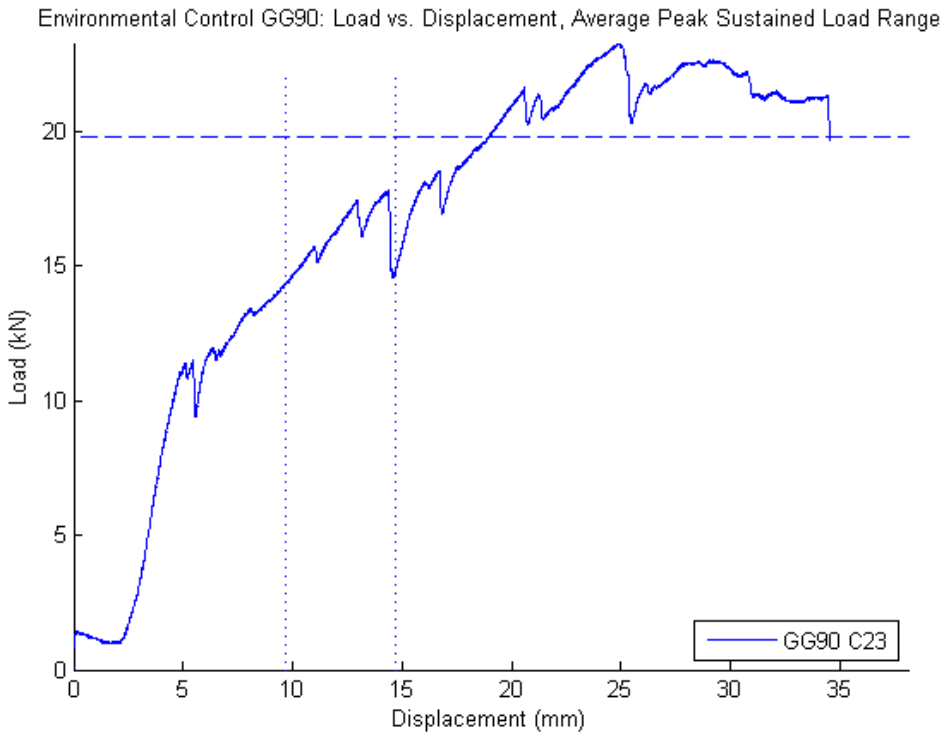

Figure 29: Load-displacement plot for determining average peak sustained load

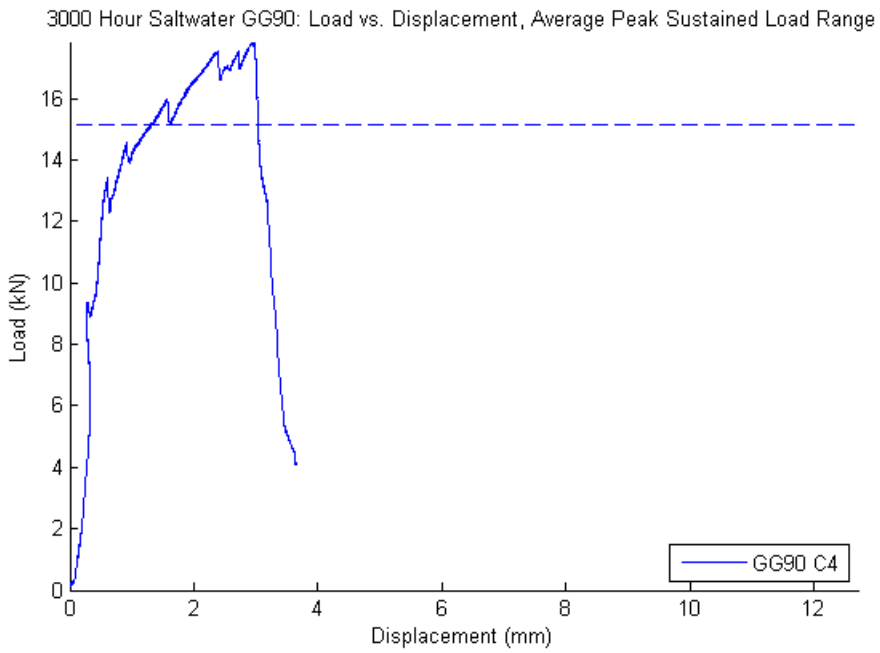

Figure 30: Load-displacement plot for average peak sustained load (2)

Conclusions

From these results it is observed that the carbon core systems are capable of withstanding environmental degradation better than the glass core systems. This is consistent with existing literature on the durability of FRP systems (Bisby, 2006; Saenz & Pantelides, 2006; Balazs & Borosnyoi, 2007; Demkowicz, 2011). The amount of reduction observed following the first round of environmental conditioning in the glass core systems may be acceptable for a short-term use of the retrofit system. However, it is possible that with continued exposure the strength of the glass core system would continue to degrade more rapidly than the carbon core system.

Although the carbon core systems were not capable of withstanding loads as great as the glass core systems across the board, the AASHTO LRFD Guide Specifications (2012) takes into account the greater environmental degradation of glass FRP systems by requiring a 35% reduction in design capacity of glass FRP systems and a 15% reduction in design capacity of a carbon FRP system. If this reduction is applied to the control condition specimen average sustained peak load (see Table 6) the reduced average sustained peak load is approximately equal for all systems. Since the increase in the flexural capacity of a bridge is dependent on the strength of the retrofit system, it is therefore best to proceed with using the two carbon core systems for small beam bend tests. These systems meet acceptability criteria for environmental exposure for both the maximum load and averaged sustained peak load and are expected to provide the most reliable strengthening system over the lifecycle of the retrofit.

Table 6: Reduced Average Sustained Peak Load for Control Condition Specimen

System Type	Mean, kN (kip)

GG90	11.9 (2.68)
GG45	11.9 (2.66)
GC90	11.6 (2.62)
GC45	13.0 (2.92)

Summary

Following design alterations, mechanical strength testing, and durability testing it was determined that the GC90 and GC45 systems would be best suited for continued study for use as flexural rehabilitation systems for flat-slab concrete bridges in Maine. Following extreme environmental exposure to 20 freeze-thaw cycles, 1000 hours of saltwater submersion and 3700 hours of saltwater submersion the carbon core FRP retrofit systems met all durability requirements, providing evidence that these systems are capable of withstanding adverse environments typically encountered in bridge applications.

The GC90 and GC45 systems will be used in small beam bend tests to provide a quantitative representation of the ability of these systems to increase the flexural capacity of flat-slab concrete bridges. If these mechanically fastened FRP strips can be installed rapidly and give adequate flexural strength increases, these systems could provide a lightweight, cost-effective rehabilitation method for the MaineDoT to use to remove or limit weight posting of aging concrete slab bridges and defer the costly replacement of such structures.

Works Cited

ACI - Committee 440. (2008). *Guide for the design and construction of externally bonded FRP systems for strengthening concrete sturctures.* Farmington HIlls, MI, USA: American Concrete Institute.

American Association of State Highway and Transportation Officials (AASHTO). (2007). *AASHTO LRFD bridge design specifications: Customary US Units.* Washinton, DC: American Association of State Highway and Transportation Officials.

American Association of State Highway and Transportation Officials (AASHTO). (2012). *Guide specifications for design of bonded FRP systems for repair and strengthening of concrete bridge elements.* Washington, DC: American Association of State Highway and Transportation Officials.

ASTM, A.S.f.T.M. (2008). Standard Test Method for Tensile Properties of Polymer Matrix Composite Materials. West Conshohocken, PA: ASTM International.

ASTM, A.S.f.t.M. (2011). Standard Test Method for Freeze-thaw and De-icing Salt Durability of Solid concrete Interlocking Paving Units. West Conshohocken, PA: ASTM International.

Balazs, C. L., & Borosnyoi, A. (2007). Long-term behavior of FRP. In *Composites in Construction: A Reality* (pp. 84-91). Reston, VA, USA: American Society of Civil Engineers.

Bisby, L. A. (2006). *ISIS eduction module 8: Durability of FRP composites for construction.* Retrieved June 2011, from ISIS Canada: www.isiscanada.com/education/download.asp

Breton, H., & Davids, W. (2012). *Bridge Safety Project, Task 4 (Deliverable 1): FRP Flexural Retrofit Designs.* Orono: University of Maine.

Breton, H., & Davids, W. (2012). *Bridge Safety Project, Task 4 (Deliverable 2): FRP Flexural Retrofit Durability Testing Plan.* Orono: University of Maine.

Demkowicz, M. (2011). Environmental durability of hybrid braided polymer matrix composites for infrastructure applications. *Masters' thesis*. Orono, ME: Univeristy of Maine.

HILTI. (2012, June). *Anchor Fastening Technical Guide.* Retrieved July 2012, from Hilti Online: http://www.us.hilti.com/fstore/holus/techlib/docs/3.2.3_HIT-HY150_MAX-SD_p60-90r30_1.pdf

Karbhari, V. M. (2005). *Using composites in seismic retrofit applications.* El Segundo: State of California Department of Transportation.

Saenz, N., & Pantelides, C. P. (2006). Short and medium term durability evaluation of FRP-confined circular concrete. *Journal of Composites for Construction, 10*(3), 244-253.

APPENDIX A: FRP Material Technical Data Sheets, Infusion and Layups Schedules

From: Tom Flanagan [mailto:tflanagan@fiberglassindustries.com]
Sent: Monday, May 07, 2012 12:52 PM
To: Jake Marquis
Cc: tmckechnie@nacomposites.com
Subject:

Jake , Sorry for the delay on this . They are making today and we'll get out today or tomorrow at the latest . Thanks Tom

From: Ziggy Ziobro
Sent: Monday, May 07, 2012 12:19 PM
To: Tom Flanagan
Subject: RE: Kenway 19 oz basecloth

Tom ,
Per your request

SW1900

Layer	Description	Material	Angle	Ends/Inch	# of Ends	Chop, Core, V-90 or Veil oz/yd^2	Yield	Effective EPI	Weight, oz/yd^2	Weight, g/ft^2	Wt % of Total	Machine setting if Chop Glass Weight g/sqm	gsm
1	Roving	2200ET700	0	7	1		225	7.00	17.92	56.45	94.5%	0	608
2	Roving	510-K-1800	90	2	1		1800	2.00	0.64	2.02	3.4%	0	22
3	Stitch	WSL Beam Yarn-185				0.40	29764	N/A	0.40	1.26	2.1%	14	14
4								N/A	0.00	0.00	0.0%	0	0
5								N/A	0.00	0.00	0.0%	0	0
6								N/A	0.00	0.00	0.0%	0	0
7								N/A	0.00	0.00	0.0%	0	0
								Total Fabric Weight	18.96	59.72	100%		643

Vectorply E-LR 1208 – Unidirectional E-Glass

VECTORPLY
Performance Composite Reinforcements

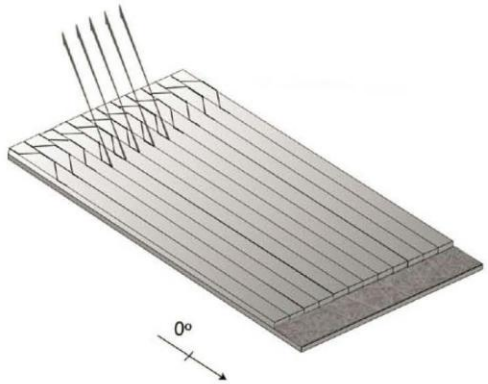

E-LR 1208

Fiber Type: E-Glass
Architecture: 0 Warp Unidirectional
Dry Thickness: 0.019 in. / 0.48 mm
Total Weight: 12.85 oz/sq.yd / 436 g/sq.m

VECTORSPORTS™

DNV

Roll Specifications			Fiber Architecture Data	
Roll Width:	Roll Weight:	Roll Length:	0 ° :	11.95 oz/sq.yd / 405 g/sq.m
50 in / 1270 mm	152 lb / 69 kg	131 yd / 120 m	45 ° :	n/a
			90 ° :	n/a
			-45 ° :	n/a
			Polyester Veil :	0.90 oz/sq.yd / 31 g/sq.m

1: Packaging: box or bag.
2: Weights do not include polyester stitching.

Laminated Properties	0 °	0 °
Laminate Weight		
(lb/sq.ft)	E-LR 1208 Resin Infused	E-LR 1208 Open Mold
Fiber	0.09	0.09
Resin	0.04	0.08
Total	0.13	0.17

Physical Properties		
	E-LR 1208 Resin Infused	E-LR 1208 Open Mold
Density (g/cc))	1.82	1.63
Fiber Content (% by Wt.)	68%	53%
Thickness (in)	0.014	0.020

Laminate Modulii		
(MSI)	E-LR 1208 Resin Infused	E-LR 1208 Open Mold
Ex	5.04	3.66
Ey	1.56	1.13
Gxy	0.73	0.51
Ex,flex.	4.79	3.48
Ey,flex.	1.48	1.07

Ultimate Stress		
(KSI)	E-LR 1208 Resin Infused	E-LR 1208 Open Mold
Long. Ten.	95	69
Long. Comp.	95	69
Trans. Ten.	31	23
Trans. Comp.	31	23
In-Plane Shear	15	10
Long. Flex.	96	70
Trans. Flex.	30	21

In-Plane Stiffness, "EA"		
10^3 lb/in	E-LR 1208 Resin Infused	E-LR 1208 Open Mold
(EA)x	69	73
(EA)y	21	23
(GA)xy	10	10

Ultimate In-Plane Load		
lb/in	E-LR 1208 Resin Infused	E-LR 1208 Open Mold
Long. Ten.	1,311	1,385
Long. Comp.	1,311	1,385
Trans. Ten.	428	452
Trans. Comp.	428	452
In-Plane Shear	202	205

Notes:

1: Resin infused laminate made with a poly / vinyl ester resin blend.

2: Open mold laminate made with poly / vinyl ester resin blend.

3: All standard reinforcements should be infused with a flow aid or Vectorfusion® reinforcements.

VECTORPLY CORPORATION

3500 Lakewood Dr. Phenix City, AL 36867 tel. 334 291 7704 fax. 334 291 7743

REV: 6/3/2011

FGI CPS-409 – Twill Woven Glass

Consistently fgi The Best

ROVCLOTH® 2977 Product Specification

Product Specification Number	Revision: A	Page 1 of 1
CPS-409		

1.0 Description

ROVCLOTH® Woven Roving is a woven fabric consisting of single end glass rovings. ROVCLOTH® features controlled wetout and excellent laminate properties. ROVCLOTH® is produced with proprietary FGI sizing technology.

2.0 Quality Specifications (Typical)

Construction	Per Inch	Yield Input	WEIGHT (OZ. /YD.^{2})	Acceptance Limits	% of Total
Warp 0°	7.0	450	8.96	± 5%	32.71
Weft 90°	7.2	225	18.43	± 5%	67.29
Total Weight (oz. /yd.^{2})			27.39	± 5%	
Thickness (inches)	.04			± .002	
Weave Style	Twill				

3.0 Width

3.1 ROVCLOTH® width is measured from selvedge ±0.5" and does not include the tails. The overall width (including two tails) is approximately 1.5" greater than the woven fields' width.

4.0 Packaging

4.1 All rolls individually stretch wrapped and palletized according to size and weight, stacking varies from 1 to 3 layers. Widths 12" and less will be boxed for shipment.

FIBER GLASS INDUSTRIES, INC.
69 EDSON ST AMSTERDAM, NY 12010 TELEPHONE 518-842-4000 FAX 518-842-4408

JB Martin TC-12-P – Plain Woven Carbon

jb martin

Texitek Division

STYLE **TC-12-P**

Carbon / Carbone

WEAVE		Plain	Taffetas		ARMURE
WARP/WEFT RATIO (weight)		50% - 50%			RATIO CHAINE/TRAME (poids)
WARP/WEFT RATIO (volume)		50% - 50%			RATIO CHAINE/TRAME (volume)
RESIN COMPATABILITY		Vinylester, Epoxy			COMPATIBILITÉ RÉSINE
COMPRESSED THICKNESS		0.021 in	0.53 mm		ÉPAISSEUR COMPRESSÉE
WET LAY UP THICKNESS		0.030 in	0.75 mm		LAMINAGE CONTACT
AREAL WEIGHT		11.9 oz/yd²	405 g/m²		MASSE SURFACIQUE
STANDARD ROLL LENGTH		109 yds	100 m		LONGUEUR STANDARD
MATERIALS					MATERIAUX
WARP					CHAINE
PRIMARY	Carbon	12 K	800 tex	Carbone	PRIMAIRE
SECONDARY	n/a			n/a	SECONDAIRE
ENDS COUNT		6.4 /in	2.5 /cm		COMPTE CHAINE
WEFT					TRAME
PRIMARY	Carbon	12 K	800 tex	Carbone	PRIMAIRE
SECONDARY	n/a			n/a	SECONDAIRE
ENDS COUNT		6.4 /in	2.5 /cm		COMPTE TRAME

JB Martin Ltd
445, St-Jacques
St-Jean sur Richelieu, QC, Canada, J3B 2M1
Tel. (450) 346-6853 Fax (450) 347-4910
email: texitek@jbmartin.ca
website: www.jbmartin.ca

DC-VEN-003-BI 2011-01-19

Technical data sheet

Kayak KF3202L-00

Toughened Epoxy Vinyl Ester Infusion Resin

Description

EPOVIA® KAYAK KF3202L-00 is an un-promoted, elastomeric modified Bisphenol-A epoxy based vinyl ester resin containing styrene monomer. EPOVIA® KAYAK KF3202L-00 is formulated for building reinforced plastic parts using closed molding processes, specifically infusion processes such as vacuum bagging, SCRIMP® and resin injection. It can be used in infusion applications that specify Derakane® 8084 and other equivalent elastomeric modified Bisphenol-A based vinyl ester resins.

Features and Benefits

- Industrial parts where toughness, fatigue and chemical resistance is required
- Infrastructure pipe construction
- Fume and vapor ducting
- Military / Naval projects for rapid infusion, high strength and improved fatigue.
- Load-bearing, structural construction members
- Automotive structural parts
- Low viscosity for easy flow through a multitude of glass fiber fabrics and cores
- Good heat resistance allows use at elevated service temperatures.
- Low shrinkage for good dimensional stability for accurate design tolerances.
- Excellent mechanical strength allows for larger safety factors in high stress applications that require improved fatigue properties.
- Un-promoted formulation that can be customized for a variety of part types.

Liquid Properties (77°F)

Liquid properties of EPOVIA® KAYAK KF3202L-00 are shown below. These values may or may not be manufacturing control criteria. They are listed as a reference guide only. Particular batches will not conform exactly to the numbers listed because storage conditions, temperature changes, age, testing equipment (type and procedure) can have significant effects on results. Products with properties outside of these readings

may perform acceptably. Final suitability of this product should be determined by the fabricator in the end use performance.

Test	EPOVIA® KAYAK KF3202L-00
Viscosity[1]	100 cps
Weight Per Gallon	8.6 lbs
Specific Gravity @ 25°C	1.03

[1]Brookfield, RV #3 spindle @ 50 rpm.

Physical Properties

The physical properties of EPOVIA® KAYAK KF3202L-00 are shown below. Properties are shown for both a neat resin casting and for a glass fiber reinforced laminate. These are typical values and are provided for reference only. Note: The physical properties of thermoset resins evolve as the resin cures. The properties given below are for well cured castings and laminates. Resin and laminates at different stages of cure will have varying properties.

Test	Test Method[4]	Neat Resin Casting[1],[3]	Laminate[2]
Tensile Strength	ASTM D638	9,860 psi (68 MPa)	82,900 psi
Tensile Modulus		526,000 psi (3,624 MPa)	6,926,000 psi
Tensile Elongation		8.6%	1.53%
Flexural Strength	ASTM D790	17,300 psi (119 MPa)	153,500 psi
Flexural Modulus		425,000 psi (2.927 MPa)	5,610,000 psi
Heat Distortion Point at 264 psi	ASTM D648	96°C/205°F	119.7°C DMA Tg
Barcol Hardness		40	52
Glass Content	ASTM D2584	--	79.7%

[1]Neat Resin Casting – Post cured at 80ºC for 2 hours, followed by 2 hours at 120ºC.
[2]Infused laminate - Laminate construction is as follows: 2 layers DevoldL1200/G50-E07 Hybon 2026
[3]Reference Cray Valley Korea
[4]CCP testing methods were used, which are similar to ASTM testing.

Application

EPOVIA® KAYAK KF3202L-00 is formulated with a low viscosity for thorough wet-out of reinforcing materials and rapid fill times. To fully realize the benefit of the low viscosity, temperature control is recommended. Resin viscosity is affected by temperature with the resin being higher in viscosity at cooler temperatures and lower in viscosity at warmer temperatures.

EPOVIA® KAYAK KF3202L-00 - Copyright 2010-2012

EPOVIA® KAYAK KF3202L-00 is un-promoted to allow for customization of fast and slow gel times for small or large parts. Sample promotion formulations for fast, slow and extended gel times are shown below. The samples formulations are provided as a guideline only. CCP recommends that gel time be checked in the customer's plant because age, temperature, humidity, promoter levels and peroxide age and type will produce varied gel times.

	Fast	Slow	Extended
Gel Time [1]	**15 min.**	**30 min.**	**100 min.**
Promoter: 12% COBALT	0.15 phr	0.15 phr	0.15 phr
Co-promoter: DMA	0.05 phr	0.05 phr	0.05 phr
Inhibitor: CCP970C951	none	0.10 phr	0.20 phr

[1] 100g mass cup gel time – 1.50% Syrgis® MEKP-925H at 77ºF (25ºC)

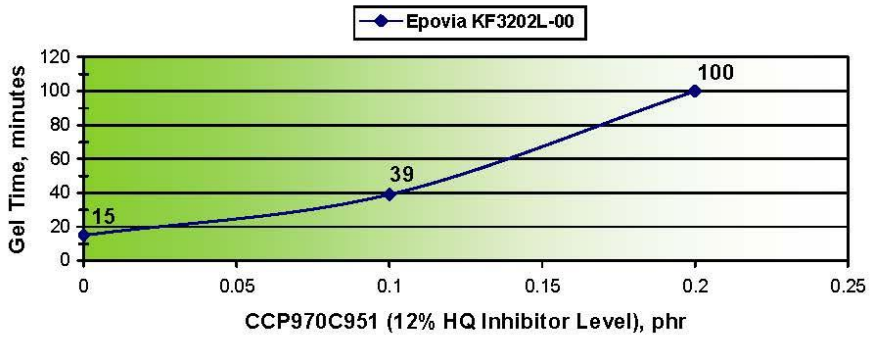

EPOVIA® KAYAK KF3202L-00 is quality control tested using Syrgis® MEKP-925H. Other MEKP catalysts such as Arkema Luperox® DHD-9, Syrgis NOROX® MEKP-925, and Chemtura HP-90 are expected to yield similar performance. Syrgis NOROX® MEKP-9 and NOROX®MEKP-9H, Akzo Nobel CADOX L-50a and CADOX D-50 may also be used, but gel and cure times may vary.

The catalyst level should not exceed 2.4% nor fall below 0.9% for proper cure. The recommended range is 1.5% at 25°C or 77°F depending on material and room temperature, humidity, air movement, and catalyst concentration.

This product should not be used when temperature conditions are below 64°F (18°C), since longer gel time, poor flow, and poor cure would be expected.

Related Products

For related products, see the EPOVIA® Epoxy Vinyl Ester Product Guide for Corrosion and Chemically Resistant Resins.

Caution

Do not add any material, other than the recommended promoters, co-promoters, inhibitors and methyl ethyl ketone peroxide to this product without the advice of a representative of CCP Composites US.

Storage

EPOVIA® KAYAK KF3202L-00 has a usage life of 6 months from date of shipment from CCP when stored at 73°F or below in a closed, factory-sealed, opaque container, and out of direct sunlight. The usage life is cut in half for every 20°F over 73°F.

MSDS / TDS

MSDS and TDS documents are found in printable format at www.ccpcompositesus.com.

COMPOSITES SAFETY INFORMATION
(October 2011)

All sales of products manufactured by CCP Composites US (CCP), and described herein, are made solely on condition that CCP's customers comply with applicable health and safety laws, regulations and orders relating to the handling of our products in the workplace. Before using, read the following information, and both the product label, and Material Safety Data Sheet pertaining to each product.

Most products contain styrene. Styrene can cause eye, skin and respiratory tract irritation. Avoid contact with eyes, skin and clothing. Impermeable gloves, safety eyewear and protective clothing should be worn during use to avoid skin and eye contact. Wash thoroughly after use.

Styrene is a solvent and may be harmful if inhaled. Reports have associated repeated and prolonged occupational overexposure to solvents with permanent brain and nervous system damage. Extended exposure to styrene at concentrations above the recommended exposure limits may cause central nervous system depression causing dizziness, headaches or nausea and, if overexposure is continued indefinitely, loss of consciousness, liver and kidney damage.

Do not ingest or breathe vapor, spray mists or dusts caused by applying, sanding, grinding and sawing products. Wear an appropriate NIOSH/MSHA approved and properly fitted respirator during application and use of these products until vapors, mists and dusts are exhausted, unless air monitoring demonstrates vapors, mists and dusts are below applicable exposure limits. Follow respirator manufacturer's directions for respirator use.

The International Agency for Research on Cancer (IARC) reclassified styrene as Group 2B, "possibly carcinogenic to humans." This revised classification was not based on new health data relating to either humans or animals, but on a change in the IARC classification system. The Styrene Information and Research Center does not agree with the reclassification and published the following statement: Recently published studies tracing 50,000 workers exposed to high occupational levels of styrene over a period of 45 years showed no association between styrene and cancer, no increase
in cancer among styrene workers (as opposed to the average among all workers), and no increase in mortality related to styrene.

Styrene is classified by OSHA and the Department of Transportation as a flammable liquid. Flammable products should be kept away from heat, sparks, and flame. Lighting and other electrical systems in the work place should be vapor-proof and protected from breakage.

Vapors from styrene may cause flash fire. Styrene vapors are heavier than air and may concentrate in the lower levels of molds and the work area. General clean air dilution or local exhaust ventilation should be provided in volume and pattern
to keep vapors well below the lower explosion limit and all air contaminants (vapor, mists and dusts) below the current permissible exposure limits in the mixing, application, curing and repair areas.

Some products may contain additional hazardous ingredients. To determine the hazardous ingredients present, their applicable exposure limits and other safety information, read the Material Safety Data Sheet for each product (identified by product number) before using. If unavailable, these can be obtained, free of charge, from your CCP representative or from: CCP Composites US, P.O. Box 419389, Kansas City, MO 64141-6389; 816-391-6053.

FIRST AID: In case of eye contact, flush immediately with plenty of water for at least 15 minutes and get medical attention; for skin, wash thoroughly with soap and water. If affected by inhalation of vapors or spray mist, remove to fresh air. If swallowed, get medical attention.

Those products have at least two components that must be mixed before use. Any mixture of components will have hazards of all components. Before opening the packages read all warning labels. Observe all precautions.

Keep containers closed when not in use. In case of spillage, absorb with inert material and dispose of in accordance with applicable regulations. Emptied containers may retain hazardous residue. Do not cut, puncture or weld on or near these containers. Follow container label warnings until containers are thoroughly cleaned or destroyed.

FOR INDUSTRIAL USE AND PROFESSIONAL APPLICATION ONLY. KEEP OUT OF REACH OF CHILDREN

CCP COMPOSITES US
WARRANTIES, DISCLAIMERS AND LIMITATION OF LIABILITY (Rev. 10/11)

Seller warrants that: (i) Buyer shall obtain good title to the product sold hereunder, (ii) at Shipment such product shall conform to Seller's specifications; and (iii) the sale or use of such product will not infringe the claims of any U.S. patent covering the product itself, but Seller does not warrant against infringement which might arise by the use of said product in any combination with other products or arising in the operation of any process. **SELLER MAKES NO OTHER WARRANTY OF ANY KIND, EXPRESS OR IMPLIED, INCLUDING WITHOUT LIMITATION ANY WARRANTY OF MERCHANTABILITY OR FITNESS FOR ANY PARTICULAR PURPOSE, EVEN IF THAT PURPOSE IS KNOWN TO SELLER. ANY APPLICATION INFORMATION OR ASSISTANCE WHICH SELLER MAY FURNISH TO BUYER IS GRATUITOUS AND SHALL IN NO WAY BE DEEMED PART OF THE SALE OF PRODUCT HEREUNDER OR A WARRANTY OF THE RESULTS OBTAINED THROUGH THE USE OF SUCH PRODUCT.**
Without limiting the generality of the foregoing, if any product fails to meet warranties mentioned above, Seller shall at Seller's option either replace the nonconforming product at no cost to Buyer or refund the Buyer the purchase price thereof. The foregoing is Buyer's sole and exclusive remedy for failure of Seller to deliver or supply product that meets the foregoing warranties. Seller's liability with respect to this contract and the product purchased under it shall not exceed the purchase price of the portion of such product as to which such liability arises. Seller shall not be liable for any injury, loss or damage, resulting from the handling or use of the product shipped hereunder whether in the manufacturing process or otherwise. In no event shall Seller be liable for special, incidental or consequential damages, including without limitations loss of profits, capital or business opportunity, downtime costs, or claims of customers or employees of Buyer. Failure to give Seller notice of any claim within thirty (30) days of shipment of the product concerned shall constitute a waiver of such claim by Buyer. Any product credit received by Buyer hereunder, if not used, shall automatically expire one (1) year from the date the credit was granted. Notwithstanding any applicable statute of limitations to the contrary, any action by Buyer relation to a claim hereunder must be instituted no later than two (2) years after the occurrence of the event upon which the claim is based. All the foregoing limitations shall apply irrespective of whether Buyer's claim is based upon breach of contract, breach of warranty, negligence, strict liability, or any other legal theory.

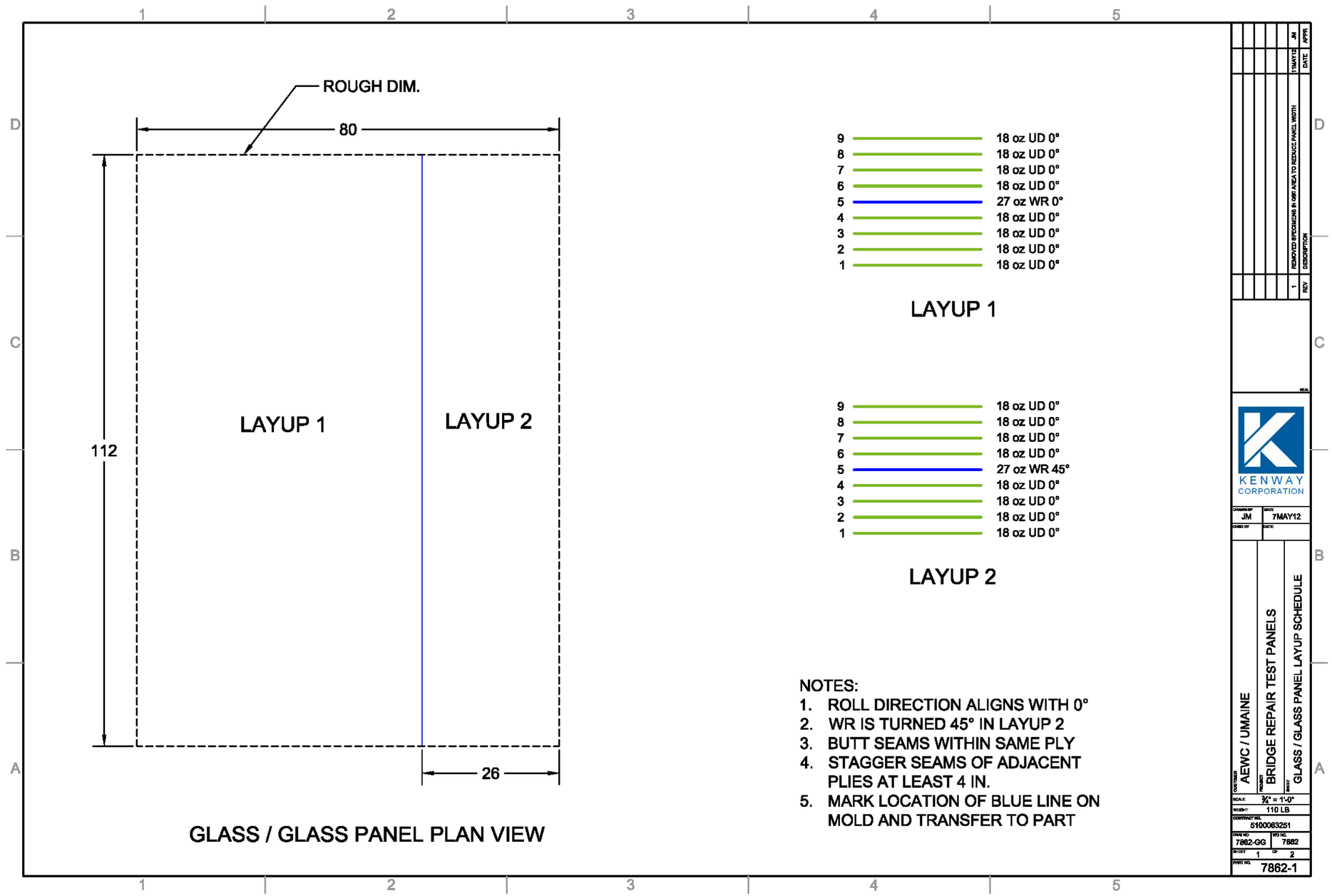
ROUGH DIM.
80
112
26
LAYUP 1
LAYUP 2
GLASS / GLASS PANEL PLAN VIEW
9 18 oz UD 0°
8 18 oz UD 0°
7 18 oz UD 0°
6 18 oz UD 0°
5 27 oz WR 0°
4 18 oz UD 0°
3 18 oz UD 0°
2 18 oz UD 0°
1 18 oz UD 0°
LAYUP 1
9 18 oz UD 0°
8 18 oz UD 0°
7 18 oz UD 0°
6 18 oz UD 0°
5 27 oz WR 45°
4 18 oz UD 0°
3 18 oz UD 0°
2 18 oz UD 0°
1 18 oz UD 0°
LAYUP 2
NOTES:
1. ROLL DIRECTION ALIGNS WITH 0°
2. WR IS TURNED 45° IN LAYUP 2
3. BUTT SEAMS WITHIN SAME PLY
4. STAGGER SEAMS OF ADJACENT PLIES AT LEAST 4 IN.
5. MARK LOCATION OF BLUE LINE ON MOLD AND TRANSFER TO PART
REV 1 DESCRIPTION REMOVED SPECIMENS IN G90 AREA TO REDUCE PANEL WIDTH DATE 7MAY12 APPR JM
KENWAY CORPORATION
DRAWN BY JM DATE 7MAY12
CHKD BY DATE
CONTRACT AEWC / UMAINE
PROJECT BRIDGE REPAIR TEST PANELS
SHEET GLASS / GLASS PANEL LAYUP SCHEDULE
SCALE 3/4" = 1'-0"
WEIGHT 110 LB
CONTRACT NO. 5100083251
DWG NO. 7862-GG
WO NO. 7862
SHEET 1 OF 2
PART NO. 7862-1

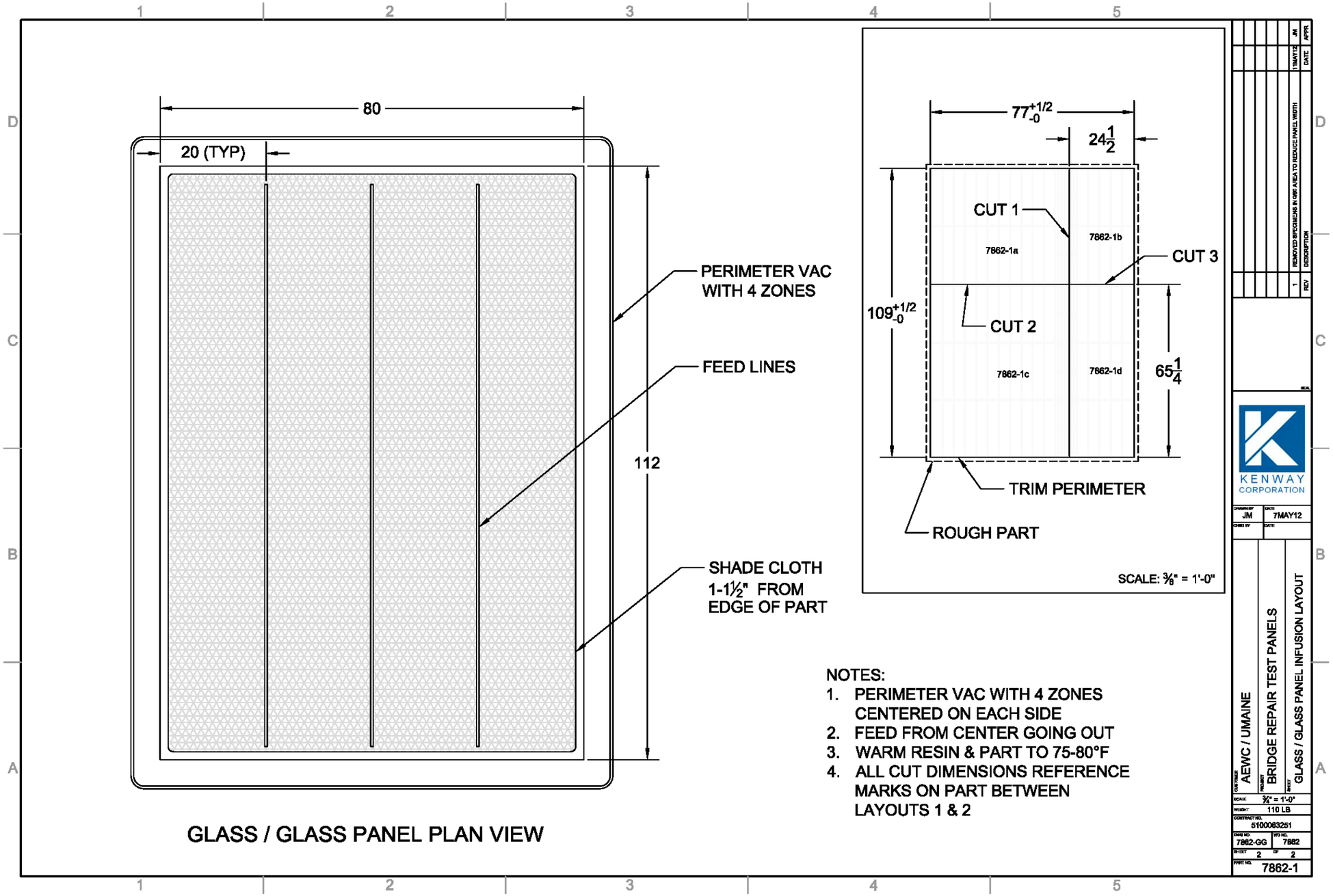
80
20 (TYP)
112
PERIMETER VAC
WITH 4 ZONES
FEED LINES
SHADE CLOTH
1-1½" FROM
EDGE OF PART
GLASS / GLASS PANEL PLAN VIEW
$77^{+1/2}_{-0}$
$24\frac{1}{2}$
$109^{+1/2}_{-0}$
$65\frac{1}{4}$
CUT 1
CUT 2
CUT 3
7862-1a
7862-1b
7862-1c
7862-1d
TRIM PERIMETER
ROUGH PART
SCALE: ⅜" = 1'-0"
NOTES:
1. PERIMETER VAC WITH 4 ZONES CENTERED ON EACH SIDE
2. FEED FROM CENTER GOING OUT
3. WARM RESIN & PART TO 75-80°F
4. ALL CUT DIMENSIONS REFERENCE MARKS ON PART BETWEEN LAYOUTS 1 & 2
REV 1 DESCRIPTION REMOVED SPECIMENS IN OBS AREA TO REDUCE PANEL WIDTH DATE 11MAY12 APPR JM
KENWAY CORPORATION
DRAWN BY JM DATE 7MAY12
CHKD BY DATE
CONTRACT AEWC / UMAINE
PROJECT BRIDGE REPAIR TEST PANELS
SHEET GLASS / GLASS PANEL INFUSION LAYOUT
SCALE ¾" = 1'-0"
WEIGHT 110 LB
CONTRACT NO. 5100083251
DWG NO. 7862-GG
WO NO. 7882
SHEET 2 OF 2
PART NO. 7862-1

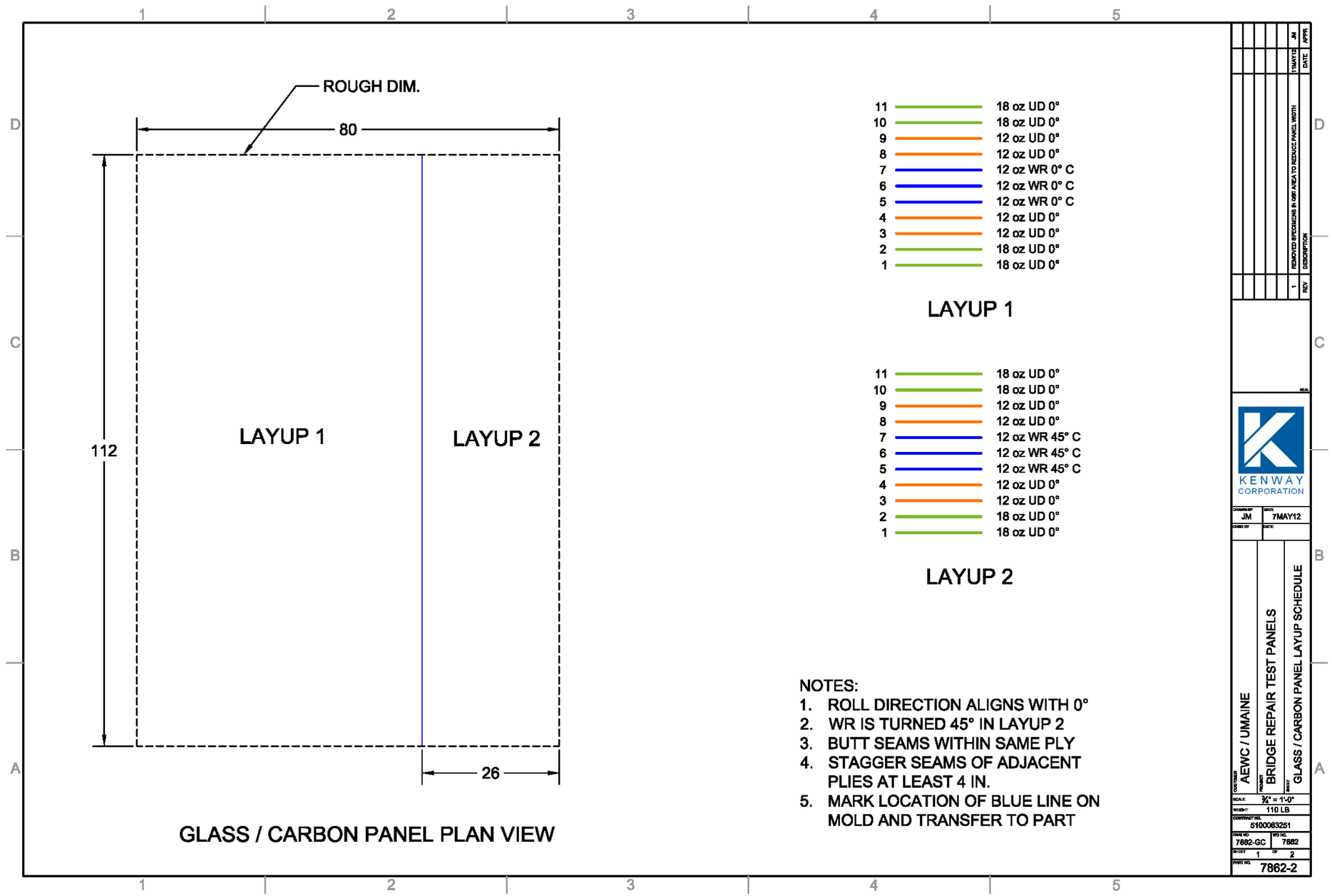
ROUGH DIM.
80
112
26
LAYUP 1
LAYUP 2
11 18 oz UD 0°
10 18 oz UD 0°
9 12 oz UD 0°
8 12 oz UD 0°
7 12 oz WR 0° C
6 12 oz WR 0° C
5 12 oz WR 0° C
4 12 oz UD 0°
3 12 oz UD 0°
2 18 oz UD 0°
1 18 oz UD 0°
LAYUP 1
11 18 oz UD 0°
10 18 oz UD 0°
9 12 oz UD 0°
8 12 oz UD 0°
7 12 oz WR 45° C
6 12 oz WR 45° C
5 12 oz WR 45° C
4 12 oz UD 0°
3 12 oz UD 0°
2 18 oz UD 0°
1 18 oz UD 0°
LAYUP 2
NOTES:
1. ROLL DIRECTION ALIGNS WITH 0°
2. WR IS TURNED 45° IN LAYUP 2
3. BUTT SEAMS WITHIN SAME PLY
4. STAGGER SEAMS OF ADJACENT PLIES AT LEAST 4 IN.
5. MARK LOCATION OF BLUE LINE ON MOLD AND TRANSFER TO PART
GLASS / CARBON PANEL PLAN VIEW
REV 1 DESCRIPTION REMOVED SPECIMENS IN G90 AREA TO REDUCE PANEL WIDTH DATE 7MAY12 APPR JM
KENWAY CORPORATION
DRAWN BY JM DATE 7MAY12
CHKED BY DATE
CONTRACT AEWC / UMAINE
PROJECT BRIDGE REPAIR TEST PANELS
SHEET GLASS / CARBON PANEL LAYUP SCHEDULE
SCALE 3/4" = 1'-0"
WEIGHT 110 LB
CONTRACT NO. 5100083251
DRWG NO. 7862-GC
WO NO. 7862
SHEET 1 OF 2
PART NO. 7862-2

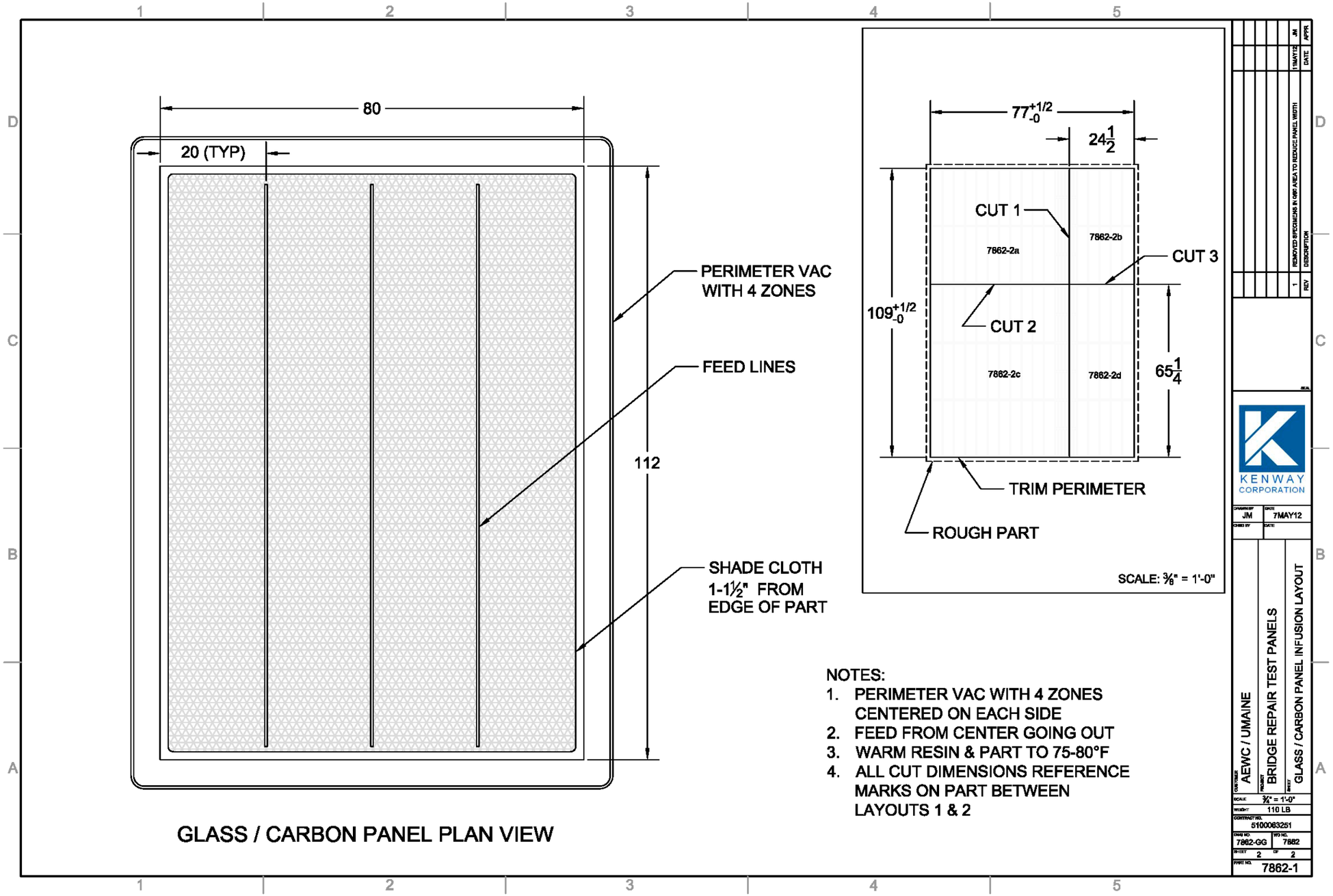
80
20 (TYP)
112
PERIMETER VAC
WITH 4 ZONES
FEED LINES
SHADE CLOTH
1-1½" FROM
EDGE OF PART
GLASS / CARBON PANEL PLAN VIEW
$77^{+1/2}_{-0}$
$24\frac{1}{2}$
$109^{+1/2}_{-0}$
$65\frac{1}{4}$
CUT 1
CUT 2
CUT 3
7862-2a
7862-2b
7862-2c
7862-2d
TRIM PERIMETER
ROUGH PART
SCALE: ⅜" = 1'-0"
NOTES:
1. PERIMETER VAC WITH 4 ZONES CENTERED ON EACH SIDE
2. FEED FROM CENTER GOING OUT
3. WARM RESIN & PART TO 75-80°F
4. ALL CUT DIMENSIONS REFERENCE MARKS ON PART BETWEEN LAYOUTS 1 & 2
REMOVED SPECIMENS IN ORIG AREA TO REDUCE PANEL WIDTH
DESCRIPTION
REV
DATE
APPR
11MAY12
JM
KENWAY CORPORATION
DRAWN BY JM
DATE 7MAY12
CHKD BY
DATE
CONTRACT AEWC / UMAINE
PROJECT BRIDGE REPAIR TEST PANELS
SHEET GLASS / CARBON PANEL INFUSION LAYOUT
SCALE ¾" = 1'-0"
WEIGHT 110 LB
CONTRACT NO. 5100083251
DWG NO. 7862-GG
WO NO. 7862
SHEET 2 OF 2
PART NO. 7862-1

APPENDIX B: ASTM D3039 Test Specimen Measurements

Table 7: Specimen Dimensions - Glass/Glass 0/90° Layup

Specimen No.	Avg. Width	Avg. Thickness	Avg. Cross-Sectional Area
4	0.996	0.2025	0.2016
8	0.993	0.2007	0.1992
9	0.99	0.2088	0.2067
10	0.99	0.2085	0.2104

Table 8: Specimen Dimensions - Glass/Glass 0/45 Layup

Specimen No.	Avg. Width	Avg. Thickness	Avg. Cross-Sectional Area
1	1.001	0.2193	0.2195
3	1.004	0.2148	0.2156
5	1.007	0.2143	0.2158
6	1.006	0.2168	0.2181
8	1.004	0.216	0.2168
10	0.997	0.2147	0.2140
11	0.999	0.2143	0.2140
12	1.000	0.2107	0.2107

Table 9: Specimen Dimensions - Glass/Carbon 0/90 Layup

Specimen No.	Avg. Width	Avg. Thickness	Avg. Cross-Sectional Area
1	0.992	0.194	0.1924
3	0.992	0.1933	0.1917
4	0.996	0.1963	0.1955
6	0.959	0.192	0.1841
8	0.994	0.188	0.1869
9	0.95	0.1942	0.1844
11	0.951	0.1943	0.1847
12	0.992	0.1888	0.1872

Table 10: Specimen Dimensions - Glass/Carbon 0/45 Layup

Specimen No.	Avg. Width	Avg. Thickness	Avg. Cross-Sectional Area
1	0.995	0.1992	0.1982
2	0.997	0.2053	0.2046
5	0.995	0.199	0.1980
7	0.995	0.1917	0.1907
8	0.986	0.1943	0.1915
9	0.996	0.1965	0.1957
10	0.995	0.1933	0.1923
11	0.999	0.1933	0.1931

APPENDIX C: ASTM D3039 Specimen Acceptability

Table 11: ASTM D3039 Tensile Strength Test Failure Modes - Glass/Glass 0/90 Layup

Specimen No.	Failure Mode	Acceptability
1	Fiber rupture and matrix cracking	A*
2	Splitting within grips	N
3	Fiber rupture and matrix cracking within grips	N
4	Longitudinal splitting	A
5	Splitting within grips	N
6	Fiber rupture and matrix cracking within grips	N
7	Longitudinal splitting	A*
8	Fiber rupture, matrix cracking, and longitudinal splitting	A
9	Fiber rupture and matrix cracking; Delamination	A
10	Fiber rupture and matrix cracking	A
11	Splitting within grips	N
12	Fiber rupture and matrix cracking within grips	N

Table 12: ASTM D3039 Tensile Strength Test Failure Modes – Glass/Glass 0/±45 Layup

Specimen No.	Failure Mode	Acceptability
1	Longitudinal splitting	A
2	Grip slip	N
3	Longitudinal splitting	A
4	Splitting within grips	N
5	Fiber rupture and matrix cracking	A
6	Fiber rupture and matrix cracking	A
7	Splitting within grips	N
8	Fiber rupture and matrix cracking	A
9	Grip slip	N
10	Longitudinal splitting	A
11	Fiber rupture and matrix cracking	A
12	Fiber rupture and matrix cracking	A

Table 13: ASTM D3039 Tensile Strength Test Failure Modes - Glass/Carbon 0/90 Layup

Specimen No.	Failure Mode	Acceptability
1	Fiber rupture and matrix cracking; Delamination	A
2	Grip slip; delamination of outer layers from core layer	N
3	Fiber rupture and matrix cracking; Delamination	A
4	Fiber rupture and matrix cracking within grips	N
5	Fiber rupture and matrix cracking; Delamination	A**
6	Fiber rupture and matrix cracking	A
7	Fiber rupture and matrix cracking; Delamination	A
8	Fiber rupture and matrix cracking within grips	N
9	Fiber rupture and matrix cracking; Delamination	A
10	Fiber rupture and matrix cracking; Delamination	A
11	Fiber rupture and matrix cracking; Delamination	A
12	Fiber rupture and matrix cracking; Delamination	A

Table 14: ASTM D3039 Tensile Strength Test Failure Modes - Glass/Carbon 0/45 Layup

Specimen No.	Failure Mode	Acceptability
1	Fiber rupture and matrix cracking; Delamination	A
2	Fiber rupture and matrix cracking; Delamination	A
3	Fiber rupture and matrix cracking; Delamination	A*
4	Fiber rupture and matrix cracking; Delamination	A*
5	Fiber rupture and matrix cracking; Delamination	A
6	Lateral failure at grip resulting in delamination	N
7	Fiber rupture and matrix cracking; longitudinal splitting; Delamination	A
8	Fiber rupture and matrix cracking; Delamination	A
9	Fiber rupture and matrix cracking; Delamination	A
10	Fiber rupture and matrix cracking; Longitudinal splitting; Delamination	A
11	Fiber rupture and matrix cracking; Delamination	A
12	Lateral failure at grip resulting in Delamination	N

*Result omitted from calculations due to noisy strain data

** Data for coupon was lost

APPENDIX D: ASTM D3039 Stress-Strain Plots

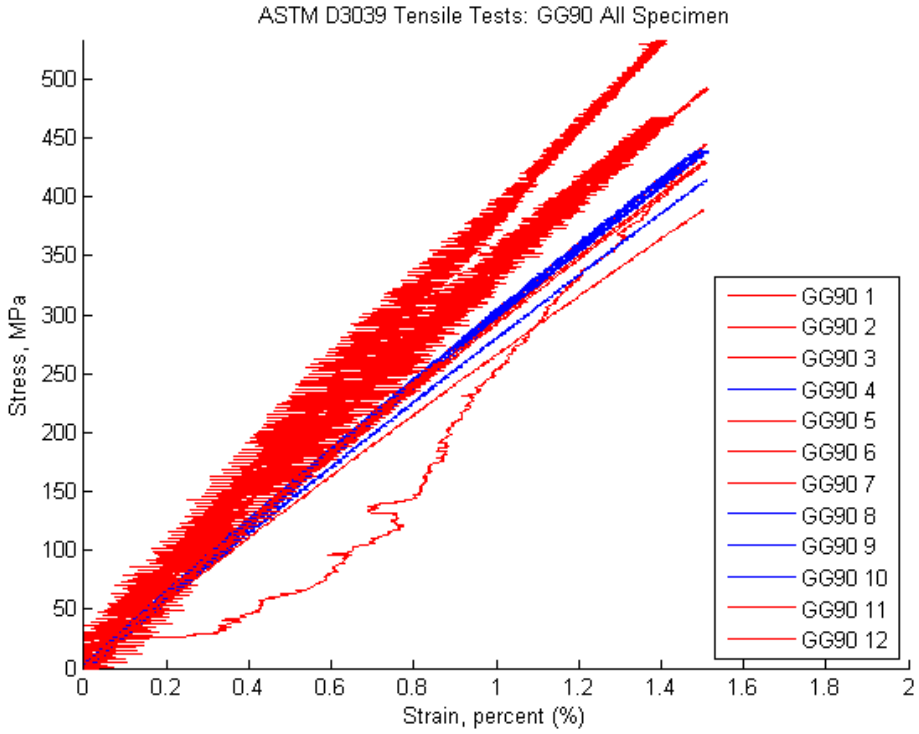

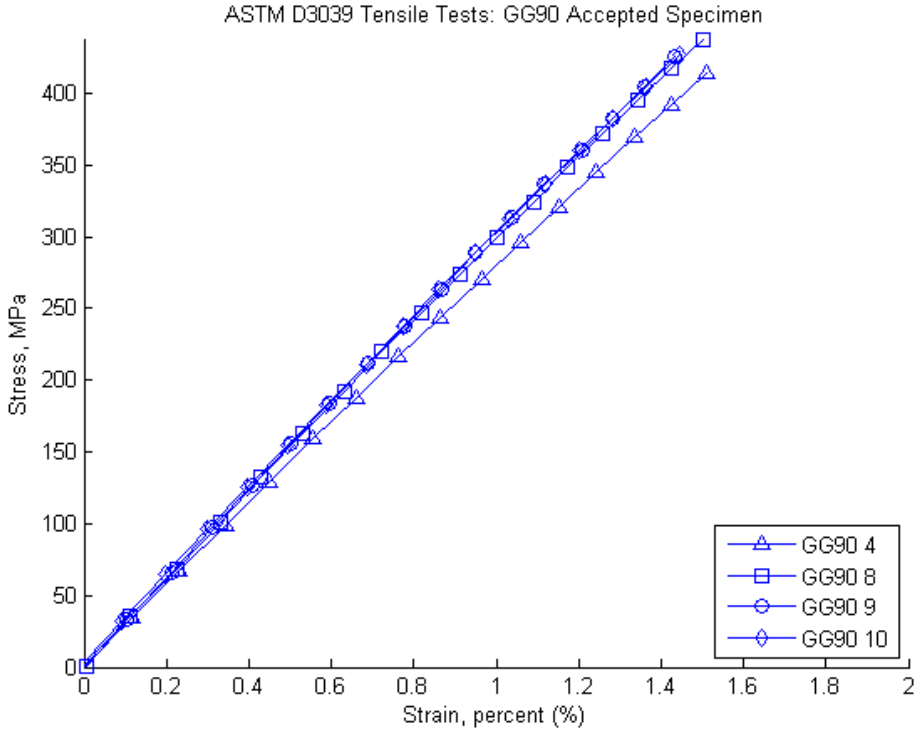

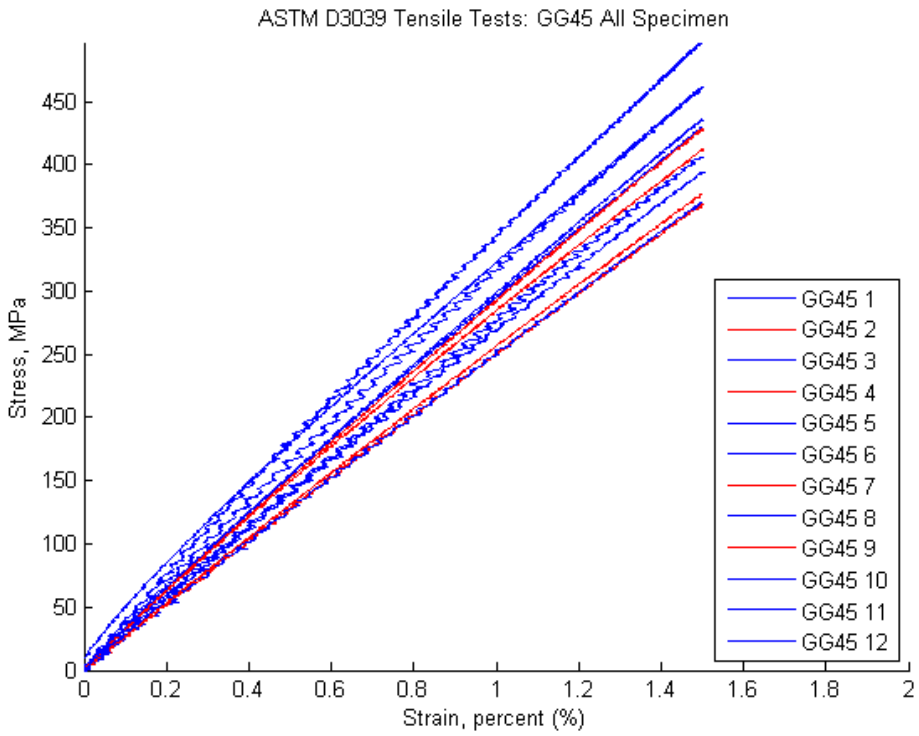
ASTM D3039 Tensile Tests: GG45 All Specimen
Stress, MPa
Strain, percent (%)
0
50
100
150
200
250
300
350
400
450
0
0.2
0.4
0.6
0.8
1
1.2
1.4
1.6
1.8
2
GG45 1
GG45 2
GG45 3
GG45 4
GG45 5
GG45 6
GG45 7
GG45 8
GG45 9
GG45 10
GG45 11
GG45 12

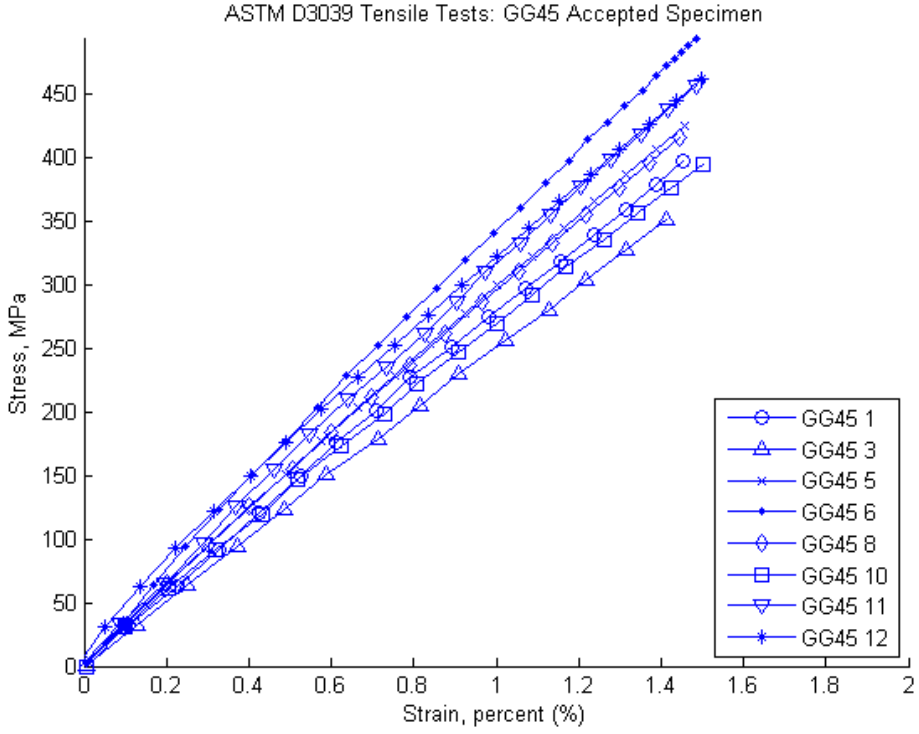
ASTM D3039 Tensile Tests: GG45 Accepted Specimen
Stress, MPa
Strain, percent (%)
0
50
100
150
200
250
300
350
400
450
0
0.2
0.4
0.6
0.8
1
1.2
1.4
1.6
1.8
2
GG45 1
GG45 3
GG45 5
GG45 6
GG45 8
GG45 10
GG45 11
GG45 12

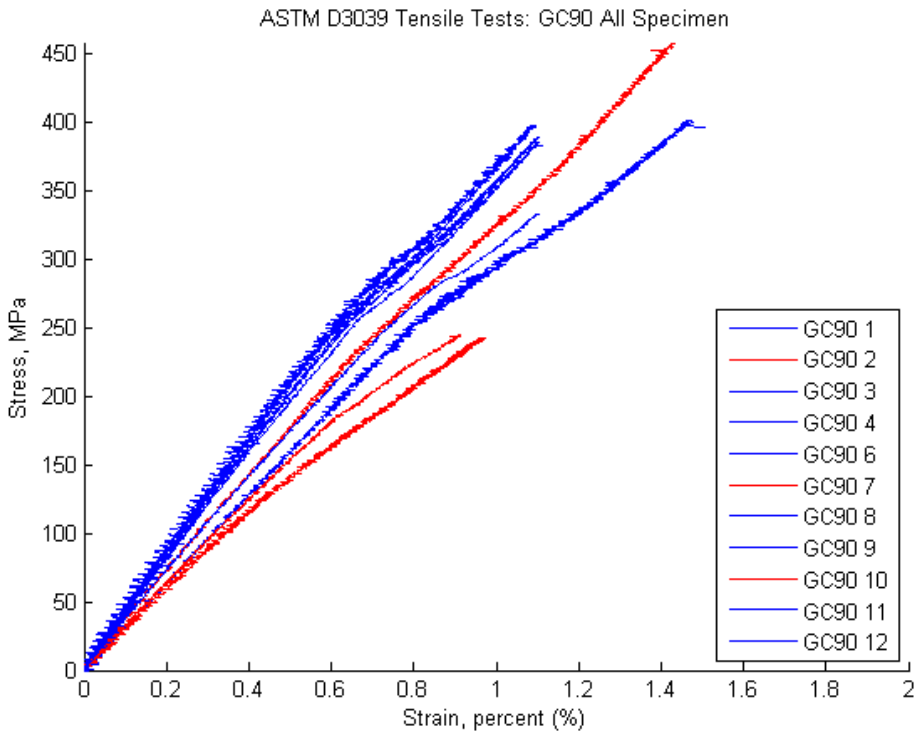
ASTM D3039 Tensile Tests: GC90 All Specimen
Stress, MPa
Strain, percent (%)
GC90 1
GC90 2
GC90 3
GC90 4
GC90 6
GC90 7
GC90 8
GC90 9
GC90 10
GC90 11
GC90 12

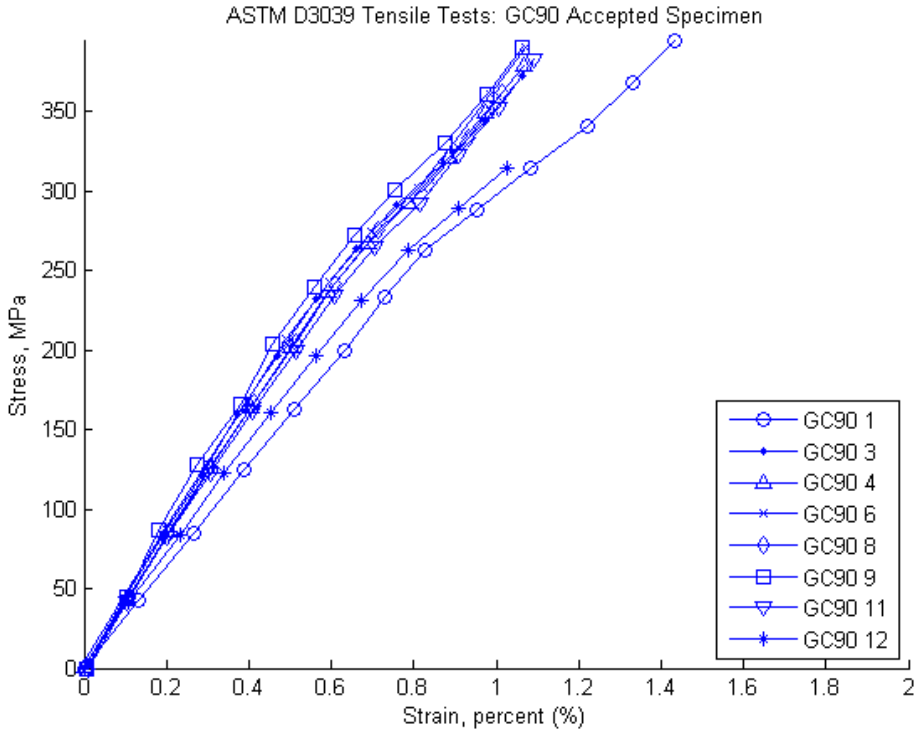
ASTM D3039 Tensile Tests: GC90 Accepted Specimen
Stress, MPa
Strain, percent (%)
GC90 1
GC90 3
GC90 4
GC90 6
GC90 8
GC90 9
GC90 11
GC90 12

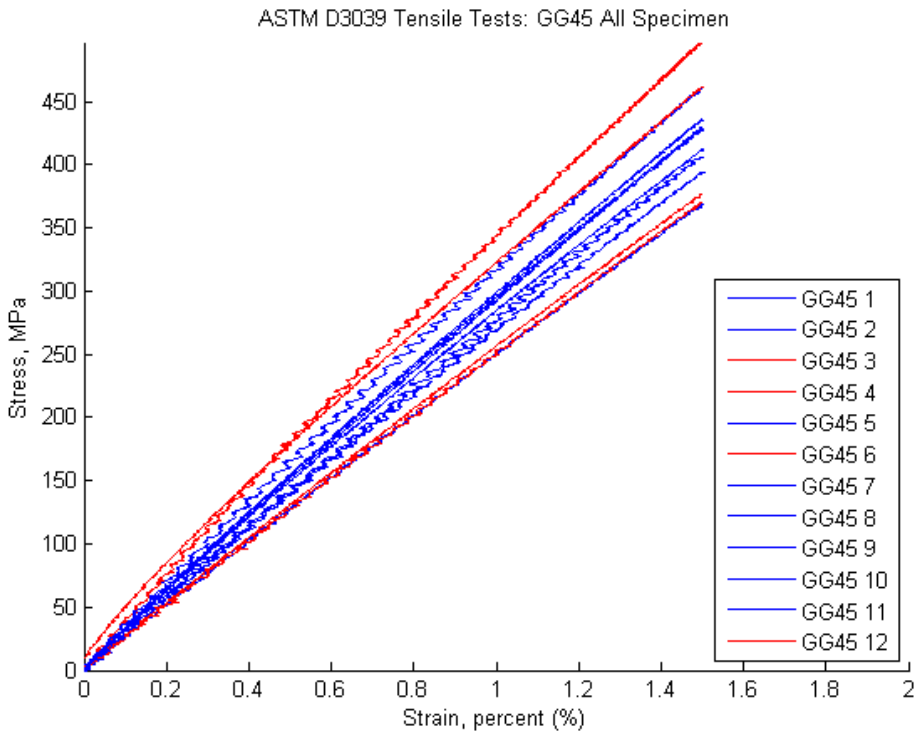
ASTM D3039 Tensile Tests: GG45 All Specimen
Stress, MPa
Strain, percent (%)
0
50
100
150
200
250
300
350
400
450
0
0.2
0.4
0.6
0.8
1
1.2
1.4
1.6
1.8
2
GG45 1
GG45 2
GG45 3
GG45 4
GG45 5
GG45 6
GG45 7
GG45 8
GG45 9
GG45 10
GG45 11
GG45 12

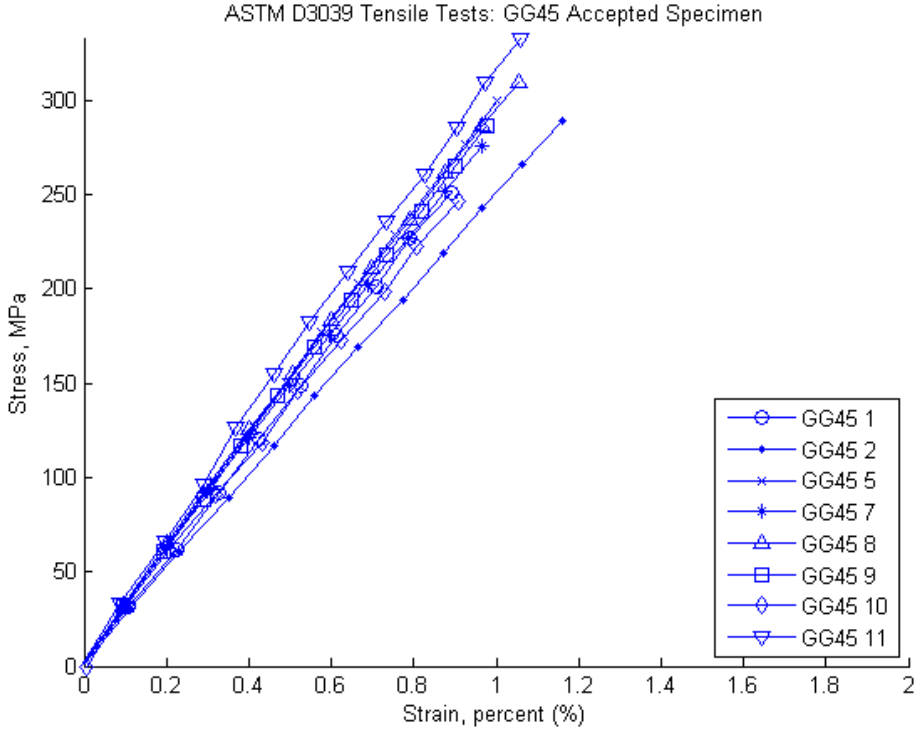
ASTM D3039 Tensile Tests: GG45 Accepted Specimen
Stress, MPa
Strain, percent (%)
0
50
100
150
200
250
300
0
0.2
0.4
0.6
0.8
1
1.2
1.4
1.6
1.8
2
GG45 1
GG45 2
GG45 5
GG45 7
GG45 8
GG45 9
GG45 10
GG45 11

APPENDIX E: ASTM D3039 Individual Specimen Test Results

Table 15: Maximum Load, Tensile Stress, and Chord Modulus - Glass/Glass 0/90° Layup

Specimen No.	Maximum Load (lbf)	Maximum Tensile Strength (psi)	Chord Modulus of Elasticity (ksi)
4	16483	81723	4083
8	16241	81495	4502
9	17198	83154	4585
10	17155	83068	4464

Table 16: Maximum Load, Tensile Stress, and Chord Modulus - Glass/Glass 0/45 Layup

Specimen No.	Maximum Load (lbf)	Maximum Tensile Strength (psi)	Elastic Chord of Modulus (ksi)
1	15749	71757	3928
3	15825	73418	3615
5	15536	71970	4509
6	15908	72918	5142
8	15319	70638	4492
10	16154	75465	4017
11	16109	75248	4480
12	16176	76813	4889

Table 17: Maximum Load, Tensile Stress, and Chord Modulus - Glass/Carbon 0/90 Layup

Specimen No.	Maximum Load (lbf)	Maximum Tensile Strength (psi)	Elastic Chord of Modulus (ksi)
1	15069	78280	4684
3	17011	88712	5922
4	17392	88927	5828
6	15993	86883	5936
8	16802	89910	5704
9	16619	90131	6401
11	16557	89631	5733
12	16686	89065	5069

Table 18: Maximum Load, Tensile Stress, and Chord Modulus - Glass/Carbon 0/45 Layup

Specimen No.	Maximum Load (lbf)	Maximum Tensile Strength (psi)	Elastic Chord of Modulus (ksi)
1	13444	67847	4199
2	14756	72093	4298
5	14953	75494	4583
7	14301	74961	4008
8	13933	72747	4536
9	15575	79597	4500
10	12824	66696	3776
11	15680	81174	4731

APPENDIX F: Durability Specimen Load-deformation Plots

GG90 Durability Specimen Average Peak Sustain Load Plots

Environmental Control Specimens

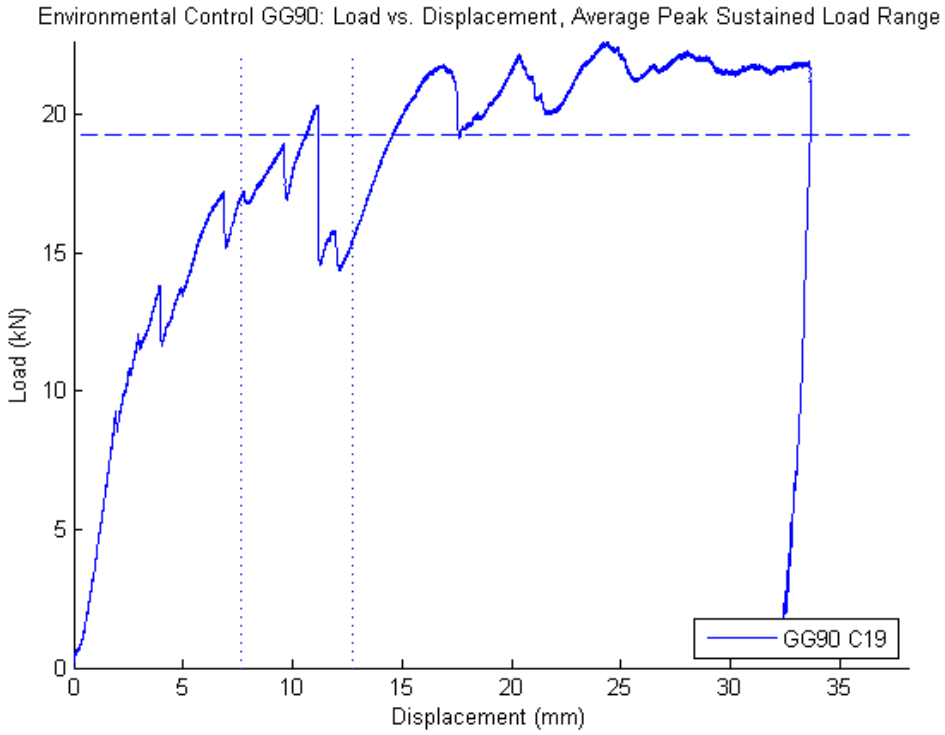

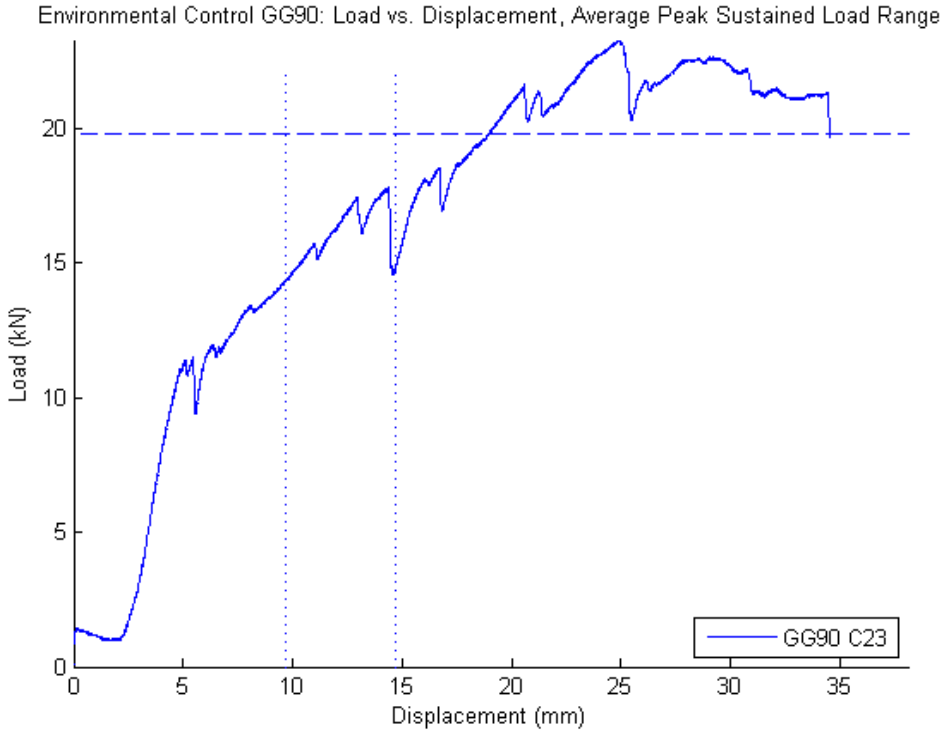

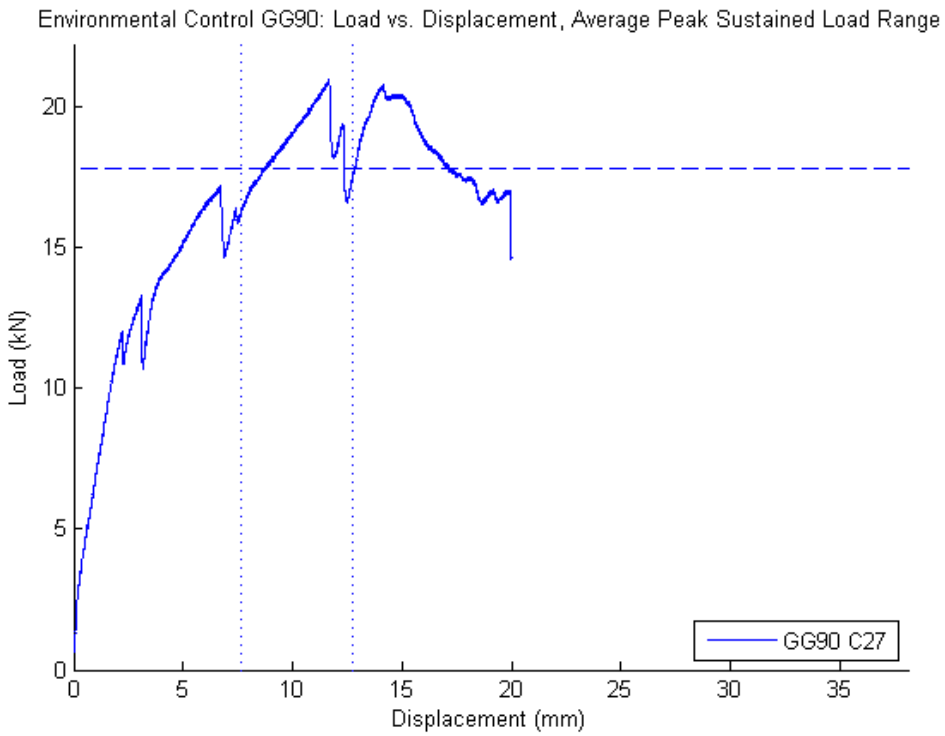
Environmental Control GG90: Load vs. Displacement, Average Peak Sustained Load Range
Load (kN)
Displacement (mm)
GG90 C27

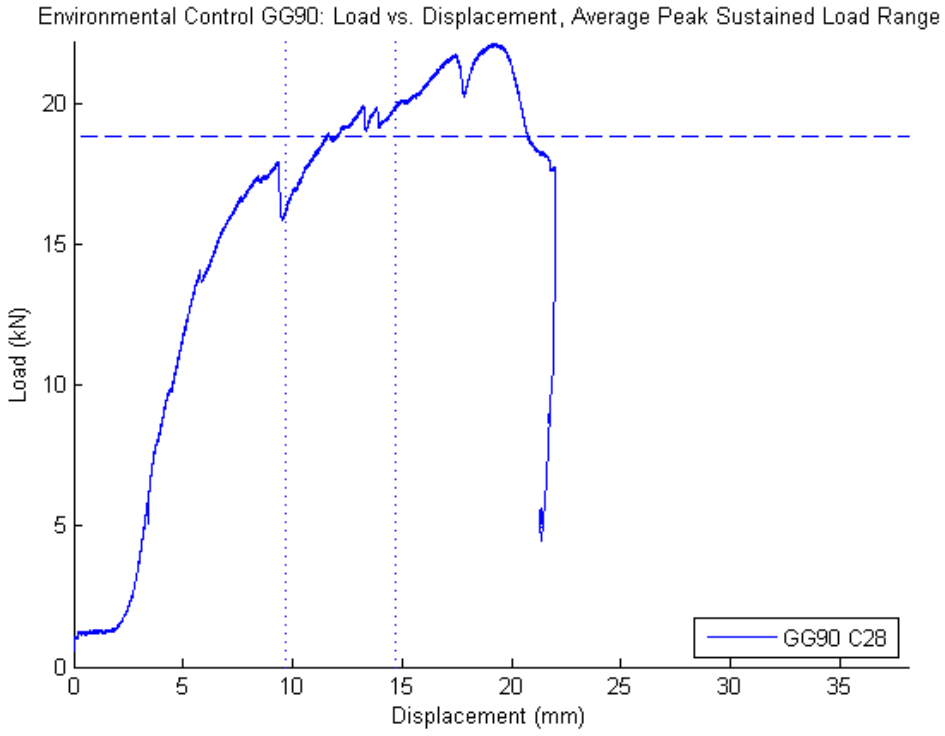
Environmental Control GG90: Load vs. Displacement, Average Peak Sustained Load Range
Load (kN)
Displacement (mm)
GG90 C28

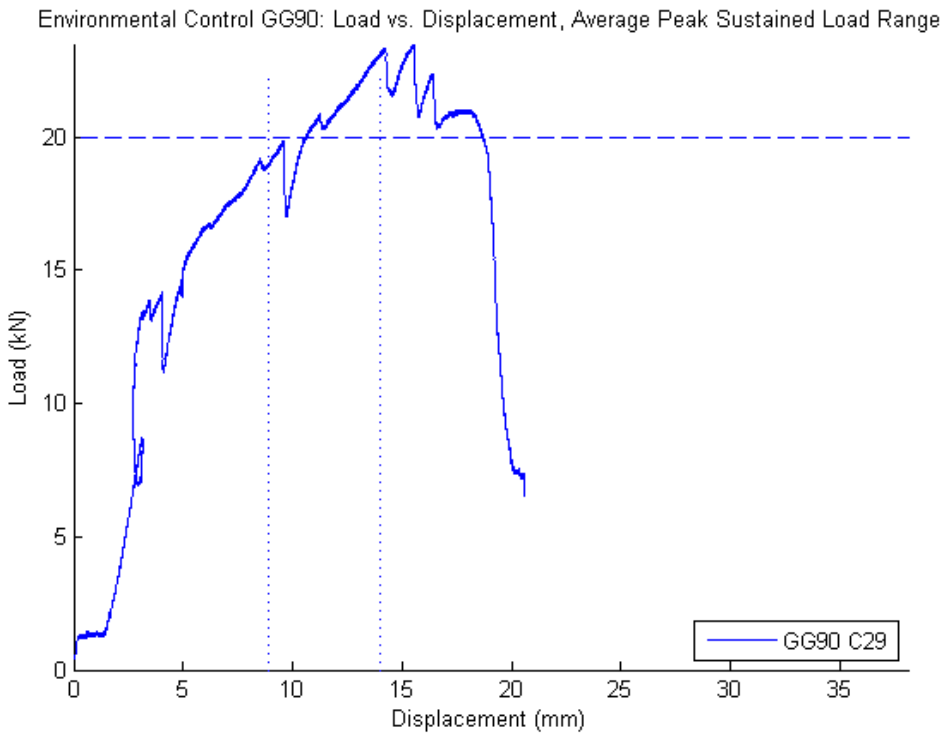
Environmental Control GG90: Load vs. Displacement, Average Peak Sustained Load Range
Load (kN)
Displacement (mm)
0
5
10
15
20
25
30
35
GG90 C29

Freeze-Thaw Specimens

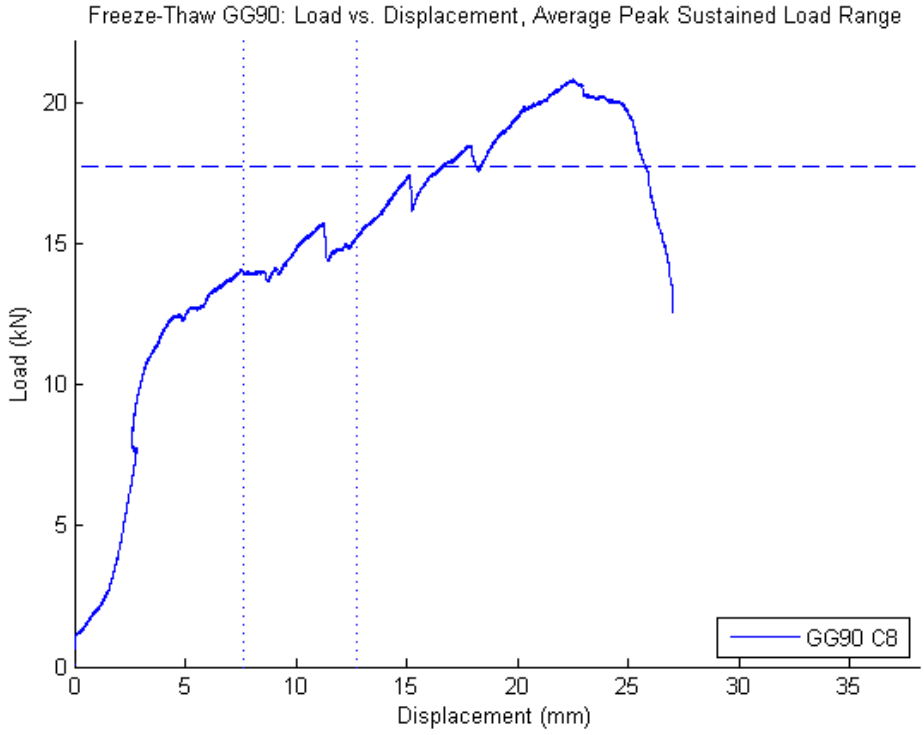

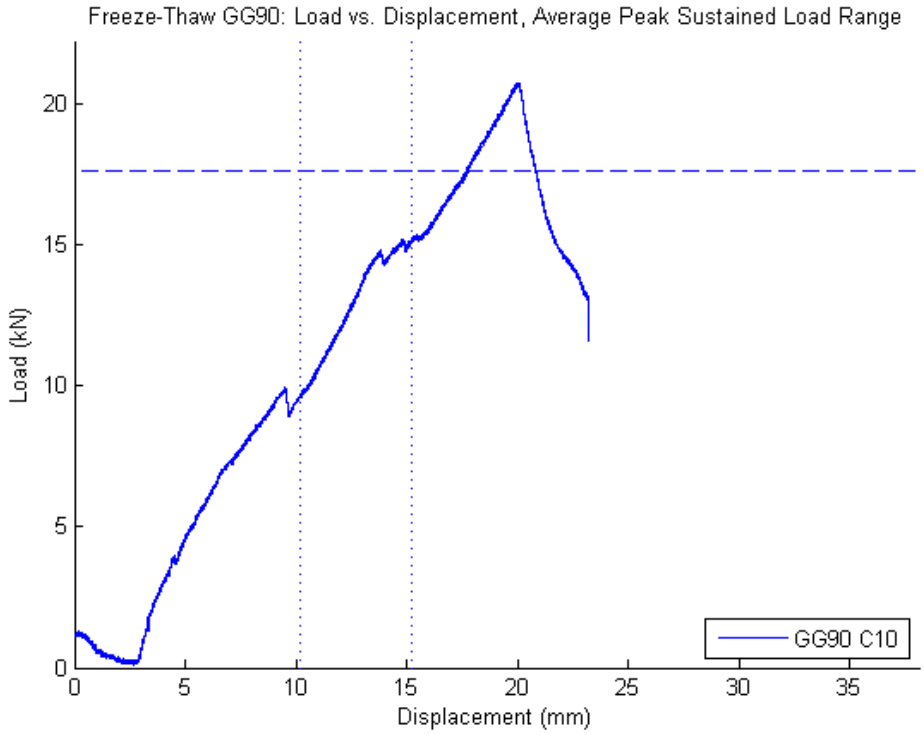

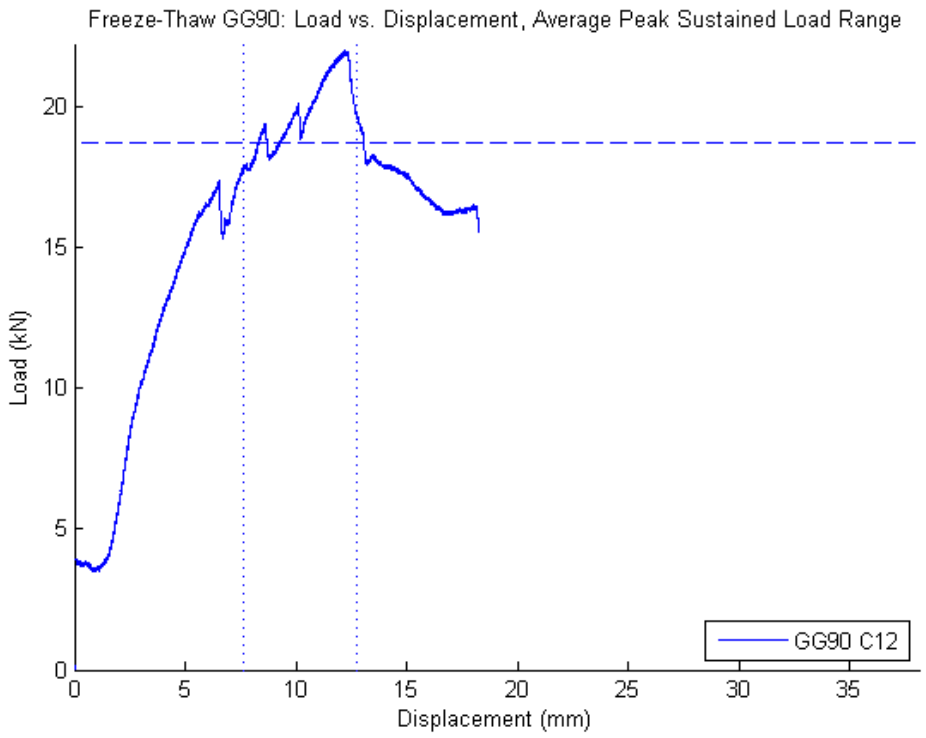
Freeze-Thaw GG90: Load vs. Displacement, Average Peak Sustained Load Range
Load (kN)
Displacement (mm)
GG90 C12

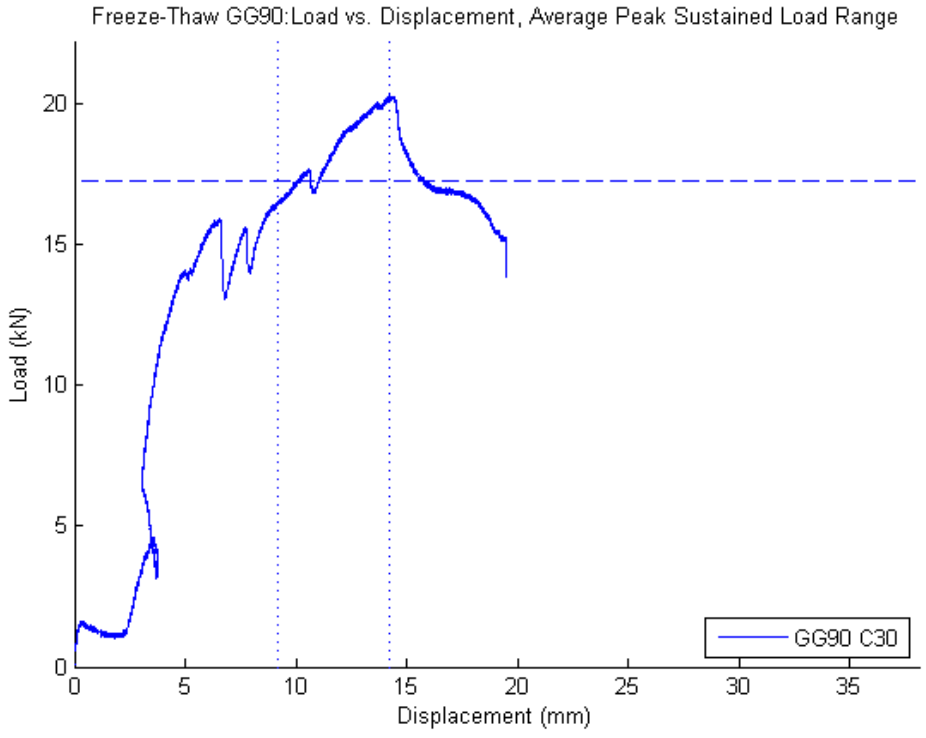
Freeze-Thaw GG90:Load vs. Displacement, Average Peak Sustained Load Range
Load (kN)
Displacement (mm)
GG90 C30

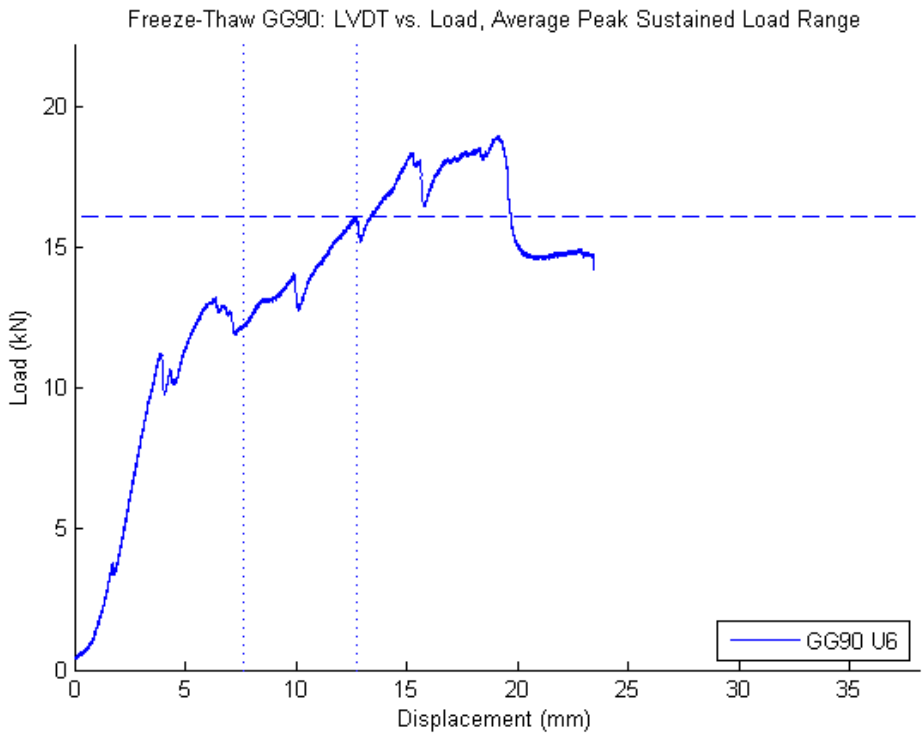
Freeze-Thaw GG90: LVDT vs. Load, Average Peak Sustained Load Range
Load (kN)
Displacement (mm)
GG90 U6
0
5
10
15
20
25
30
35

1000 Hour Saltwater Specimens

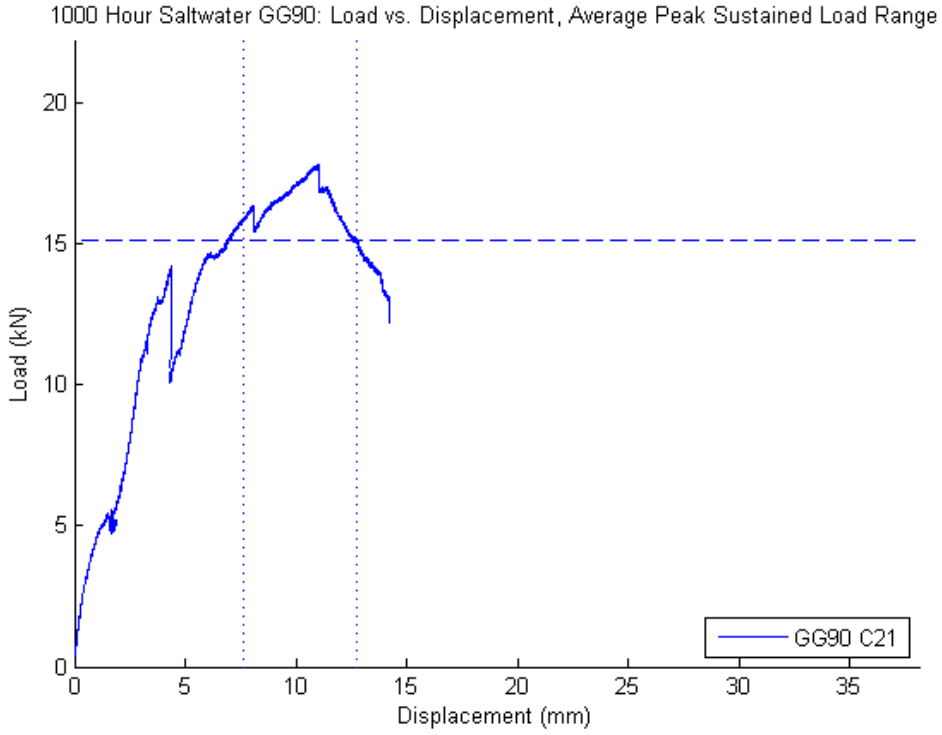

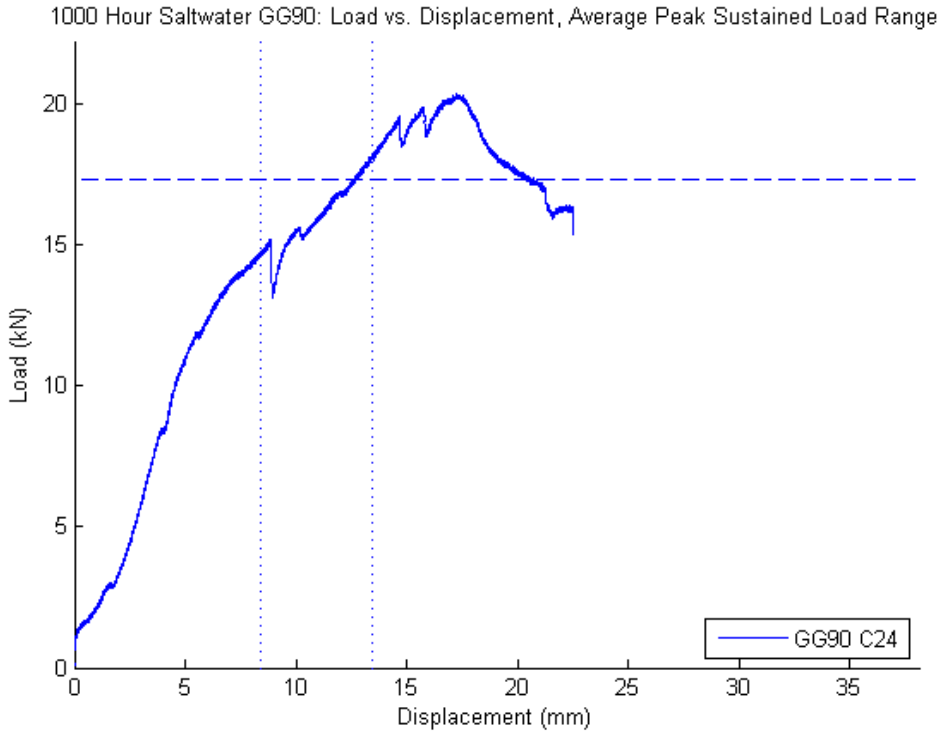

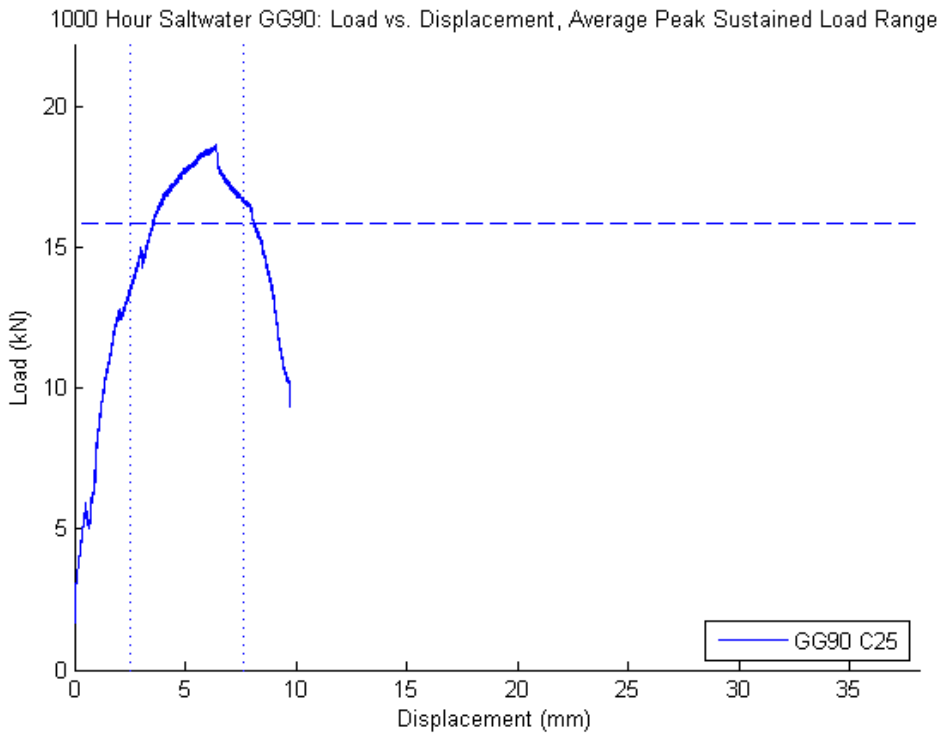
1000 Hour Saltwater GG90: Load vs. Displacement, Average Peak Sustained Load Range
Load (kN)
Displacement (mm)
GG90 C25

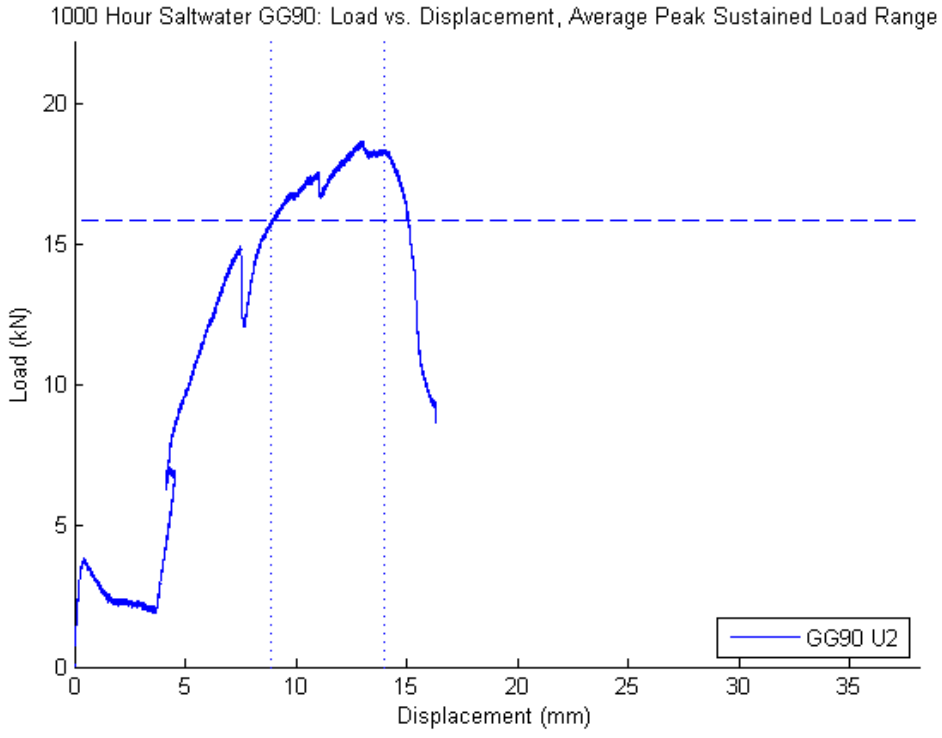
1000 Hour Saltwater GG90: Load vs. Displacement, Average Peak Sustained Load Range
Load (kN)
Displacement (mm)
GG90 U2

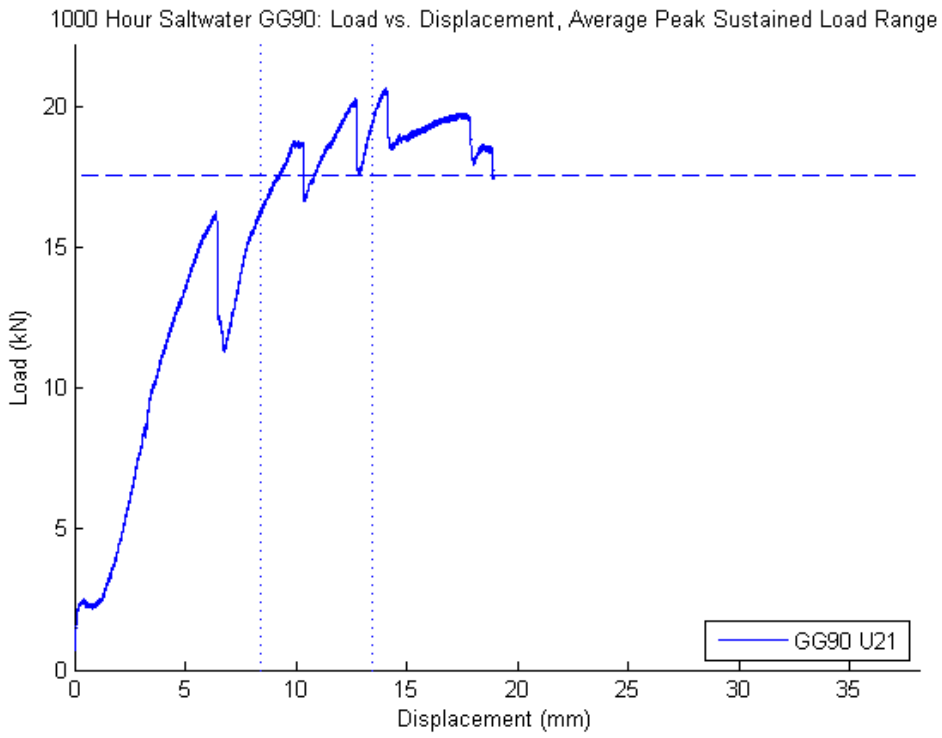
1000 Hour Saltwater GG90: Load vs. Displacement, Average Peak Sustained Load Range
Load (kN)
Displacement (mm)
GG90 U21
0
5
10
15
20
25
30
35

3000 Hour Saltwater Specimens

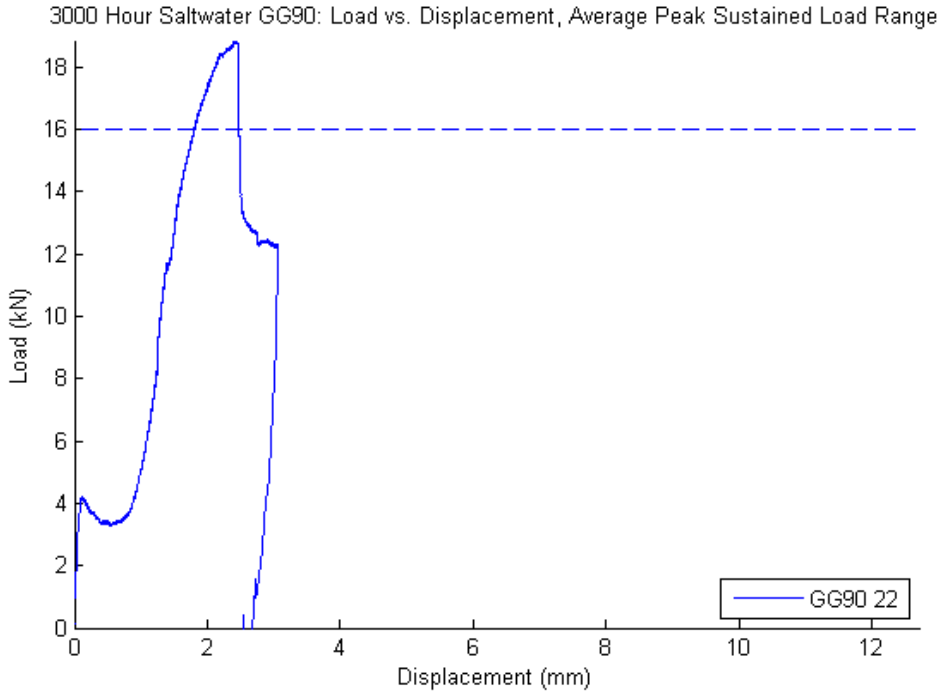

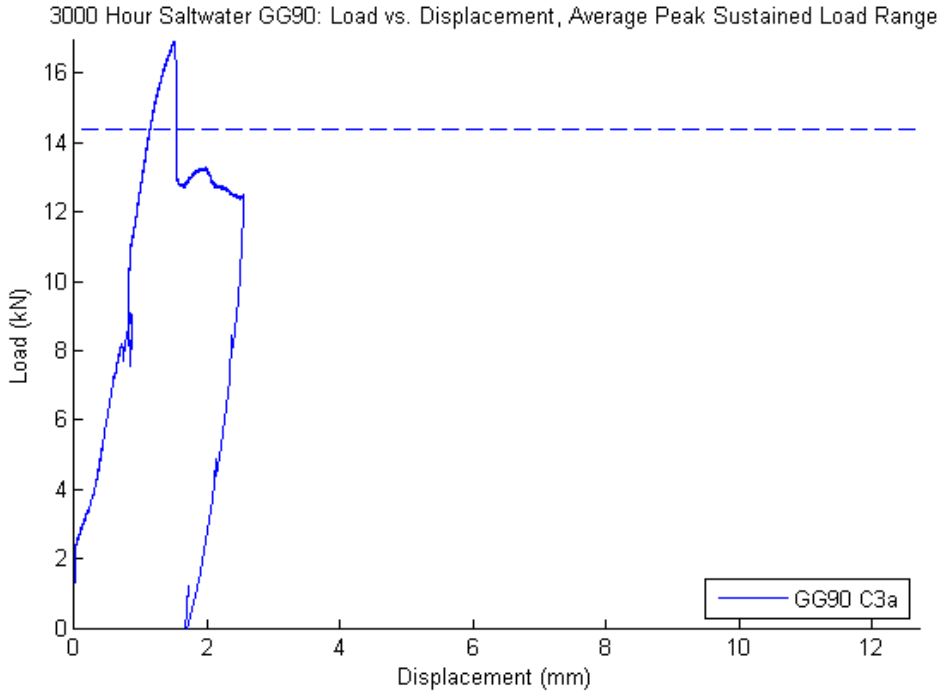

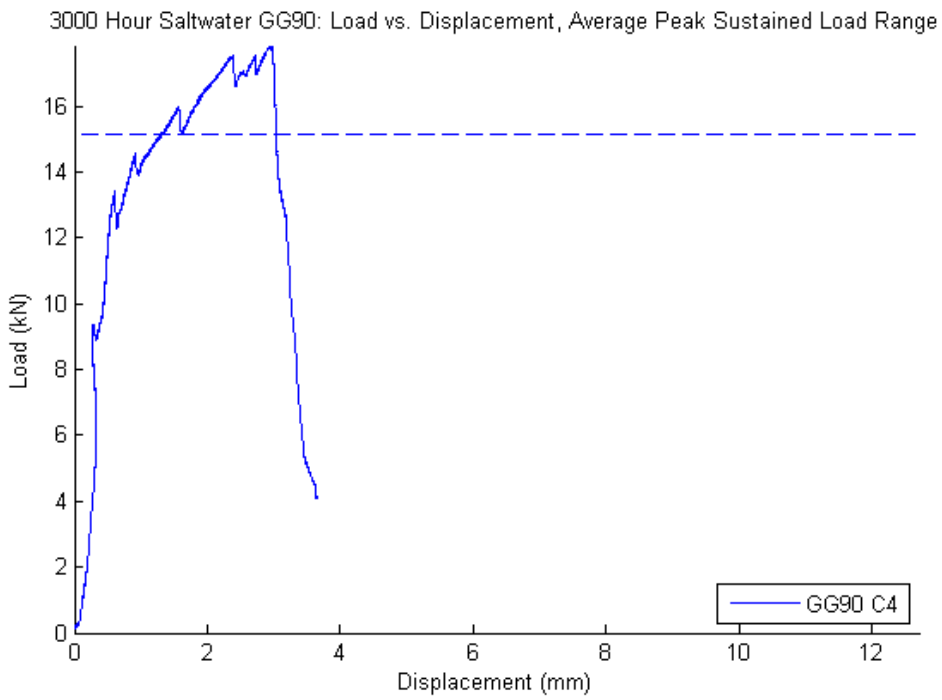
3000 Hour Saltwater GG90: Load vs. Displacement, Average Peak Sustained Load Range
Load (kN)
Displacement (mm)
GG90 C4

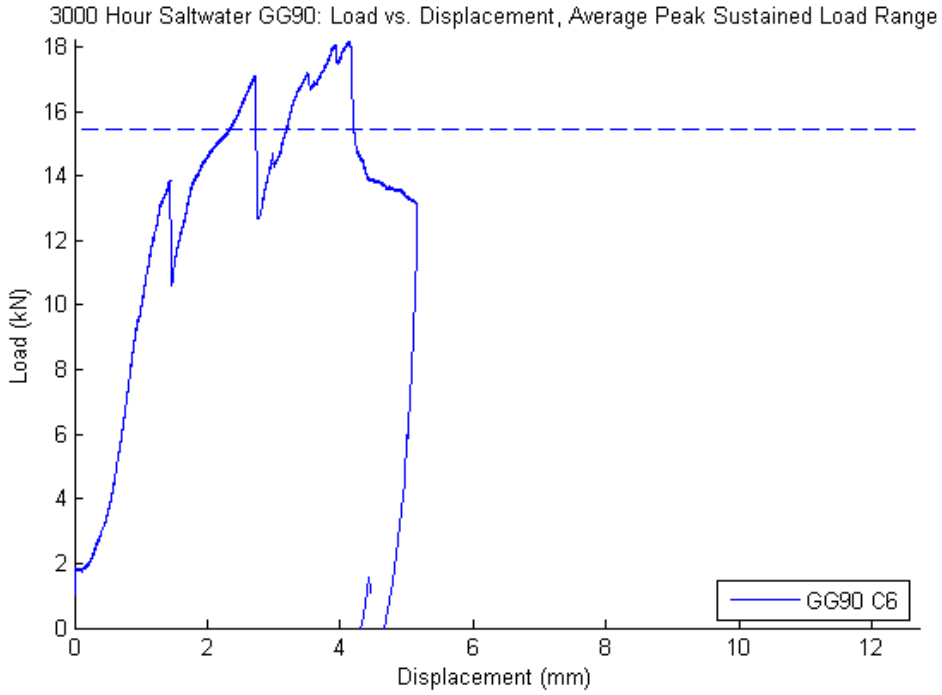
3000 Hour Saltwater GG90: Load vs. Displacement, Average Peak Sustained Load Range
Load (kN)
Displacement (mm)
GG90 C6

GG45 Durability Specimen Average Peak Sustain Load Plots

Environmental Control Specimens

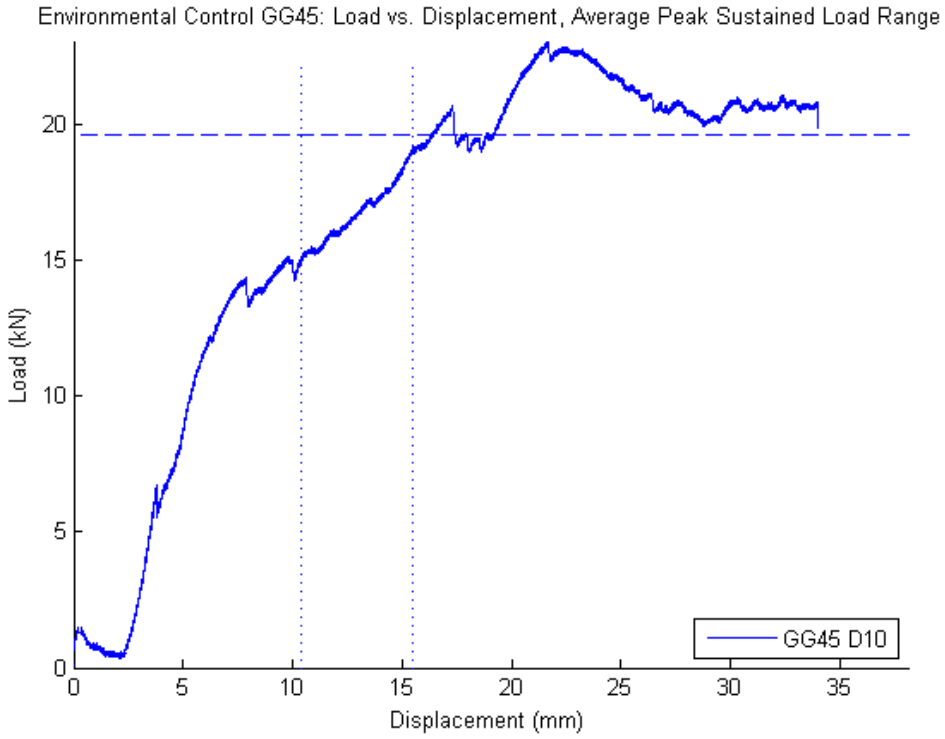

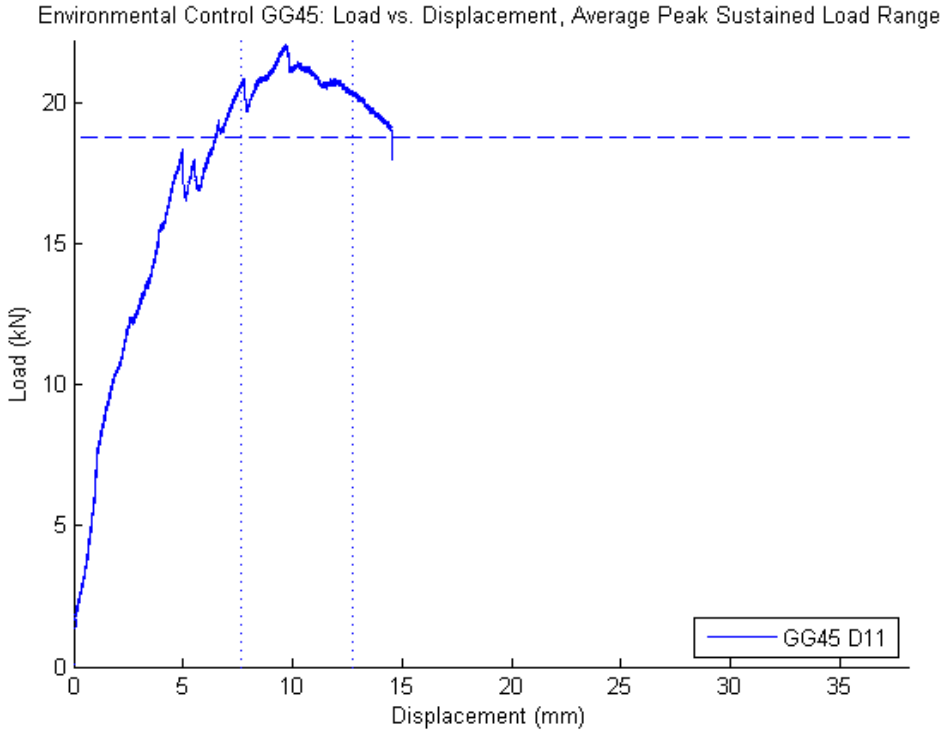

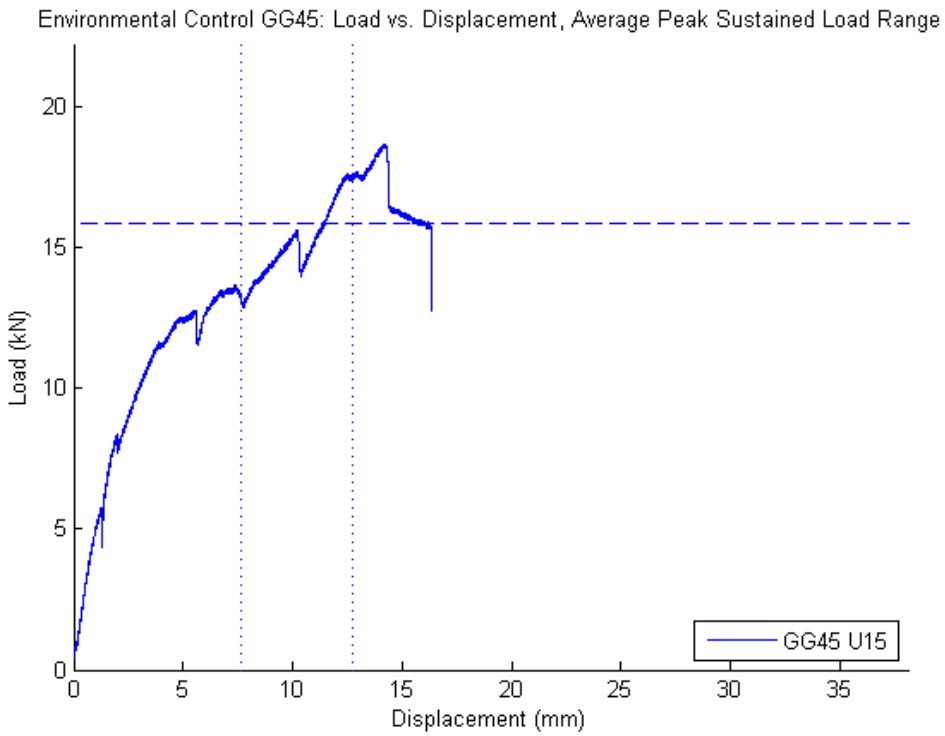
Environmental Control GG45: Load vs. Displacement, Average Peak Sustained Load Range
Load (kN)
Displacement (mm)
GG45 U15

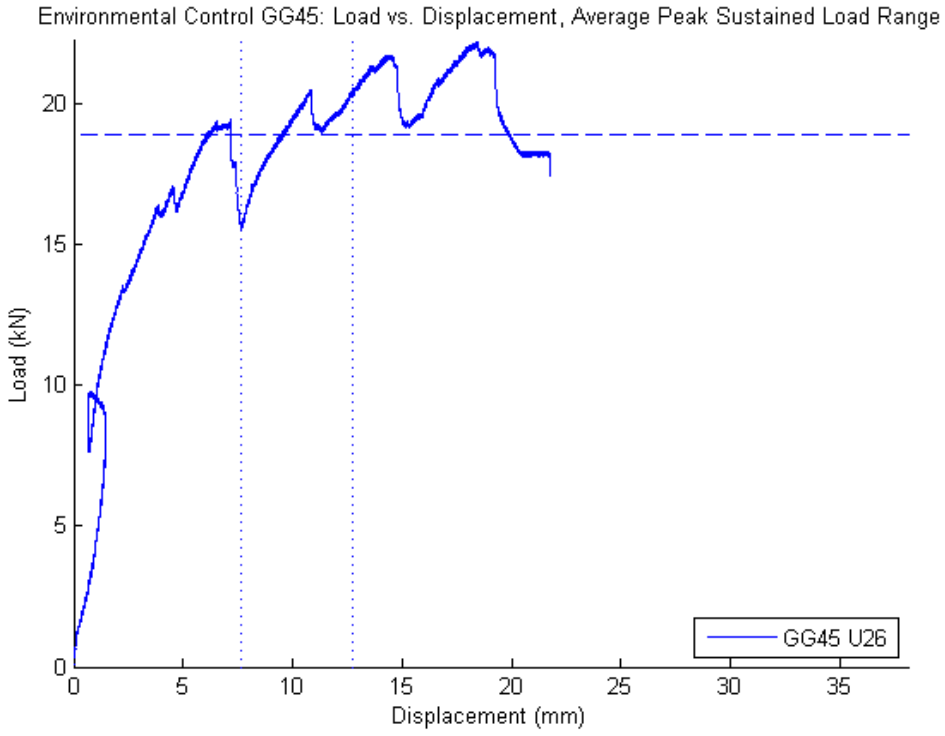
Environmental Control GG45: Load vs. Displacement, Average Peak Sustained Load Range
Load (kN)
Displacement (mm)
GG45 U26

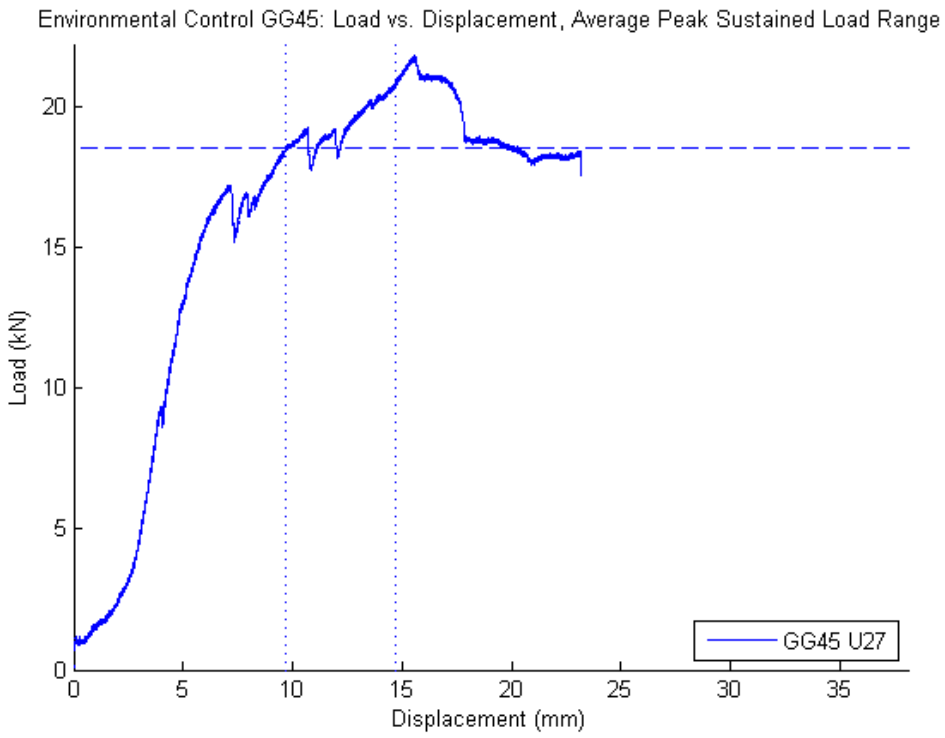
Environmental Control GG45: Load vs. Displacement, Average Peak Sustained Load Range
Load (kN)
Displacement (mm)
0
5
10
15
20
25
30
35
GG45 U27

Freeze-Thaw Specimens

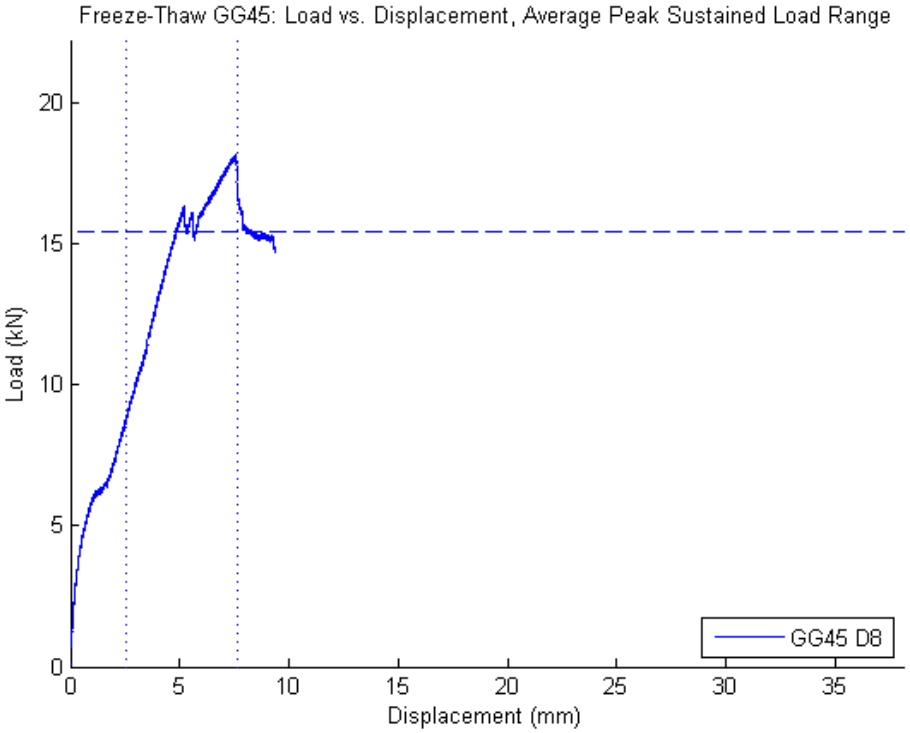

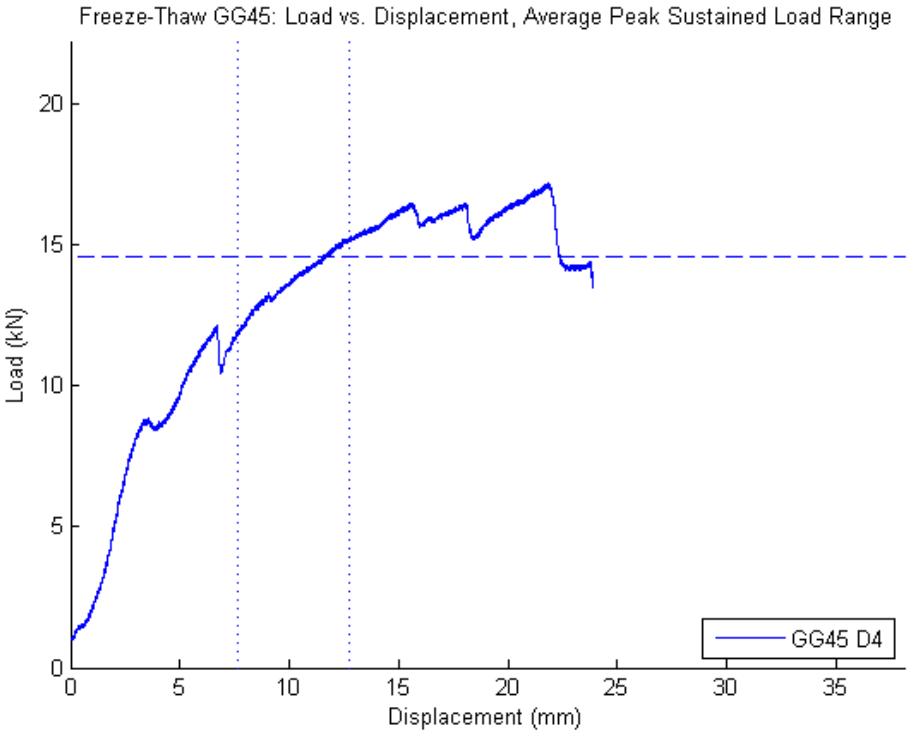

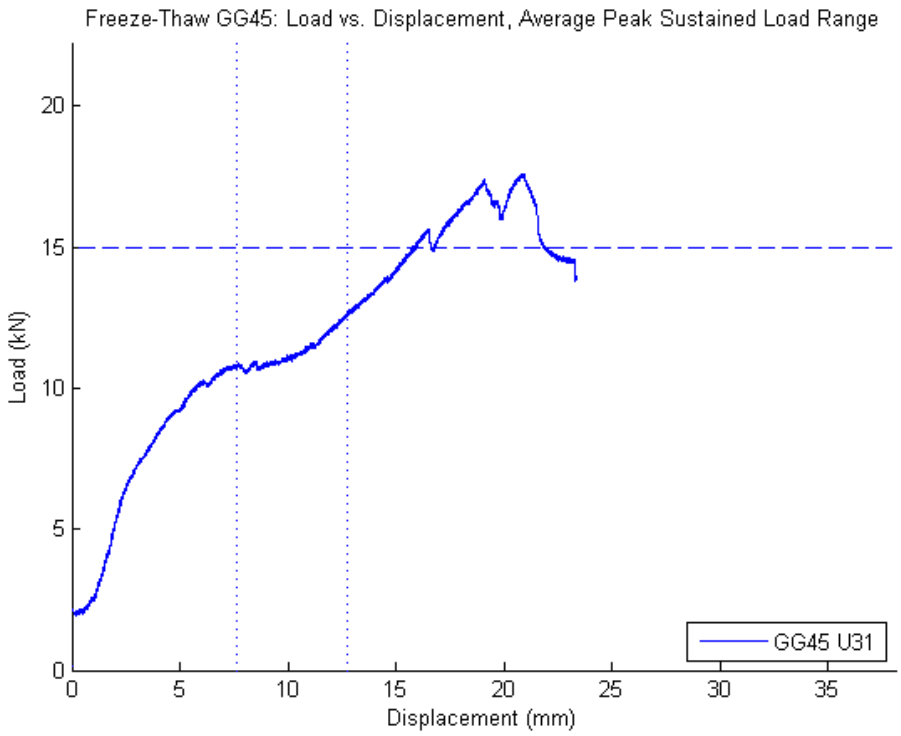
Freeze-Thaw GG45: Load vs. Displacement, Average Peak Sustained Load Range
Load (kN)
Displacement (mm)
GG45 U31

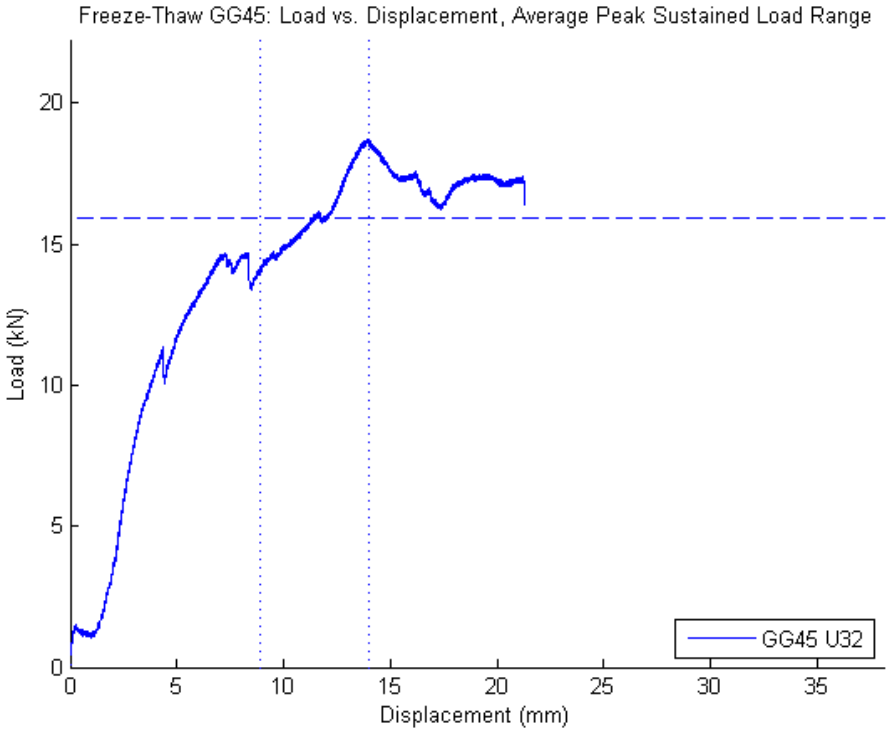
Freeze-Thaw GG45: Load vs. Displacement, Average Peak Sustained Load Range
Load (kN)
Displacement (mm)
GG45 U32

1000 Hour Saltwater Specimens

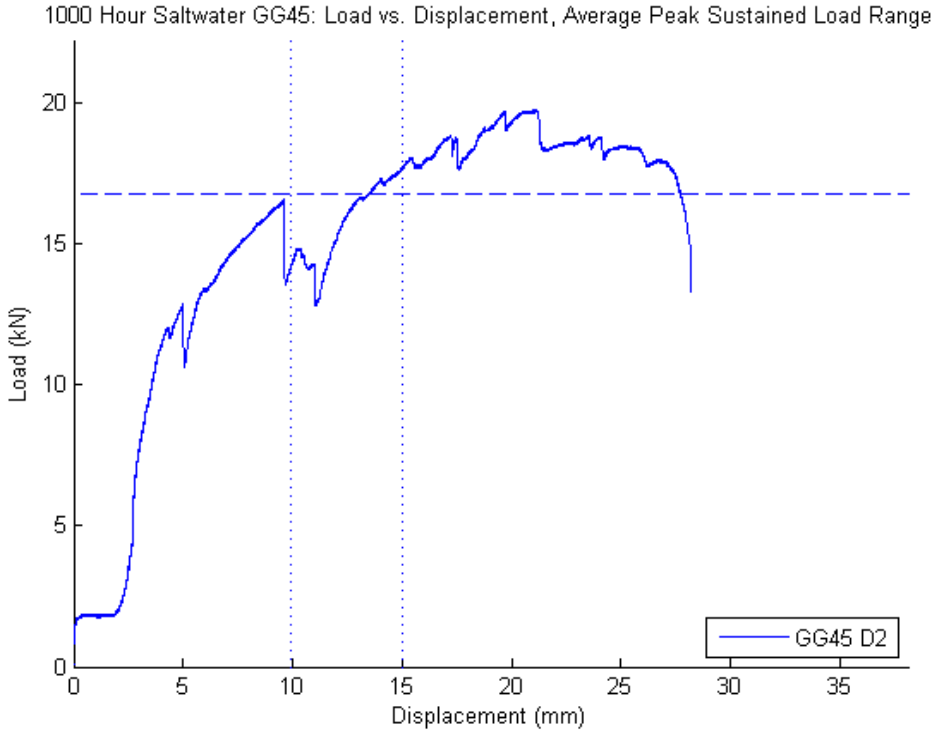

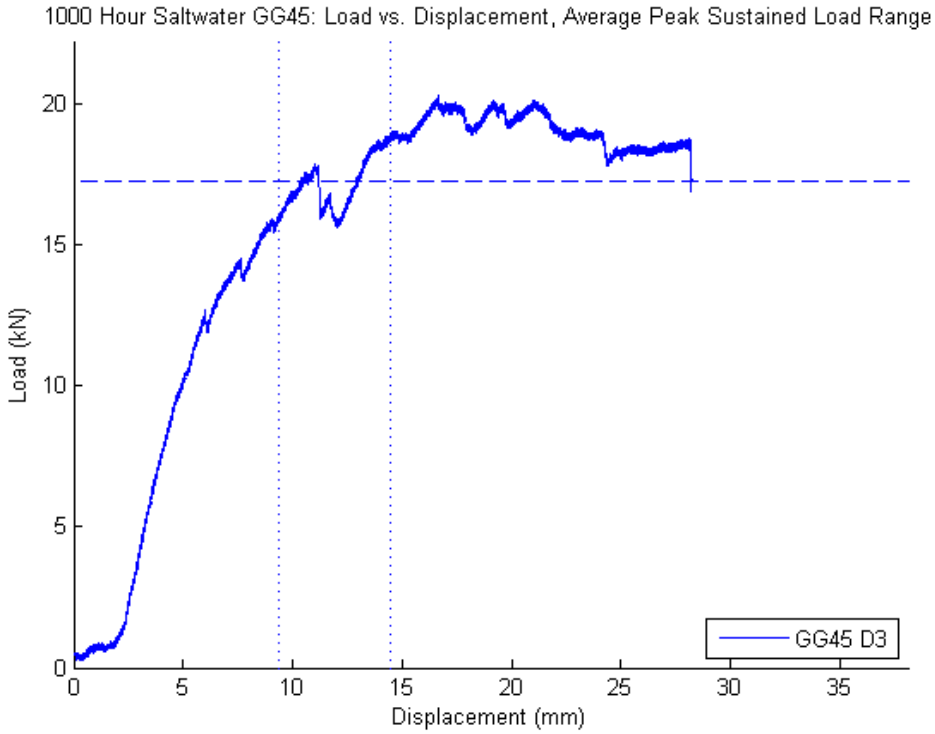

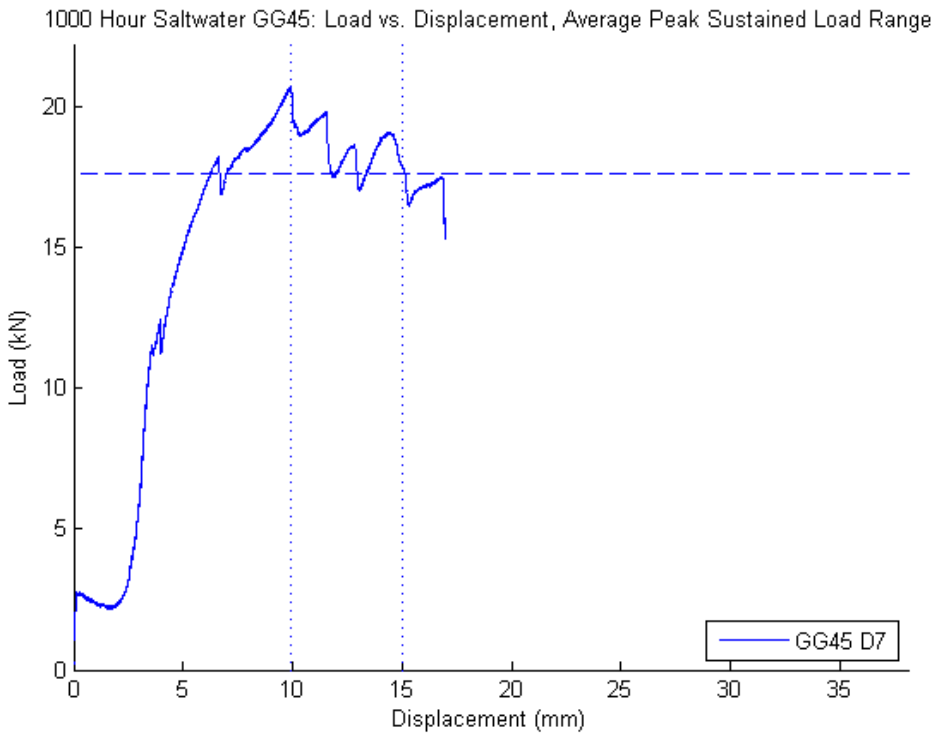
1000 Hour Saltwater GG45: Load vs. Displacement, Average Peak Sustained Load Range
Load (kN)
Displacement (mm)
GG45 D7

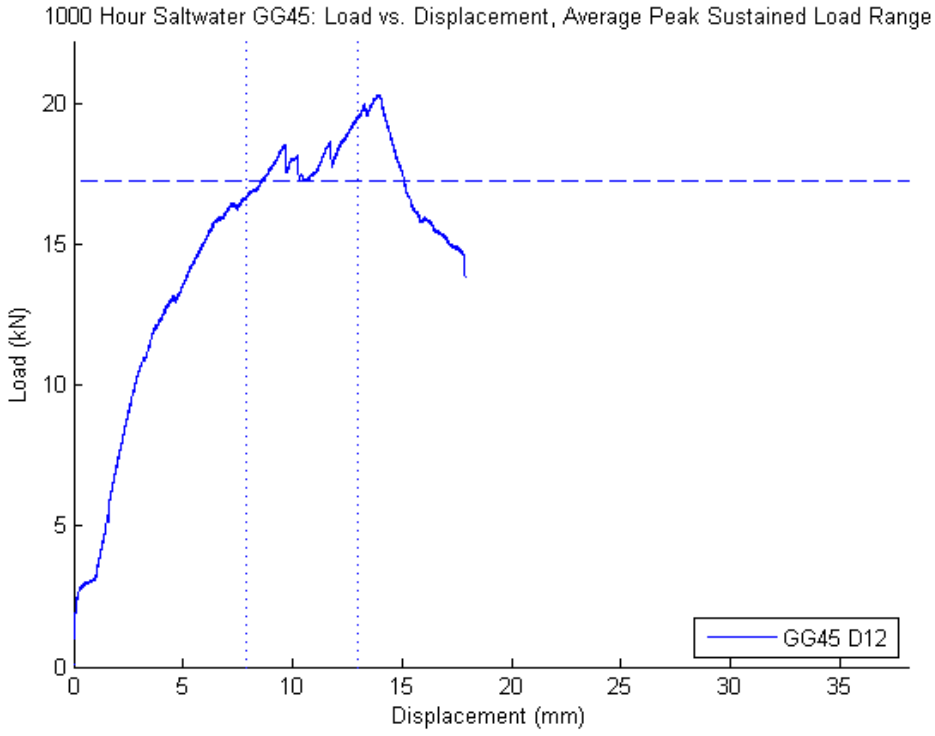
1000 Hour Saltwater GG45: Load vs. Displacement, Average Peak Sustained Load Range
Load (kN)
Displacement (mm)
GG45 D12

3000 Hour Saltwater Specimens

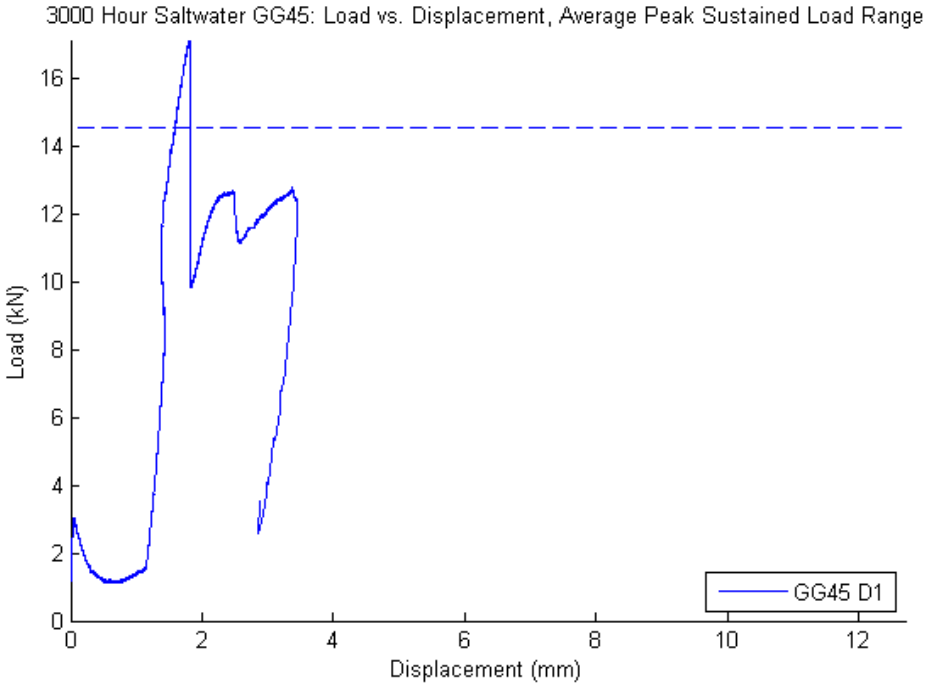

GC90 Durability Specimen Average Peak Sustain Load Plots

Environmental Control Specimens

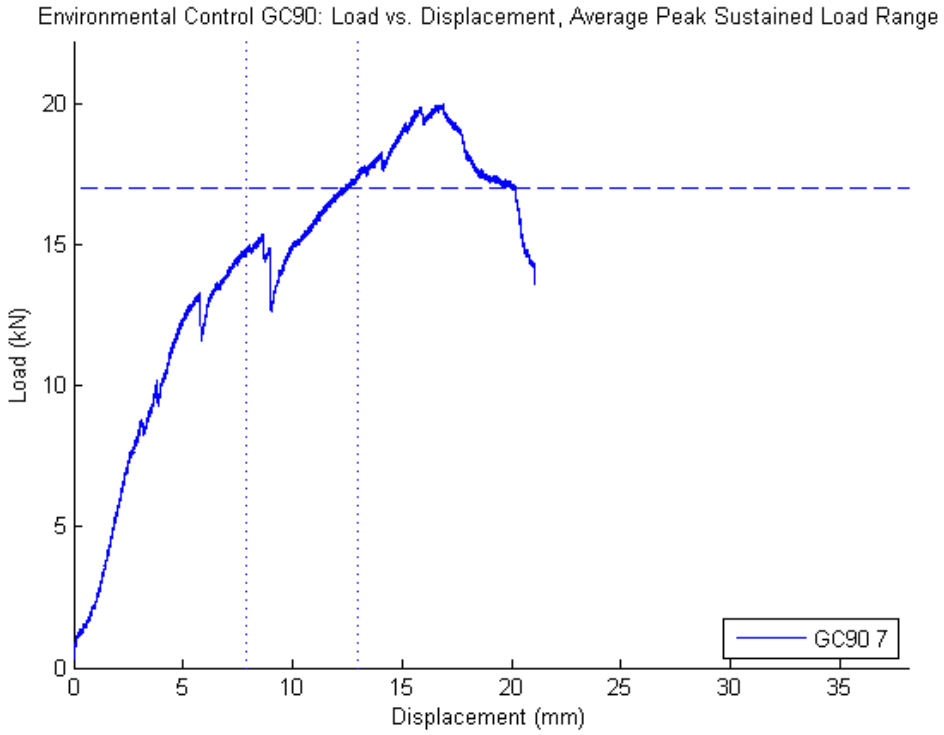

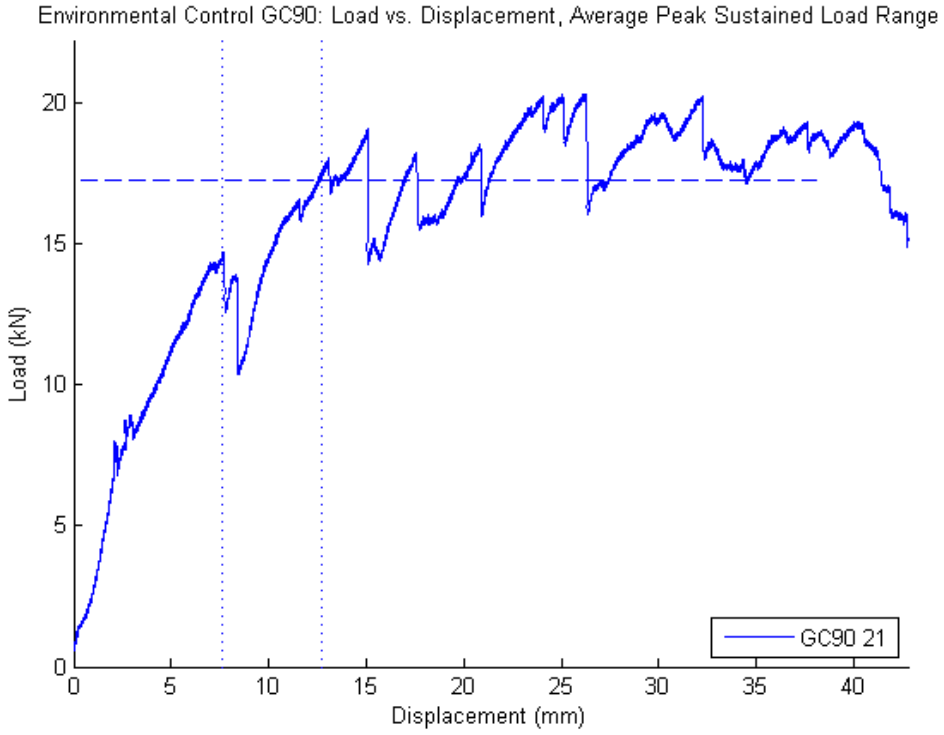

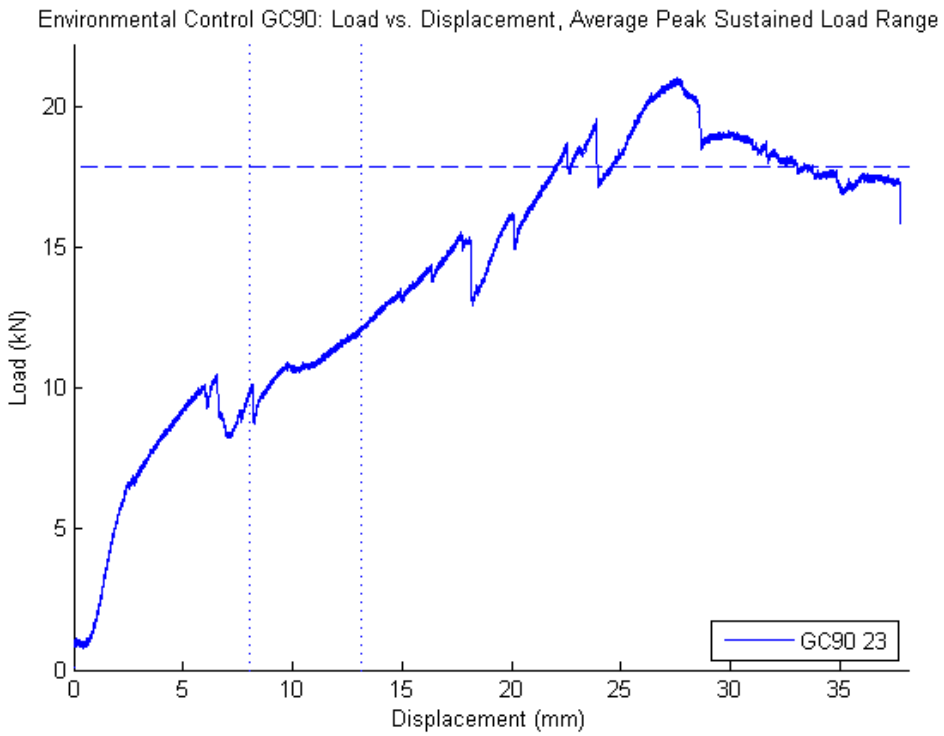
Environmental Control GC90: Load vs. Displacement, Average Peak Sustained Load Range
Load (kN)
Displacement (mm)
GC90 23

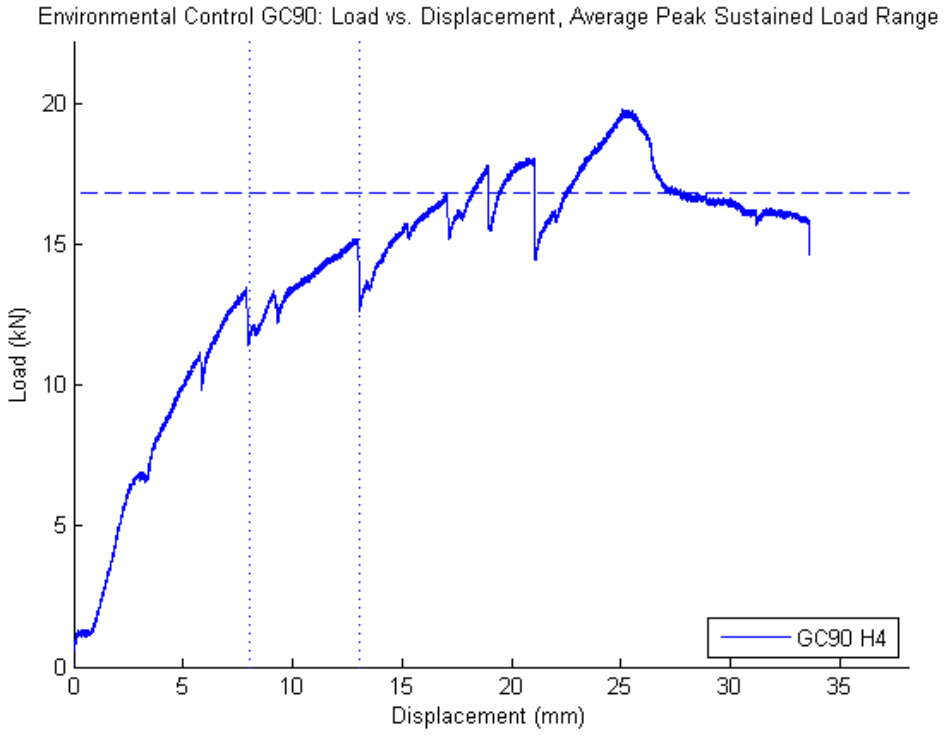
Environmental Control GC90: Load vs. Displacement, Average Peak Sustained Load Range
Load (kN)
Displacement (mm)
GC90 H4

Freeze-Thaw Specimens

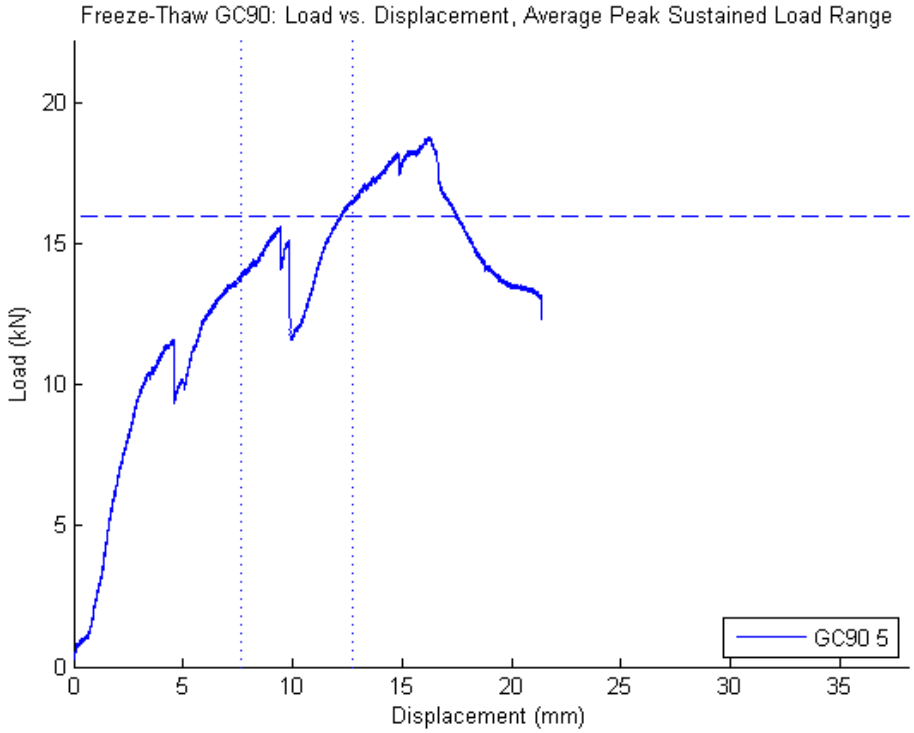

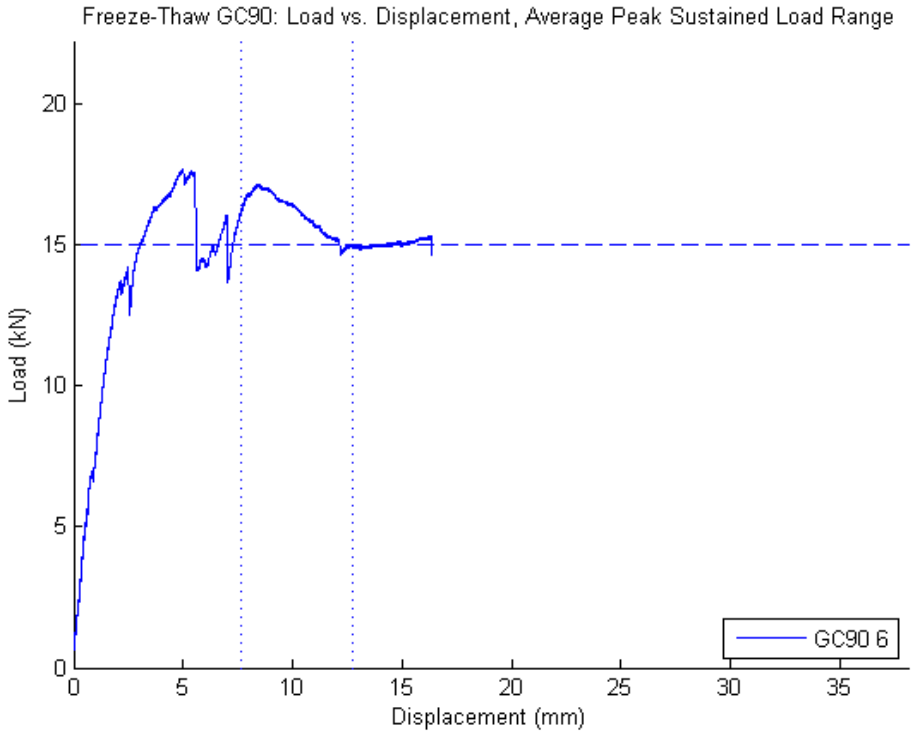

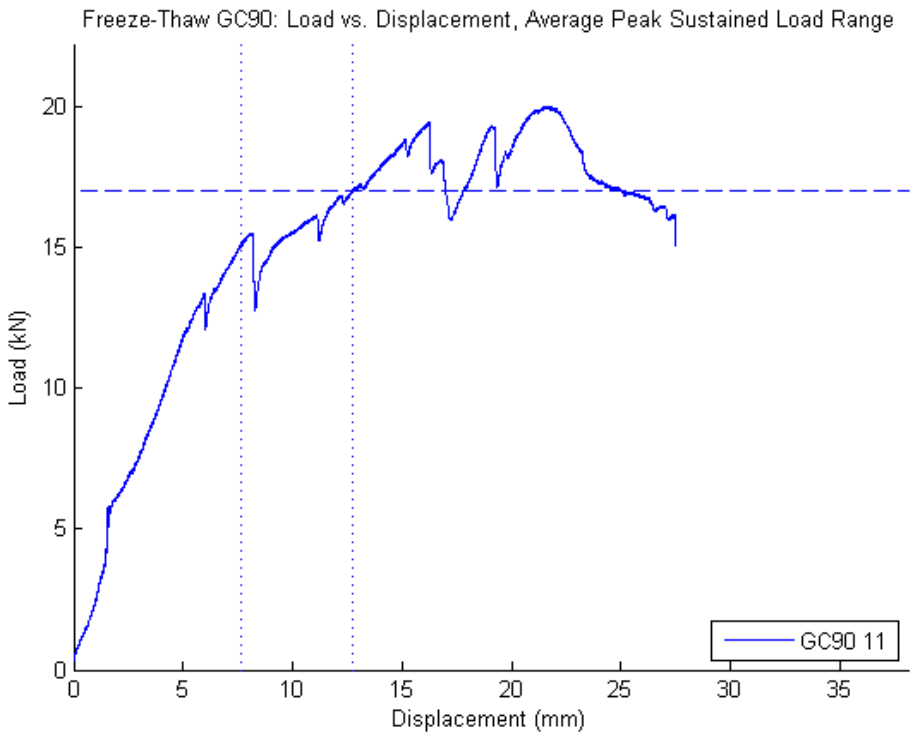
Freeze-Thaw GC90: Load vs. Displacement, Average Peak Sustained Load Range
Load (kN)
Displacement (mm)
GC90 11

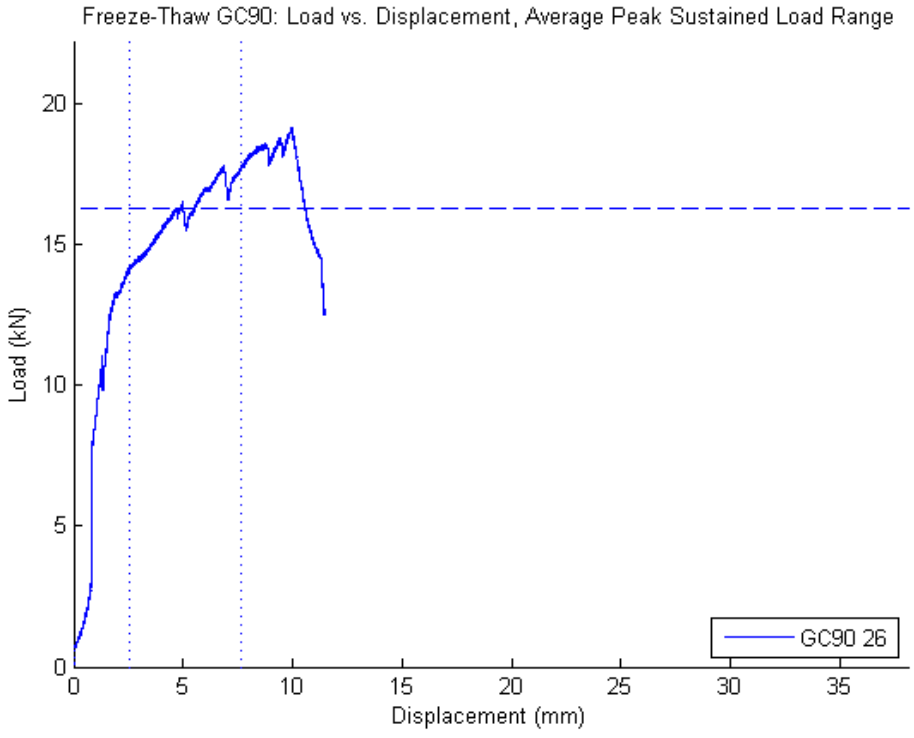
Freeze-Thaw GC90: Load vs. Displacement, Average Peak Sustained Load Range
Load (kN)
Displacement (mm)
GC90 26

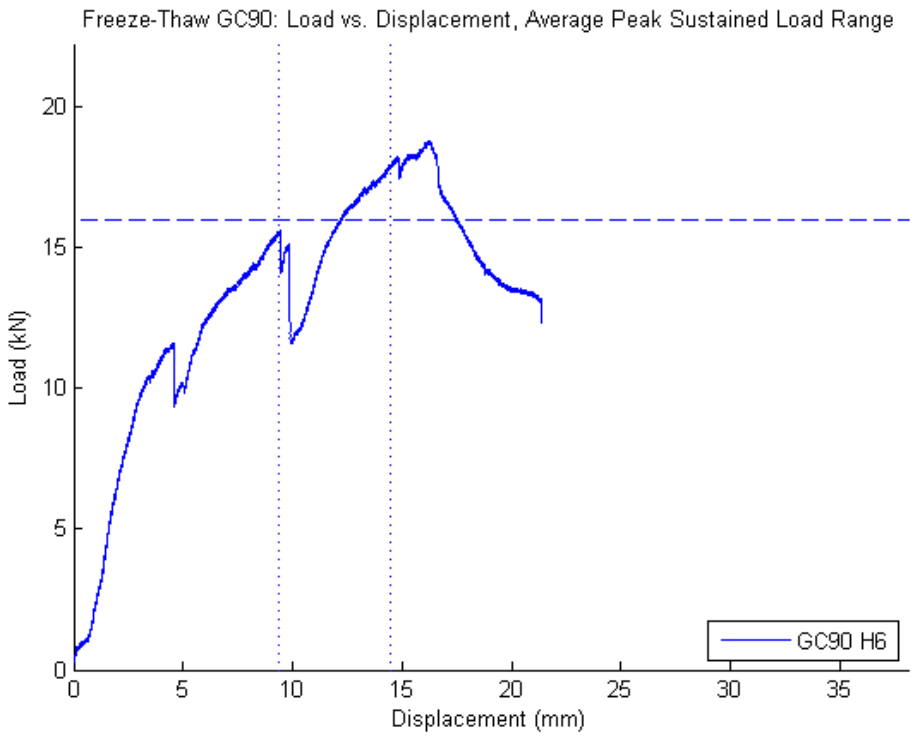
Freeze-Thaw GC90: Load vs. Displacement, Average Peak Sustained Load Range
Load (kN)
Displacement (mm)
GC90 H6
0
5
10
15
20
25
30
35

1000 Hour Saltwater Specimens

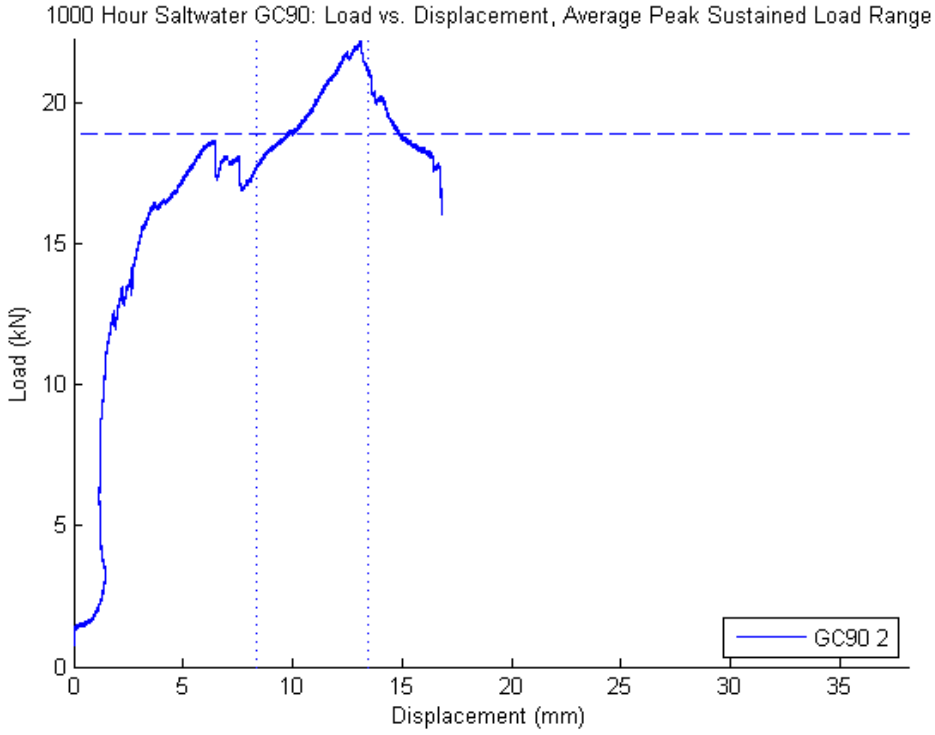

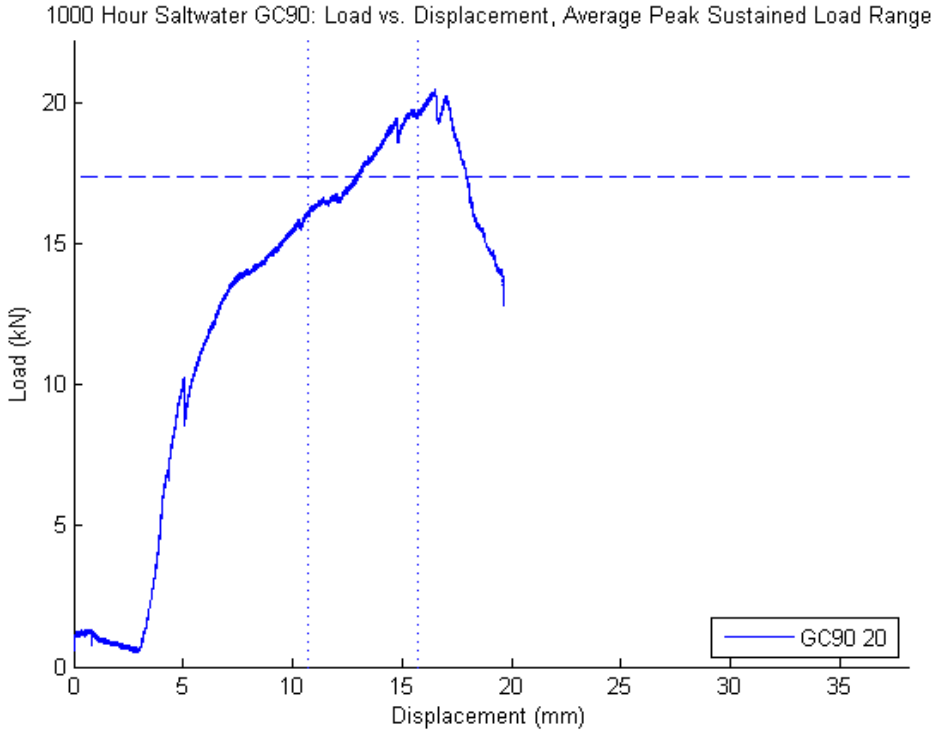

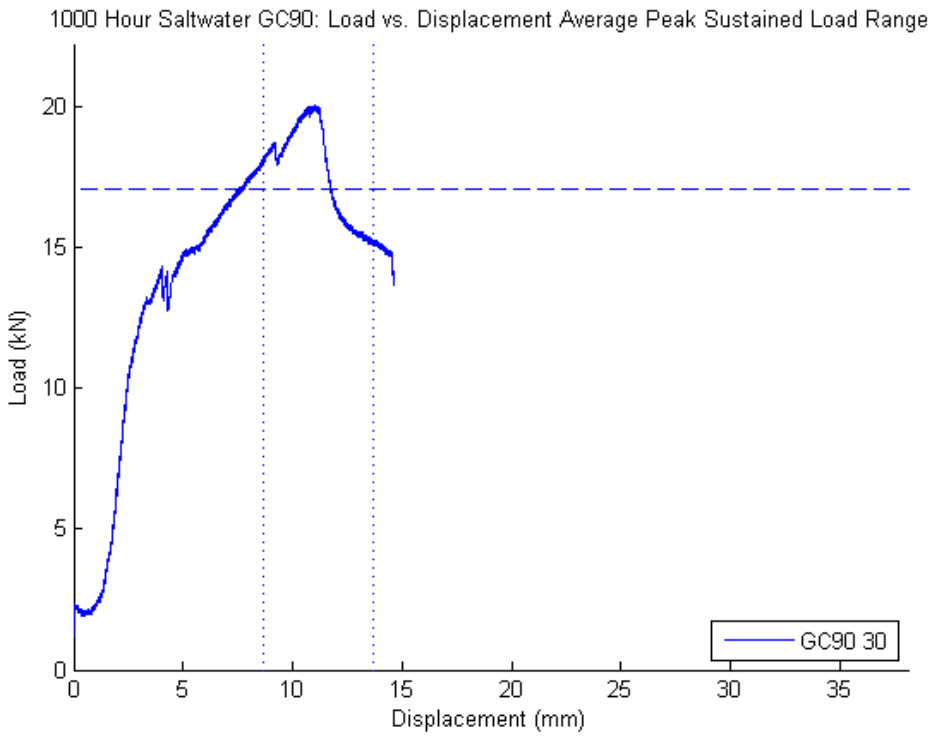
1000 Hour Saltwater GC90: Load vs. Displacement Average Peak Sustained Load Range
Load (kN)
Displacement (mm)
GC90 30
0
5
10
15
20
25
30
35

3000 Hour Saltwater Specimens

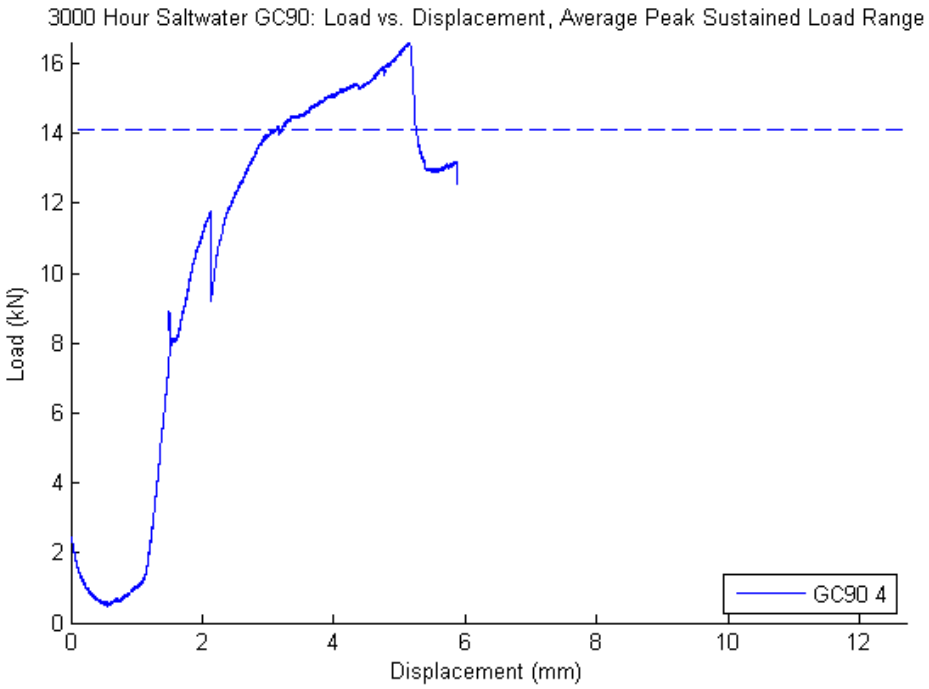

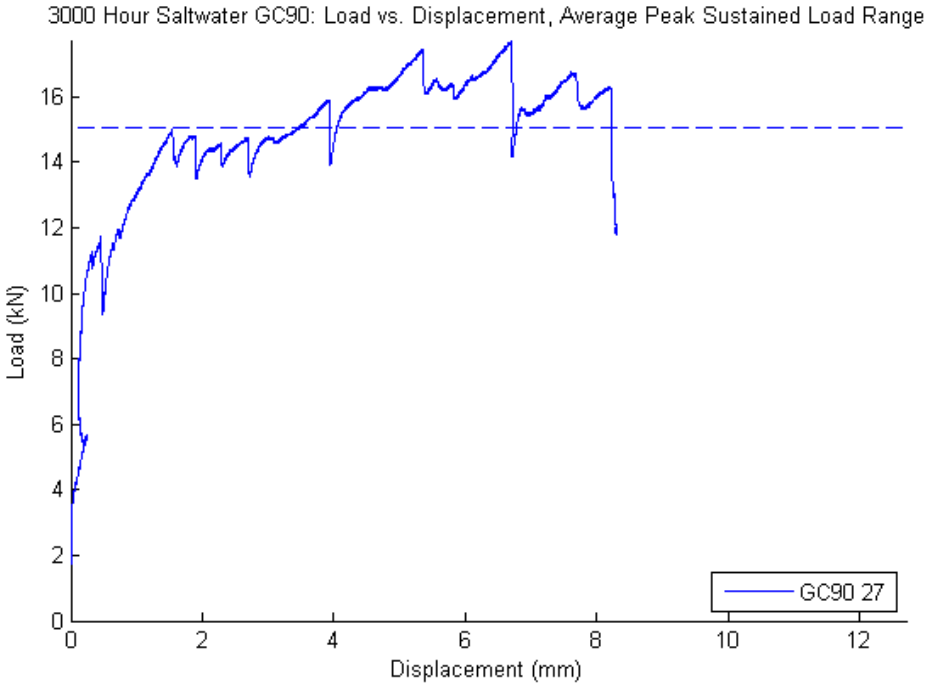

GC45 Durability Specimen Average Peak Sustain Load Plots

Environmental Control Specimens

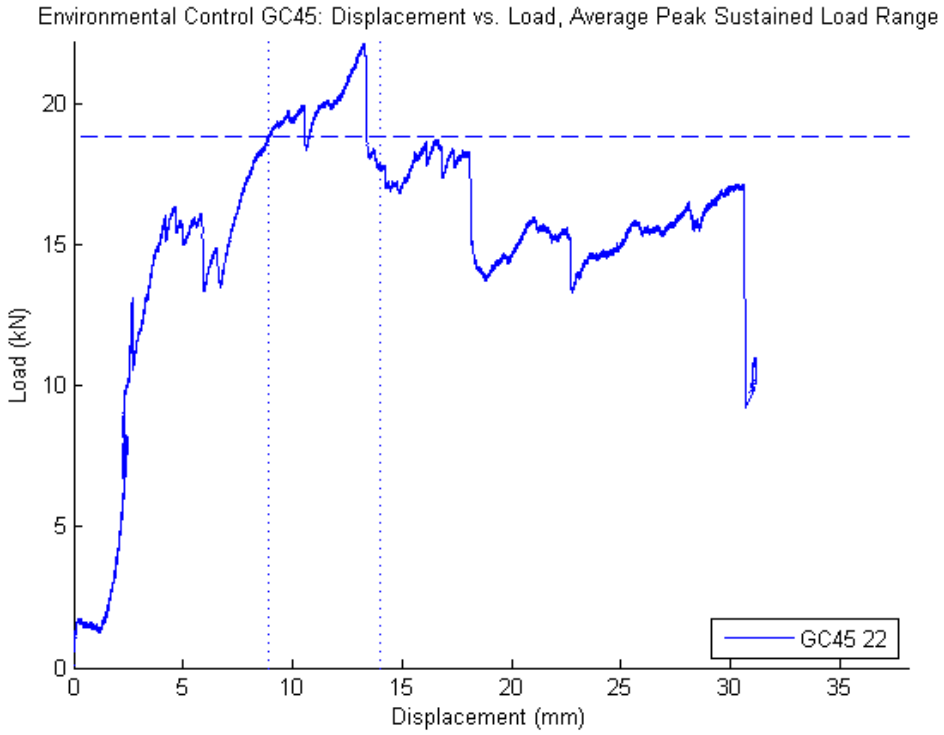

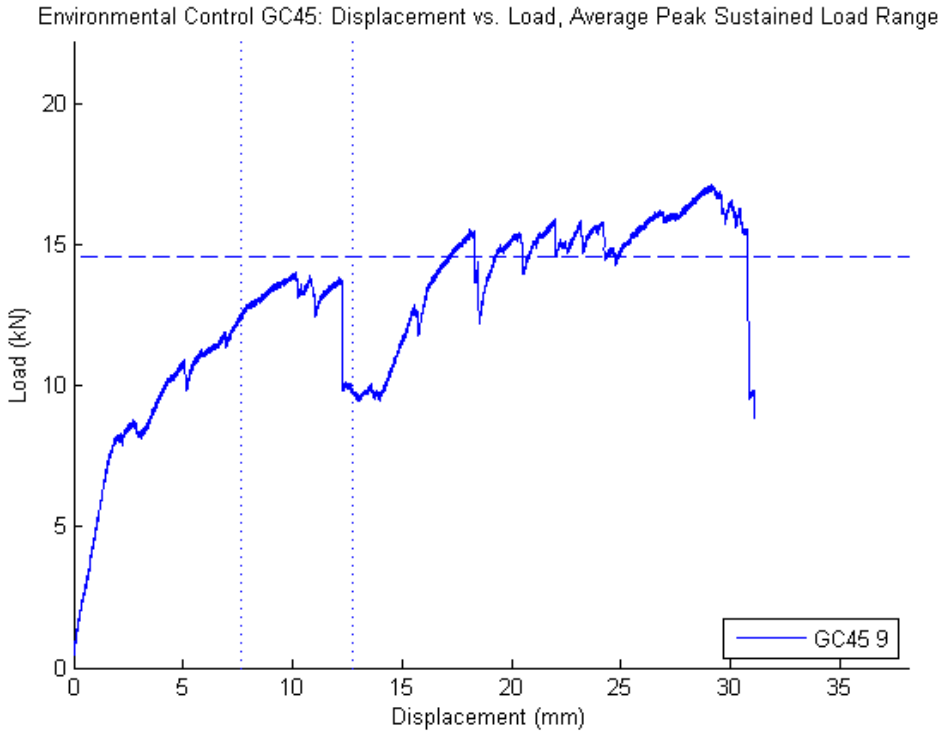

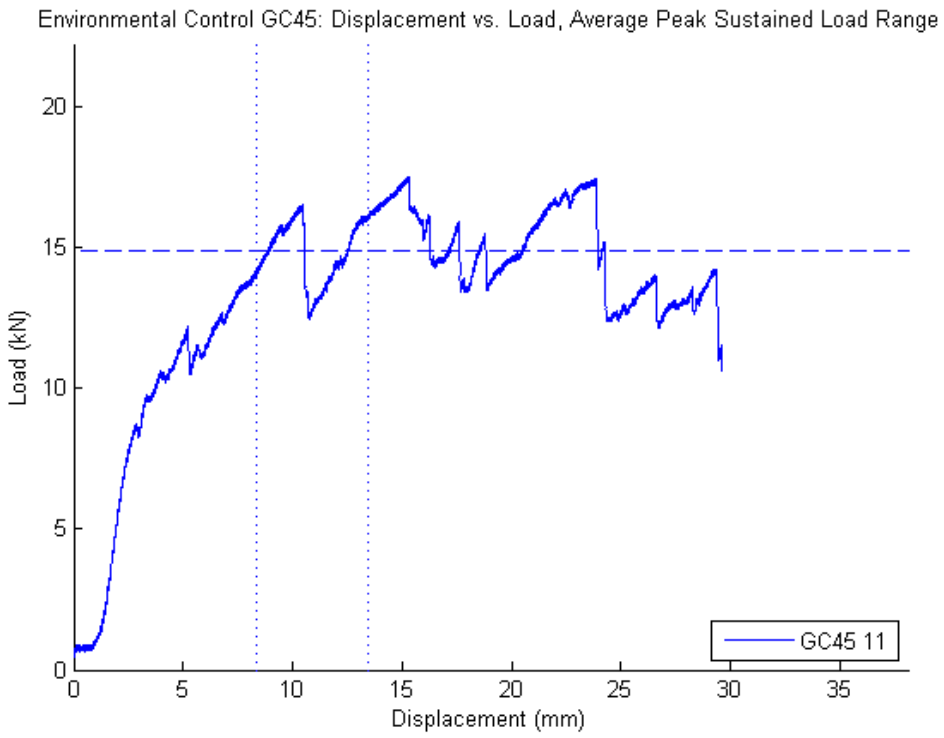
Environmental Control GC45: Displacement vs. Load, Average Peak Sustained Load Range
Load (kN)
Displacement (mm)
GC45 11

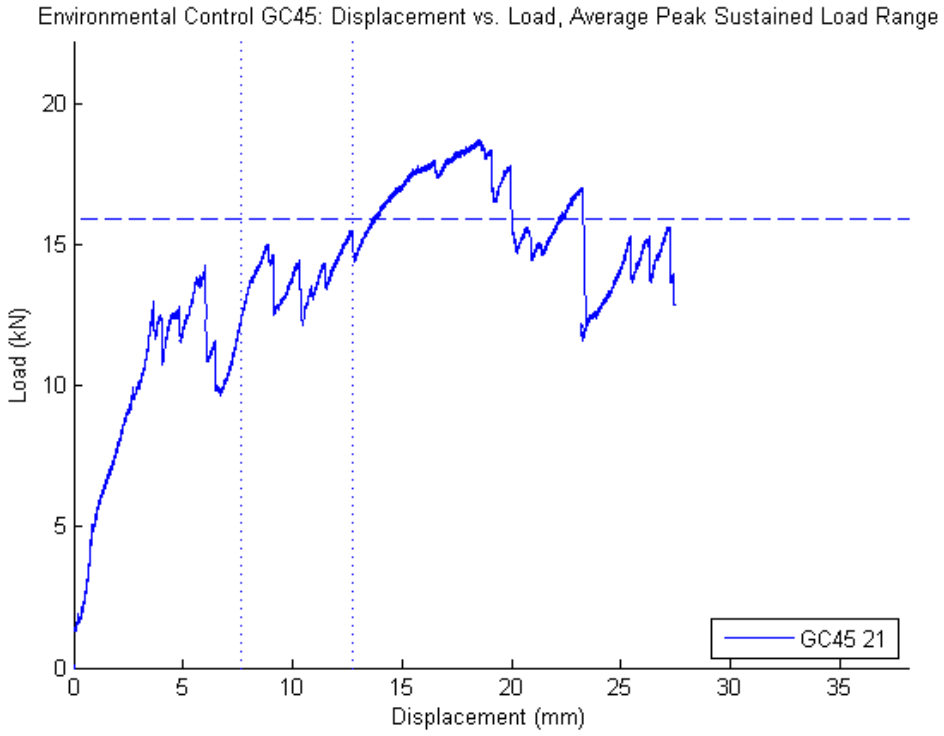
Environmental Control GC45: Displacement vs. Load, Average Peak Sustained Load Range
Load (kN)
Displacement (mm)
GC45 21

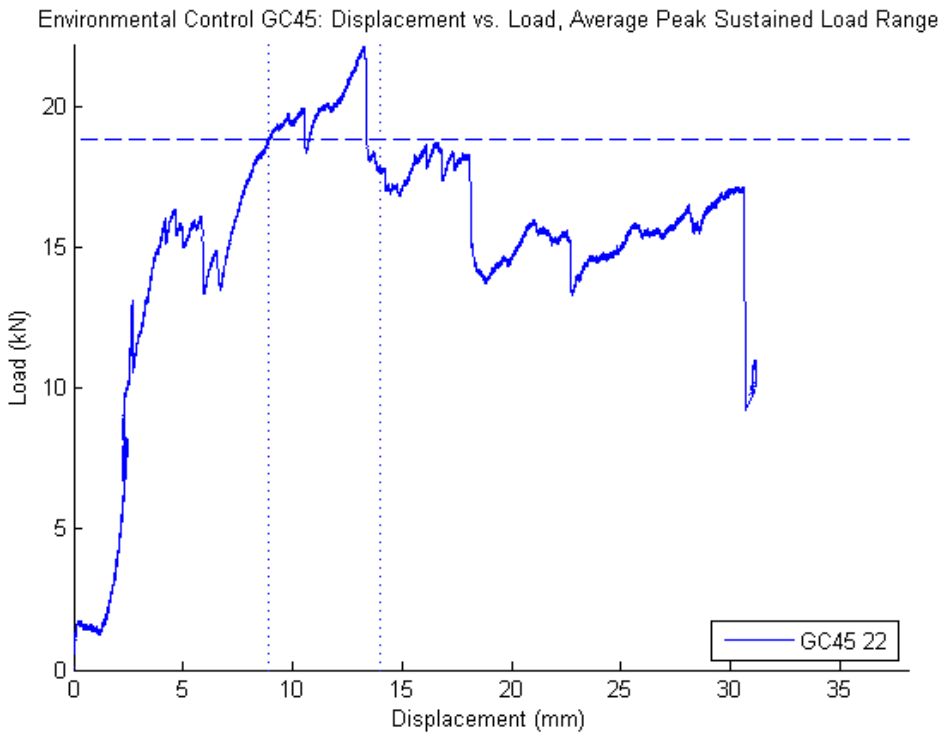
Environmental Control GC45: Displacement vs. Load, Average Peak Sustained Load Range
Load (kN)
Displacement (mm)
0
5
10
15
20
25
30
35
GC45 22

Freeze-Thaw Specimens

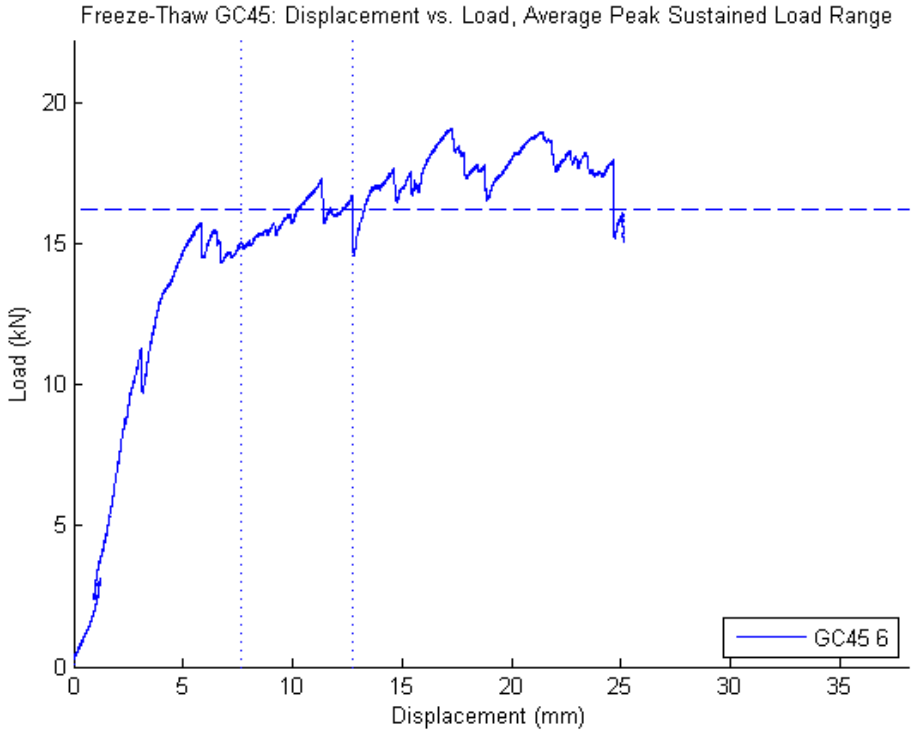

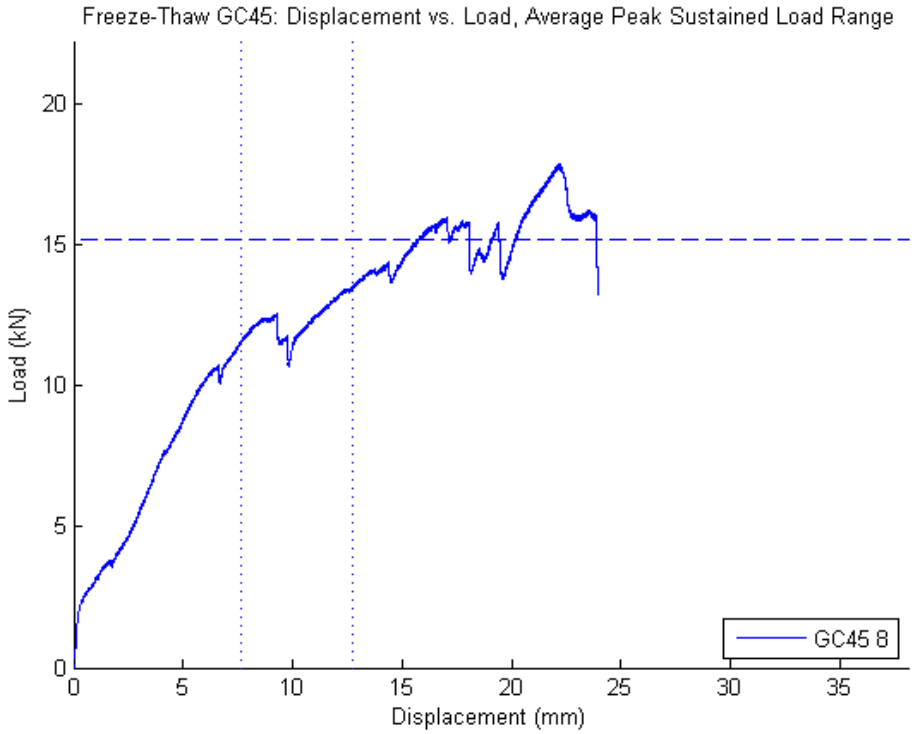

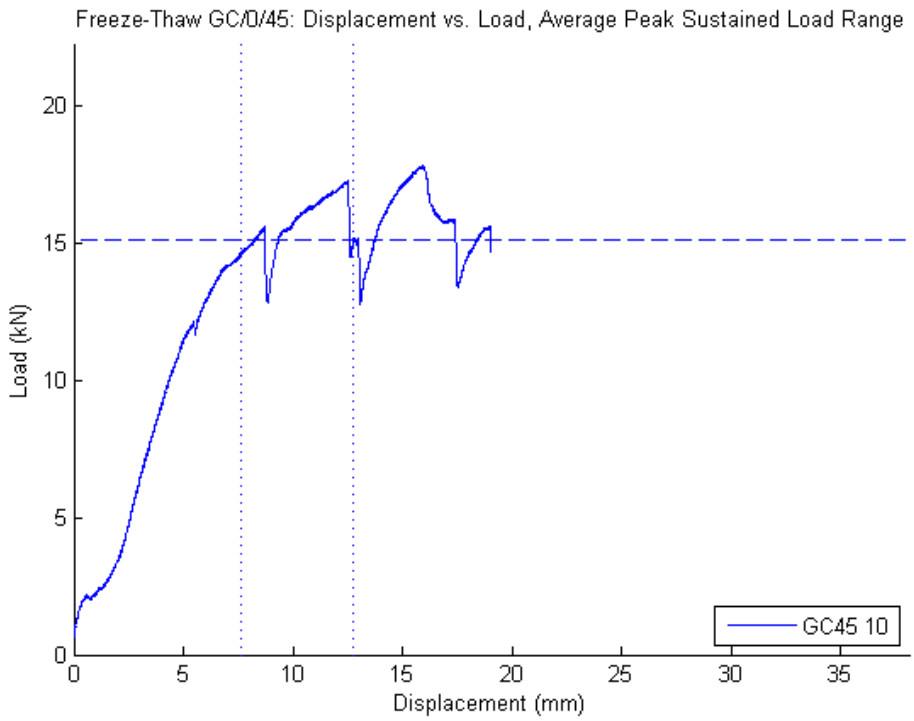
Freeze-Thaw GC/0/45: Displacement vs. Load, Average Peak Sustained Load Range
Load (kN)
Displacement (mm)
GC45 10

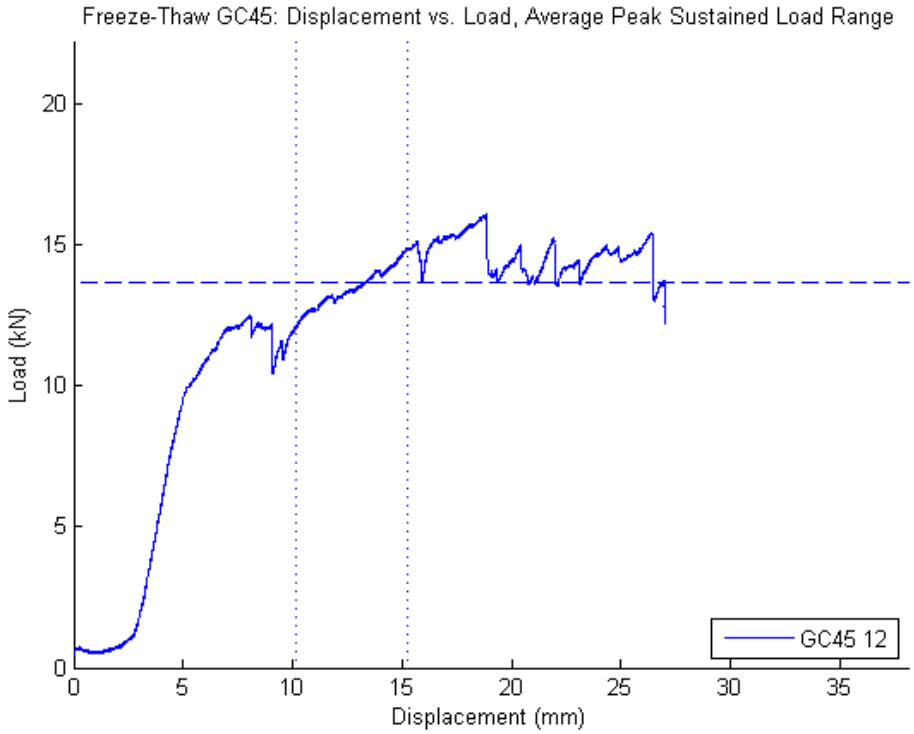
Freeze-Thaw GC45: Displacement vs. Load, Average Peak Sustained Load Range
Load (kN)
Displacement (mm)
GC45 12

1000 Hour Saltwater Specimens

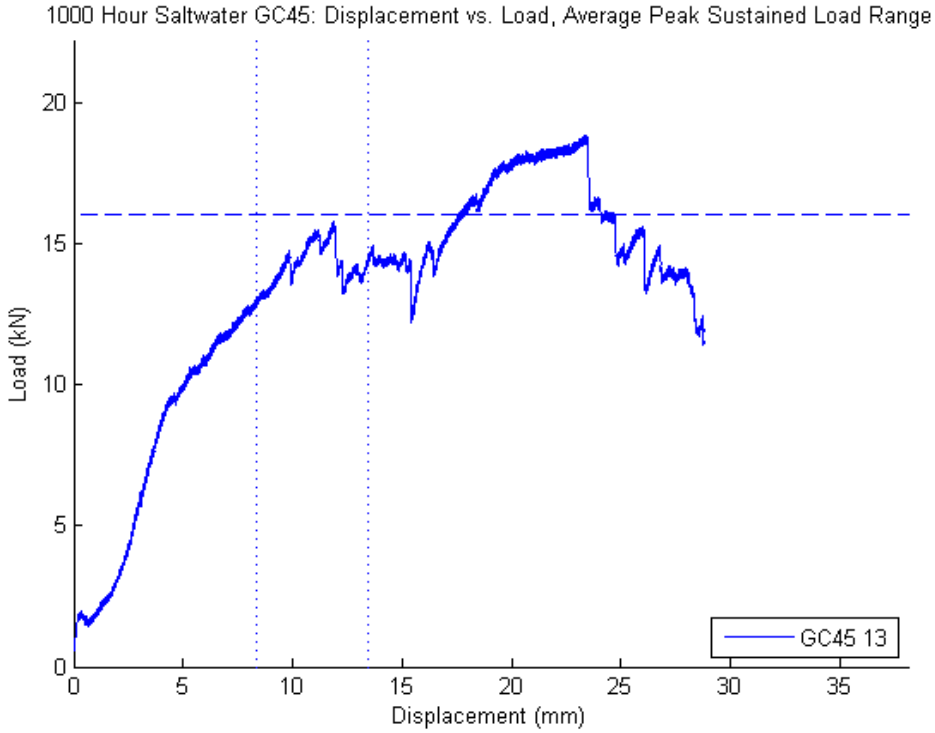

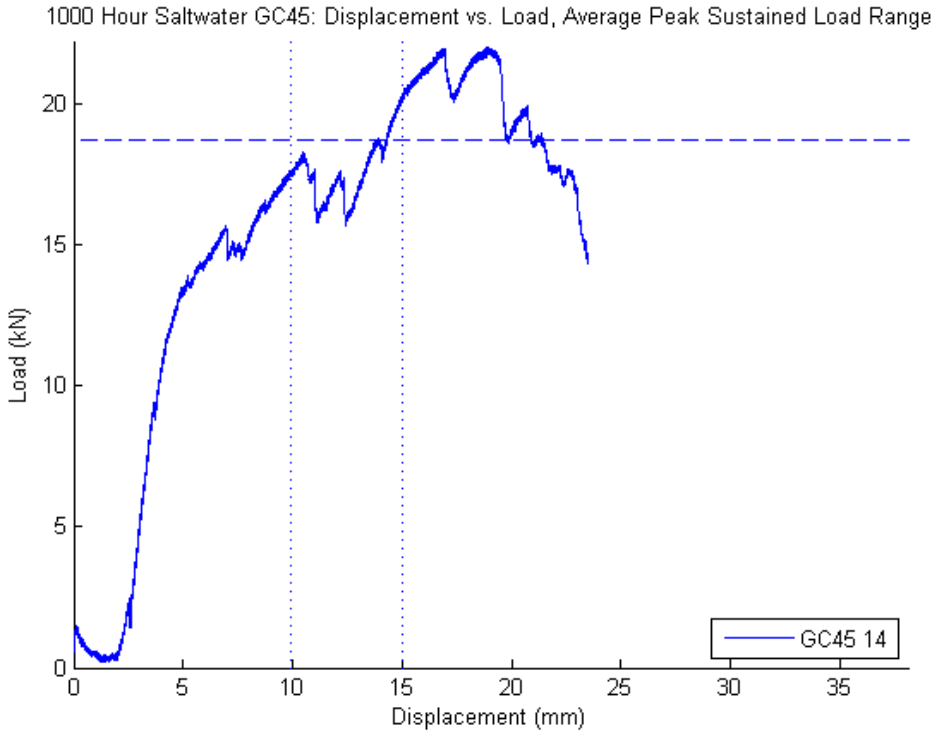

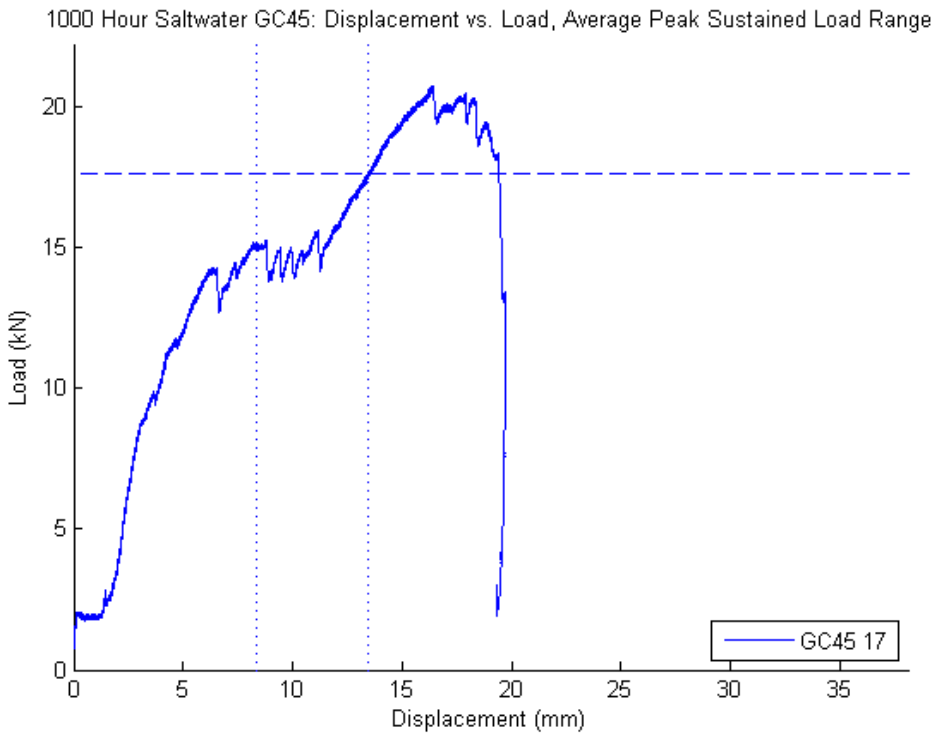
1000 Hour Saltwater GC45: Displacement vs. Load, Average Peak Sustained Load Range
Load (kN)
Displacement (mm)
GC45 17

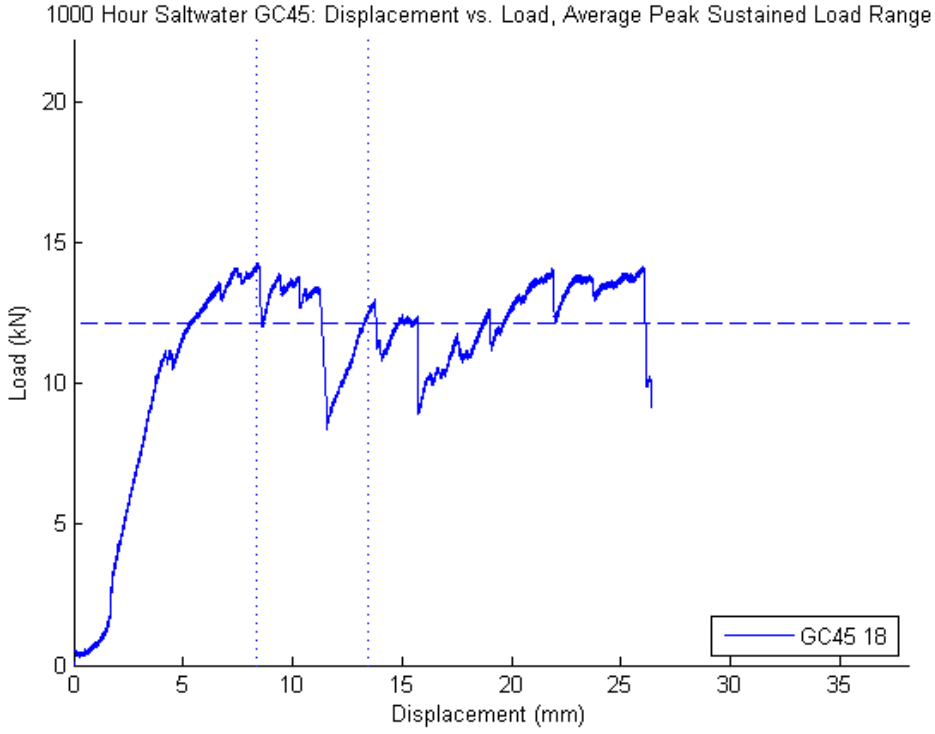
1000 Hour Saltwater GC45: Displacement vs. Load, Average Peak Sustained Load Range
Load (kN)
Displacement (mm)
GC45 18

3000 Hour Saltwater Specimens

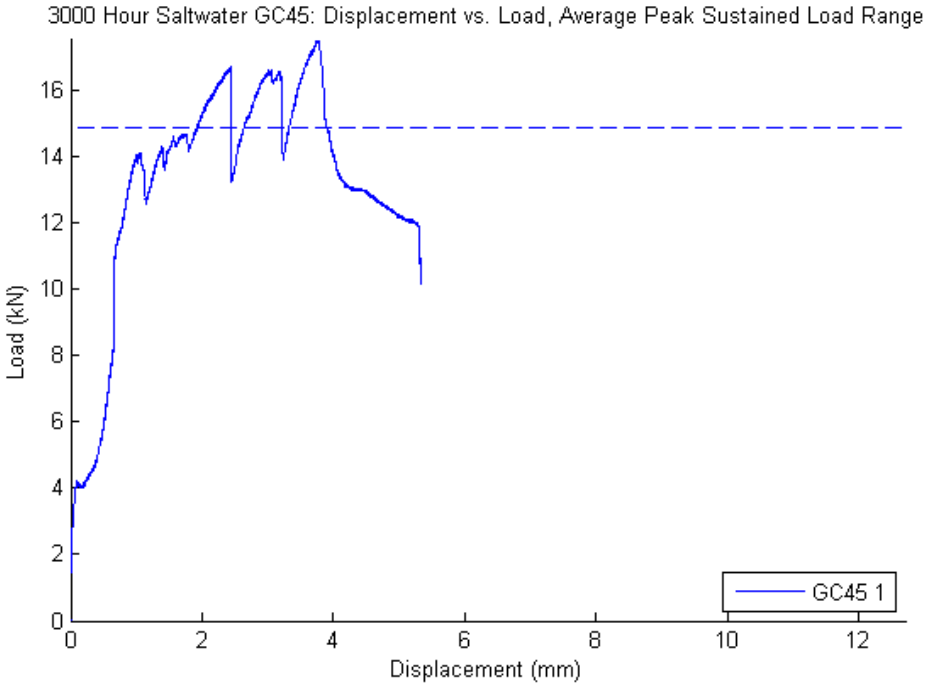

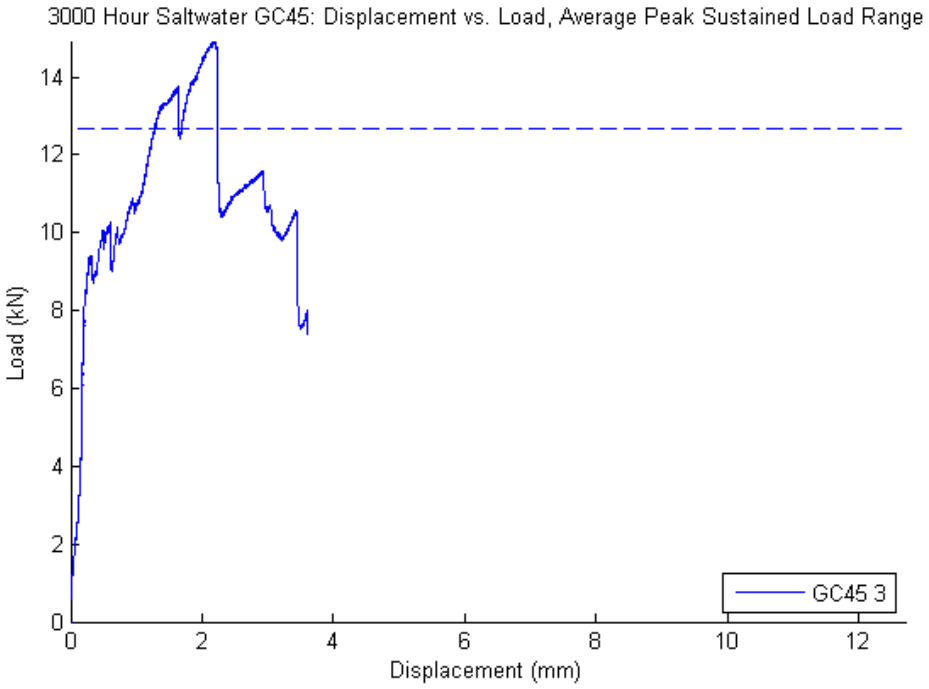

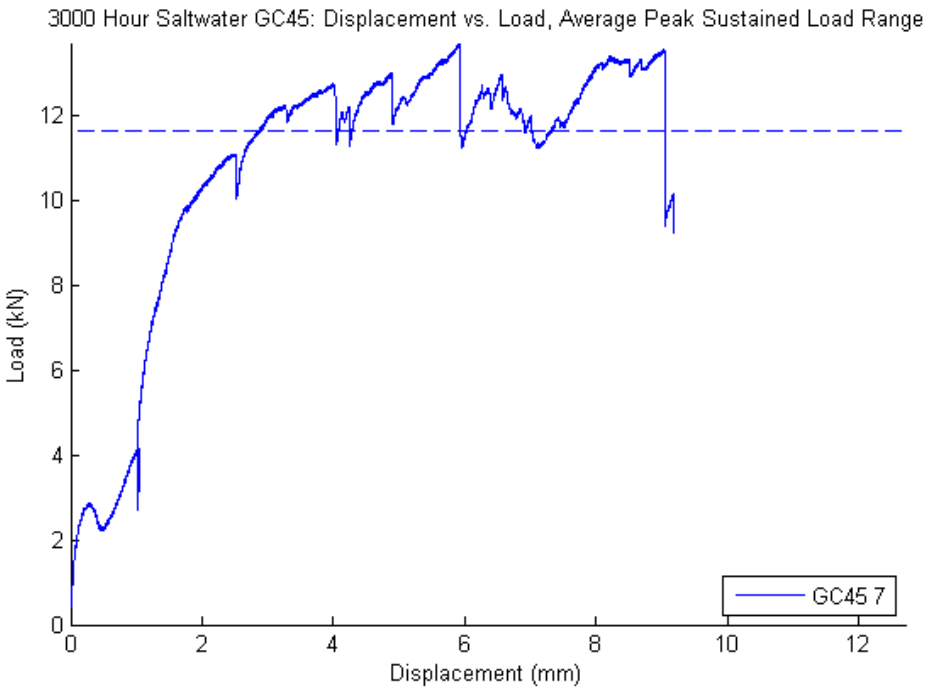
3000 Hour Saltwater GC45: Displacement vs. Load, Average Peak Sustained Load Range
Load (kN)
Displacement (mm)
GC45 7
0
2
4
6
8
10
12

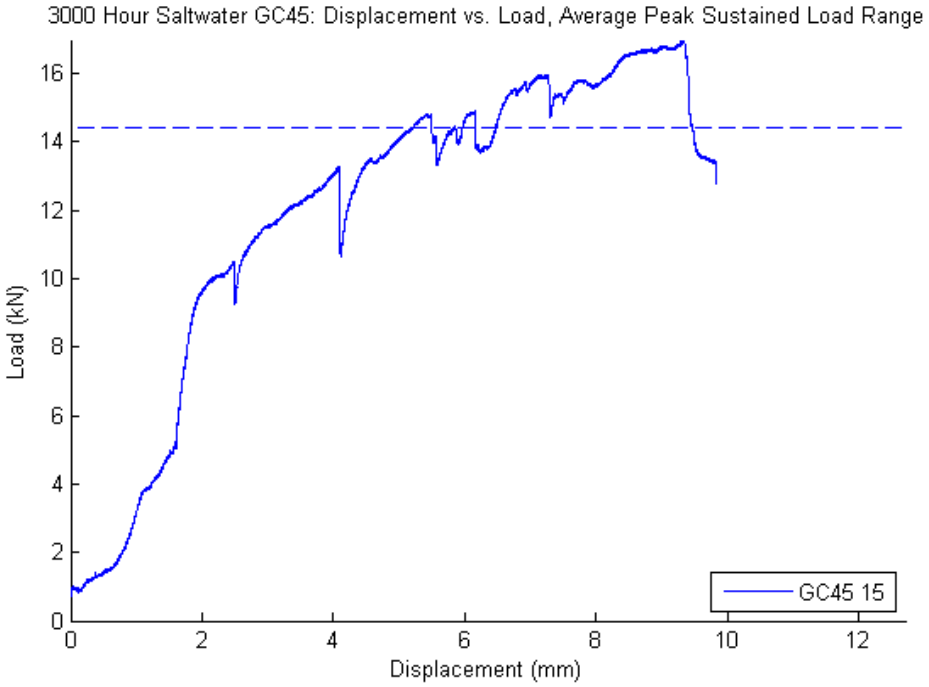
3000 Hour Saltwater GC45: Displacement vs. Load, Average Peak Sustained Load Range
Load (kN)
Displacement (mm)
GC45 15
0
2
4
6
8
10
12
14
16

Bridge Safety Project

Task 4 (Deliverable 5): FRP Flexural Retrofit Environmental Durability and Small Beam Bending Testing and Analysis

6/30/2014

Caleb Frederick, M.S. Candidate in Civil and Environmental Engineering
Bill Davids, PhD, PE, John C. Bridge Professor and Chair of Civil and Environmental Engineering

University of Maine Advanced Structures and Composites Center and Department of Civil and Environmental Engineering

Contents

Introduction

This engineering report for the Maine Department of Transportation (MaineDOT) satisfies deliverable 5 of Task 4 for the UMaine Advanced Structures and Composites Center Bridge Safety project funded by MaineDOT.

Deliverable 4 of Task 4 (Breton & Davids, 2013a) contained discussion and results of environmental durability testing performed previously at the UMaine Advanced Structures and Composites Center. At the time of that report, 10,000 hour saltwater immersion specimens were being conditioned. This report discusses the results of the 10,000 hour specimens.

Deliverable 3 of Task 4 (Breton & Davids, 2013b) contained discussion and results of small beam bend tests. The small beams discussed in that report were manufactured with 60ksi reinforcing steel. It was determined that tests would be performed on beams manufactured with 40ksi reinforcing steel to better represent existing flat slab bridges. This report discusses the results of the 40ksi small beam bend specimens.

The scope of deliverable 5 of Task 4 includes the presentation and discussion of results of single-fastener, tension-bearing testing of environmental durability specimens, discussion of results of small beam bend tests of beams manufactured with 40ksi reinforcing steel, and discussion of results of small beam fatigue tests of beams manufactured with 60ksi reinforcing steel.

The results of the environmental durability testing reported here are intended to provide more information on the four FRP reinforcement systems considered in this ongoing study. The results of the 40ksi small beam bend testing are intended to provide understanding of the effectiveness of the FRP retrofit systems for slabs with lower-grade reinforcing. The results of the 60ksi small beam fatigue testing are intended to provide understanding of the effectiveness of the FRP retrofit systems over the life span of the bridge.

Environmental Durability Assessment of FRP Retrofit Systems

Environmental testing was performed by Breton (Breton, 2013) to select optimum FRP external reinforcement. Her testing included specimens that were subjected to freeze-thaw cycling and saltwater immersion (de-icing salts). Preliminary saltwater testing included specimens that were submersed for 1,000 hours and 3,000 hours. Following these tests 10,000 hour saltwater immersion specimens were conditioned. The results of the 10,000 hour specimens are discussed in this chapter.

Environmental specimens were conditioned and tested in accordance with the *Guide Specifications for Design of Bonded FRP Systems for Repair and Strengthening of Concrete Bridge Elements* (American Association of State Highway and Transportation Officials (AASHTO), 2012). The test specimens consisted of an FRP coupon attached to a rectangular concrete prism using stainless steel epoxy anchors. Elastic modulus, average peak sustained

bearing load capacity, and tensile strength retention were determined through single-fastener, tension-bearing testing.

Test Specimen

Environmental tests were performed on specimens that encompassed the whole reinforcement system, including concrete, FRP, adhesive, and stainless steel anchors. The specimens were constructed by Breton and are discussed in *Mechanically Fastened Fiber-Reinforced Polymer (FRP) Flexural Retrofit Systems for Reinforced Concrete Flat-Slab Bridges*(Breton, 2013). A brief description of the specimens will be provided here. An epoxy adhesive was used to hold a stainless steel threaded rod in a concrete prism. An FRP coupon was attached to the concrete prism using this threaded rod. Specimens were conditioned in this configuration. For testing purposes, the concrete prism was post tensioned and a steel plate was added after conditioning. The steel plate allowed for direct loading into the connection and reduce eccentricity of the loading. Individual components of the test specimens are discussed in the following sections.

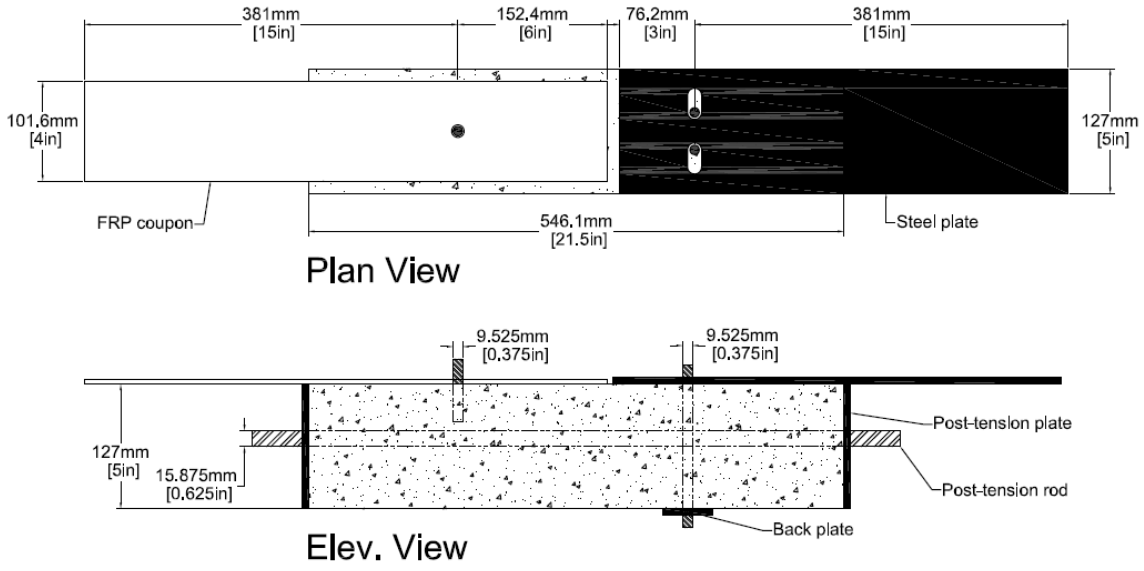

Figure 1: Environmental Durability Test Specimen (Breton, 2013)

Epoxy Adhesive and Mechanical Fasteners

FRP coupons were installed using the same method as described in Section 4.1.1 of Breton (Breton, 2013); a brief explanation of the installation process will be presented here. A Hilti hammer drill was used to drill an 11.1mm (0.438in) hole into the concrete prism. The holes were approximately 38.1mm (1.5in) deep. The holes were thoroughly cleaned with a wire brush to remove any debris left from the drilling process.

To attach the FRP to the concrete specimens a HILTI epoxy and stainless steel threaded rod was used as anchors. HILTI HIT-HY 150 MAX-SD injectable mortar was used as the adhesive. The adhesive was applied using a specialized HILTI caulking gun and mixing tube. After a hole was filled with adhesive a 63.5mm (2.5in) long, 9.53mm (0.375in) diameter stainless steel threaded

rod was inserted into the hole. Following the 30 minute epoxy cure time, a stainless steel washer and nut were tightened to a torque of 16.9kN-m (12.5kip-ft) (HILTI, 2012).

Post-Tensioned Concrete Prism

The concrete portion of the environmental durability specimen was cast as a rectangular prism with dimensions of 127 × 127 × 546.1mm (5 × 5 × 21.5in). These prisms were originally designed for use with powder actuated fasteners. It was determined by Breton that powder actuated fasteners would be inadequate for use in this system (Breton, 2013). The dimensions of the concrete prisms, however, were adequate for one threaded rod fastener to allow for single-fastener, tension-bearing testing. The formwork used for the concrete prisms is shown in Figure 2. Two 9.53mm (0.375in) threaded rods were cast into the prisms to connect the steel plate used for loading to the prism. Through the center of the prism a 19.05mm (0.75in) inner diameter PVC pipe was placed to allow for post-tensioning the prism. Post-tensioning was used to confine the concrete during loading.

Figure 2: Formwork for Environmental Durability Concrete Prism (Breton, 2013)

FRP System Coupons

FRP reinforcing systems were cut into coupons measuring 101.6mm (4in) wide by 457.2mm (18in) long. A 12.7mm (0.5in) diameter hole was drilled into each coupon to accommodate the stainless steel threaded rod used to attach it to the concrete prism. The hole was drilled 152.4mm (6in) from the coupon end and on the center line in the longitudinal direction. All four FRP reinforcing systems were used in this study: GG45, GG90, GC45, and GC90. “GG” specimens were manufactured with fiberglass skins and fiberglass cores, whereas “GC” specimens were manufactured with fiberglass skins and carbon fiber cores. Specimens with “45” had the core material oriented at +/-45°, while specimens with “90” had the core material oriented at 0°/90°. The outer fiberglass skins were oriented at 0°/90° for all reinforcing systems.

Testing Plan

An environmental durability test matrix was developed by Breton for the reinforcing systems (Breton & Davids, 2012). This testing matrix included 10,000hr saltwater exposure specimens. The 10,000hr specimens were still conditioning upon the completion of Breton's work and were tested in December, 2013.

Saltwater (De-icing Salt) Exposure

The specimens were conditioned in a 3% NaCl solution for 10,192 hours. The NaCl solution was created using road salt supplied by Facilities Management at the University of Maine. The solution was maintained during conditioning by constant circulation supplied by aquarium pumps. During conditioning some water evaporation occurred that went unnoticed for approximately one month. As a result, six specimens were not fully submerged for the full 10,000 hours (Figure 3). These specimens were marked and tracked during testing. Upon review of the results there was no notable effect of the partial submersion.

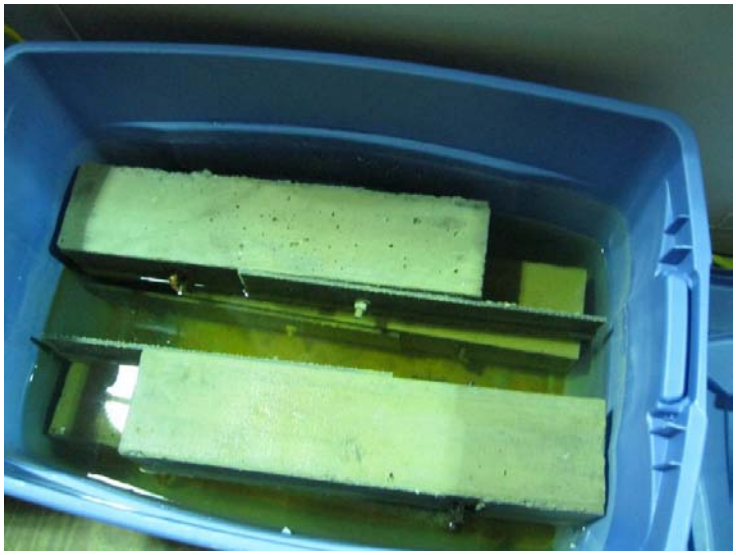

Figure 3: Partially Submerged Environmental Durability Specimens

Test Method

Upon the completion of environmental conditioning, specimens were loaded in single-fastener tension-bearing loading. Load, actuator position, and displacement due to connection slip were recorded throughout testing. All four FRP reinforcement systems were included in this testing, despite the decision to only use the GC system for small beam testing. A compressive force was introduced into the concrete prism through post-tensioning. The prism was post-tensioned using a 15.876mm (0.625in) threaded rod and heavy-hex nuts tightened to 122N-m (90ft-lb) of torque. This resulted in a compressive force of 34.9kN (7850lbf) (Breton, 2013).

The specimens were tested by attaching a steel plate to the concrete prism (Figure 4). All connections were torqued to 16.9N-m (12.5ft-lb). An LVDT was used to measure the displacement due to FRP connection slip. The LVDT was attached using wood clamps (Figure 4). The lower clamp was attached to the FRP strip flush with the actuator grips, while the upper clamp was attached to the concrete prism at the center of the connection.

A load rate of 2.54mm/min (0.10in/min) was used to test the environmental specimens. Specimens were loaded until it was evident that the connection could no longer support continued loading. This differs slightly from the method used by Breton, in which concrete cracking was considered failure (Breton & Davids, 2013b). As a result of this, the 10,000 hour specimens were loaded for a longer duration than many of the 1,000hr and 3,000hr specimens.

Figure 4: Envionmental Durability Specimen

Results

Bearing failure at the connection was evident in all 10,000hr specimens. Concrete cracking occurred in almost all specimens under sustained loading. A typical bearing failure is shown in Figure 5. Concrete cracking around the anchor rods for the steel plate is shown in Figure 6. One specimen displayed significant concrete cracking around the FRP anchor hole. The cracking was so significant that the anchor rod was loose after failure and could be removed from the concrete prism by hand (Figure 7). It was determined that data from this test was still useable, as the concrete cracking occurred following bearing failure. The average maximum load carried by each reinforcement system is shown in Table 1.

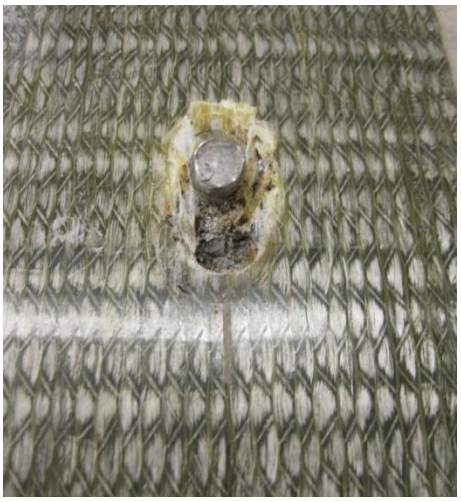

Figure 5: Typical Bearing Failure of 10,000hr Environmental Durability Specimen

Figure 6: Concrete Cracking at Steel Plate Connection

Figure 7: Significant Concrete Cracking Following Bearing Failure

Table 1: Average Maximum Load by Specimen Type

Specimen Type (Number of Specimens)	Mean, kN (kip)	Coefficient of Variation (%)	Percent Retention (%)
GG90 (5)	22.2 (4.98)	7.9	98.4
GG45 (4)	20.6 (4.62)	8.4	95.3
GC90 (5)	19.3 (4.33)	9.0	94.8
GC45 (4)	18.2 (4.08)	13.1	94.9

The performance criteria chosen for this study specify that 10,000 hour saltwater exposure specimens must retain 85% strength relative to control specimens. It can be seen in Table 1 that all FRP reinforcing systems meet this criteria. Control values were taken from Breton and Davids (Breton & Davids, 2013b). Environmental durability data was also analyzed using the average sustained peak load. The average sustained peak load as defined by Breton is as follows:

> "Based on the original acceptability criteria and the load-displacement plots for tested specimen the average peak sustained load range was defined using the two following points:
>
> - Initial point – the first recorded occurrence of 85% of peak load prior to the occurrence of peak load

- Final point – the first recorded occurrence of 85% peak load following the occurrence of peak load" (Breton, 2013)

This definition of average sustained peak load was used for this data series. Due to the continued loading mentioned previously, the average sustained peak loads found using this definition are higher than the loads reported for control specimens, as can be seen in Table 2. As a result, it is difficult to draw conclusions using the average sustained peak load under the current definition. Figure 8 shows a typical load displacement curve showing the location of the average sustained peak load. The location of the average sustained peak load is shown where the dashed, horizontal line intersects the load-displacement curve. A load displacement plot for each specimen is provided in APPENDIX A.

Table 2: Average Sustained Peak Load by System

Specimen Type (Number of Specimens)	Mean, kN (kip)	Coefficient of Variation (%)	Percent Retention (%)
GG90 (5)	20.3 (4.57)	7.3	110.8*
GG45 (4)	18.7 (4.20)	7.6	102.4*
GC90 (5)	17.7 (3.99)	9.6	129.4*
GC45 (4)	16.6 (3.72)	13.1	108.2*

*Due to load method reported in Test Method

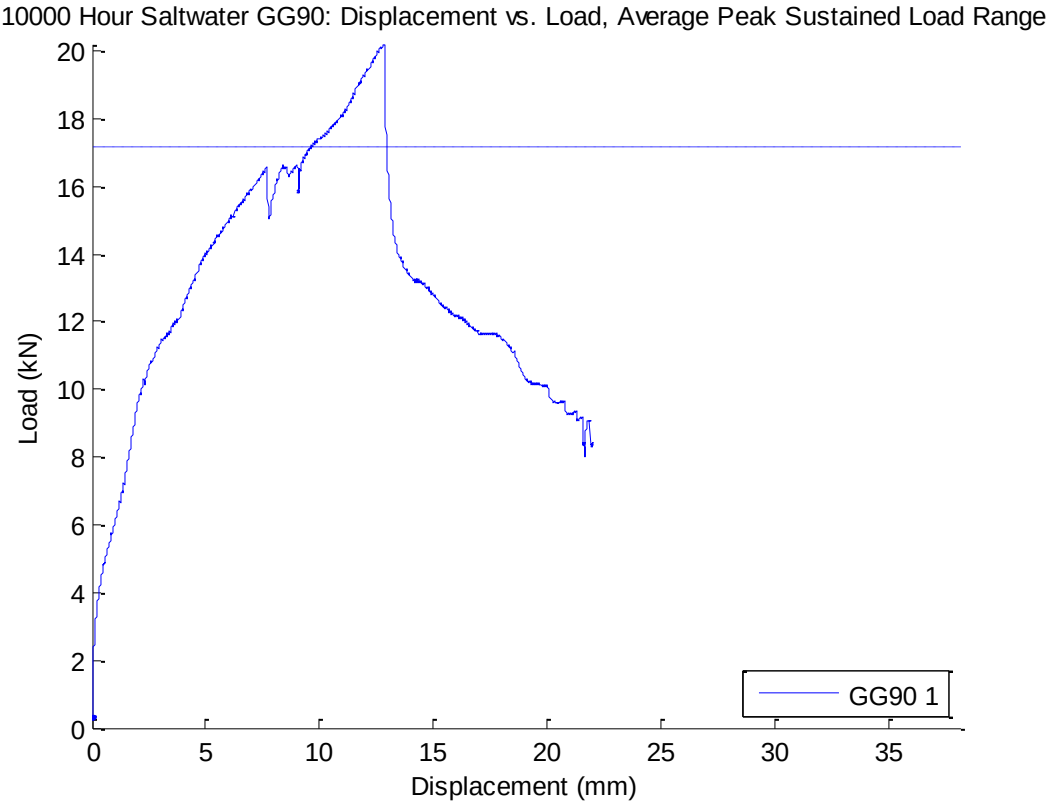

Figure 8: Load-displacement Plot for Average Peak Sustained Load

Conclusions

It can be seen that both systems performed well in terms of ultimate strength after experiencing environmental conditioning. The data indicates that after 10,000 hours of saltwater exposure the glass core systems were able to carry slightly higher loads than the carbon core specimens. This contradicts the data reported by Breton (Breton, 2013). The decision to move forward with the carbon core system only is still justifiable. As explained in Breton and Davids (2013b), a reduced design capacity is required by AASHTO when FRP systems are subjected to environmental effects. A 35% reduction is required for glass systems, while a 15% reduction is required for carbon systems. However, a concern is the apparent degradation of the epoxy used to bond the anchors to the concrete. In aggressive environments, the epoxy used here may not be appropriate.

Flexural Strength Testing of FRP-Reinforced Concrete Beam Specimen

In 2013, reinforced concrete beams with external FRP reinforcement were tested to explore the increase in capacity of an FRP strengthened beam compared with a non-FRP strengthened beam. These tests were of interest due to the larger loads being applied to these bridges. Existing concrete flat slab bridges may not have the load capacity to handle today's larger trucks (Poulin, 2012). Original beam testing was conducted with beams that were cast with 60ksi steel rebar, which is typical for modern construction. Based on the success of the FRP reinforcement further tests were conducted on beams cast with 40ksi steel rebar, which was typical of construction from the period these bridges were built (Poulin, 2012). As with the previous tests, two FRP reinforcement systems were used: GC45 and GC90. The two systems are made up of a carbon fiber core and fiberglass skins. The carbon fiber core is oriented at +/- 45° to the longitudinal axis in the GC45 reinforcing, and 0°/90° in the GC90 reinforcing. A more detailed discussion of the reinforcement systems is provided in the Masters' thesis written by Breton (Breton, 2013).

The beams were tested following the same procedures as Breton. First, to simulate service loads, an initial loading scheme to produce flexural cracks in the concrete and strain in the reinforcing steel was run. The specimens were then externally reinforced with a strip of the mechanically fastened FRP (MF-FRP) and loaded until failure. The observed failure mode, concrete crushing in the moment span, was the same as observed by Breton. The GC45 system provided a 34% increase in ultimate moment and a 27% decrease in center span deflection. The GC90 system provided a 43% increase in ultimate moment and a 31% decrease in center span deflection. The results presented here are similar to the results presented by Breton (Breton, 2013).

Test Specimen

The concrete beams used to evaluate the reinforcement systems were cast at the University of Maine's Advanced Structures and Composites Center in accordance with the American Concrete Institute (ACI) (ACI - Committee 318, 2008). The beams were designed to represent flat-slab concrete bridges by maintaining the same span-to-depth and reinforcement ratios of the design bridge. The Levant Bridge (MaineDOT Bridge #5253) was used as the design bridge. As noted

in Breton's thesis, the compressive strength of the specimens is higher than that of the Levant Bridge (Breton, 2013). Another discrepancy that exists between the specimens and the Levant Bridge is the grade of the reinforcing steel. The specimens were built with Grade 40 reinforcing steel, compared to the Grade 33 reinforcing steel that is likely present in the Levant Bridge.

The following sections discuss the specimen design and details of the reinforcing material. Specimens were labeled according to the FRP strip used to strengthen them. Strips were pre-labeled by Breton; this number system was kept for these specimens. For example, only two GC90 specimens were tested and were labeled with their predetermined numbers (4 and 5 in this case), resulting in '40_090_4' and '40_090_5', with no specimen 1-3.

Design of Beam Specimen

The Levant Bridge (MaineDOT Bridge #5253), which was used as the design bridge, has a span-to-depth ratio of 16.2 and a reinforcement ratio of 0.0077 (Breton, 2013). The properties were maintained in the construction of the flexural specimens. Table 3 provides the as-built beam dimensions of the specimens.

Table 3: Beam Specimen Dimensions

Width, mm (in)	Depth, mm (in)	Length, mm (in)	Span, mm (in)
305 (12)	203 (8)	3962 (156)	3353 (132)

MF-FRP Dimensions and Details

The FRP strips were cut to a length of 3.042m (9.79ft). Holes to accommodate the anchors were drilled with a diameter of 12.7mm (0.5in). The holes were drilled 73.0mm (2.875in) from the ends with a spacing of 127mm (5in). Holes were numbered starting on the north end of the beam, resulting in holes 1-12 on the northern half of the span and holes 13-24 on the southern half. The strips had a width of 101.6mm (4in). The average thickness for the GC45 and GC90 strips was 5.46mm (0.215in) and 5.41mm (0.213in), respectively.

Reinforcing Steel Tensile Strength Tests

To obtain the true yield strength of the reinforcing steel used in the beam specimens, tensile tests were performed. The results of these tests showed that the reinforcing steel had an average yield strength of 372MPa (54ksi). The experimental yield strength is 35% higher than the minimum specified design value. The theoretical capacity of both FRP strengthened and non-strengthened beam specimens was better approximated using the experimental yield strength.

Test Specimen and Test Method

Rebar specimens were extracted and tested following flexural failure of beams; refer to Breton's thesis for the manner of extraction (Breton, 2013). Upon completion of the flexural testing, the beams were flipped over so that the flexural face was accessible. At one end of the beam, concrete was scored and removed to expose the steel reinforcement. The steel was then removed from the beam using a grinding wheel. The extracted rebar specimens varied in length from 311mm to 457mm (12.25in to 18in). All specimens were long enough to provide for adequate

grip length and the required 203mm (8in) gauge length except for one. However, this specimen's data was unusable do to an error in testing that was unrelated to the length of the specimen, which is discussed below. The actual cross-sectional area of the rebar specimens was found to be less than $0.31in^2$, the nominal cross-sectional area for a No. 5 bar.

The rebar was testing in accordance with ASTM A370 (ASTM, 2012) in a 500kN (110kip) capacity MTS actuator at a load rate of 12.7mm/min (0.5in/min). Load and position data were collected during the test and used to calculate the stress and strain of each specimen. Specimen labels corresponded with the beam they were extracted from. As noted above, the data from one specimen, 45_2A, was unusable due to an error. The load rate was set to cover 1in over the course of two minutes (resulting in 0.5in/min). Due to the way the testing program was set up the test stopped after 1in of movement. The program was changed to allow for 3in of deflection. This change inadvertently changed the load rate to 6in/min. The specimen failed in 18 seconds, and the first data point was collected after yield had already occurred. This error was corrected before any further testing was conducted to ensure that the load rate of 0.5in/min was used.

Results and Conclusions

All specimens failed by rupture, following necking within the gauge length. As mentioned above, the data from specimen 45_2A was unusable, and will be excluded from this discussion. The yield stress of each specimen was determined using the autographic diagram method, or "top of knee" method as defined in ASTM A370 (ASTM, 2012). The yield point for each specimen is provided in Table 4. A graphical overlay of all rebar specimen load-displacement plots is presented in Figure 9.

An average yield stress for the reinforcing steel of 372MPa (54ksi) was calculated using the nominal area and average yield force. The average yield strain was found to be 0.0019 by assuming the steel's elastic modulus to be 200,000MPa (29,000ksi). Grade 40, No. 5 reinforcing steel has a nominal yield force and yield strain of 55.2kN (12.4kip) and 0.00138 respectively.

Table 4: Reinforcing Steel Cross-sectional Area and Yield Force

Specimen Label	Cross-sectional Area, mm^2 (in^2)	Yield Force, kN (kip)
'control'	164 (0.254)	76.3 (17.1)
'45_1A'	165 (0.256)	76.5 (17.2)
'090_4'	165 (0.256)	73.8 (16.6)
'090_5'	171 (0.265)	71.3 (16.0)
Average	167 (0.258)	74.5 (16.7)
Std. Dev.	3.20 (0.0050)	2.45 (0.55)
CoV (%)	1.9	3.3

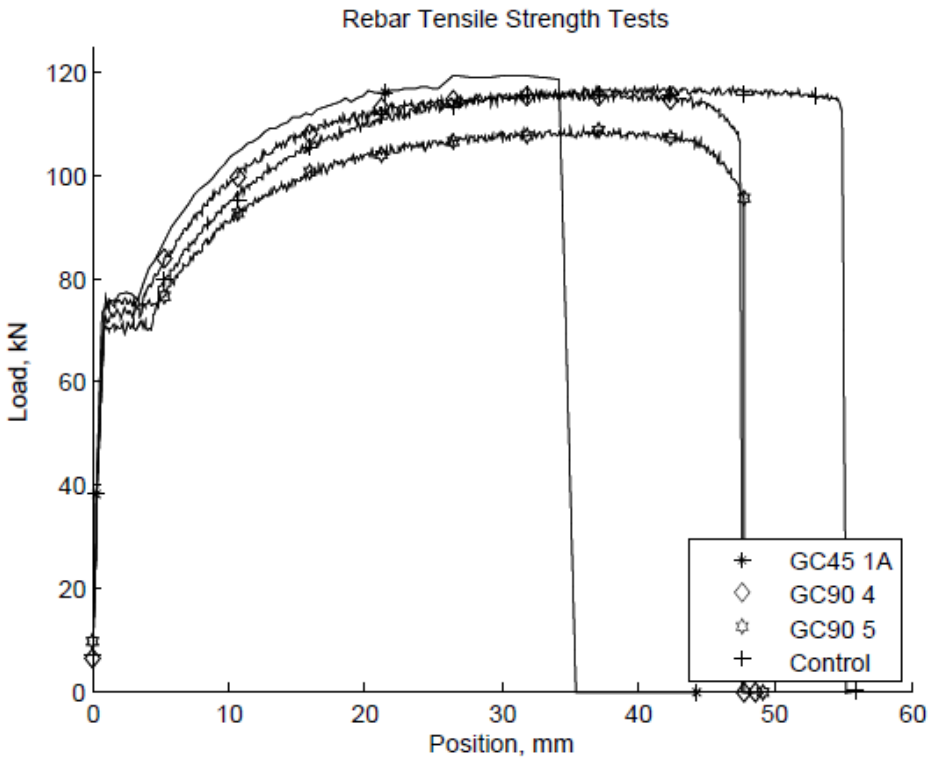

Figure 9: Reinforcing Steel Load-Displacement Overlay

Flexural Capacity Test Method and Instrumentation

Flexural specimens were loaded with a 490kN (110kip) capacity Instron actuator. The specimens were first subjected to an initial loading phase, which produced flexural cracks in the beam. This made the beam a better representation of concrete that had been in service and was a candidate

for retrofitting. Following the initial loading sequence, the beam was loaded to failure, which was used to assess the strength gain provided by the MF-FRP systems. Anticipated nominal flexural capacities for beam specimens were calculated in accordance with the ACI design guidelines (ACI - Committee 440, 2008). Nominal flexural capacities were calculated with both assumed and real concrete and steel strength values (see APPENDIX B). Table 5 contains the expected moment capacities and FRP stresses of FRP-strengthened beams.

Table 5: Concrete and Steel Strengths

Concrete and Steel Strength	Assumed Strengths f'c = 28.3MPa (4100psi) fy = 276MPa (40ksi)		As-built Strengths f'c = 28.3MPa (4100psi) Fy = 372MPa (54ksi)	
	Nominal Moment Capacity kN-m (kip-ft)	FRP Stress at Capacity MPa (ksi)	Nominal Moment Capacity kN-m (kip-ft)	FRP stress at Capacity MPa (ksi)
GC45	49.5 (36.5)	316.3 (45.9)	50.6 (37.3)	299.6 (43.5)
GC90	36.6 (27.0)	193.1 (28)	53.4 (39.4)	345.9 (50.2)

Loading Procedures

Flexural specimens were tested using the same method as Breton, which is thoroughly explained in section 5.2.1 of Breton's thesis (Breton, 2013). A brief discussion of the loading procedures will be presented here. As stated above, all specimens underwent an initial loading sequence to form flexural cracks. The initial loading sequence began with the load ramping up to 21.8kN (4.9kip) over a period of 6.75min. This load was then held for 10s. The load was then ramped down to 0.89kN (0.2kip) over a period of 6.75min. This load was held for 10s. This process was then repeated once and then the beam was fully unloaded. Following the initial loading sequence, an FRP strip was attached to the specimen. Specimens were then loaded to failure at a rate of 12.7mm/min (0.5in/min).

Beam Specimen Instrumentation

The specimens were instrumented similarly to Breton, with two string pots located at mid-span, one LVDT at each end to measure support compression, a strain gage on one of the steel reinforcing bars, and eight strain gages on the FRP strips. The FRP strain gages were placed in redundant locations over the half span of the FRP. Instrumentation labeling was consistent with that used by Breton, with the exception of the FRP strain gages (Breton, 2013). FRP strain gage locations were changed due to space availability in the lab. The northern half span of the beam was instrumented for these tests. Strain gages 1 and 2 were kept as the northerly-most gages, which moved them to near the supports. This in turn moved strain gages 7 and 8 to mid-span. A diagram of the FRP strain gage locations can be seen in Figure 10.

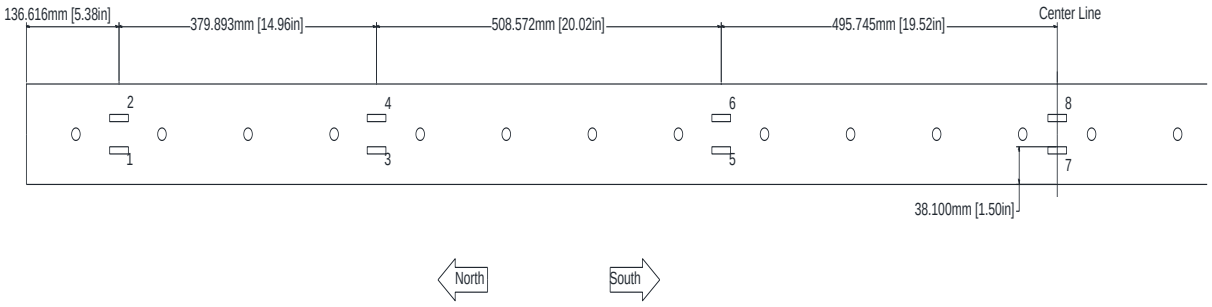

Figure 10: FRP Strain Gage Locations (as seen from under specimen)

MF-FRP Installation

Upon completion of the initial loading sequence an FRP reinforcing strip was adhered to the flexural face of the beam using 3M™ VHB™ 5952 industrial double-sided, visco-elastic foam tape (3M, 2011). Once adhered, 11.1mm (0.438in) holes were drilled into the concrete beam with a Hilti hammer drill. The FRP strip was used as a template for this process. The holes were approximately 38.1mm (1.5in) deep. The holes were thoroughly cleaned with a wire brush to remove any debris left from the drilling process.

To attach the FRP to the beam specimens a HILTI epoxy and stainless steel threaded rods were used as anchors. HILTI HIT-HY 150 MAX-SD injectable mortar was used as the adhesive. The adhesive was applied using a specialized HILTI caulking gun and mixing tube. After a hole was filled with adhesive a 63.5mm (2.5in) long, 9.53mm (0.375in) diameter stainless steel threaded rod was inserted into the hole. Following the 30 minute cure time of the adhesive, stainless steel washers and nuts were tightened to a torque of 16.9kN-m (12.5kip-ft). (HILTI, 2012).

Some problems were encountered during the installation process. The most notable issue was the inconsistency of the concrete beam dimensions. During casting, portions of the formwork deformed, causing the depth of the beams to vary over their lengths. This caused problems with installing the FRP because the strips were fairly stiff. It was difficult to adhere the FRP using the VHB tape. This also caused an issue where the FRP couldn't be in full contact with the concrete beam. In some anchor rods the 16.9kN-m (12.5kip-ft) torque was reached before the FRP was pulled into full contact because of the drastic section changes in the beam and relative stiffness of the FRP. An example of this can be seen in Figure 11. Shims were not placed between the FRP and the concrete, which forced the system to rely on bearing of the FRP at anchors for short lengths along the beam.

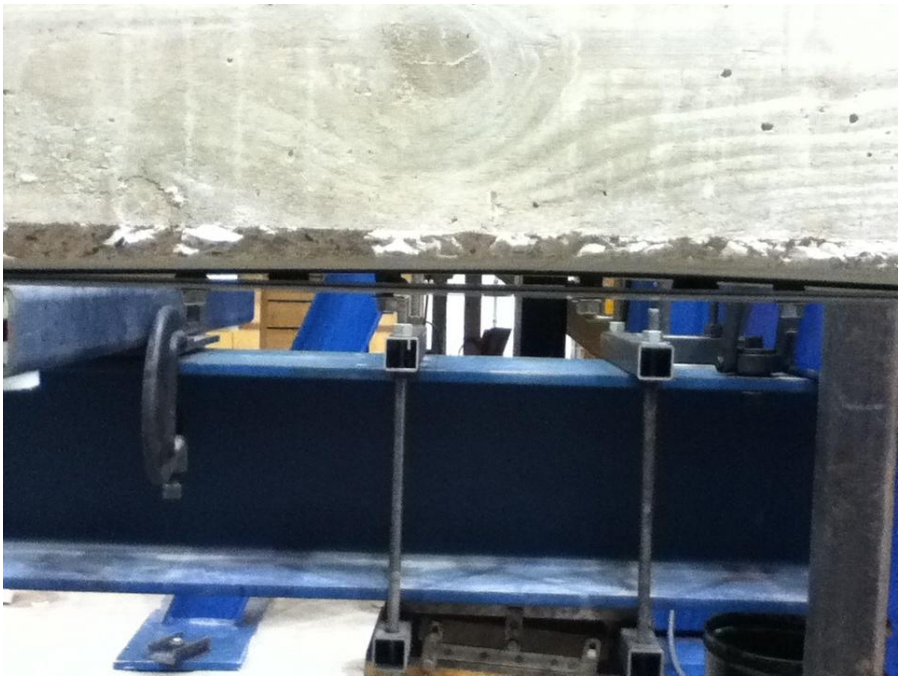

Figure 11: Gap between FRP and Beam Flexural Face

Flexural Behavior

Flexural cracks were produced during the preloading sequence to simulate a beam after service conditions. Steel strain gage data from several of the beams indicate that the steel exceeded yield during the preloading sequence. It was apparent that the rebar strain gages were malfunctioning on these specimens, as a clearly defined yield point can be seen for every specimen (see Figure 12). For all specimens this yield point occurs at a load higher than the applied service load of 22kN (5kip) used to cause initial cracking.

All specimens tested failed due to concrete crushing under failure loading and showed permanent deformation. It was observed that the reinforcing steel yielded by examining the load-deflection plots of the beam specimens. A "knee" is visible in all specimens indicating yield of the steel. The FRP strengthened specimens exhibit a bilinear response, indicating where the FRP reinforcing strip begins to carry the load. Figure 12 shows the load vs. mid-span deflection plot of all specimens.

A plot was generated showing rebar strain vs. load for all specimens except '45_1A', which had a broken strain gage. Figure 13, Figure 14, and Figure 15 show the rebar strain vs. load plots for the control, GC45, and GC90 specimens, respectively. The vertical dotted line represents the average yield strain of 0.0019, while the horizontal dotted line represents the yield load determined by the "top of knee" method. As previously mentioned, some rebar strain gages appeared to record questionable data; this can be seen in Figure 12, where it is clear that the steel never yielded.

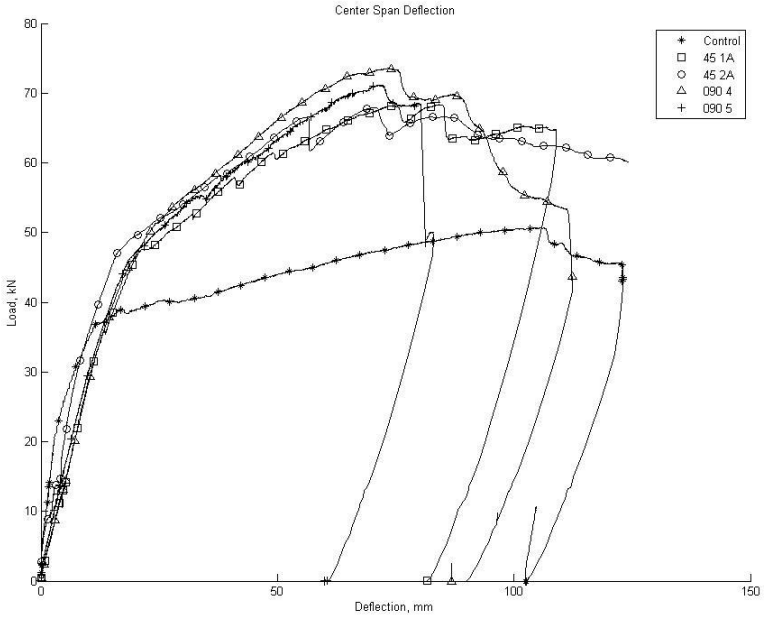

Figure 12: Load vs. center span deflection of flexural beam tests

Other instrumentation issues were encountered during testing. The west string pot began providing faulty data between the preloading sequence and the failure loading for GC45_1A. This issue was not noticed until the string pot completely failed during testing of Fatigue_045_1 (discussed below). As a result of this west string pot data is not available for the failure loading of specimen 'GC45_1A' and both the preloading sequence and failure loading of specimen 'GC90_5'. For these specimens, mid-span deflection was presented using only data from the east string pot. During the testing of 'GC45_2A' the specimen deflected so much that the spreader beam came into contact with an LVDT and began loading the LVDT. This caused the load increase substantially and the LVDT to malfunction. As a result, useable data from 'GC45_2A' stops around 125mm of deflection. This can be noted in Figure 12, as the Load – Deflection curve for 'GC45_2A' ends before unloading.

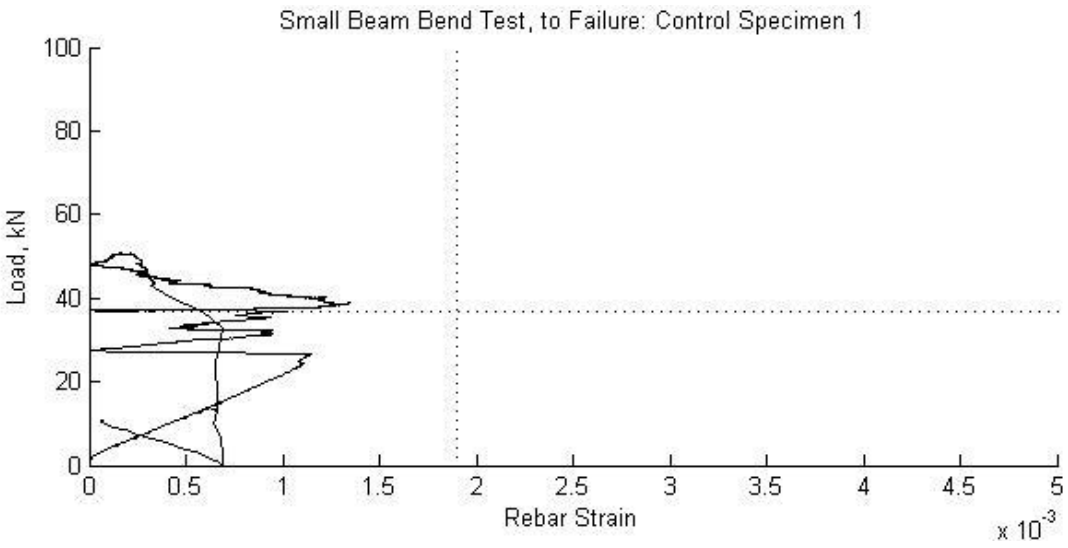

Figure 13: Rebar strain vs. load: 40ksi control specimen

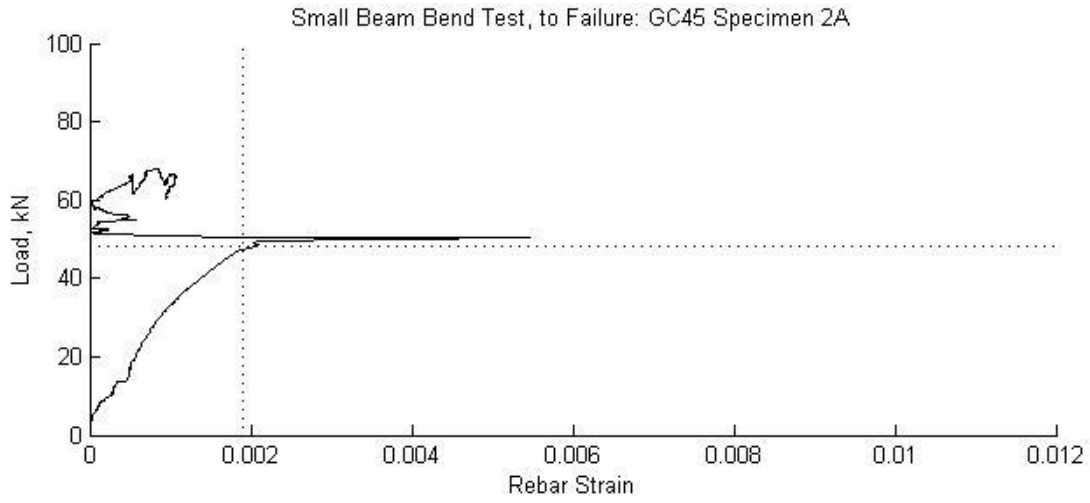

Figure 14: Rebar strain vs. load: 40ksi GC45 specimen

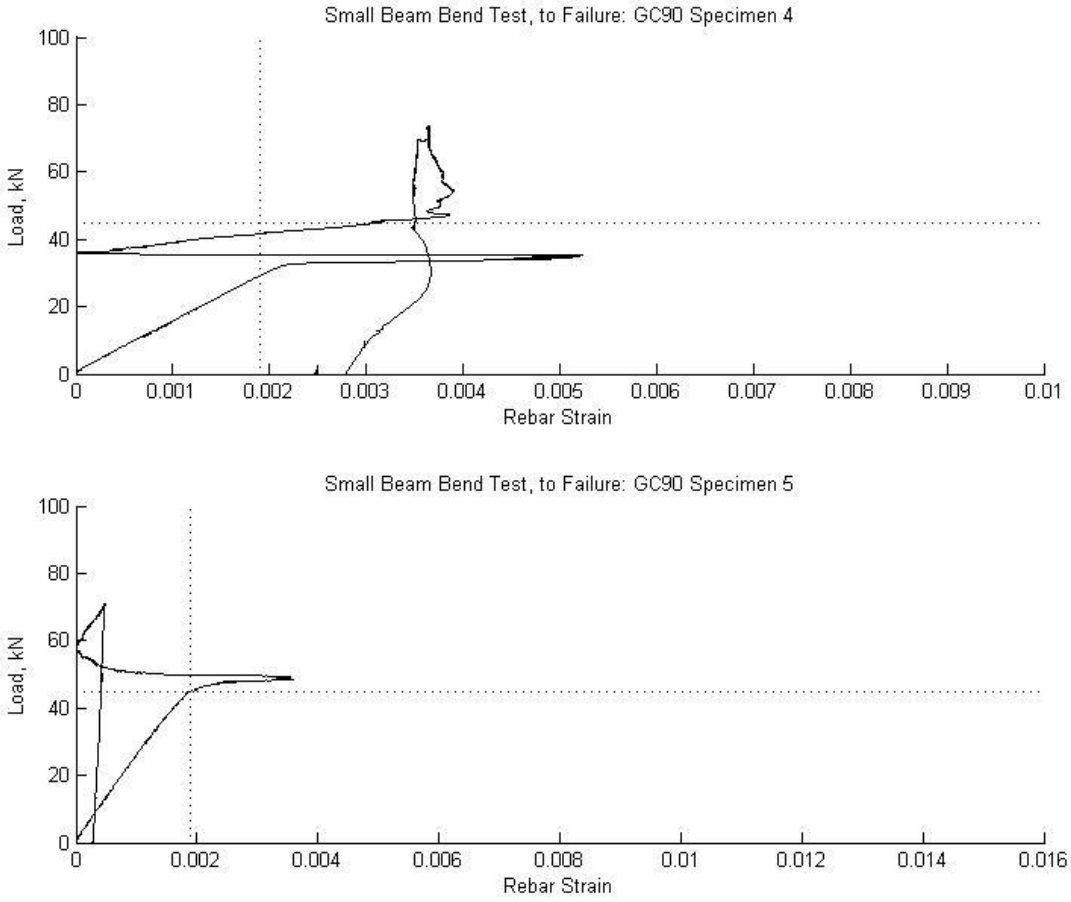

Figure 15: Rebar strain vs. load: 40ksi GC90 specimens

The GC45 system provided an increase in yield and ultimate moment capacity of 28% and 34%, respectively. The GC90 system provided an increase in yield and ultimate moment capacity of 31% and 43%, respectively. As mentioned, not all strain gage data was considered to be accurate. Due to this yield load was determined using the 'top of knee' method from the load-displacement data. This yield load was used to determine the yield moment for the small beam specimens. The yield moments are presented in Table 6 - Table 7. Ultimate capacity was determined to be the highest load that the specimen withstood during failure loading. Ultimate capacity values are presented in Table 9 - Table 11. The ultimate moment capacity for the GC45 and GC90 systems was 24.7% and 24.3% less than the expected as built moment capacities, respectively.

Table 6: Yield Moment of Control Specimen

Specimen	Yield Moment by 'Top of Knee' Method kN-m (kip-ft)
Control	20.73 (15.29)

Table 7: Yield Moment of GC45 Specimens

Specimen	Yield Moment by 'Top of Knee' Method kN-m (kip-ft)
GC45_1A	26.57 (19.59)
GC45_2A	26.55 (19.58)
Avg.	16.56 (19.59)
Std.	0.013 (0.010)
CoV (%)	0.05

Table 8: Yield Moment of GC90 Specimens

Specimen	Yield Moment by 'Top of Knee' Method kN-m (kip-ft)
GC90_4	28.63 (21.12)
GC90_5	25.83 (19.05)
Avg.	27.23 (20.08)
Std.	1.978 (1.459)
CoV (%)	7.26

Table 9: Maximum Response of Control Specimen

Specimen	Max. Moment kN-m (kip-ft)	Max. Shear kN (kip)	Max. Mid-span Deflection, West mm (in)	Max. Mid-span Deflection, East mm (in)
Control	28.34 (20.90)	25.36 (5.70)	102.15 (4.02)	109.16 (4.30)

Table 10: Maximum Response of GC45 Specimens

Specimen	Max. Moment kN-m (kip-ft)	Max. Shear kN (kip)	Max. Mid-span Deflection, West mm (in)	Max. Mid-span Deflection, East mm (in)
GC45_1A	38.21 (28.18)	34.19 (7.69)	- -	84.17 (3.31)
GC45_2A	37.94 (27.99)	33.95 (7.63)	72.61 (2.86)	68.68 (2.70)
Avg.	38.08 (28.09)	34.07 (7.66)	72.61 (2.86)	76.43 (3.01)
Std.	0.190 (0.140)	0.170 (0.038)	- -	10.953 (0.431)
CoV (%)	0.50	0.50	- -	14.33

Table 11: Maximum Response of GC90 Specimens

Specimen	Max. Moment kN-m (kip-ft)	Max. Shear kN (kip)	Max. Mid-span Deflection, West mm (in)	Max. Mid-span Deflection, East mm (in)
GC90_4	41.13 (30.34)	36.80 (8.27)	75.07 (2.96)	71.65 (2.82)
GC90_5	39.77 (29.33)	35.58 (8.00)	- -	71.65 (2.82)
Avg.	40.45 (29.83)	36.19 (8.14)	75.07 (2.96)	71.65 (2.82)
Std.	0.965 (0.712)	0.863 (0.194)	- -	0.000 (0.000)
CoV (%)	2.39	2.39	- -	0.00

All beam specimens underwent flexural failure in the moment span. The control specimen failed due to concrete crushing just ahead of the load head, as can be seen in Figure 16. The control beam exhibited permanent deflection, yielded steel reinforcement, and flexural cracks. All FRP strengthened beams failed due to concrete crushing under a load head (see Figure 17). All FRP strengthened specimens exhibited permanent deflection, yielded steel reinforcement, and flexural cracks. In both figures large flexural cracks can be observed. Figure 17 shows anchor withdrawal, which is not considered to be the failure mode. The anchors withdrew during continued loading after beam failure and did not have an effect on the beam's capacity. The phenomenon of bent anchors discussed by Breton in section 5.2.4 of *Mechanically Fastened Fiber-Reinforced Polymer (FRP) Flexural Retrofit Systems for Reinforced Concrete Flat-Slab Bridges* (Breton, 2013) was also observed in all FRP strengthened specimens.

Figure 16: Control Beam Failure

Figure 17: Typical FRP Strengthened Beam Failure

FRP Strains

During testing several strain gages failed to provide data. However, at least one FRP strain gage was functional at each redundant location with the exception of mid-span of 'GC45-1A', where both gage 7 and 8 failed. As discussed previously, strain gage numbering differed from that used by Breton; the numbering used for these tests is displayed in Figure 10.

The variations of strain in the FRP strip over the half span are shown in Figure 18 - Figure 21. Three loadings were used to represent strain: 1) half the load required to yield the reinforcing steel, 2) the load required to yield the reinforcing steel, and 3) the ultimate load. A solid vertical line represents the location of the load head, 0.55m from mid-span of the beam. As distance from mid-span increased the strain in the FRP decreased. The strain also increases following the yield of the reinforcing steel, as the FRP begins to take more direct load.

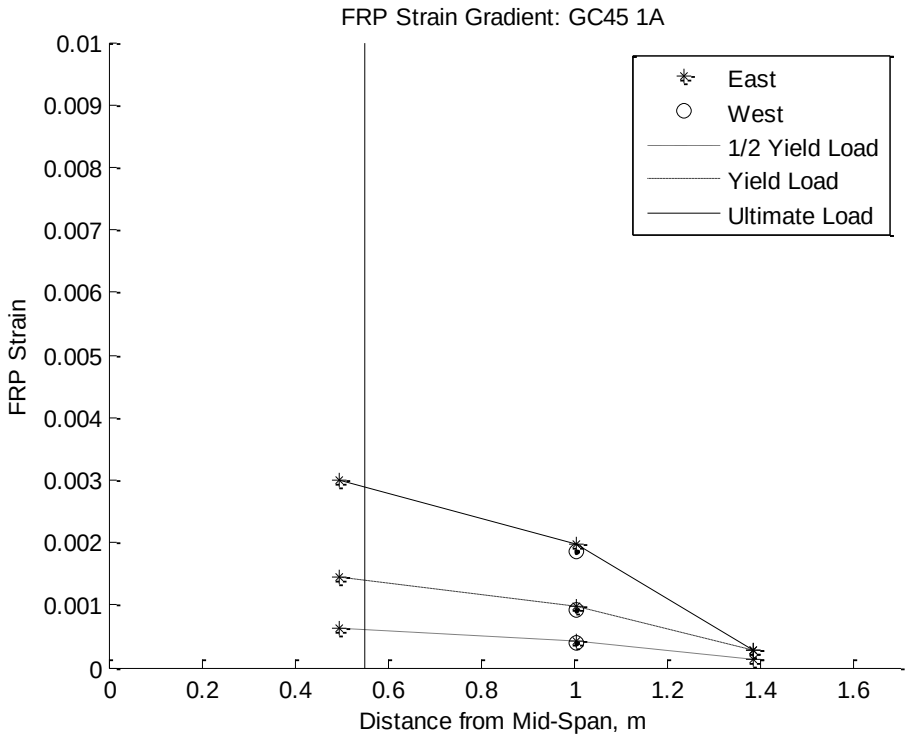

Figure 18: Variation of Strain in GC45_1A

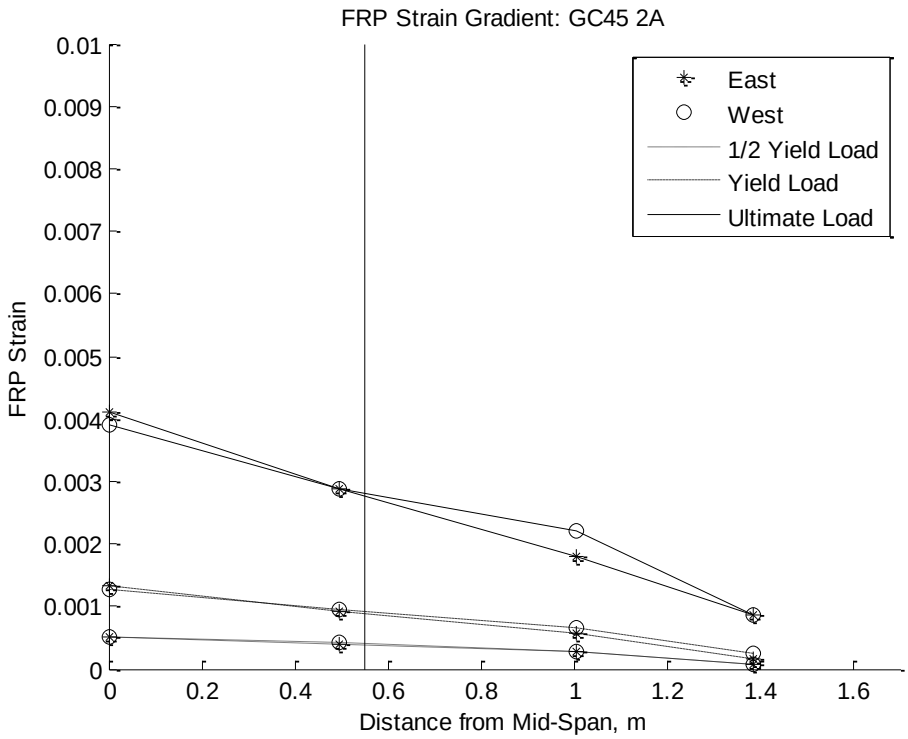

Figure 19: Variation of Strain in GC45_2A

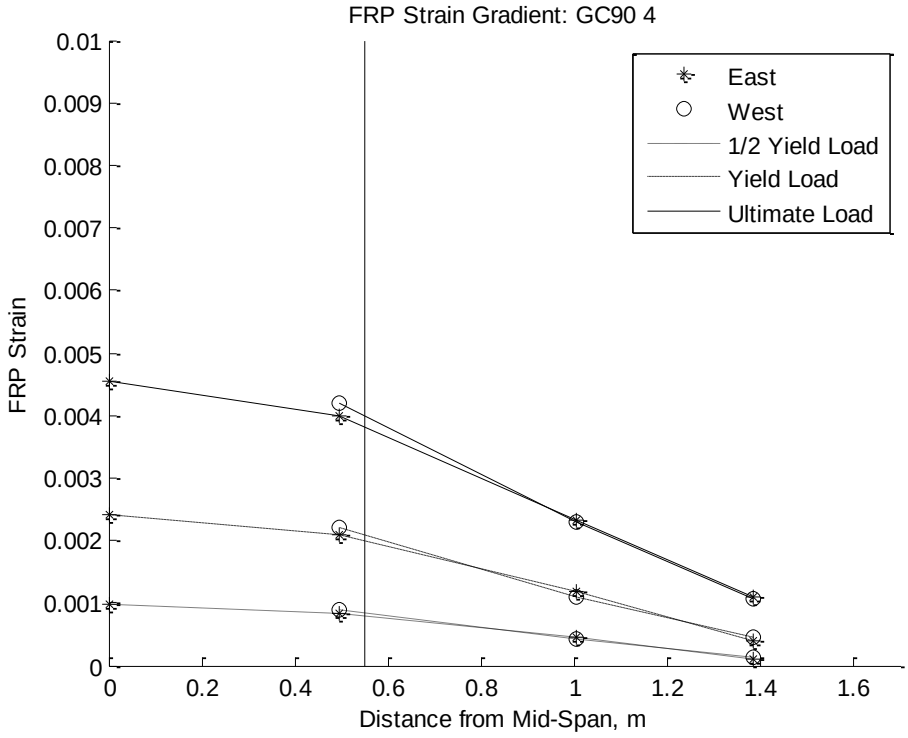

Figure 20: Variation of Strain in GC90_4

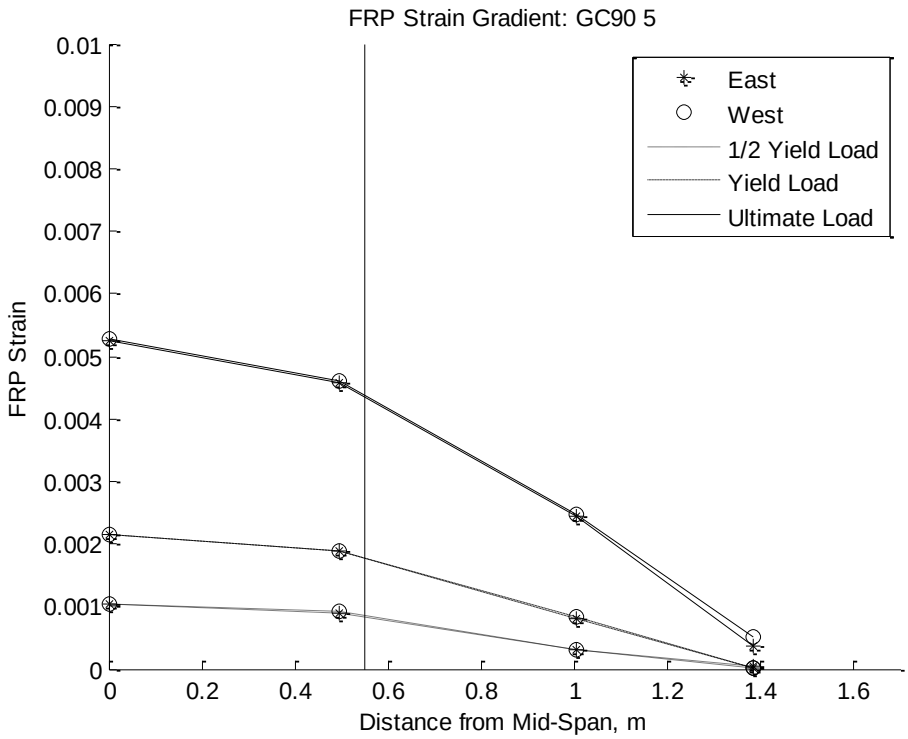

Figure 21: Variation of Strain in GC90_5

The variation of FRP strain by gage location for GC90 5 is shown in Figure 22. Similar plots for all beam specimens are presented in APPENDIX C. These plots show the FRP strain for each strengthened specimen over the duration of the failure loading. The gages within the load span (gages 5-8) experience significantly higher strains than those outside of the load span (gages 1-4). This indicates that the FRP experiences more tensile force within the load span. However, more bearing force is applied to the FRP outside of the load span where the shear is largest. The strain in the FRP is significantly affected by whether or not the steel reinforcement has yielded. This can be seen in the previously mentioned plots displayed in Figure 18 - Figure 21. It can be noted that prior to steel yield the strain increases more slowly than after steel yielding occurs.

Strain data was used to determine the tensile forces and the average bearing force in the FRP. Tensile and bearing forces were calculated following the same procedure as Breton (Breton, 2013). FRP tensile forces and FRP bearing forces are presented in Table 12-Table 13 and Table 14-Table 15, respectively.

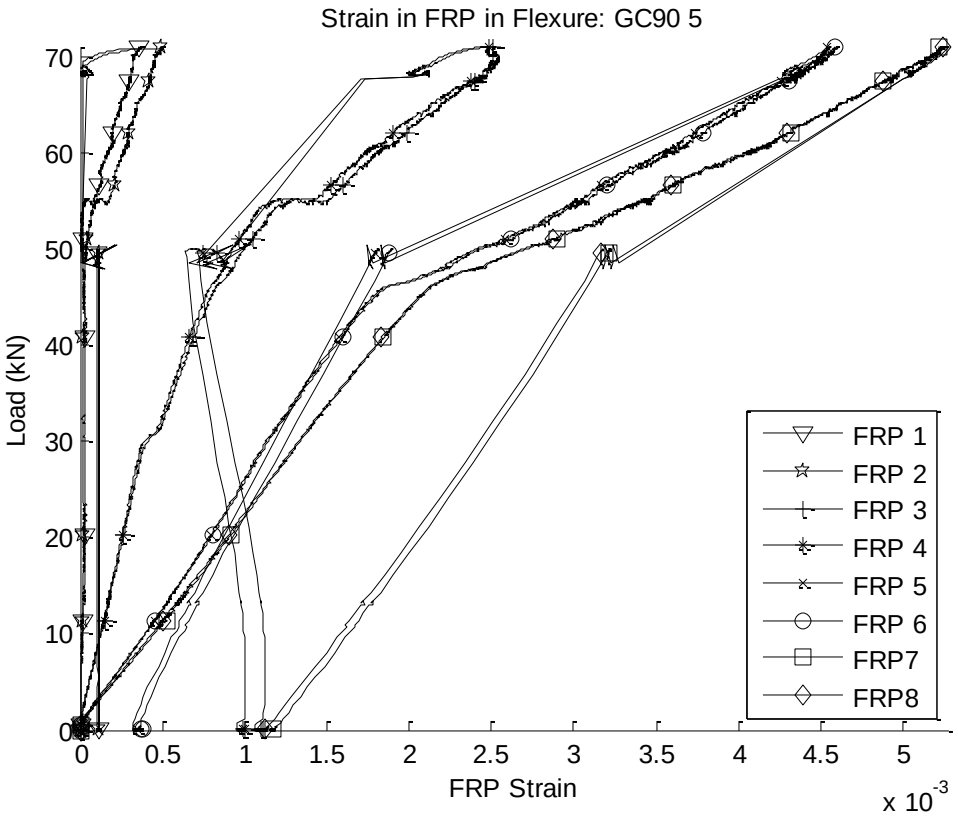

Figure 22: Strain in GC90 5 over duration of failure loading

Table 12: Tensile force in GC45 reinforcement at strain gage locations

	Gage 1&2 kN (kip)	Gage 3&4 kN (kip)	Gage 5&6 kN (kip)	Gage 7&8 kN (kip)
½ Yield Load				
GC45 1A	3.9 (0.9)	11.4 (2.6)	18.0 (4.0)	--
GC45 2A	2.4 (0.5)	8.0 (1.8)	11.6 (2.6)	14.7 (3.3)
Avg.	3.1 (0.7)	9.7 (2.2)	14.8 (3.3)	--
Std.	1.0 (0.2)	2.4 (0.5)	4.5 (1.0)	--
COV (%)	32.4	24.7	30.6	--
Yield Load				
GC45 1A	7.7 (1.7)	27.0 (6.1)	40.9 (9.2)	--
GC45 2A	5.8 (1.3)	17.5 (3.9)	26.6 (6.0)	36.8 (8.3)
Avg.	6.7 (1.5)	22.3 (5.0)	33.7 (7.6)	--
Std.	1.4 (0.3)	6.7 (1.5)	10.1 (2.3)	--
COV (%)	20.2	30.1	29.8	--
Ultimate Load				
GC45 1A	28.0 (6.3)	52.2 (11.7)	94.8 (21.3)	--
GC45 2A	29.3 (6.6)	73.0 (16.4)	67.1 (15.1)	110.7 (24.9)
Avg.	28.6 (6.4)	62.6 (14.1)	80.9 (18.2)	--
Std.	0.9 (0.2)	14.7 (3.3)	19.6 (4.4)	--
COV (%)	3.2	23.5	24.2	--

Table 13: Tensile force in GC90 reinforcement at strain gage locations

	Gage 1&2 kN (kip)	Gage 3&4 kN (kip)	Gage 5&6 kN (kip)	Gage 7&8 kN (kip)
½ Yield Load				
GC90 4	4.1 (0.9)	16.7 (3.7)	32.2 (7.2)	36.0 (8.1)
GC90 5	1.1 (0.3)	11.1 (2.5)	33.3 (7.5)	38.3 (8.6)
Avg.	2.6 (0.6)	13.9 (3.1)	32.8 (7.4)	37.1 (8.4)
Std.	2.1 (0.5)	4.0 (0.9)	0.8 (0.2)	1.6 (0.4)
COV (%)	81.5	28.6	2.3	4.3
Yield Load				
GC90 4	15.2 (3.3)	42.1 (9.5)	79.4 (17.8)	88.7 (19.9)
GC90 5	0.8 (0.2)	30.0 (6.8)	69.6 (15.6)	79.2 (17.8)
Avg.	8.0 (1.8)	36.1 (8.1)	74.5 (16.7)	83.9 (18.9)
Std.	10.2 (2.3)	8.5 (1.9)	6.9 (1.6)	6.7 (1.5)
COV (%)	126.7	23.6	9.3	8.0
Ultimate Load				
GC90 4	40.0 (9.0)	85.4 (19.2)	151.4 (34.0)	168.0 (37.8)
GC90 5	16.6 (3.7)	91.4 (20.6)	169.5 (38.1)	194.4 (43.7)
Avg.	28.3 (6.4)	88.4 (19.9)	160.4 (36.1)	181.2 (40.7)
Std.	16.5 (3.7)	4.3 (1.0)	12.8 (2.9)	18.6 (4.2)
COV (%)	58.3	4.8	8.0	10.3

Table 14: Average bearing force per anchor in GC45 specimens

	Anchors 2-4 kN (kip)	Anchors 5-8 kN (kip)	Anchors 9-12 kN (kip)
½ Yield Load			
GC45 1A	1.9 (0.4)	1.6 (0.4)	--
GC45 2A	1.4 (0.3)	0.9 (0.2)	1.0 (0.2)
Avg.	1.6 (0.4)	1.3 (0.3)	--
Std.	0.3 (0.1)	0.5 (0.1)	--
COV (%)	21.0	41.7	--
Yield Load			
GC45 1A	4.8 (1.1)	3.5 (0.8)	--
GC45 2A	2.9 (0.7)	2.3 (0.5)	3.4 (0.8)
Avg.	3.9 (0.9)	2.9 (0.6)	--
Std.	1.3 (0.3)	0.8 (0.2)	--
COV (%)	34.4	29.2	--
Ultimate Load			
GC45 1A	6.0 (1.4)	10.7 (2.4)	--
GC45 2A	10.9 (2.5)	-1.5 (-0.3)*	14.5 (3.3)
Avg.	8.5 (1.9)	--	--
Std.	3.4 (0.8)	--	--
COV (%)	40.7	--	--

* Negative difference between FRP strain is assumed to result in zero bearing force at the anchor. Value excluded from avg., std. and COV calculations

Table 15: Average bearing force per anchor in GC90 specimens

	Anchors 2-4 kN (kip)	Anchors 5-8 kN (kip)	Anchors 9-12 kN (kip)
½ Yield Load			
GC90 4	3.1 (0.7)	3.8 (0.9)	1.3 (0.3)
GC90 5	2.3 (0.6)	5.6 (1.2)	1.7 (0.4)
Avg.	2.8 (0.6)	4.7 (1.1)	1.5 (0.3)
Std.	0.5 (0.1)	1.2 (0.3)	0.3 (0.1)
COV (%)	16.2	25.0	18.9
Yield Load			
GC90 4	6.7 (1.5)	9.3 (2.1)	3.1 (0.7)
GC90 5	7.3 (1.6)	9.9 (2.2)	3.2 (0.7)
Avg.	7.0 (1.6)	9.6 (2.2)	3.1 (0.7)
Std.	0.4 (0.1)	0.4 (0.1)	0.1 (0.0)
COV (%)	5.9	4.1	2.3
Ultimate Load			
GC90 4	11.3 (2.6)	16.5 (3.7)	5.5 (1.2)
GC90 5	18.7 (4.2)	19.5 (4.4)	8.3 (1.9)
Avg.	15.0 (3.4)	18.0 (4.0)	6.9 (1.6)
Std.	5.2 (1.2)	2.1 (0.5)	2.0 (0.4)
COV (%)	34.6	11.8	28.3

Hole elongation at connection locations, indicating bearing failure of the FRP, was observed in both the GC45 and the GC90 specimens. Hole elongation within the moment span can be seen in Figure 23 and Figure 24. Similar to the observations made by Breton (Breton, 2013), hole elongation was more significant in the shear span than it was in the moment span, which is to be expected, as can be seen in the average bearing forces per anchor presented in Table 14 and

Table 15. The magnitude of the hole elongation in these four specimens was observed to be smaller than the hole elongation reported by Breton. This supports her statement that hole elongation was likely due to the large deflections that occurred during failure loading (Breton, 2013). Beams reinforced with 40ksi steel had less capacity than the beams tested by Breton, which contained 60ksi reinforcing steel. As a result, less deflection, and therefore less hole elongation, was recorded as the beam's ultimate capacity was reached.

Figure 23: Hole elongation in a GC45 FRP strip within the load span, after failure

Figure 24: Hole elongation in a GC90 FRP strip within the load span, after failure

The FRP reinforcing used in these tests was the same material used by Breton; therefore the material properties reported in her thesis are valid for this report. The elastic modulus of both the GC45 and GC90 reinforcing strips was determined through ASTM D3039 (ASTM, 2008) testing performed by Breton and is summarized in Table 16. The ultimate tensile capacity of the FRP strip was calculated by Breton and is also reported in Table 16 (Breton, 2013). The elastic modulus was used to calculate the stress at maximum load for all strengthened specimens. The maximum stress was compared with the ultimate capacity of the FRP strip to determine the utilization of the FRP reinforcing. At beam failure, it was determined that 21.3% of the GC45 reinforcing strip's strength was utilized and 31.6% of the GC90 reinforcing strip's strength was utilized, on average. Maximum strain, maximum stress, and FRP utilization for GC45 and GC90 reinforcing strips are presented in Table 17 and Table 18, respectively.

Table 16: FRP Mechanical Properties

FRP System		GC45	GC90
Max. Tensile Stress MPa (ksi)	*Avg.*	509 (73.8)	605 (87.7)
	STD	35.2 (5100)	27.1 (3930)
	COV (%)	6.9	4.5
Elastic Modulus MPa (ksi)	*Avg.*	29800 (4329)	39000 (5660)
	STD	2220 (322)	3720 (539)
	COV (%)	7.4	9.5

Table 17: GC45 Maximum Strain, Maximum Stress, and FRP Utilization

	Max. Strain ($\times 10^{-3}$)	Max. Stress, MPa (ksi)	FRP Capacity Utilization (%)
GC45 1A	3.33	99.1 (14.4)	19.5
GC45 2A	3.95	117.7 (17.1)	23.1
Avg.	3.64	108.4 (15.7)	21.3
Std.	0.44	13.2 (1.9)	2.6
COV (%)	12.14	12.1	12.1

Table 18: GC90 Maximum Strain, Maximum Stress, and FRP Utilization

	Max. Strain ($\times 10^{-3}$)	Max. Stress, MPa (ksi)	FRP Capacity Utilization (%)
GC90 4	4.55	177.3 (25.7)	29.3
GC90 5	5.27	205.3 (29.8)	33.9
Avg.	4.91	191.3 (27.8)	31.6
Std.	0.51	19.8 (2.9)	3.3
COV (%)	10.35	10.4	10.4

Summary and Conclusions

To determine the viability of the MF-FRP reinforcing systems tested by Breton on older structures, beam specimens were constructed with 40ksi reinforcing steel. The Levant Bridge (MDOT Bridge #5253) was used as the design bridge for the 40ksi specimens.

Tension tests were performed on portions of reinforcing steel removed from specimens after beam failure to obtain a true yield strength. The rebar portions were taken from the ends of the beams to ensure that they had not yet experienced yield. After tension testing was completed it was determined that the average yield stress of the rebar was 372MPa (54ksi), which corresponds to a yield strain of 0.0019. These values were used to determine more accurate beam capacities.

Beam specimens were subjected to an initial loading sequence designed to produce flexural cracks and develop service level strain in the rebar. Beams were than strengthened by either GC45 or GC90 reinforcing strips. The GC45 system provided an increase in yield and ultimate moment capacity of 28% and 34%, respectively, and provided a decrease in mid-span deflection of 27%. The GC90 system provided an increase in yield and ultimate moment capacity of 31% and 43%, respectively, and provided a decrease in mid-span deflection of 31%. At beam failure, it was determined that 21.3% of the GC45 reinforcing strip's strength was utilized and 31.6% of the GC90 reinforcing strip's strength was utilized, on average. The effect of the FRP reinforcement was less significant when compared with the 60ksi beams. Concrete crushing within the load span was the failure mode observed in all FRP strengthened beams. All beams exhibited permanent deformation, yielded reinforcing steel, and flexural cracks. Strain in the FRP strips was seen to be greatest within the load span and less at the ends of the beams. It was also observed that bearing force was greater outside the load span, where shear forces between

the FRP and the concrete were greatest. These results agree with the results reported by Breton (Breton, 2013).

It can be concluded that both the GC45 and GC90 reinforcing systems are effective at increasing flexural capacity of the beams tested here. The systems also allow good ductility prior to failure. The strength increase of the 40 ksi beams due to the FRP reinforcing was less pronounced than that observed by Breton for beams with 60 ksi reinforcing (Breton, 2013). However, the strength increase provided by the FRP reinforcing strips is still significant.

Fatigue Testing of FRP-Reinforced Concrete Beam Specimen

The results of small beam bend tests showed that both FRP reinforcing systems were viable options for externally reinforcing flat-slab concrete bridges. The results of the environmental durability tests also showed that both systems maintained their strength after extended environmental exposure. Fatigue tests were conducted to assess the overall performance of the MR-FRP systems after representative service life.

Test Specimen

The concrete beams used for fatigue testing were the same as those used in static testing conducted by Breton. The beams were constructed with 60ksi reinforcing steel; all other properties were consistent with the beams discussed previously in the Flexural Strength Testing of FRP-Reinforced Concrete Beam Specimen section of this report.

FRP reinforcement used for fatigue tests was the same material used in small beam bend tests. The first three fatigue specimens were reinforced with GC45 strips. Due to a shortage of GC45 reinforcement, the fourth fatigue specimen was reinforced with a GC90 strip.

Test Method and Instrumentation

Fatigue specimens were tested in the same test fixture as the small beam bend specimens. However, a different actuator was used for fatigue testing. The 490kN (110kip) actuator used in small beam flexure tests was incapable of cycling fast enough to be feasible for fatigue testing. Instead, a 245kN (55kip) actuator was used. A detailed discussion of the loading procedure is presented below.

Loading Procedures

Specimens were subjected to the same preloading sequence that was used in the small beam flexure tests. The preloading sequence was designed to produce flexural cracks and create a surface more representative of an in-service concrete beam. Following preloading, an FRP strip was installed following the same procedure as was used for the small beam flexure tests, as described previously. Following FRP installation the specimen underwent an initial service test. The beam was then loaded in a sinusoidal manner, with periodic service tests.

Static Service Test Loading

Service tests were performed on the fatigue specimens at regular intervals. A static test was performed prior to beginning the fatigue cycle to determine baseline behavior of the specimen. The first fatigue specimen had service tests performed every 20,000 cycles until the beam reached 100,000 cycles, after which service tests were performed every 100,000 cycles. The greater frequency at the beginning of the testing ensured that there were no unintended negative effects of the fatigue loading on either the specimen or the test fixture. It was determined that the test fixture was performing adequately during fatigue. As a result service tests on all other specimens were conducted at intervals of 100,000 cycles.

Table 19: Service Loads

	Fatigue_045_1	**Fatigue_045_2**	**Fatigue_045_3**	**Fatigue_090_4**
Service Load kN (kip)	53.4 (12.0)	48.9 (11.0)	48.9 (11.0)	44.5 (10.0)

Sinusoidal Fatigue Loading

To fatigue the specimens a sinusoidal loading was used. A 0.67kN (0.15kip) preload was placed on the beam. The load was then ramped up to 24.5kN (5.5kip) over a time of two minutes. When the specimen reached 24.5kN (5.5kip) the cyclic loading began. For all fatigue specimens the lower load during fatigue was 24.5kN (5.5kip). The lower load represents the dead load of the curbing and the self weight of the bridge. The upper load of the cycle was the service load presented in Table 19, above. The initial service load of 53.4kN (12.0kip) represents the load required to produce the design live load moment. It was changed for subsequent tests as discussed below. All beams were fatigued at a rate of 1.3Hz. The initial plan was to fatigue each beam for two million cycles, which is generally accepted as a good representation of a bridge girder's life span (Richie, 2003). The actual number of cycles performed is presented in Table 20. The wide range of cycles is discussed in detail in Fatigue Behavior, below.

Table 20: Fatigue Cycles to Failure

	Fatigue_045_1	**Fatigue_045_2**	**Fatigue_045_3**	**Fatigue_090_4**
Number of Cycles	851,693	2,604,258	1,030,287	2,000,025

Fatigue Specimen Instrumentation

Fatigue beams were instrumented in the same manner as the small beam flexure specimens. During fatigue loading load and position were collected directly from the load cell. No other instrumentation was hooked up during the cyclic loading to preserve the instrumentation. During service tests all instrumentation was installed and data was being collected. This instrumentation included: two string pots to measure center span deflection, two LVDTs (one at each beam end) to measure support compression, eight FRP strain gages placed consistently with Figure 10, and one strain gage attached to the embedded reinforcing steel. As noted before, the west string pot was broken during the first fatigue testing. As a result only data from the east string pot is

available for Fatigue_045_1. The string pot was replaced before the remaining beams were tested.

Fatigue Behavior

As mentioned above, the magnitude of the service load and the number of cycles varied depending on the specimen. The service load was originally set as 53.4kN (12.0kip) as discussed above. Fatigue_045_1 failed due to rebar fracture during fatigue loading at 851,693 cycles. Due to this, the service load was dropped to 48.9kN (11.0kip) to lower the stress in the rebar during fatigue loading. As can be seen in Table 20, Fatigue_045_2 withstood the initial two million cycles. It was determined that the beam would be run to three million. Fatigue_045_2 also experienced rebar fracture during fatigue at 2,604,258 cycles. Due to the fact that Fatigue_045_2 completed the initial two million cycles with little issue it was decided that Fatigue_045_3 would be tested with a service load of 48.9kN (11.0kip). Fatigue_045_3 failed during fatigue loading just over one million cycles. As a result of this, a monotonic test to failure post-fatigue could not be completed on any of these specimens. It was decided that the fourth beam, Fatigue_090_4, would be tested at a lower service load to ensure it reached two million cycles, where it was statically loaded to failure. Rebar fracture was also observed by Borowicz (Borowicz, 2002), who conducted similar tests. Results and observations for each beam are presented in detail below.

Fatigue_045_1

Fatigue_045_1 failed during fatigue loading due to rebar fracture. Data from the strain gage on the steel reinforcing bar was used to determine the stress in the rebar during service tests. The allowable fatigue stress range in steel reinforcing for infinite fatigue life specified by AASHTO is 165.5MPa (24.0ksi) (American Association of State Highway and Transportation Officials (AASHTO), 2012). Figure 25 shows that Fatigue_045_1 exceeded this limit. The average fatigue stress range was approximately 270MPa (39ksi). Both steel reinforcing bars in the specimen fracture during fatigue, as can be seen in Figure 26. As a result of the rebar failure it was decided that this beam would not be monotonically loaded after fatigue.

Permanent deflection was evident as a result of fatigue loading. Figure 27 shows the load displacement curve data from the service tests performed on Fatigue_045_1. Data from the final service test is not reported due to an error during testing. It can also be seen from Figure 27 that the stiffness of the beam was relatively unchanged during fatigue loading.

FRP strain data was collected during service tests. Figure 28 shows the variation of FRP strain based on the distance the gage was from mid-span of the beam. The vertical line represents the location of the load head. The lower load data presented corresponds with the lower fatigue value of 24.5kN (5.5kip). It can be observed that there is little change in FRP strain due to fatigue loading. This can also be observed in Figure 29, which shows the strain at strain gages 7 and 8 as a function of elapsed cycles. Similar plots for all gage locations can be found in APPENDIX D.

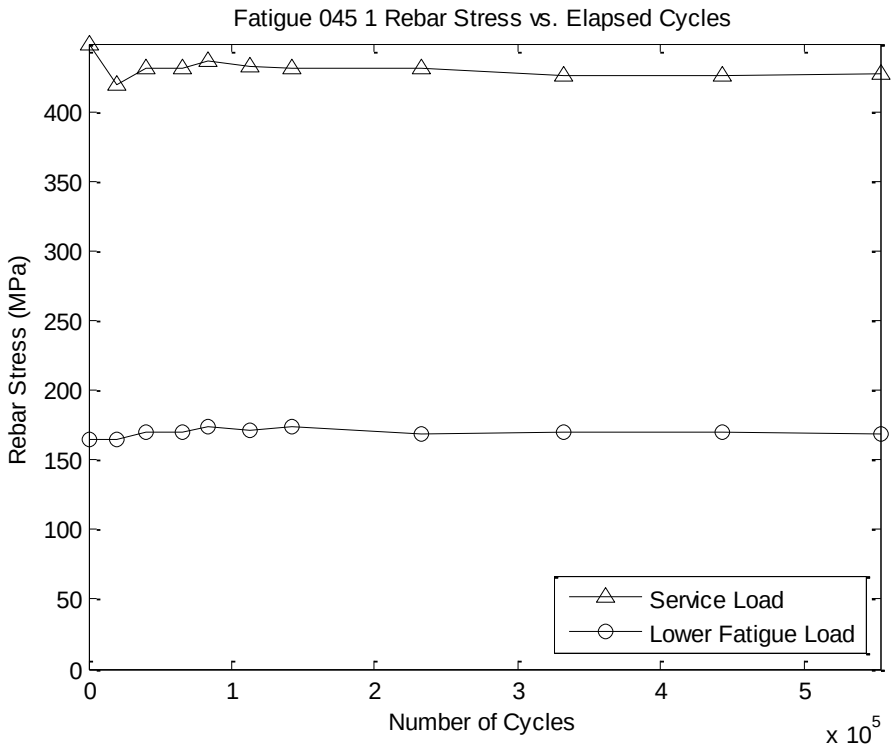

Figure 25: Fatigue_045_1 Rebar Stress

Figure 26: Fatigue_045_1 Rebar Fracture (Left: East rebar, Right: West rebar)

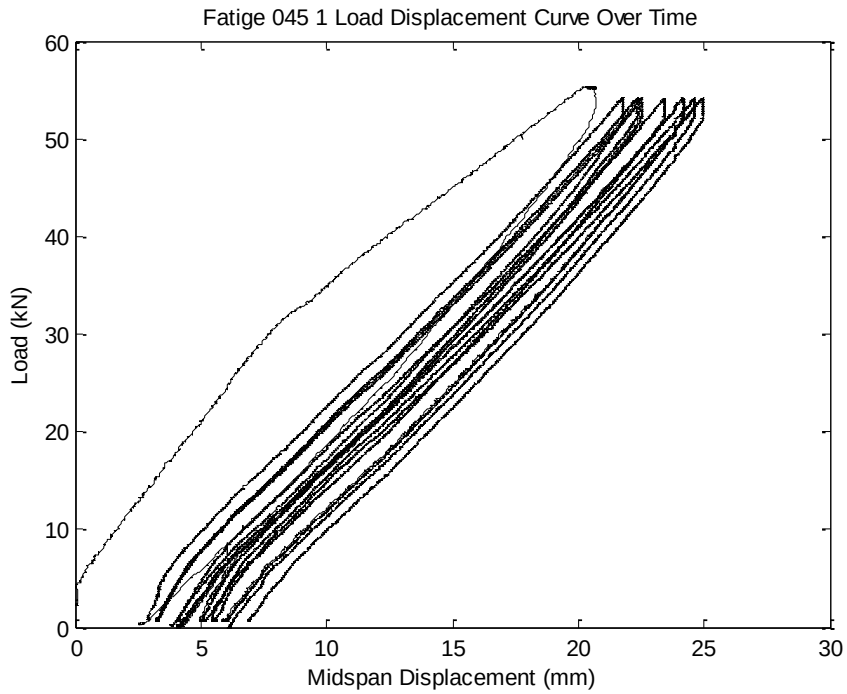

Figure 27: Fatigue_045_1 Service Test Mid-span Displacement Data

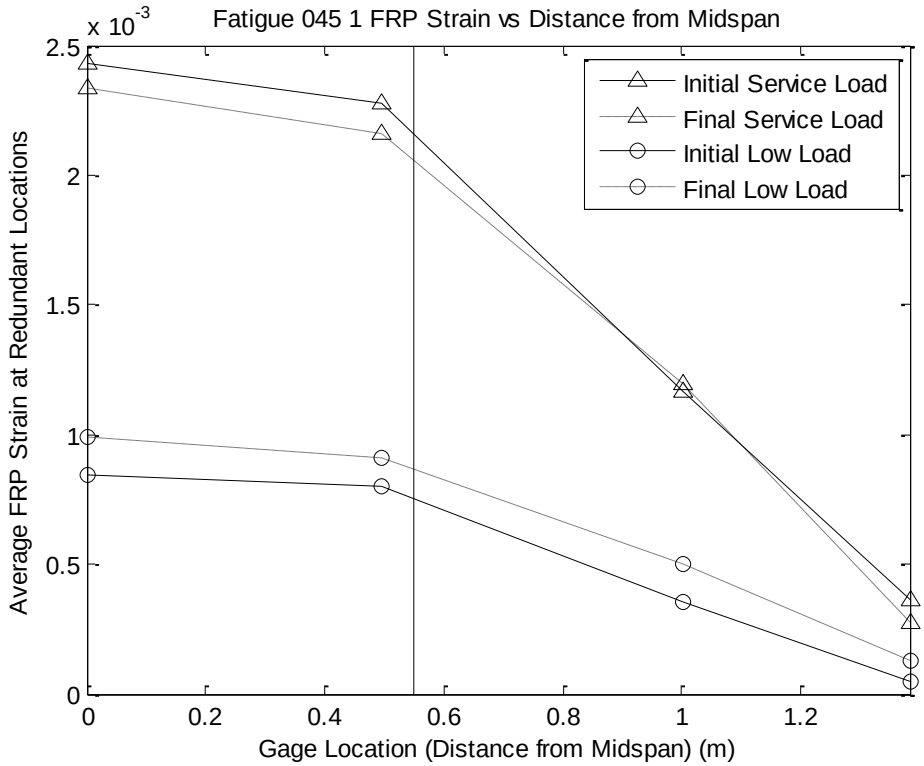

Figure 28: Variation in FRP Strain in Fatigue_045_1

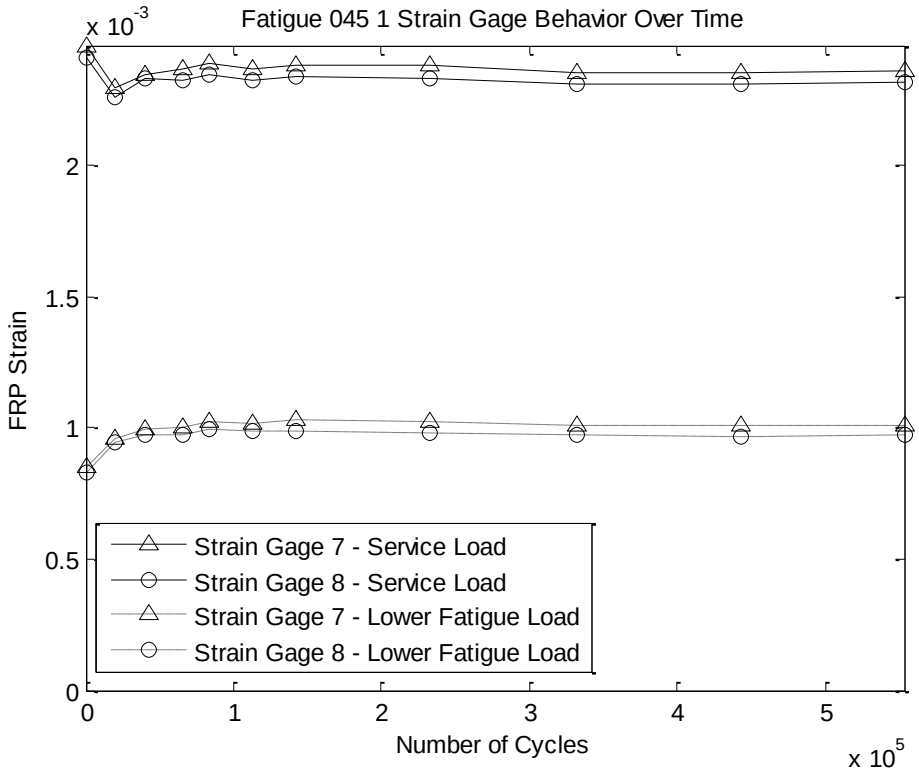

Figure 29: Mid-span FRP Strain Over Time

Fatigue_045_2

Fatigue_045_2, like Fatigue_045_1, experienced rebar fracture during fatigue loading. Only one reinforcing bar in Fatigue_045_2 fractured, as can be seen in Figure 30. It was decided that this beam would be loaded to failure to assess the behavior of the FRP strip. Fatigue_045_2 showed permanent displacement as fatigue cycles increased and relatively no loss of stiffness, as can be seen in Figure 31.

Figure 32 shows the variation of FRP strain based on the distance the gage was from mid-span of the specimen. The vertical line represents the location of the load head. The lower load data is the strain when the load first reaches the lower fatigue value of 24.5kN (5.5kip) during the service tests. It can be observed that there is little change in FRP strain due to fatigue loading. This can also be observed in Figure 33, which shows the strain at strain gages 7 and 8 as a function of elapsed cycles. Similar plots for all gage locations can be found in APPENDIX D.

Figure 30: Fatigue_045_2 Rebar Fracture (Left: Both bars. Right: Close up of Fractured Bar)

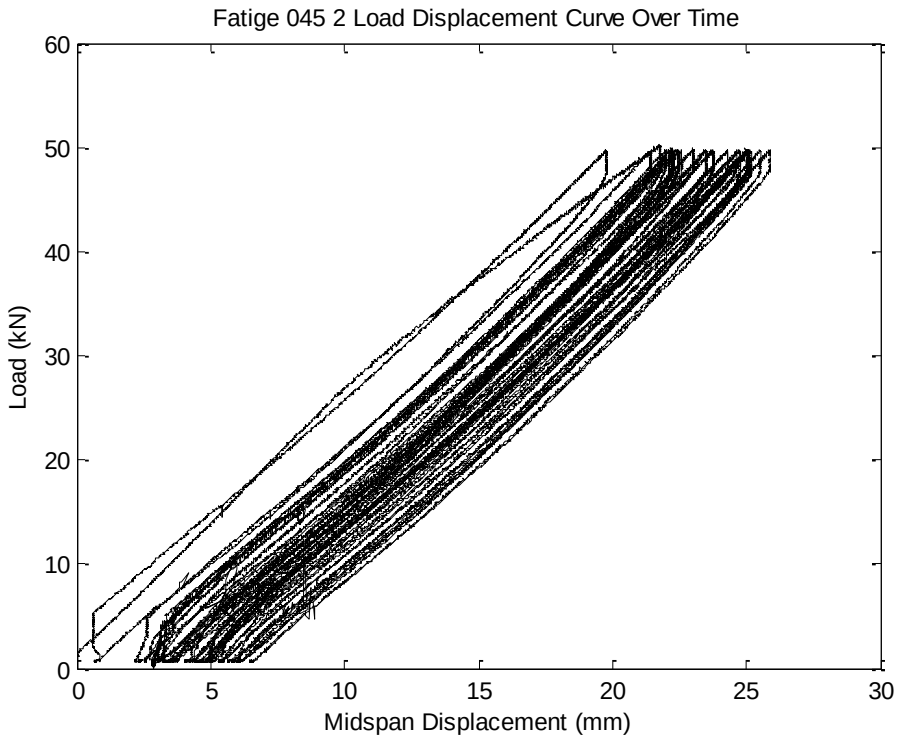

Figure 31: Fatigue_045_2 Service Test Mid-span Displacement Data

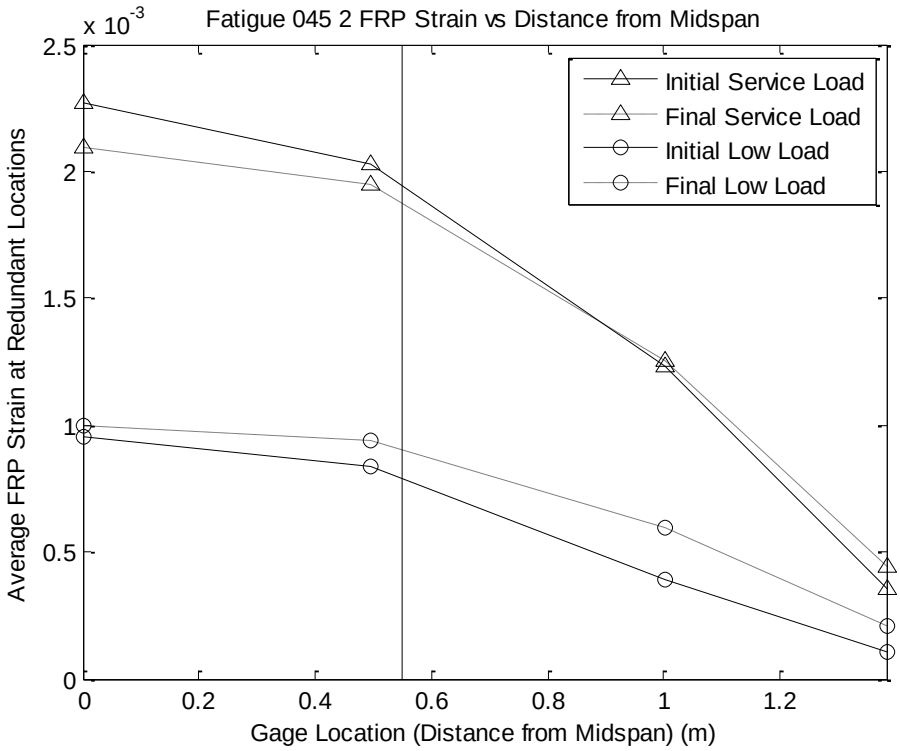

Figure 32: Variation in FRP Strain in Fatigue_045_2

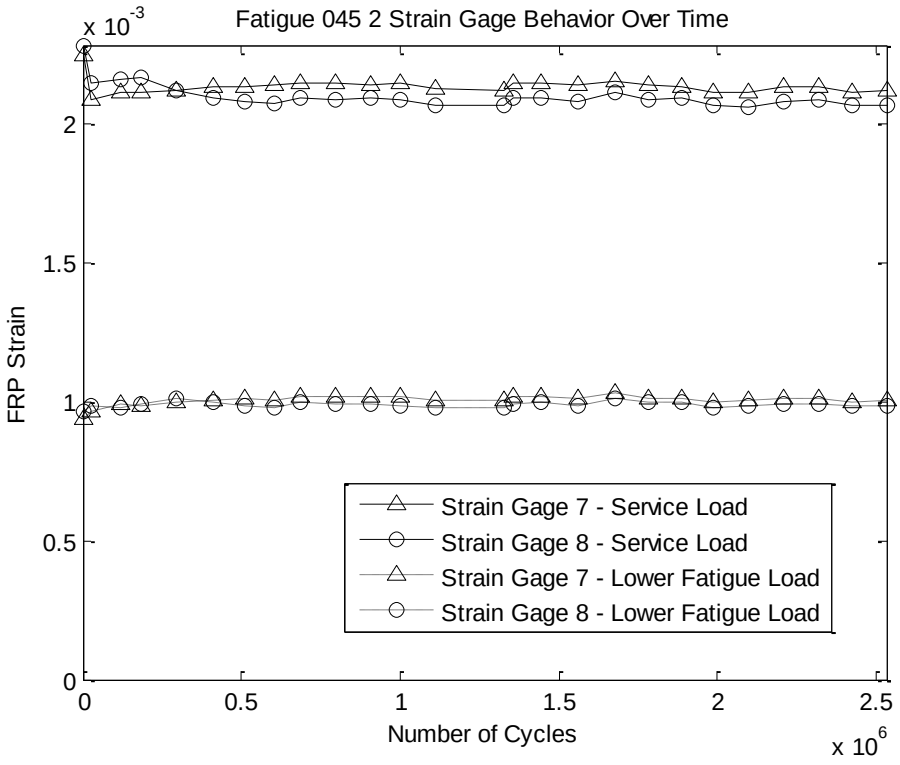

Figure 33: Mid-span FRP Strain Over Time

As previously mentioned, it was determined that Fatigue_045_2 would be tested to failure, despite apparent rebar fracture. The specimen was loaded at a rate of 12.7mm/min (0.5in/min) to failure. This is the same procedure used to conduct the static tests. Breton determined that the average capacity of a specimen reinforced with a GC45 reinforcing strip was 97.0kN (21.8 kip) (Breton, 2013). Fatigue_045_2 reached a capacity of 66.0kN (14.8kip). There is a noticeable drop in load where the stiffness of the system changes, as can be seen in Figure 34. This may be due to anchor bolts failing in shear due to the increased loading of anchors that resulted from rebar failure.

Failure loading produced large flexural cracks at the location of the fractured rebar, as can be seen in Figure 35. Figure 36 shows concrete crushing, which was also present. During failure it was noted that some anchors sheared or withdrew from the concrete, as can be seen in Figure 37. This was attributed to the large deflection seen during failure loading and the large load applied to the anchors.

Figure 34: Fatigue_045_2 Load vs. Center Span Displacement

Figure 35: Flexural Crack Following Failure Loading (West Side of Specimen)

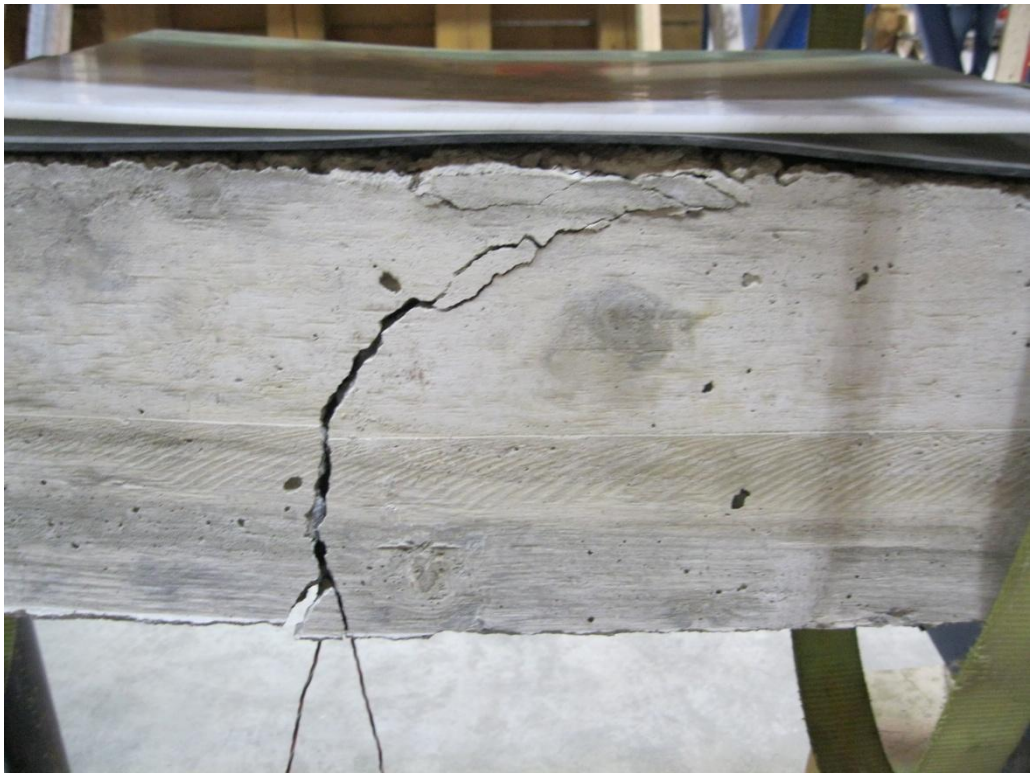

Figure 36: Flexural Crack Following Failure Loading (East Side of Specimen)

Figure 37: Anchor Withdrawal Following Failure Loading

Fatigue_045_3

Fatigue_045_3 also experienced rebar fracture during fatigue loading. Like Fatigue_045_2, only one reinforcing bar in Fatigue_045_3 fractured, shown in Figure 38. It was decided that this beam would also be loaded to failure to assess the behavior of the FRP strip. Fatigue_045_3 showed permanent displacement as fatigue cycles increased. It showed a slight loss of stiffness, as can be seen in Figure 39.

Figure 40 shows the variation of FRP strain based on the distance the gage was from mid-span of the specimen. The vertical line represents the location of the load head. The lower load data is the strain when the load first reaches the lower fatigue value of 24.5kN (5.5kip) during the service tests. It can be observed that there is some change in FRP strain due to fatigue loading over the half span. It can be noted in Figure 41, which shows the strain at strain gages 7 and 8 as a function of elapsed cycles, that there is a steady decline in FRP strain in this specimen. Similar plots for all gage locations can be found in APPENDIX D.

Figure 38: Fatigue_045_3 Rebar Fracture

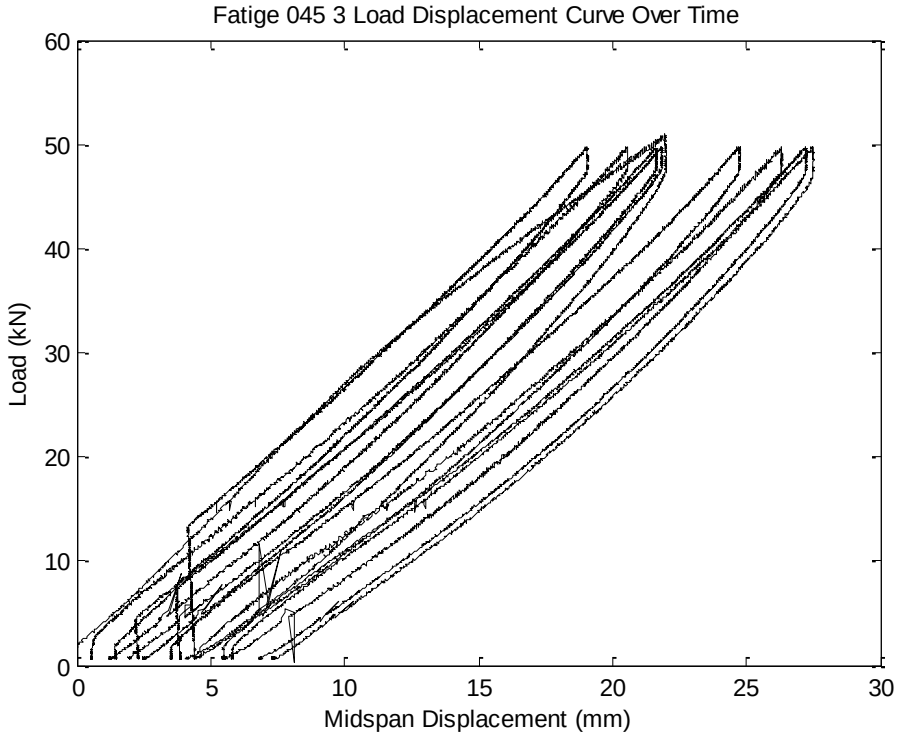

Figure 39: Fatigue_045_3 Service Test Mid-span Displacement Data

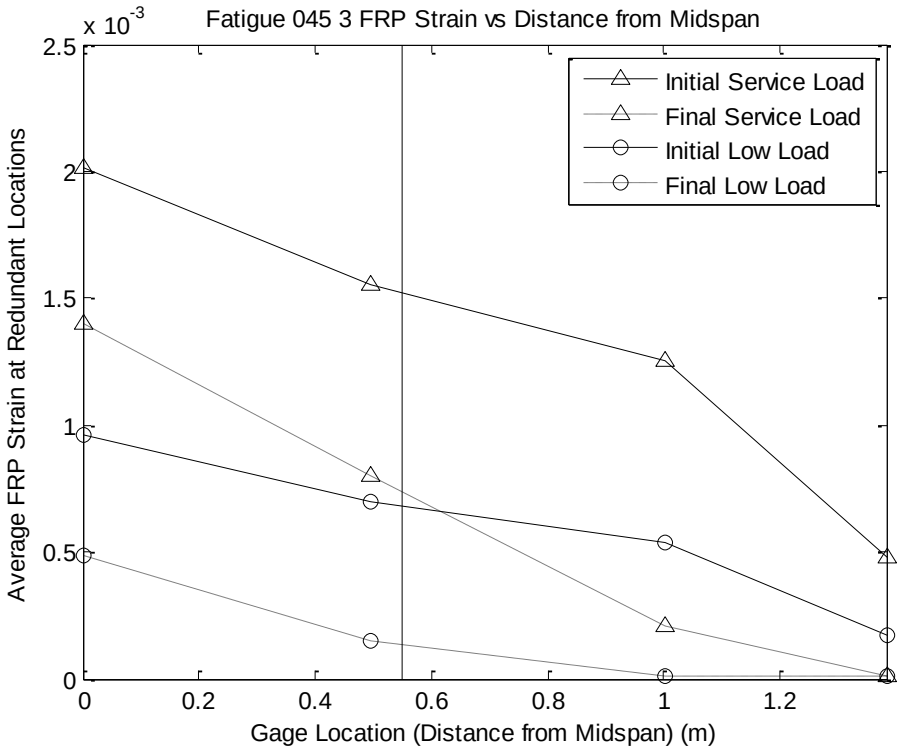

Figure 40: Variation in FRP Strain in Fatigue_045_3

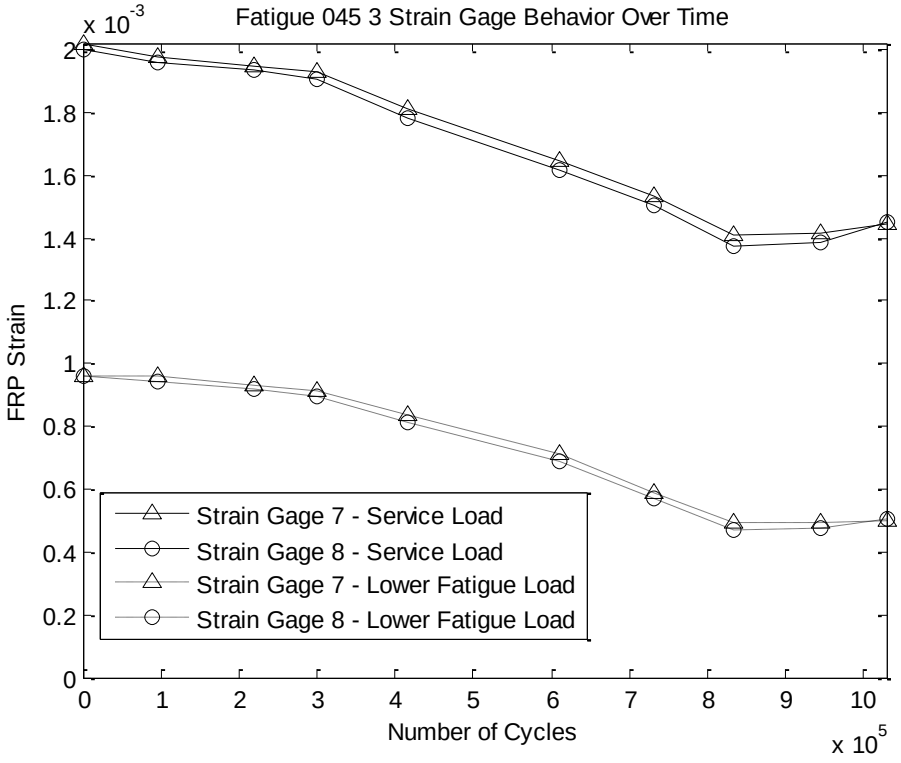

Figure 41: Mid-span FRP Strain Over Time

Fatigue_045_3 was loaded to failure following fatigue cycling. Fatigue cycling was stopped when it became apparent internal reinforcement had been compromised. A large flexural crack was accompanied by permanent deflection that indicated an internal reinforcing bar had fractured. Several FRP anchors were sheared off as well. It isn't known which event occurred first. During failure loading, several large flexural cracks formed and significant concrete crushing was noted. Figure 42 - Figure 44 show the effects of failure loading. Fatigue_045_3 held sustained load throughout the test, as can be seen in Figure 45. The beam could have withstood further loading, but the test was stopped due to the large deflections. These large deflections likely contributed to further anchor shear and FRP bearing. Figure 46 shows the significant damage to the FRP reinforcing strip and the anchor. The capacity of Fatigue_045_3 was 48.6kN (10.9kip).

Figure 42: Fatigue_045_3 Following Failure Loading (West Side of Specimen)

Figure 43: Fatigue_045_3 Following Failure Loading (East Side of Specimen)

Figure 44: Sheared FRP Anchors in Fatigue_045_3 Following Failure Loading

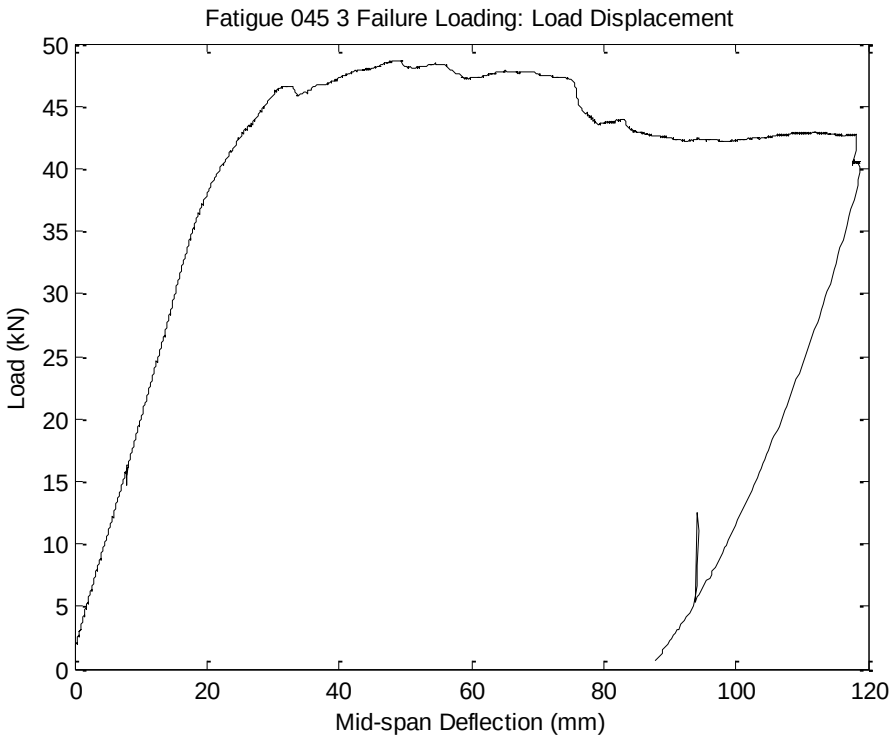

Figure 45: Fatigue_045_3 Load vs. Center Span Displacement

Figure 46: FRP Bearing Following Failure in Fatigue_045_3

Fatigue_090_4

To accurately assess the effects of fatigue loading a beam with intact rebar would need to be loaded to failure following fatigue cycling. The service load (upper load during fatigue cycling) was lowered to 44.5kN (10.0kip) to ensure that rebar fracture would not occur. The 44.5kN (10.0kip) load was determined through data analysis from Fatigue_045_1. Rebar strain from Fatigue_045_1 was used to determine the corresponding stress in the rebar. It was determined that a 44.5kN (10.0kip) produced a rebar fatigue stress range of approximately 165.5MPa (24ksi), AASHTO's limit for infinite fatigue life (American Association of State Highway and Transportation Officials (AASHTO), 2012).

The fatigue loading was stopped after 2 million cycles and the beam was loaded monotonically to failure. While conducting the first static service test, the beam was accidentally loaded to 48.9kN (11.0kip) because the test program had not been changed after Fatigue_045_3. This was corrected for all other service tests.

The stiffness of Fatigue_090_4 was constant throughout the fatigue testing and permanent deflection was observed, as can be seen in Figure 47. A small spike in the data can be seen at the end of each test. The cause of this jump was not found, and during testing there was no visible evidence that the beam was suddenly loaded. It should also be noted that the load and displacement data collected from LabView during the final service test and failure loading was inaccurate. Load and position data directly from the Instron load cell was substituted for these tests.

Strain gage 1 malfunctioned during testing. As a result of this only data from strain gage 2 was used to present results near the support. Figure 48 shows the variation of strain over the half span. Strain at mid-span as a function of cycles can be seen in Figure 49, plots for other gage locations can be found in APPENDIX D. Figure 48 and Figure 49 show the consistency of FRP strain, which changed only slightly as fatigue cycles elapsed. The set of data representing the final service test was gathered during failure loading. The load rate during failure (12.7mm/min (0.5in/min)) was faster than the rate used in service tests. This fact could contribute to the reduced FRP strain during the final serviceability test. However, it is also possible that damage to the FRP or anchors had begun to accumulate, reducing the effectiveness of the FRP reinforcing.

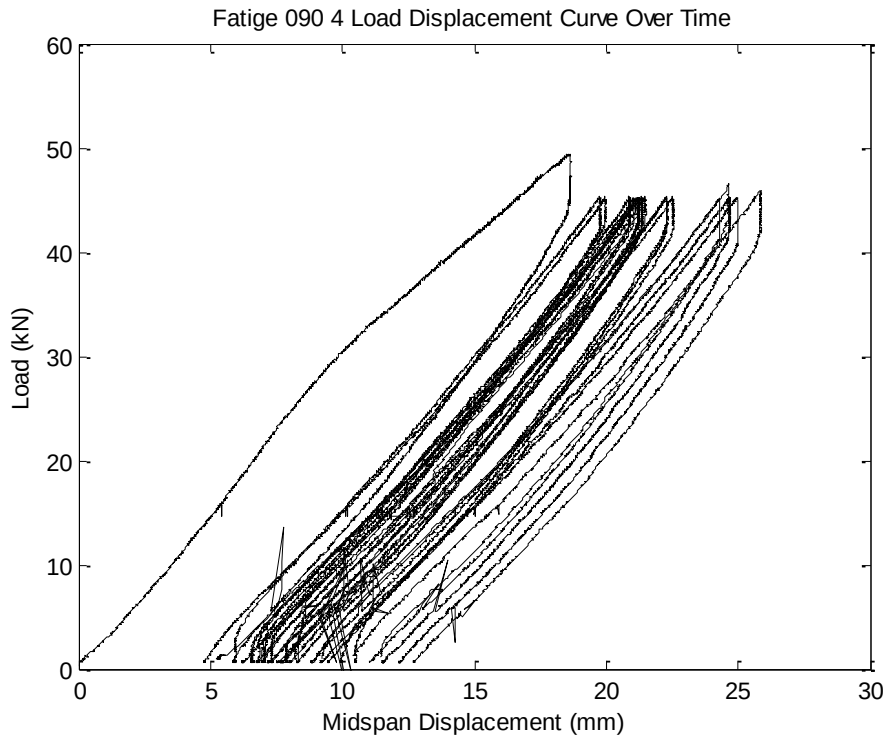

Figure 47: Fatigue_090_4 Service Test Mid-span Displacement Data

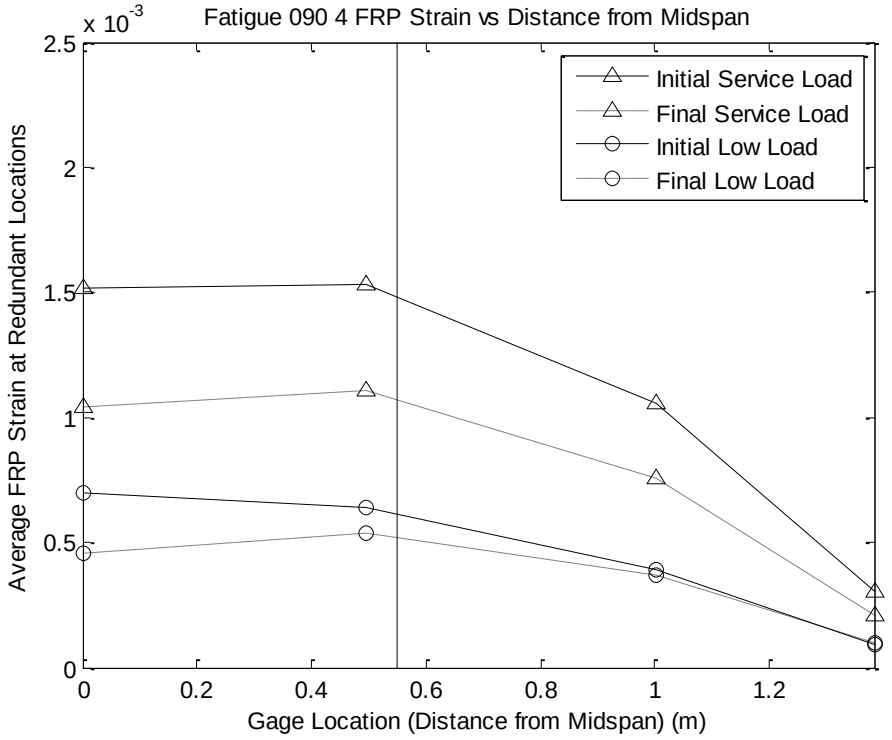

Figure 48: Variation in FRP Strain in Fatigue_090_4

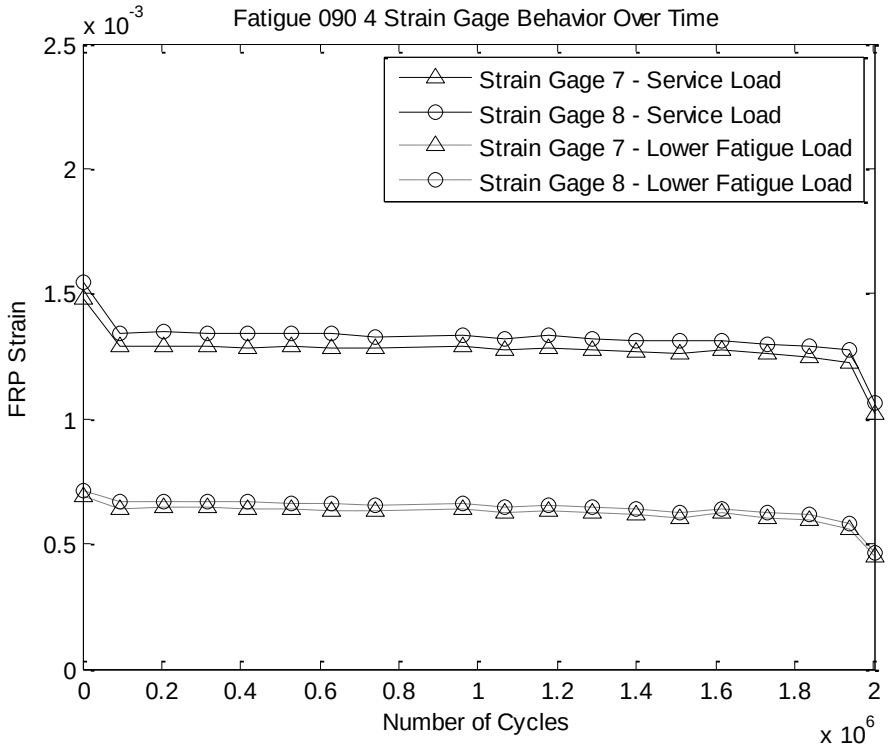

Figure 49: Mid-span FRP Strain Over Time

Fatigue_090_4 was the first beam loaded to failure with two intact steel reinforcing bars. The load-displacement curve, Figure 50, shows a clear yield point of the steel reinforcement. Using the top of knee method used in static testing the yield point was found to be 65kN (14.6kip). The capacity of Fatigue_090_4 was 84.7kN (19.0kip). Unfatigued beams without external reinforcement (control specimens) tested by Breton had an average capacity of 65.9kN (14.8kip) (Breton, 2013). Following fatigue, the GC90 reinforcement increased the capacity of the beam by 28.5% as compared to a beam without external FRP reinforcement that was not subjected to fatigue loading. Unfatigued beams with GC90 reinforcement tested by Breton had an average capacity of 98.5kN (22.1kip) (Breton, 2013). The ultimate capacity of the fatigued specimen was 14.0% less than a beam reinforced with GC90 that was not subjected to fatigue loading. Figure 51 shows the FRP strain over the duration of failure loading; similar plots for all fatigue specimens taken to failure can be seen in Appendix D.

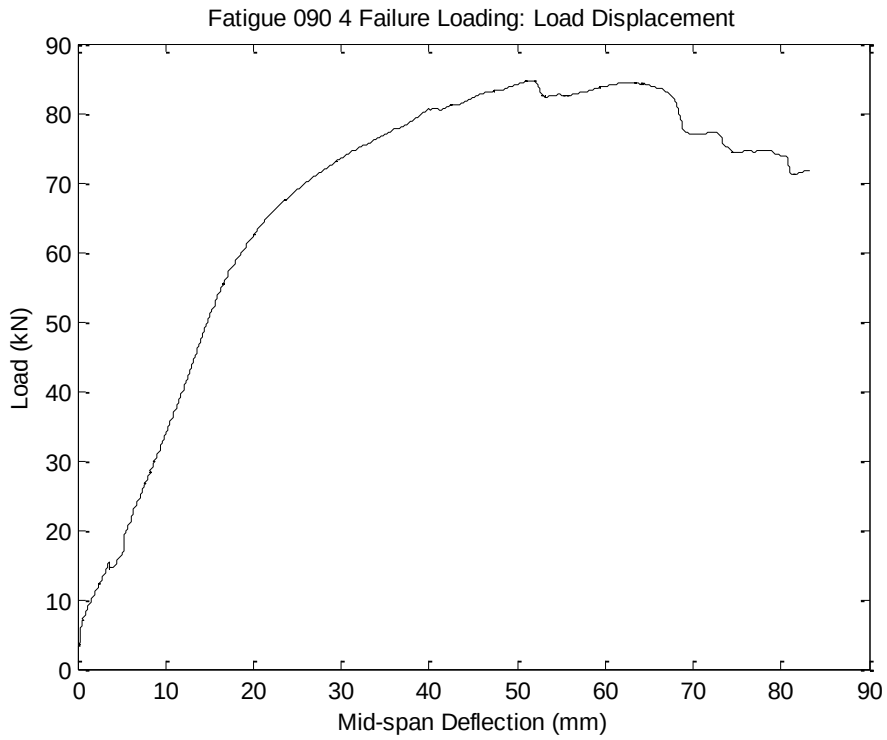

Figure 50: Fatigue_090_4 Load vs. Center Span Displacement

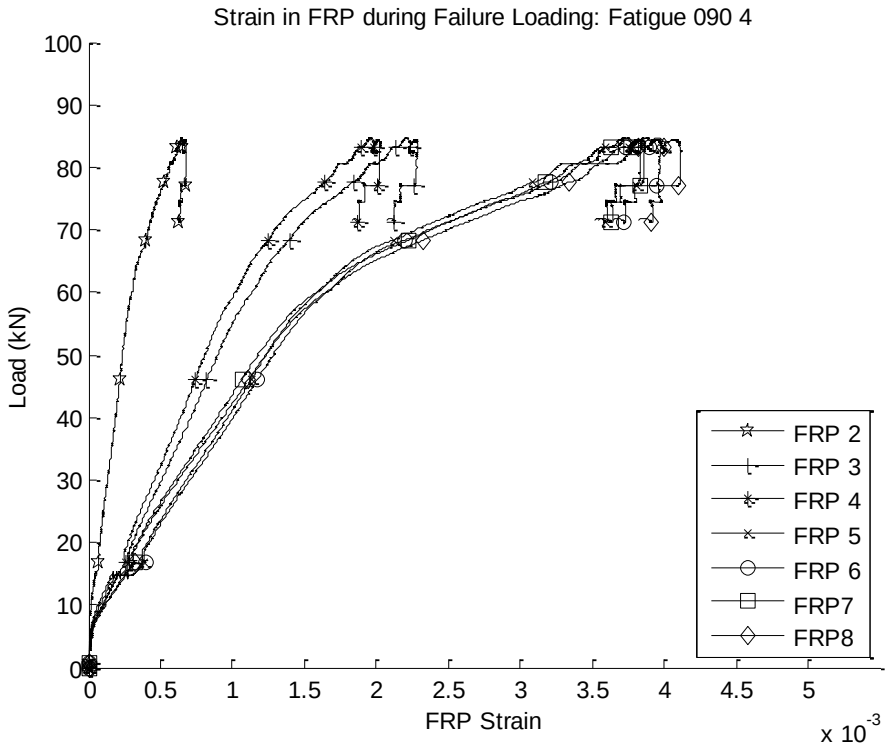

Figure 51: Strain in Fatigue_090_4 over Duration of Failure Loading

Fatigue Beam Comparison

Strain data was used to determine the tensile forces and the average bearing force in the FRP. Tensile and bearing forces were calculated following the same procedure as Breton (Breton, 2013). This was done at three distinct loadings: 1) 24.5kN (5.5kip): the lower load used for fatigue, 2) the service load for the specimen (varied by specimen, refer to Table 19), and 3) the ultimate load from failure loading. FRP tensile forces for Fatigue_045 and Fatigue_090 specimens are presented in Table 21 and Table 23, respectively. The average bearing force applied to the FRP anchors for Fatigue_045 and FRP_090 specimens are presented in Table 22 and Table 24, respectively.

Only one reinforcing bar was instrumented during testing. During failure loading for Fatigue_045_2 the rebar strain data did not register any reading, indicating that it was attached to the rebar that fractured. This also confirmed that the rebar failed prior to failure loading during fatigue. Rebar strain data was collected during failure loading of Fatigue_045_3, indicating that the bar was likely not fractured prior to loading. Conclusions about the other reinforcing bar in Fatigue_045_3 cannot be drawn from the rebar strain data. Figure 52 shows the rebar strain data from failure loading tests where rebar strain data was present.

Table 21: Tensile force in Fatigue_045 Specimens at strain gage locations

	Gage 1&2 kN (kip)	Gage 3&4 kN (kip)	Gage 5&6 kN (kip)	Gage 7&8 kN (kip)
24.5kN (5.5kip) Low Load				
Fatigue_045_1	3.6 (0.8)	14.3 (3.2)	25.9 (5.8)	28.2 (6.3)
Fatigue_045_2	6.0 (1.4)	17.0 (3.8)	26.8 (6.0)	28.4 (6.4)
Fatigue_045_3	0.2 (0.04)	0.2 (0.05)	4.6 (1.0)	14.3 (3.2)
Avg.	3.3 (0.7)	10.5 (2.4)	19.1 (4.3)	23.6 (5.3)
Std.	2.9 (0.7)	9.0 (2.0)	12.6 (2.8)	8.1 (1.8)
COV (%)	90.1	85.8	65.9	34.2
Service Load				
Fatigue_045_1	7.7 (1.7)	34.1 (7.7)	61.5 (13.8)	66.6 (15.0)
Fatigue_045_2	12.6 (2.8)	35.8 (8.1)	55.6 (12.5)	59.7 (13.4)
Fatigue_045_3	0.2 (0.04)	7.1 (1.6)	23.2 (5.2)	41.2 (9.3)
Avg.	6.8 (1.5)	25.7 (5.8)	46.8 (10.5)	55.8 (12.6)
Std.	6.2 (1.4)	16.1 (3.6)	20.6 (4.6)	13.1 (2.9)
COV (%)	91.5	62.8	44.0	23.5
Ultimate Load				
Fatigue_045_1	--	--	--	--
Fatigue_045_2	16.8 (2.8)	84.2 (18.9)	147.0 (33.1)	165.8 (37.3)
Fatigue_045_3	0.8 (0.2)	20.9 (4.7)	62.3 (14.0)	116.5 (26.2)
Avg.	8.8 (2.0)	52.5 (11.8)	104.7 (23.5)	141.2 (31.7)
Std.	11.3 (2.5)	44.7 (10.1)	59.9 (13.5)	34.9 (7.8)
COV (%)	129.2	85.2	57.3	24.7

Table 22: Average bearing force per anchor in Fatigue_045 specimens

	Anchors 2-4 kN (kip)	Anchors 5-8 kN (kip)	Anchors 9-12 kN (kip)
24.5kN (5.5kip) Low Load			
Fatigue_045_1	2.7 (0.6)	2.9 (0.7)	0.8 (0.2)
Fatigue_045_2	2.8 (0.6)	2.4 (0.5)	0.5 (0.1)
Fatigue_045_3	0.01 (0.002)	1.1 (0.2)	3.2 (0.7)
Avg.	1.8 (0.4)	2.1 (0.5)	1.5 (0.3)
Std.	1.6 (0.4)	0.9 (0.2)	1.5 (0.3)
COV (%)	86.1	44.0	99.7
Service Load			
Fatigue_045_1	6.6 (1.5)	6.8 (1.5)	1.7 (0.4)
Fatigue_045_2	5.8 (1.3)	4.9 (1.1)	1.4 (0.3)
Fatigue_045_3	1.7 (0.4)	4.0 (0.9)	6.0 (1.3)
Avg.	4.7 (1.1)	5.3 (1.2)	3.0 (0.7)
Std.	2.6 (0.6)	1.4 (0.3)	2.6 (0.6)
COV (%)	55.6	27.1	85.7
Ultimate Load			
Fatigue_045_1	--	--	--
Fatigue_045_2	16.8 (3.8)	15.7 (3.5)	6.3 (1.4)
Fatigue_045_3	5.0 (1.1)	10.3 (2.3)	18.1 (4.1)
Avg.	10.9 (2.5)	13.0 (2.9)	12.2 (2.7)
Std.	8.4 (1.9)	2.8 (0.9)	8.3 (1.9)
COV (%)	76.4	29.2	68.6

Table 23: Tensile force in Fatigue_090 Specimen at strain gage locations

	Gage 1&2 kN (kip)	Gage 3&4 kN (kip)	Gage 5&6 kN (kip)	Gage 7&8 kN (kip)
24.5kN (5.5kip) Low Load				
Fatigue_090_4	3.7 (0.8)	13.7 (3.1)	19.8 (4.4)	16.9 (3.8)
Service Load				
Fatigue_090_4	7.8 (1.8)	27.9 (6.3)	41.0 (9.2)	38.6 (8.7)
Ultimate Load				
Fatigue_090_4	22.5 (5.1)	73.2 (16.4)	133.0 (29.9)	135.4 (30.4)

Table 24: Average bearing force per anchor in Fatigue_090 specimen

	Anchors 2-4 kN (kip)	Anchors 5-8 kN (kip)	Anchors 9-12 kN (kip)
24.5kN (5.5kip) Low Load			
Fatigue_090_4	2.5 (0.6)	1.5 (0.3)	-1.0 (-0.2)*
Service Load			
Fatigue_090_4	5.0 (1.1)	3.3 (0.7)	-0.8 (-0.1)*
Ultimate Load			
Fatigue_090_4	12.7 (2.8)	15.0 (3.4)	0.8 (0.2)

* Negative difference between FRP strain is assumed to result in zero bearing force at the anchor. Value excluded from avg., std. and COV calculations

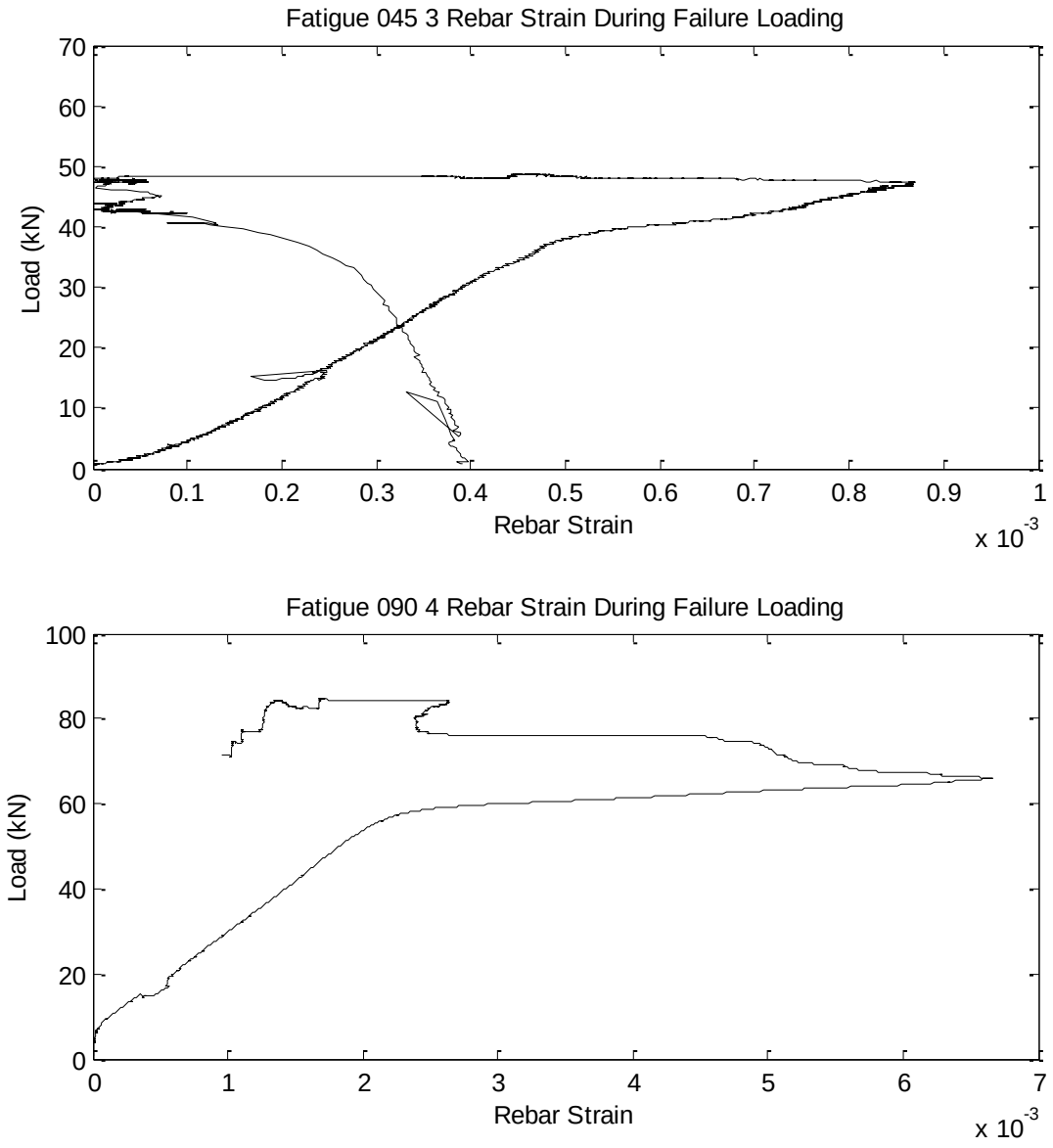

Figure 52: Rebar Strain during Failure Loading

Summary and Conclusions

To assess the viability of the MF-FRP reinforcing systems for bridge applications fatigue testing was performed. Beam specimens were subjected to an initial loading sequence to produce flexural cracks and develop service level strain in the rebar. The beams were then externally reinforced with either GC45 or GC90 reinforcing strips. Beams were then loaded in a fatigue cycle designed to simulate the life span of the structure. The first three specimens all failed due to rebar fracture during fatigue. Two of those specimens were then loaded to failure, although conclusions about the full effects of fatigue couldn't be drawn from these beams due to the rebar

fractures that occurred during fatigue testing. The final specimen did not experience rebar fracture during fatigue testing, and was tested to failure after 2,000,000 cycles of loading that produced a rebar stress corresponding to the AASHTO upper limit for an infinite fatigue life. The beam showed a 28.5% increase in strength as compared to an un-fatigued, unreinforced beam, but a 14.0% decrease in strength as compared to an un-fatigued beam reinforced with a GC90 reinforcing strip.

All fatigue specimens demonstrated permanent deflection throughout the fatigue process. The stiffness of the beams remained relatively unchanged throughout fatigue. Prior to rebar fracture in the three beams that exhibited rebar fracture, there was no sign of FRP damage. This, combined with the strength gains shown in the fourth fatigue specimen, indicate that both the GC45 and GC90 reinforcing systems performed reasonably well under fatigue loading. However, rebar fatigue stress is clearly a design consideration that may limit the amount of strength gain that can be achieved with mechanically fastened FRP flexural reinforcing. Further, given that only one specimen was tested to a large number of load cycles without experiencing rebar fracture, definite conclusions regarding the fatigue performance of the mechanically fastened FRP used in this study cannot be drawn.

Works Cited

3M. (2011, June). *3M VHB(TM) Tapes.* Retrieved 2012, from 3M in the United States: solution.3m.com

ACI - Committee 318. (2008). *Building code requirements for structural concrete (ACI 318-08) and commentary.* American Concrete Institute.

ACI - Committee 440. (2008). *Guide for the design and construction of externally bonded FRP systems for strengthening concrete structures.* Farmington Hills, MI, USA: American Concrete Institute.

ACI - Committee 440. (2011). *Guide of accelerated conditioning protocols for durability of internal and external fiber reinforced polymer (FRP) reinforcement for concrete.* Farmington Hills, MI, USA: American Concerete Institue.

American Association of State Highway and Transportation Officials (AASHTO). (2012). *Guide specifications for design of bonded FRP systems for repair and strengthening of concrete bridge elements.* Washington, DC: American Association of State Highway and Transportation Officials.

ASTM. (2012). ASTM A370 Standard Test Methods and Definitions for Mechanical Testing of Steel Products. West Conshohocken, Pa: ASTM International.

ASTM. (2011). ASTM C1645 Standard Test Method for Freeze-thaw and De-icing Salt Durability of Solid concrete Interlocking Paving Units. West Conshohocken, PA: ASTM International.

ASTM. (2008). ASTM D3039 Standard Test Method for Tensile Properties of Polymer Matrix Composite Materials. West Conshohocken, PA: ASTM International.

Borowicz, D. (2002). Rapid Strengthening of Concrete Beams with Powder-Actuated Fastening Systems and Fiber Reinforced Polymer (FRP) Composite Materials. *Masters' Thesis* . Madison, WI: University of Wisconsin.

Breton, H. (2013). Mechanically Fastened Fiber-Reinforced Polymer (FRP) Flexural Retrofit Systems for Reinforced Concrete Flat-Slab Bridges. *Masters' Thesis* . Orono, ME: University of Maine.

Breton, H., & Davids, W. (2012). *Bridge Safety Project, Task 4 (Deliverable 2): FRP Flexural Retrofit Durability Testing Plan.* Orono: University of Maine.

Breton, H., & Davids, W. (2013). *Bridge Safety Project, Task 4 (Deliverable 3): Small Beam Bend Tests.* Orono: University of Maine.

Breton, H., & Davids, W. (2013). *Bridge Safety Project, Task 4 (Deliverable 4): FRP Flexural Retrofit Environmental Durability Testing and Analysis.* Orono: University of Maine.

HILTI. (2012, June). *Anchor Fastening Technical Guide.* Retrieved July 2012, from Hilti Online: http://www.us.hilti.com/fstore/holus/techlib/docs/3.2.3_HIT-HY150_MAX-SD_p60-90r30_1.pdf

Poulin, T. (2012). Development of Improved Analytical Load Ratin Procedures for Flat-Slab Concrete Bridges. *Masters' Thesis* . Orono, ME: University of Maine.

Richie, M. (2003). Fatigue Behavior of FRP-Reinforced Douglas-Fir Glued Laminated Bridge Girders. *Masters' Thesis* . Orono, ME: University of Maine.

APPENDIX A: Durability Specimen Load-deformation Plots

GG90 Durability Specimen Average Peak Sustained Load Plots

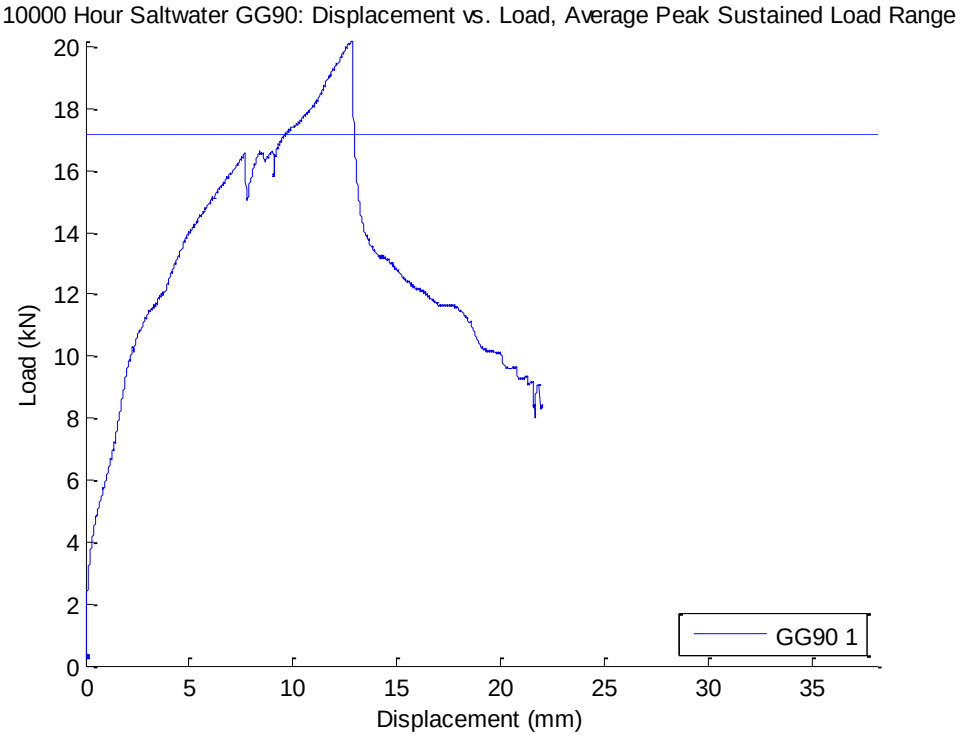

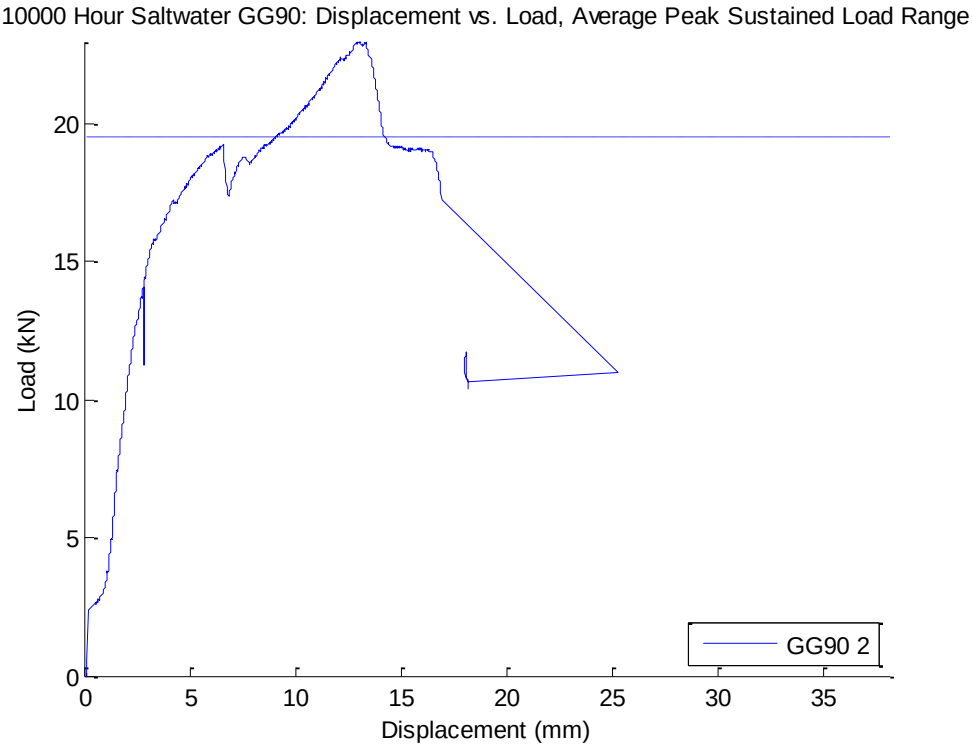

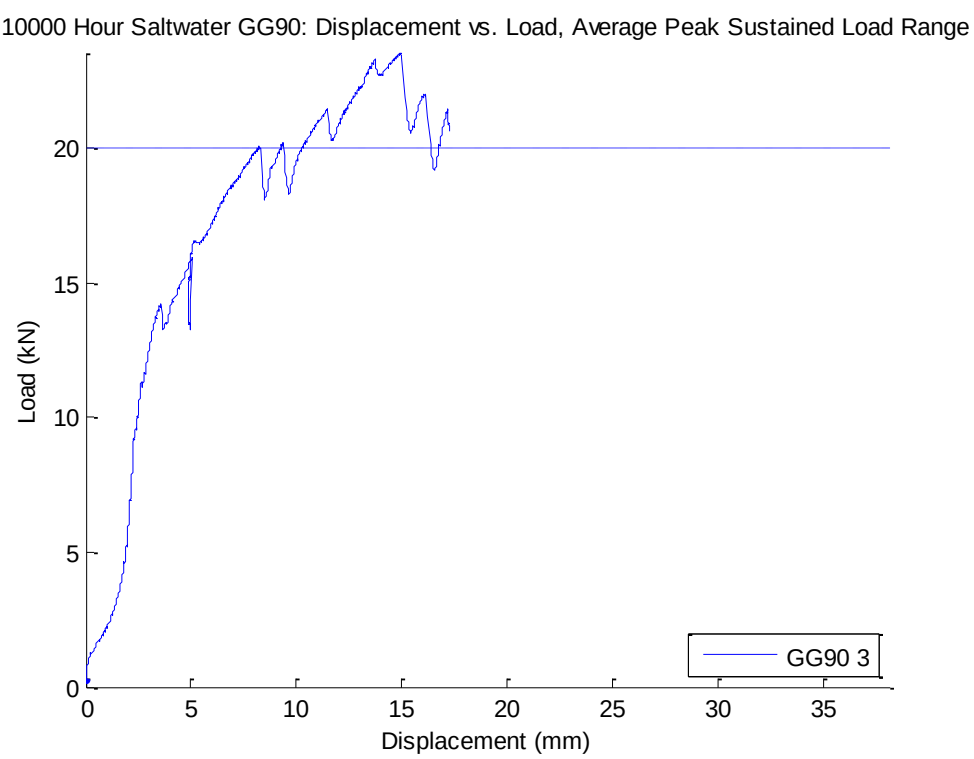
10000 Hour Saltwater GG90: Displacement vs. Load, Average Peak Sustained Load Range
Load (kN)
Displacement (mm)
GG90 3
0
5
10
15
20
25
30
35

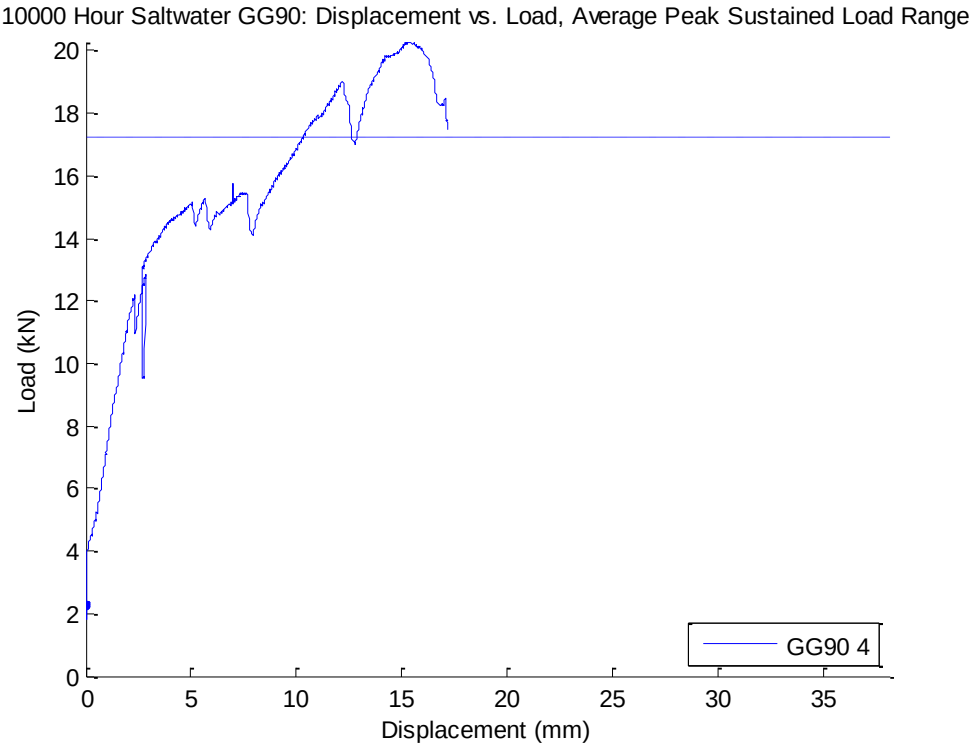
10000 Hour Saltwater GG90: Displacement vs. Load, Average Peak Sustained Load Range
Load (kN)
Displacement (mm)
GG90 4
0
2
4
6
8
10
12
14
16
18
20
25
30
35

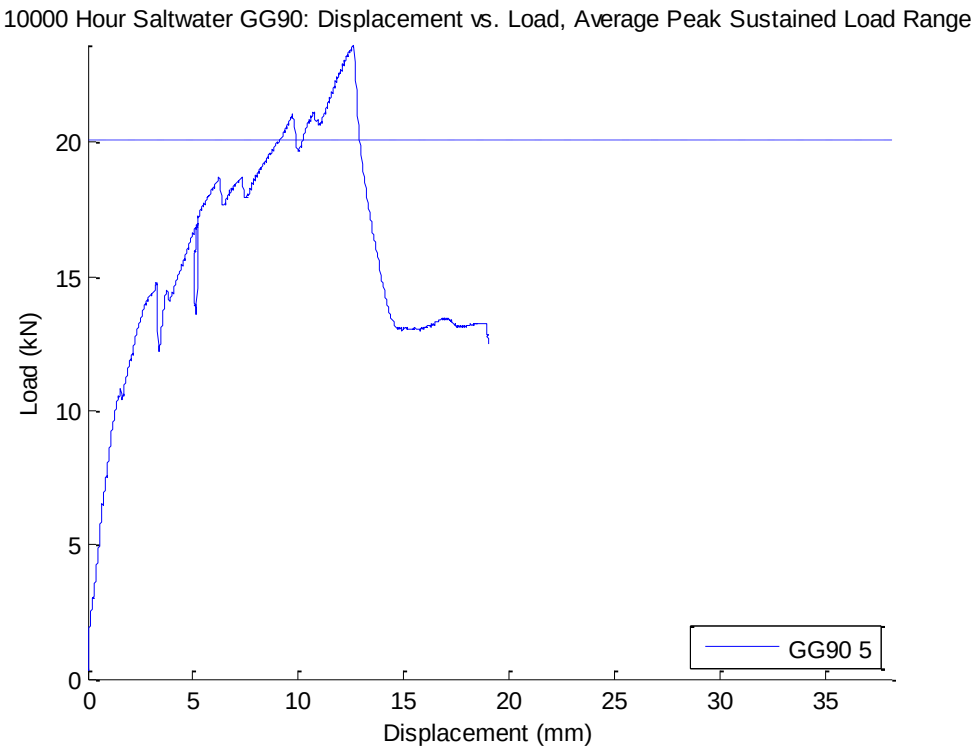
10000 Hour Saltwater GG90: Displacement vs. Load, Average Peak Sustained Load Range
Load (kN)
Displacement (mm)
0
5
10
15
20
25
30
35
GG90 5

GG45 Durability Specimen Average Peak Sustained Load Plots

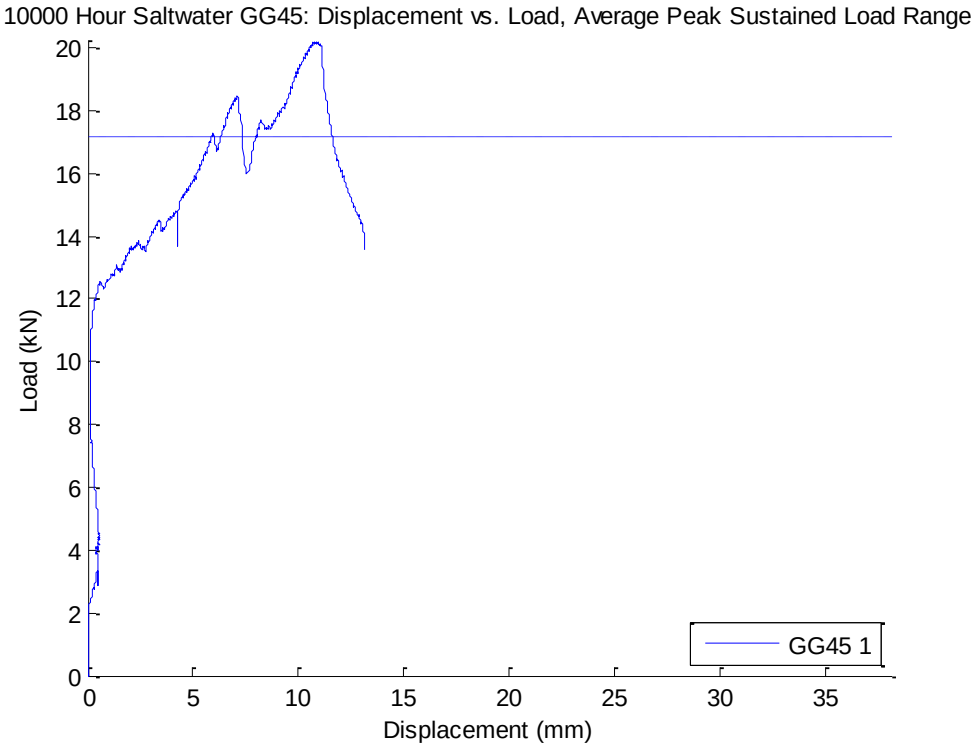

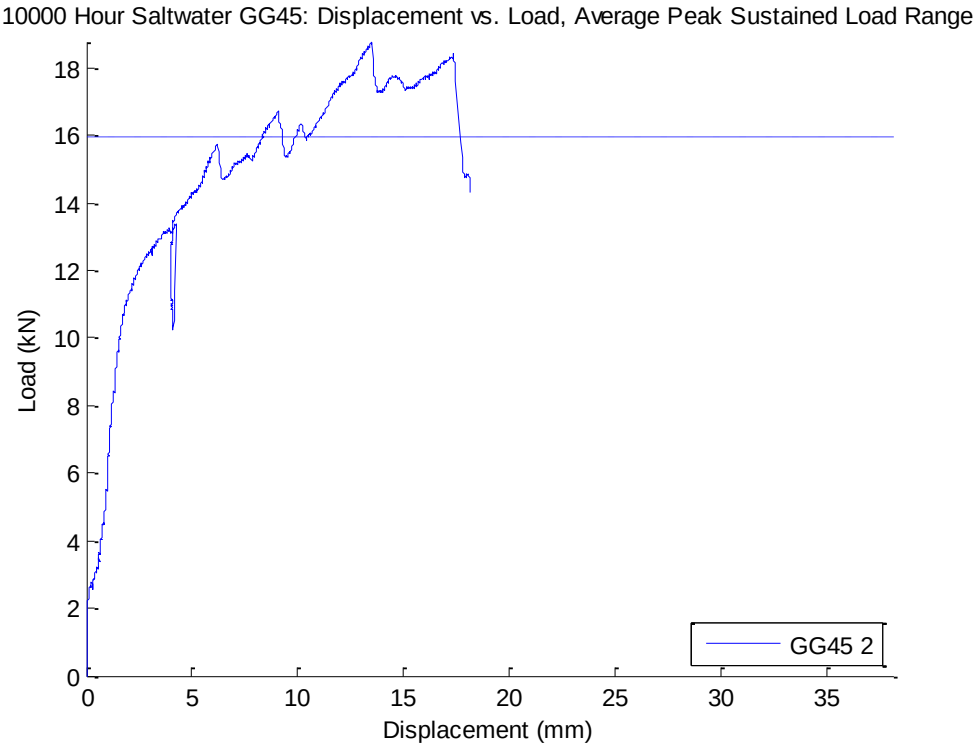

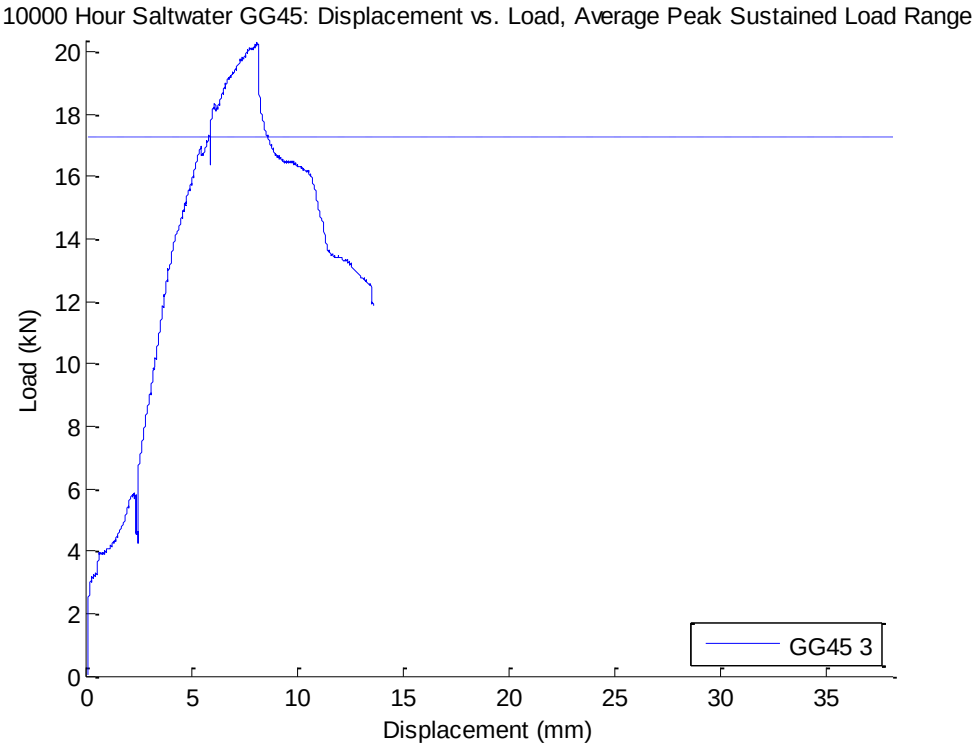
10000 Hour Saltwater GG45: Displacement vs. Load, Average Peak Sustained Load Range
Load (kN)
Displacement (mm)
GG45 3

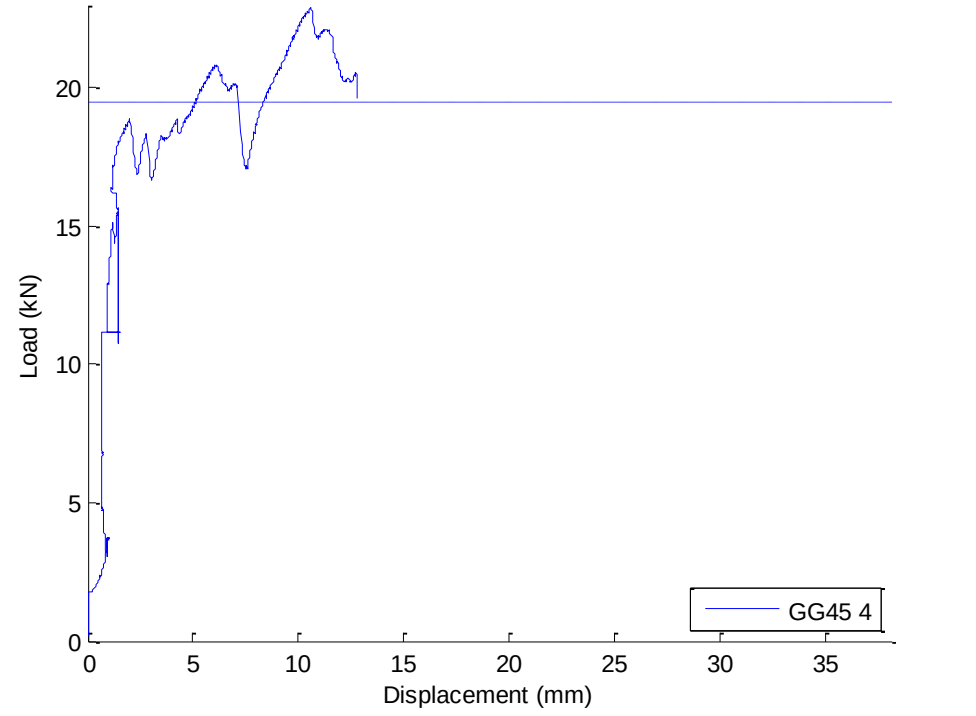
10000 Hour Saltwater GG45: Displacement vs. Load, Average Peak Sustained Load Range
Load (kN)
Displacement (mm)
GG45 4

GC90 Durability Specimen Average Peak Sustained Load Plots

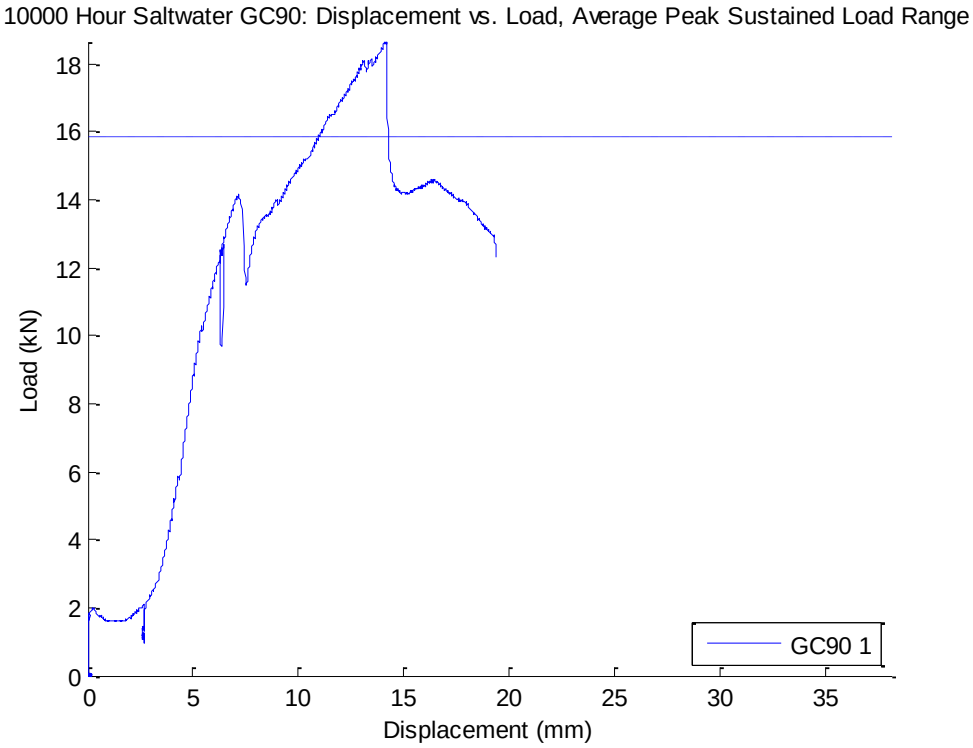

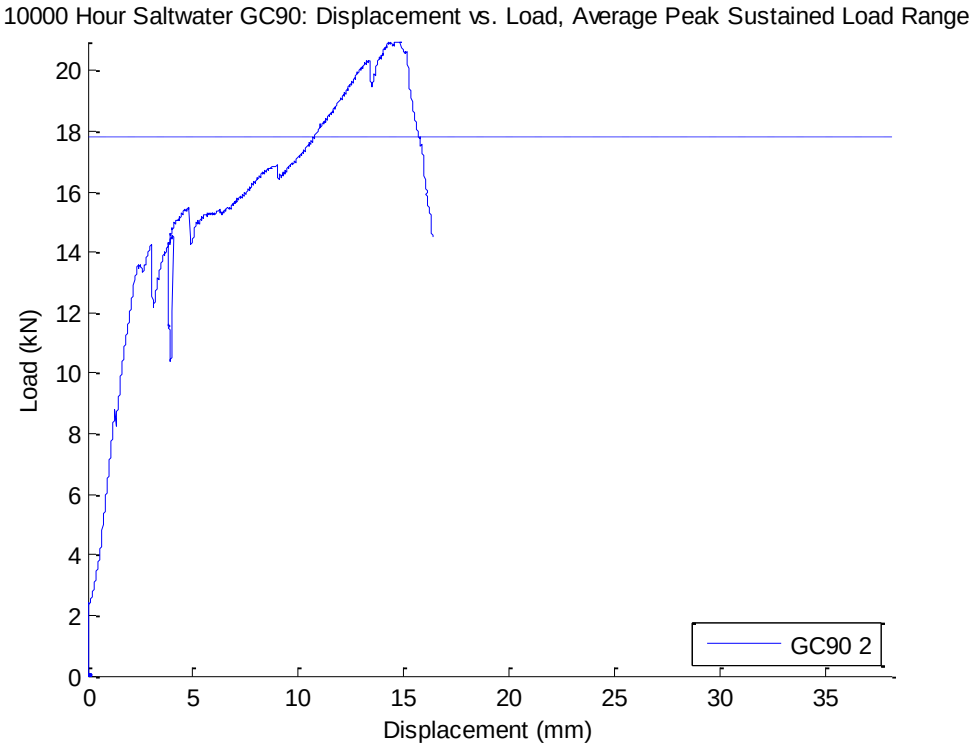

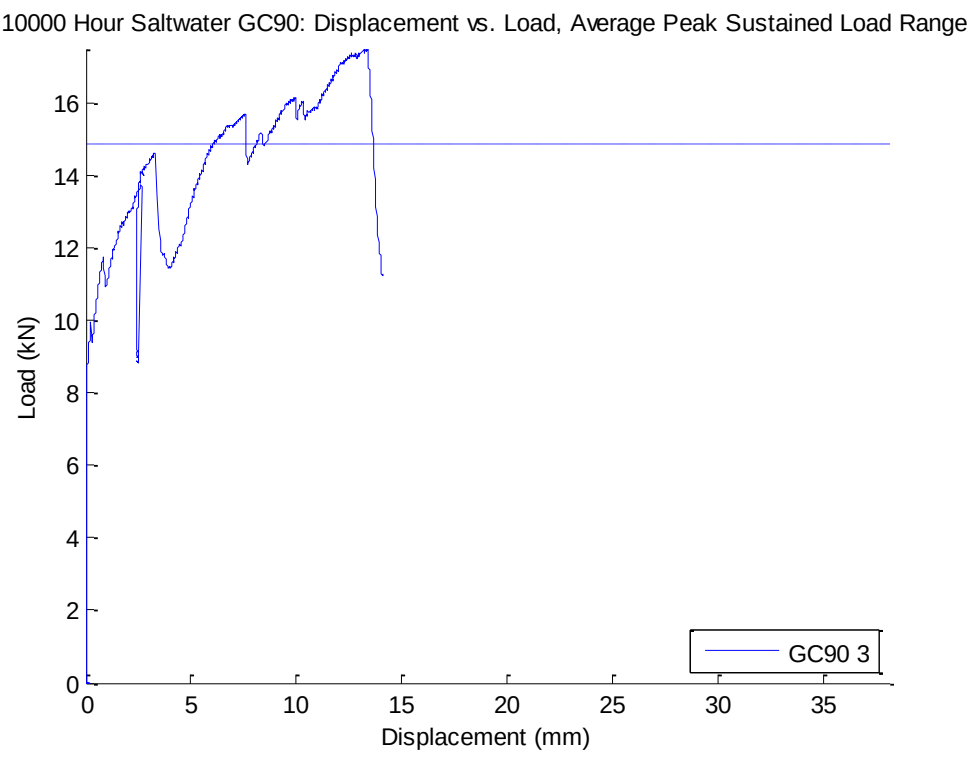
10000 Hour Saltwater GC90: Displacement vs. Load, Average Peak Sustained Load Range
Load (kN)
Displacement (mm)
GC90 3
0
2
4
6
8
10
12
14
16
0
5
10
15
20
25
30
35

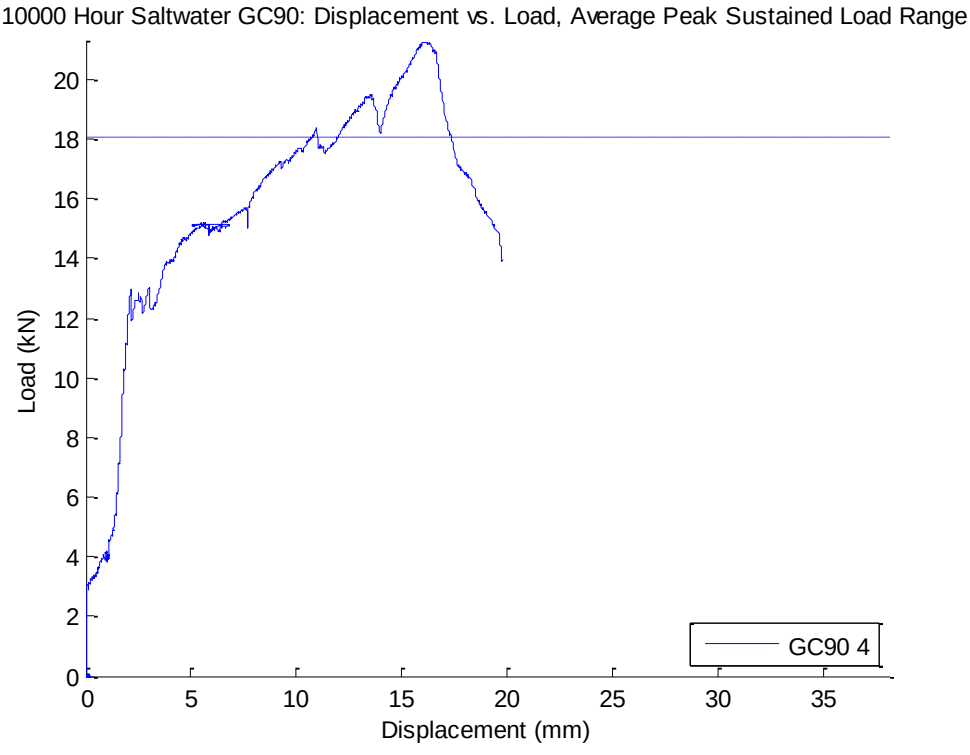
10000 Hour Saltwater GC90: Displacement vs. Load, Average Peak Sustained Load Range
Load (kN)
Displacement (mm)
GC90 4
0
2
4
6
8
10
12
14
16
18
20
0
5
10
15
20
25
30
35

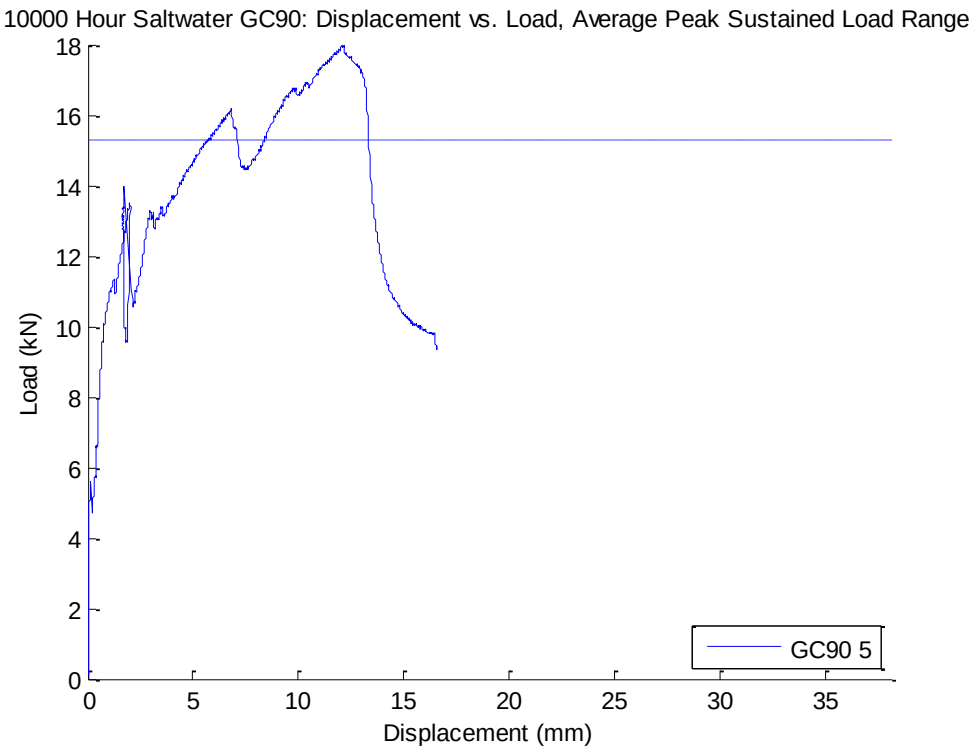
10000 Hour Saltwater GC90: Displacement vs. Load, Average Peak Sustained Load Range
Load (kN)
Displacement (mm)
GC90 5
0
2
4
6
8
10
12
14
16
18
0
5
10
15
20
25
30
35

GC45 Durability Specimen Average Peak Sustained Load Plots

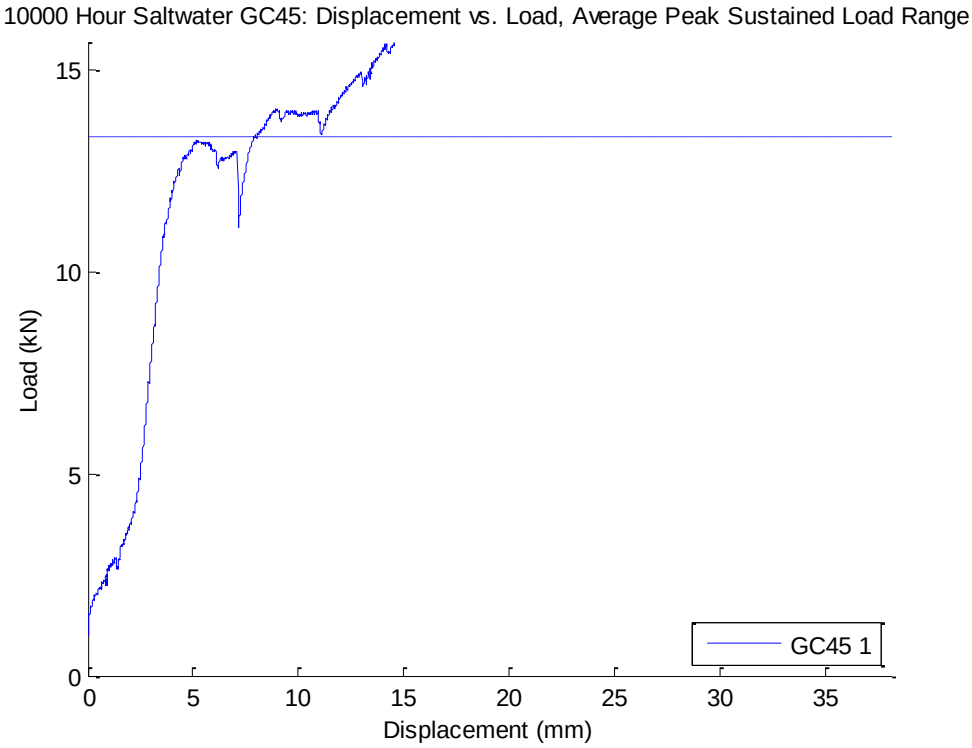

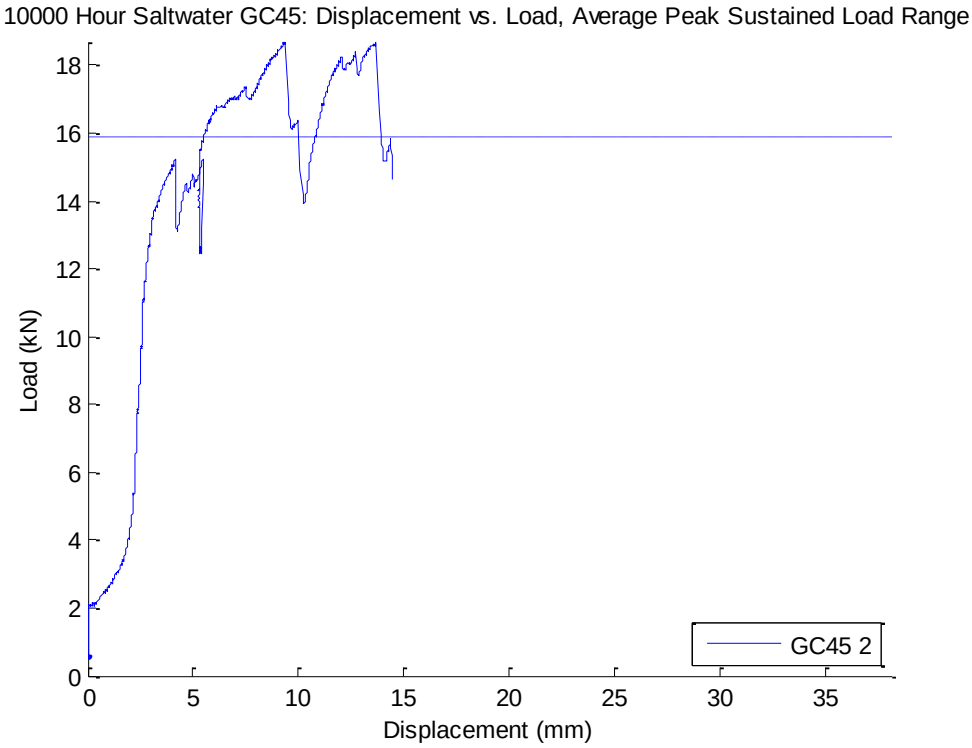

10000 Hour Saltwater GC45: Displacement vs. Load, Average Peak Sustained Load Range

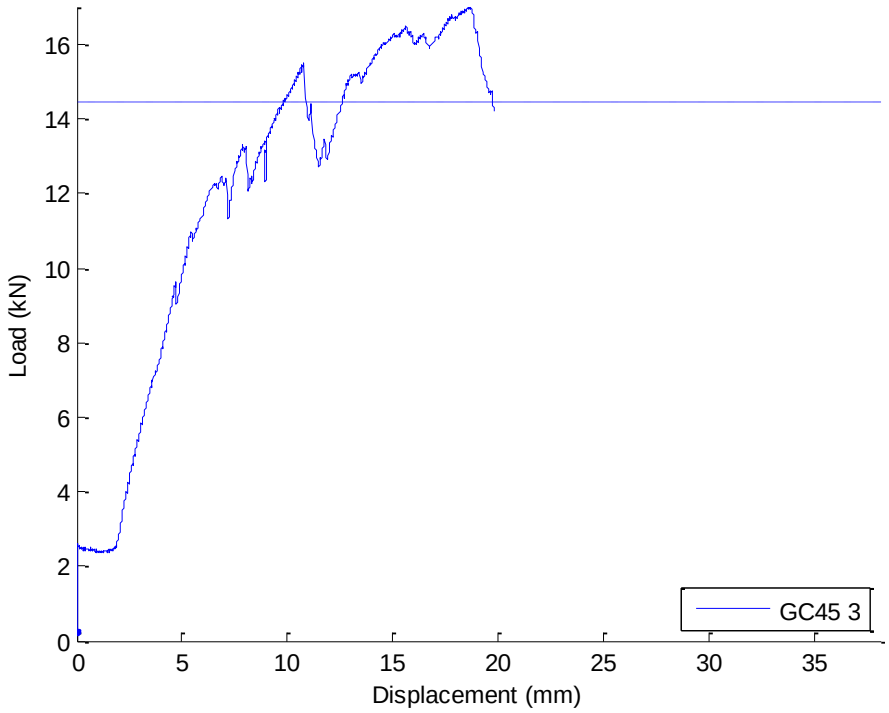

10000 Hour Saltwater GC45: Displacement vs. Load, Average Peak Sustained Load Range

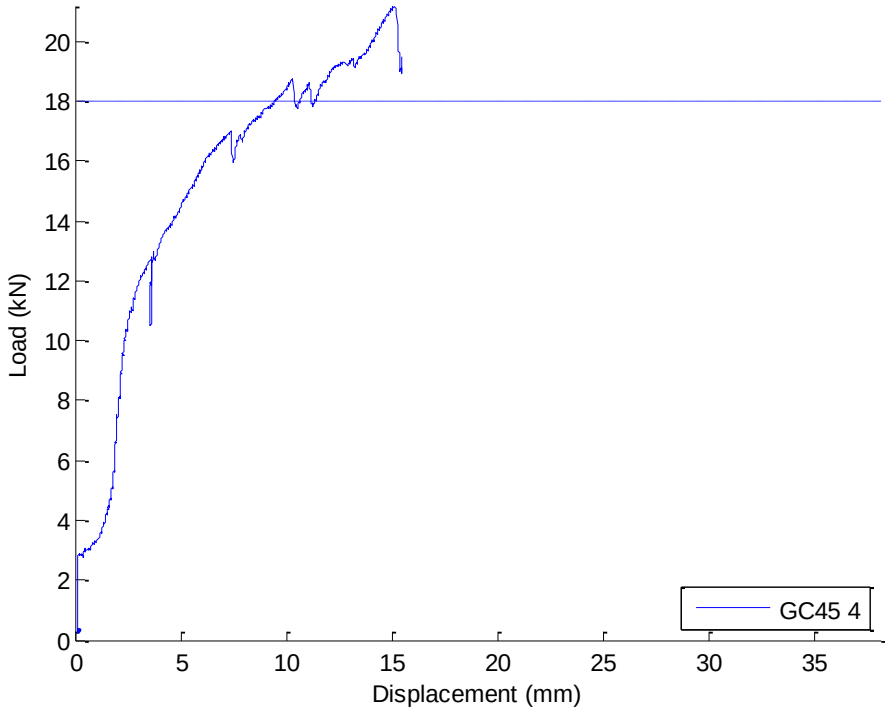

APPENDIX B: Small Beam Flexural Capacities

Anticipated Capacity of Non-Strengthened Beam Specimens

Beam span (center-line to center-line of support) $L := 11ft$

Beam width $b := 12in$

Beam depth $h := 8in$

Concrete compressive strength $f'c := 4100psi$

$\psi_f := 1$

$C_E := 1$

$\phi := 1$

$$\beta_1 := 1.05 - 0.05\frac{f'c}{1000psi} = 0.85$$

Concrete MoE $$Ec := 57000psi\sqrt{\frac{f'c}{psi}} = 3650ksi$$

Steel yield strength $fy := 40ksi$

Steel MoE $Es := 29000ksi$

Reinforcement clear cover $clr := 1.5in$

Depth to reinforcement $d := h - clr = 6.5in$

Area of reinforcing steel (2 #5 bars) $As := 0.62in^2$

Distributed dead weight of beam $w_D := 150pcf \cdot b \cdot h = 100plf$

Dead load moment $$M_D := \frac{w_D \cdot L^2}{8} = 1.5kip \cdot ft$$

Cracking Moment Load:

Rupture stress $$fr := 6psi \cdot \sqrt{\frac{f'c}{psi}} = 384psi$$

Modular ratio $$n_s := \frac{Es}{Ec} = 7.946$$

Transformed steel area $$As_n := (n_s - 1) \cdot As = 4.3in^2$$

Neutral axis $$y := \frac{b \cdot h \cdot \frac{h}{2} + As_n \cdot clr}{b \cdot h + As_n} = 3.9in$$

Moment of Inertia $$I := \frac{b \cdot h^3}{12} + b \cdot h \cdot \left(\frac{h}{2} - y\right)^2 + As_n \cdot (y - clr)^2 = 538in^4$$

Cracking moment $$Mcr := \frac{fr \cdot I}{y} = 4.4kip \cdot ft$$

Actuator load required in 4-point bend to produce Mcr (less the amount of moment caused by dead weight of the beam)

$$Pcr := 2\cdot\left(Mcr - M_D\right)\cdot\frac{3}{L} = 1.6\,kip$$

Service Load:

Given

$$y_{cr} := 1in$$

$$0 = b\cdot\left(d - y_{cr}\right)\cdot\frac{\left(d - y_{cr}\right)}{2} - n_s\cdot As\cdot y_{cr}$$

$$y_{cr} := Find\left(y_{cr}\right) = 4.564in$$

Depth of uncracked concrete

$$c := d - y_{cr} = 1.936in$$

Cracked moment of inertia

$$I_{cr} := \frac{b\cdot c^3}{12} + b\cdot c\cdot\left(\frac{c}{2}\right)^2 + n_s\cdot As\cdot y_{cr}^2 = 131.6in^4$$

Concrete elastic limit

$$fc := 0.45\,f'c = 1845psi$$

Service Moment

$$Ms := \frac{fc\cdot I_{cr}}{c} = 10.5\,kip\cdot ft$$

Actuator load required in 4-point bend to produce Ms (less the amount of moment caused by dead weight of the beam)

$$Ps := 2\cdot\left(Ms - M_D\right)\frac{3}{L} = 4.9\,kip$$

Failure Load:

Depth of stress block

$$a := \frac{As\cdot fy}{0.85\,f'c\cdot b} = 0.593in$$

Nominal moment capacity

$$Mn := As\cdot fy\cdot\left(d - \frac{a}{2}\right) = 12.8\,kip\cdot ft$$

Actuator load required in 4-point bend test

$$P := 2\cdot\left(Mn - M_D\right)\cdot\frac{3}{L} = 6.2\,kip$$

Service modulus of rupture

$$fr := 7.5\sqrt{\frac{f'c}{psi}}\cdot psi = 480.2psi$$

Service cracking moment

$$Mcr_s := \frac{fr\cdot b\cdot h^3}{12}\cdot\frac{2}{h} = 5.1\,kip\cdot ft$$

Effective moment of inertia

$$Ie := \min\left[\left(\frac{Mcr_s}{Mn}\right)^3\cdot\frac{b\cdot h^3}{12} + \left[1 - \left(\frac{Mcr_s}{Mn}\right)^3\right]\cdot I_{cr}, \frac{b\cdot h^3}{12}\right] = 155.9in^4$$

Anticipated Capacity of GC90-Strengthened Beam Specimens

Actuator load required in 4-point bend to produce Mcr (less the amount of moment caused by dead weight of the beam)

$$Pcr := 2\cdot\left(Mcr - M_D\right)\cdot\frac{3}{L} = 1.6\,kip$$

Service Load:

Given

$$y_{cr} := 1in$$

$$0 = b\cdot\left(d - y_{cr}\right)\cdot\frac{\left(d - y_{cr}\right)}{2} - n_s\cdot As\cdot y_{cr}$$

$$y_{cr} := Find\left(y_{cr}\right) = 4.564in$$

Depth of uncracked concrete

$$c := d - y_{cr} = 1.936in$$

Cracked moment of inertia

$$I_{cr} := \frac{b\cdot c^3}{12} + b\cdot c\cdot\left(\frac{c}{2}\right)^2 + n_s\cdot As\cdot y_{cr}^{\,2} = 131.6in^4$$

Concrete elastic limit

$$fc := 0.45\,f'c = 1845psi$$

Service Moment

$$Ms := \frac{fc\cdot I_{cr}}{c} = 10.5\,kip\cdot ft$$

Actuator load required in 4-point bend to produce Ms (less the amount of moment caused by dead weight of the beam)

$$Ps := 2\cdot\left(Ms - M_D\right)\frac{3}{L} = 4.9\,kip$$

Failure Load:

Depth of stress block

$$a := \frac{As\cdot fy}{0.85\,f'c\cdot b} = 0.593in$$

Nominal moment capacity

$$Mn := As\cdot fy\cdot\left(d - \frac{a}{2}\right) = 12.8\,kip\cdot ft$$

Actuator load required in 4-point bend test

$$P := 2\cdot\left(Mn - M_D\right)\cdot\frac{3}{L} = 6.2\,kip$$

Service modulus of rupture

$$fr := 7.5\sqrt{\frac{f'c}{psi}}\cdot psi = 480.2psi$$

Service cracking moment

$$Mcr_s := \frac{fr\cdot b\cdot h^3}{12}\cdot\frac{2}{h} = 5.1\,kip\cdot ft$$

Effective moment of inertia

$$Ie := \min\left[\left(\frac{Mcr_s}{Mn}\right)^3\cdot\frac{b\cdot h^3}{12} + \left[1 - \left(\frac{Mcr_s}{Mn}\right)^3\right]\cdot I_{cr}, \frac{b\cdot h^3}{12}\right] = 155.9in^4$$

Anticipated Capacity of GC45-Strengthened Beam Specimens

Assumed Beam Properties: $f_y = 40\text{ksi}$, $A_s = 0.62\text{in}^2$

FRP width $b_f := 4\text{in}$

FRP depth $t_f := 0.22\text{in}$

FRP area $A_f := b_f \cdot t_f = 0.88\text{in}^2$

Depth to FRP $d_f := h + \frac{t_f}{2} = 8.11\text{in}$

FRP MoE $E_f := 4500\text{ksi}$

FRP ultimate stress $f_{fu} := 71\text{ksi}$

Strain in concrete under dead load $\varepsilon_{bi} := \frac{M_D \cdot y}{I \cdot E_c} = 3.6 \times 10^{-5}$

Stress & Strain equations

$$\varepsilon_f(c) := 0.003\left(\frac{d_f - c}{c}\right)$$

$$f_f(c) := \min\left(E_f \cdot \varepsilon_f(c), f_{fu} \cdot C_E\right)$$

$$\varepsilon_s(c) := \min\left[\frac{f_y}{E_s}, \left(\varepsilon_f(c) + \varepsilon_{bi}\right) \cdot \left(\frac{d - c}{d_f - c}\right)\right]$$

$$f_s(c) := E_s \cdot \varepsilon_s(c)$$

Determine depth to N.A

Given $c := 1\text{in}$

$$c = \frac{A_s \cdot f_s(c) + A_f \cdot f_f(c)}{0.85 f'_c \cdot b \cdot \beta_1}$$

Depth to neutral axis $c_{45} := \text{Find}(c) = 1.8\text{in}$

Depth of compression block $a_{45} := c_{45}\beta_1 = 1.6\text{in}$

Stress in steel at failure $f_s(c_{45}) = 40\text{ksi}$

Stress in FRP at failure $f_f(c_{45}) = 45.87\text{ksi}$

Moment Capacity $M_{45} := \phi \cdot \left[A_s \cdot f_s(c_{45}) \cdot \left(d - \frac{a_{45}}{2}\right) + A_f \cdot f_f(c_{45}) \cdot \left(d_f - \frac{a_{45}}{2}\right)\right] = 36.5\text{kip}\cdot\text{ft}$

Actuator load required in 4-point bend test $P_{45} := 2 \cdot \left(M_{45} - M_D\right) \cdot \frac{3}{L} = 19.1\text{kip}$

As-built Capacity of GC90-Strengthened Beam Specimens

As-Built Beam Properties:

$f_y := 54\,ksi$ $A_s := 2 \cdot 0.275\,in^2$

FRP width $b_f := 4\,in$

FRP depth $t_f := 0.2\,in$

FRP area $A_f := b_f \cdot t_f = 0.84\,in^2$

Depth to FRP $d_f := h + \frac{t_f}{2} = 8.105\,in$

FRP MoE $E_f := 5600\,ksi$

FRP ultimate stress $f_{fu} := 87\,ksi$

Strain in concrete under dead load $\varepsilon_{bi} := \frac{M_D \cdot y}{I \cdot E_c} = 3.6 \times 10^{-5}$

Stress & Strain equations

$\varepsilon_f(c) := 0.003\left(\frac{d_f - c}{c}\right)$

$f_f(c) := \min\left(E_f \cdot \varepsilon_f(c), C_E \cdot f_{fu}\right)$

$\varepsilon_s(c) := \min\left[\frac{f_y}{E_s}, \left(\varepsilon_f(c) + \varepsilon_{bi}\right) \cdot \left(\frac{d - c}{d_f - c}\right)\right]$

$f_s(c) := E_s \cdot \varepsilon_s(c)$

Determine depth to N.A Given $c := 1\,in$

$$c = \frac{A_s \cdot f_s(c) + A_f \cdot f_f(c)}{0.85 f'_c \cdot b \cdot \beta_1}$$

Depth to neutral axis $c_{90} := \text{Find}(c) = 2 \cdot in$

Depth of compression block $a_{90} := c_{90} \cdot \beta_1 = 1.7\,in$

Stress in steel at failure $f_s(c_{90}) = 54\,ksi$

Stress in FRP at failure $f_f(c_{90}) = 50.17\,ksi$

Moment Capacity $M_{90} := \phi \cdot \left[A_s \cdot f_s(c_{90}) \cdot \left(d - \frac{a_{90}}{2}\right) + \psi_f \cdot A_f \cdot f_f(c_{90}) \cdot \left(d_f - \frac{a_{90}}{2}\right)\right] = 39.4\,kip \cdot ft$

Actuator load required in 4-point bend test $P_{90} := 2 \cdot \left(M_{90} - M_D\right) \cdot \frac{3}{L} = 20.7\,kip$

As-built Capacity of GC45-Strengthened Beam Specimens

As-Built Beam Properties:

$f_y := 54\,ksi$ $A_s := 2 \cdot 0.275\,in^2$

FRP width $b_f := 4\,in$

FRP depth $t_f := 0.22\,in$

FRP area $A_f := b_f \cdot t_f = 0.88\,in^2$

Depth to FRP $d_f := h + \frac{t_f}{2} = 8.11\,in$

FRP MoE $E_f := 4500\,ksi$

FRP ultimate stress $f_{fu} := 71\,ksi$

Strain in concrete under dead load $\varepsilon_{bi} := \frac{M_D \cdot y}{I \cdot E_c} = 3.6 \times 10^{-5}$

Stress & Strain equations

$$\varepsilon_f(c) := 0.003\left(\frac{d_f - c}{c}\right)$$

$$f_f(c) := \min\left(E_f \cdot \varepsilon_f(c), C_E \cdot f_{fu}\right)$$

$$\varepsilon_s(c) := \min\left[\frac{f_y}{E_s}, \left(\varepsilon_f(c) + \varepsilon_{bi}\right) \cdot \left(\frac{d - c}{d_f - c}\right)\right]$$

$$f_s(c) := E_s \cdot \varepsilon_s(c)$$

Determine depth to N.A

Given $c := 1\,in$

$$c = \frac{A_s \cdot f_s(c) + A_f \cdot f_f(c)}{0.85 f'_c \cdot b \cdot \beta_1}$$

Depth to neutral axis $c_{45} := \text{Find}(c) = 1.9\,in$

Depth of compression block $a_{45} := c_{45}\beta_1 = 1.6\,in$

Stress in steel at failure $f_s(c_{45}) = 54\,ksi$

Stress in FRP at failure $f_f(c_{45}) = 43.45\,ksi$

Moment Capacity $M_{45} := \phi \cdot \left[A_s \cdot f_s(c_{45}) \cdot \left(d - \frac{a_{45}}{2}\right) + \psi_f \cdot A_f \cdot f_f(c_{45}) \cdot \left(d_f - \frac{a_{45}}{2}\right)\right] = 37.3\,kip \cdot ft$

Actuator load required in 4-point bend test $P_{45} := 2 \cdot \left(M_{45} - M_D\right) \cdot \frac{3}{L} = 19.5\,kip$

APPENDIX C: Small Beam Bend Test FRP Strain by Gage Location

GC90 Specimens – FRP Strain by Gage Location

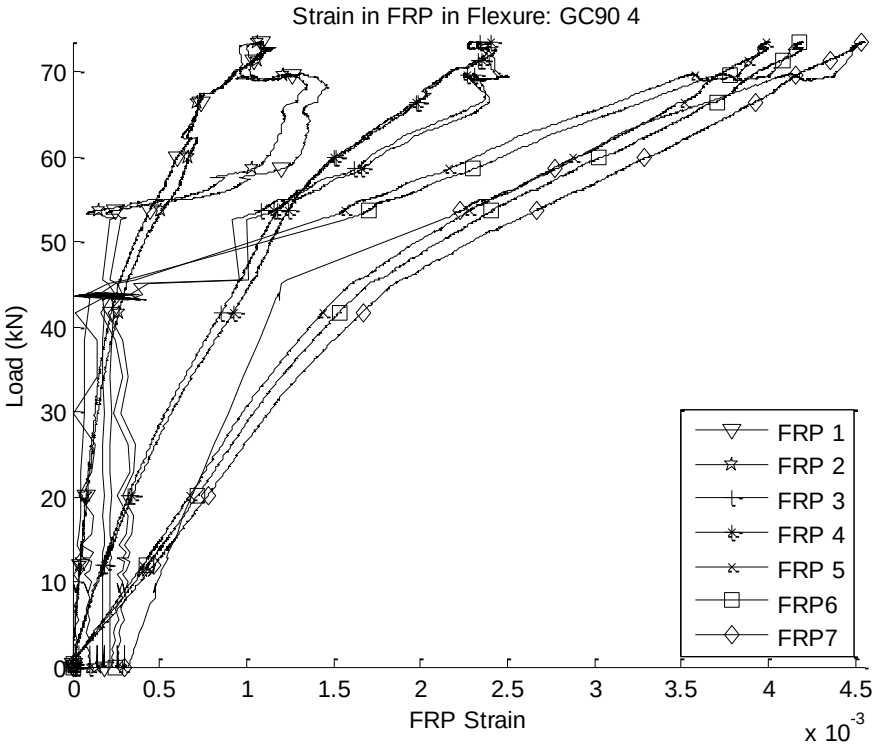

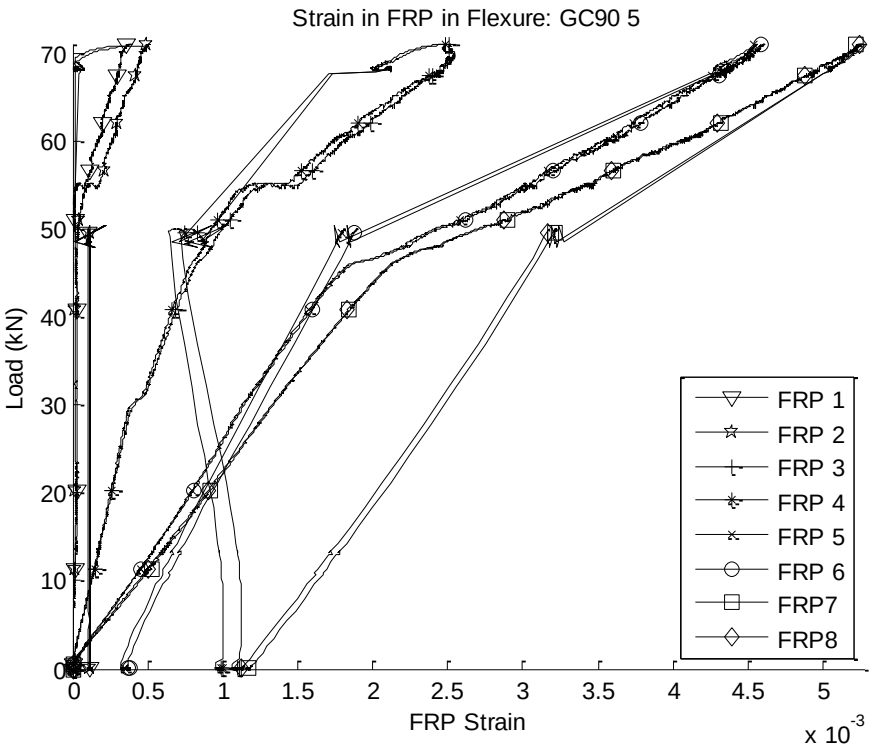

GC45 Specimens – FRP Strain by Gage Location

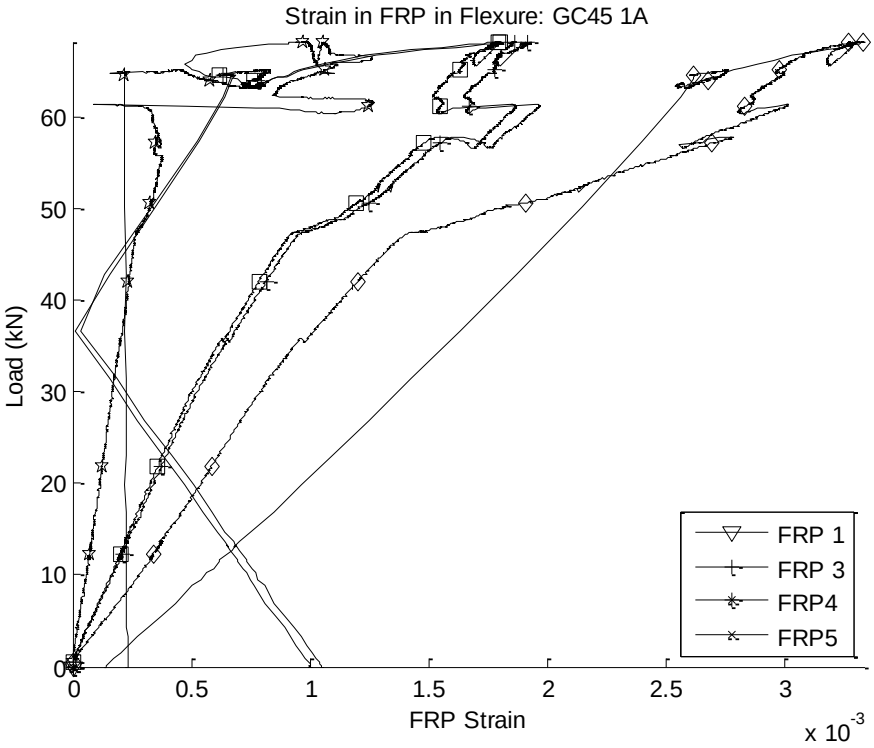

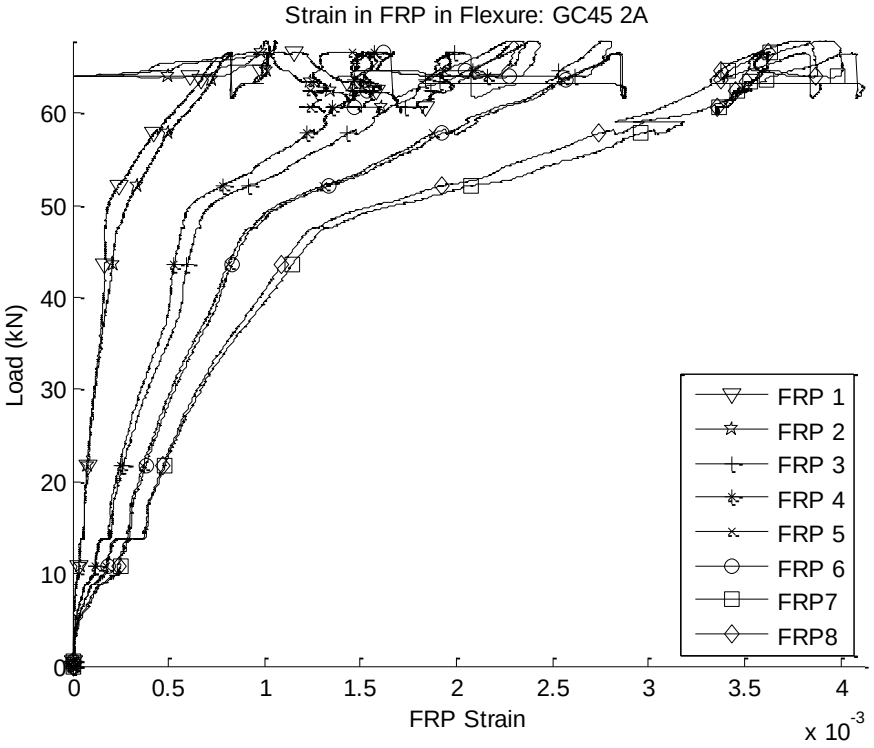

APPENDIX D: Fatigue Test FRP Strain by Redundant Gage Location over Time

Fatigue_045_1

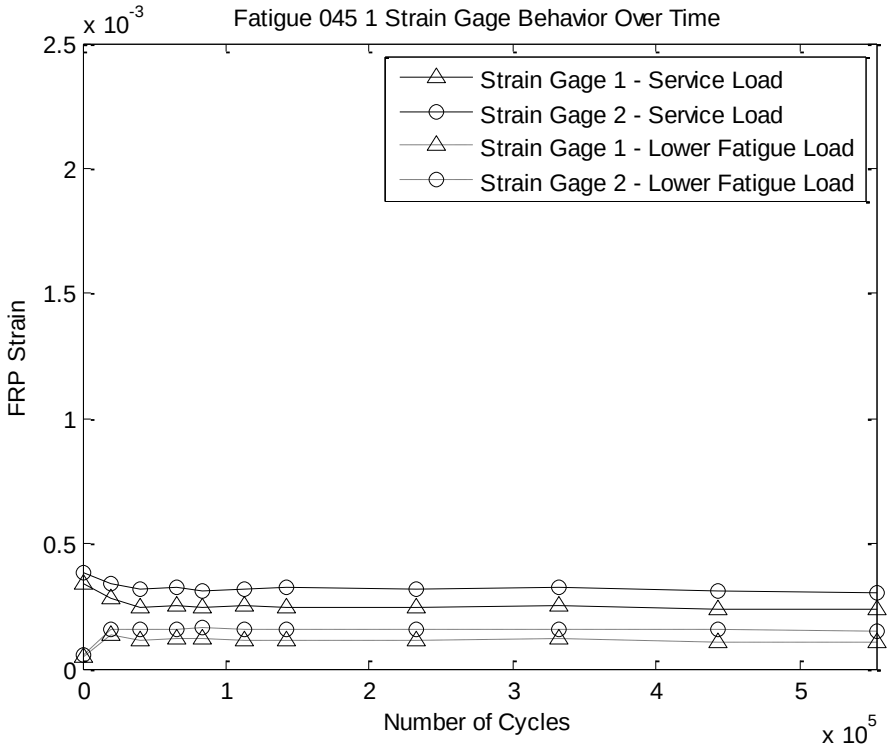

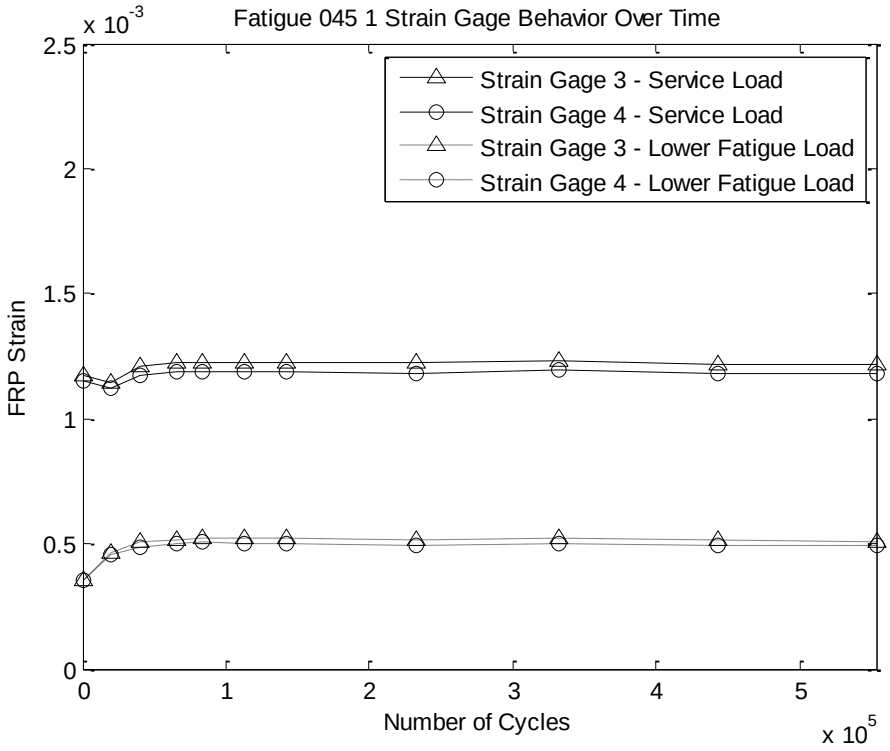

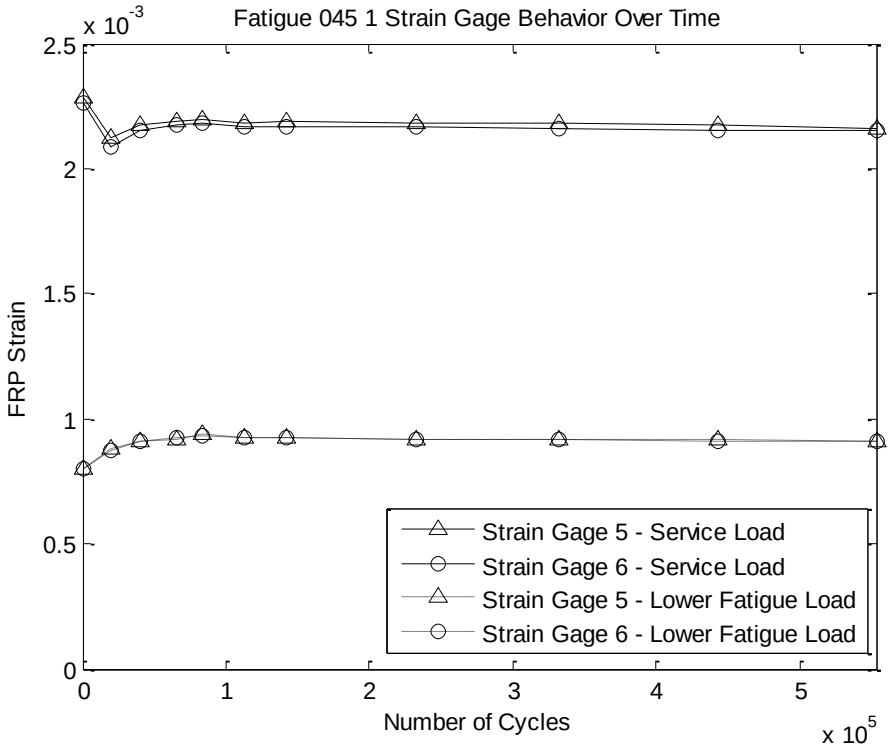
Fatigue 045 1 Strain Gage Behavior Over Time
x 10^-3
2.5
2
1.5
1
0.5
0
FRP Strain
0
1
2
3
4
5
Number of Cycles
x 10^5
Strain Gage 5 - Service Load
Strain Gage 6 - Service Load
Strain Gage 5 - Lower Fatigue Load
Strain Gage 6 - Lower Fatigue Load

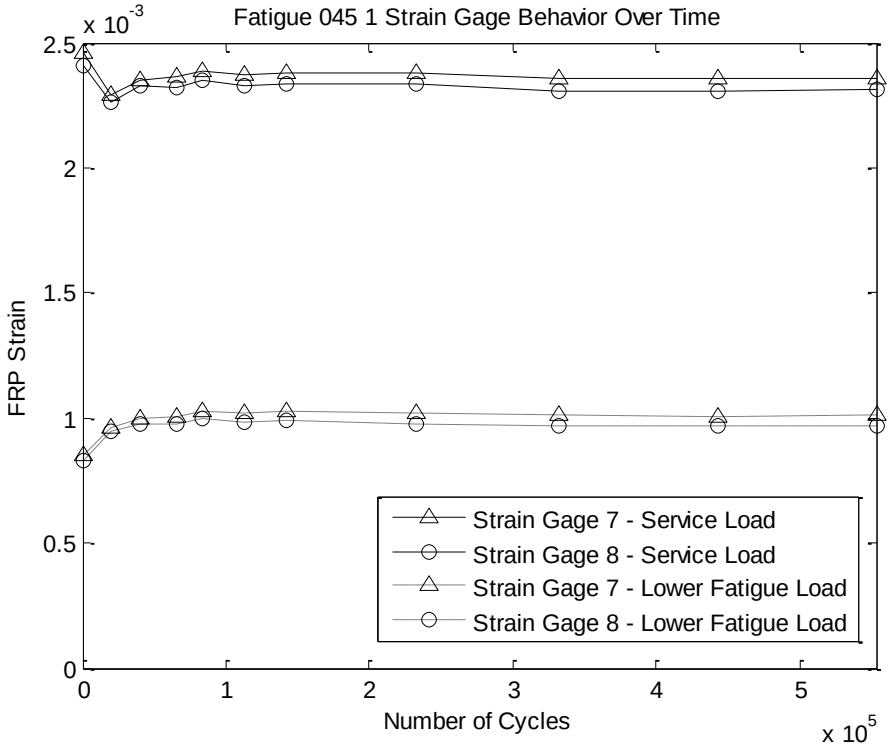
Fatigue 045 1 Strain Gage Behavior Over Time
x 10^-3
2.5
2
1.5
1
0.5
0
FRP Strain
0
1
2
3
4
5
Number of Cycles
x 10^5
Strain Gage 7 - Service Load
Strain Gage 8 - Service Load
Strain Gage 7 - Lower Fatigue Load
Strain Gage 8 - Lower Fatigue Load

Fatigue_045_2

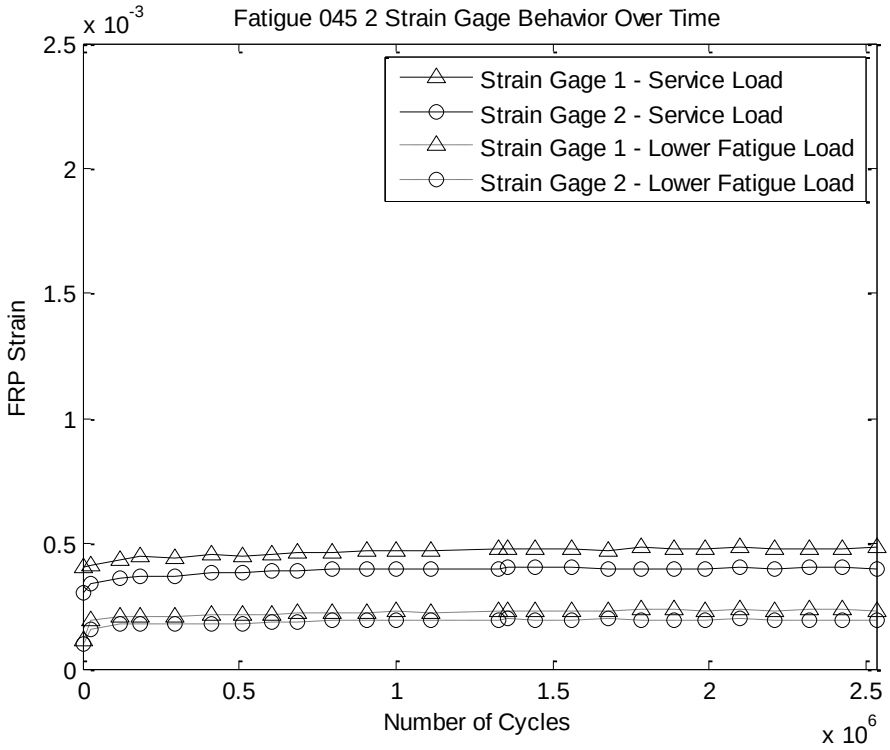

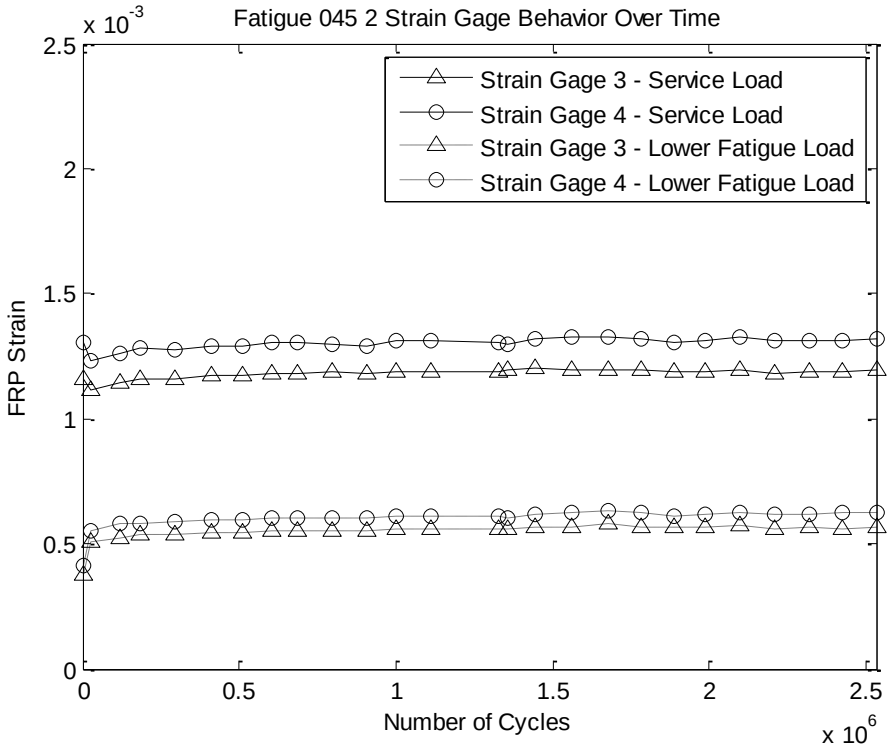

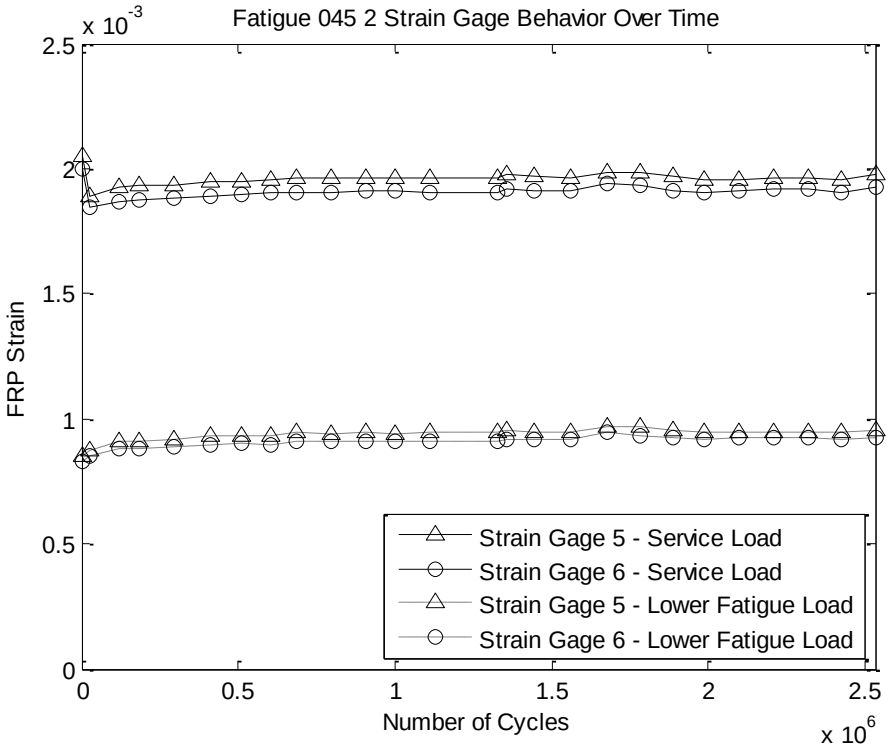
Fatigue 045 2 Strain Gage Behavior Over Time
x 10^-3
FRP Strain
Number of Cycles
x 10^6
Strain Gage 5 - Service Load
Strain Gage 6 - Service Load
Strain Gage 5 - Lower Fatigue Load
Strain Gage 6 - Lower Fatigue Load

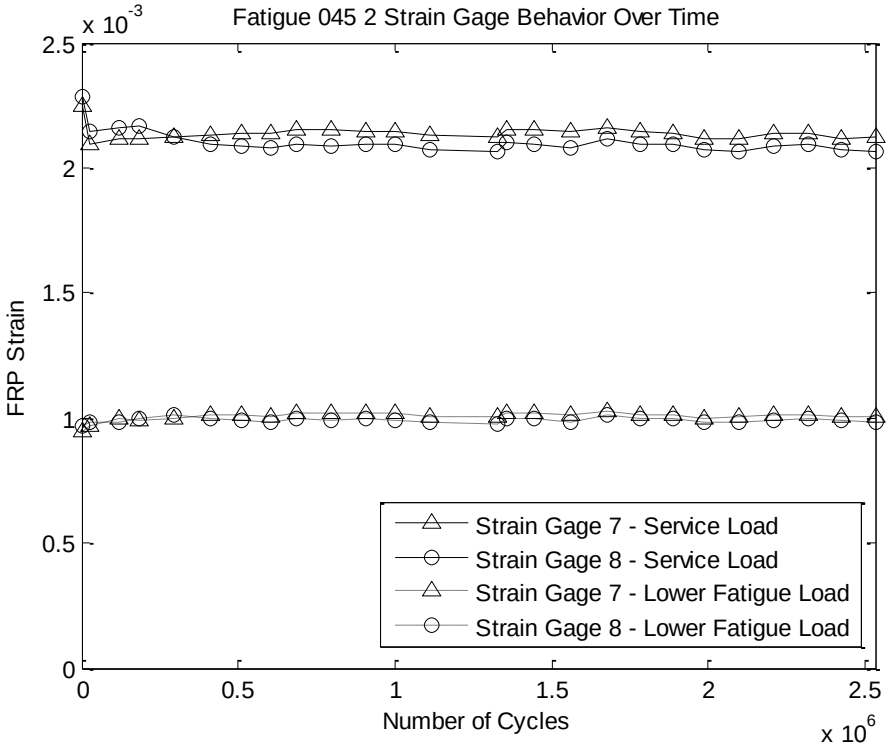
Fatigue 045 2 Strain Gage Behavior Over Time
x 10^-3
FRP Strain
Number of Cycles
x 10^6
Strain Gage 7 - Service Load
Strain Gage 8 - Service Load
Strain Gage 7 - Lower Fatigue Load
Strain Gage 8 - Lower Fatigue Load

Fatigue_045_3

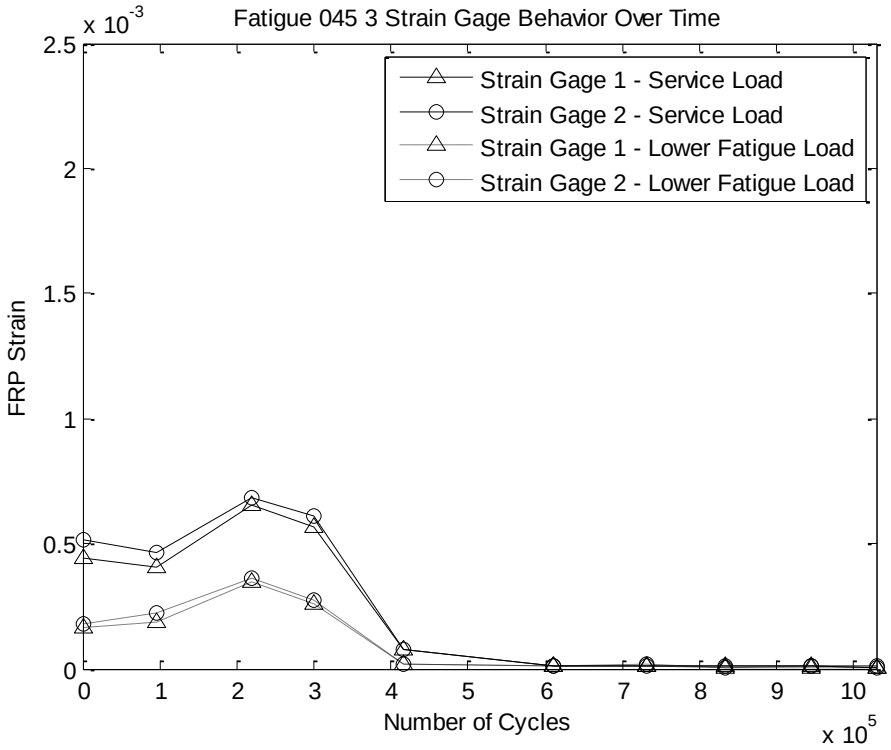

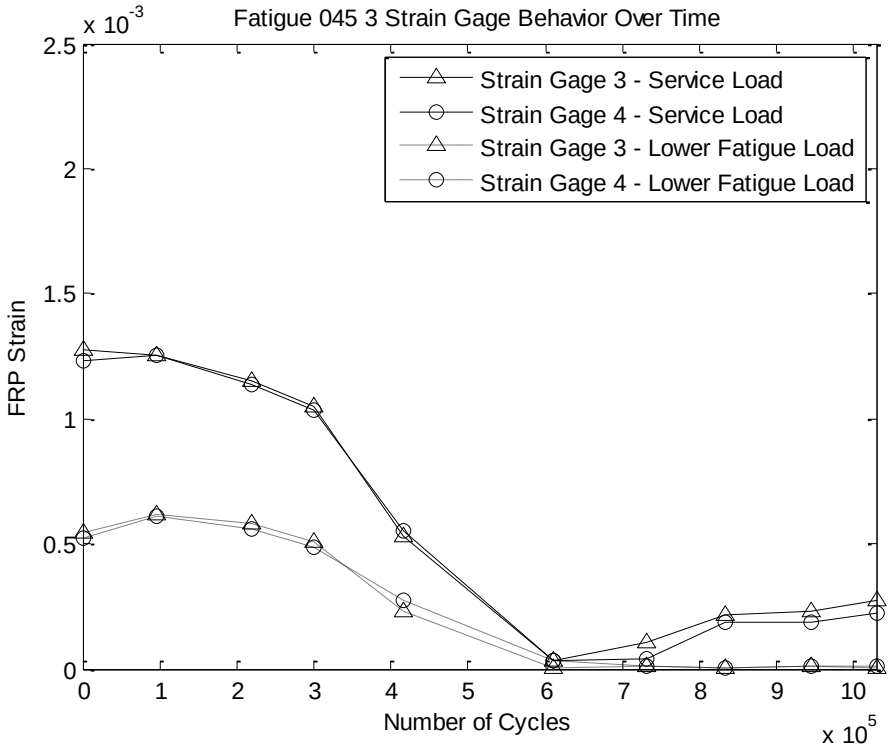

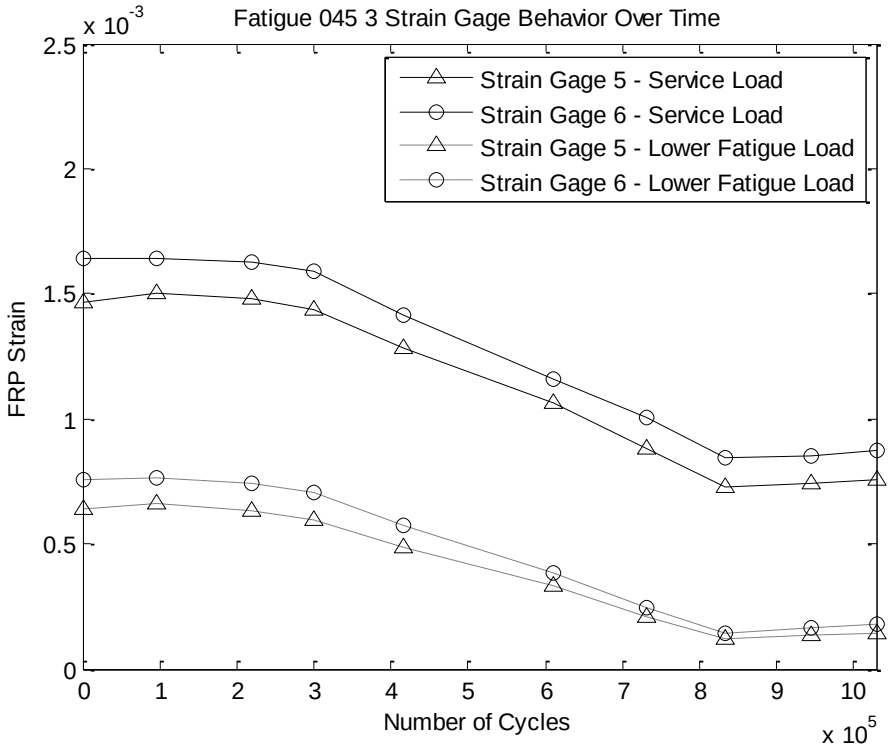
Fatigue 045 3 Strain Gage Behavior Over Time
x 10^-3
2.5
2
1.5
1
0.5
0
FRP Strain
Strain Gage 5 - Service Load
Strain Gage 6 - Service Load
Strain Gage 5 - Lower Fatigue Load
Strain Gage 6 - Lower Fatigue Load
0 1 2 3 4 5 6 7 8 9 10
Number of Cycles
x 10^5

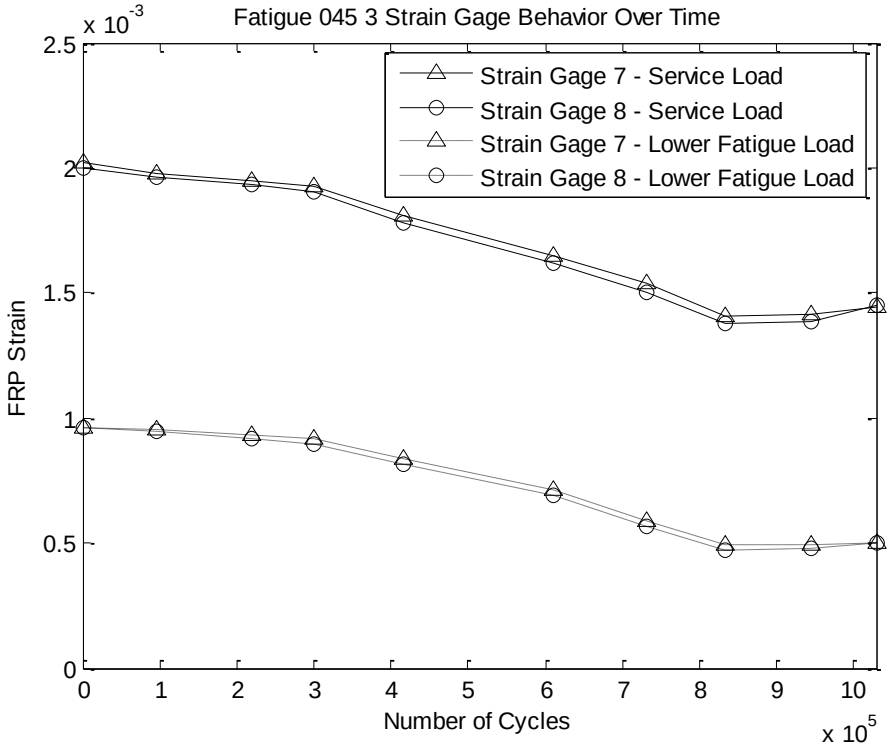
Fatigue 045 3 Strain Gage Behavior Over Time
x 10^-3
2.5
2
1.5
1
0.5
0
FRP Strain
Strain Gage 7 - Service Load
Strain Gage 8 - Service Load
Strain Gage 7 - Lower Fatigue Load
Strain Gage 8 - Lower Fatigue Load
0 1 2 3 4 5 6 7 8 9 10
Number of Cycles
x 10^5

Fatigue_090_4

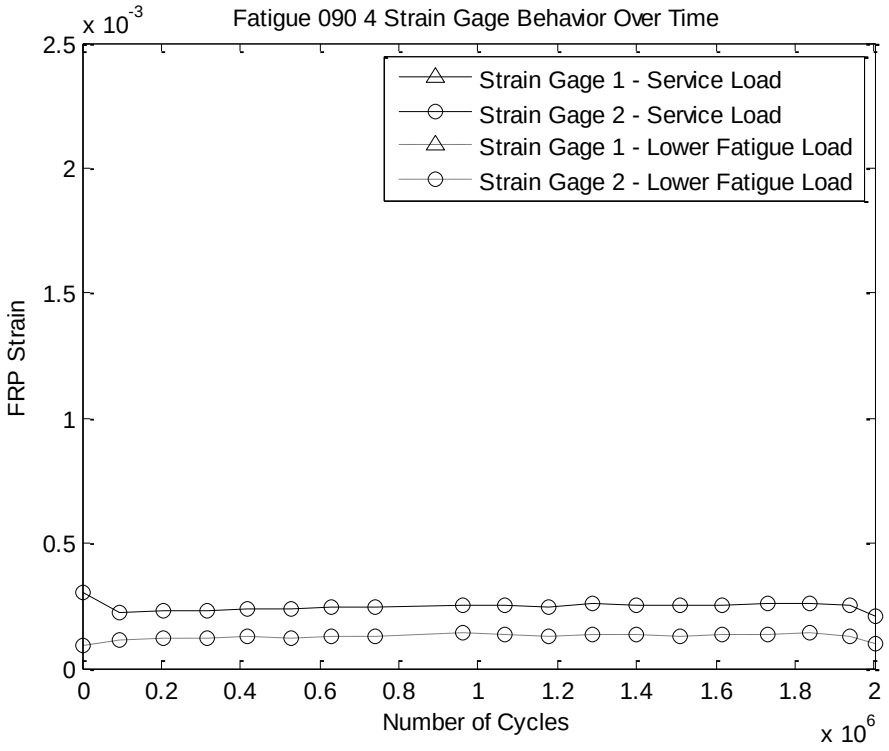

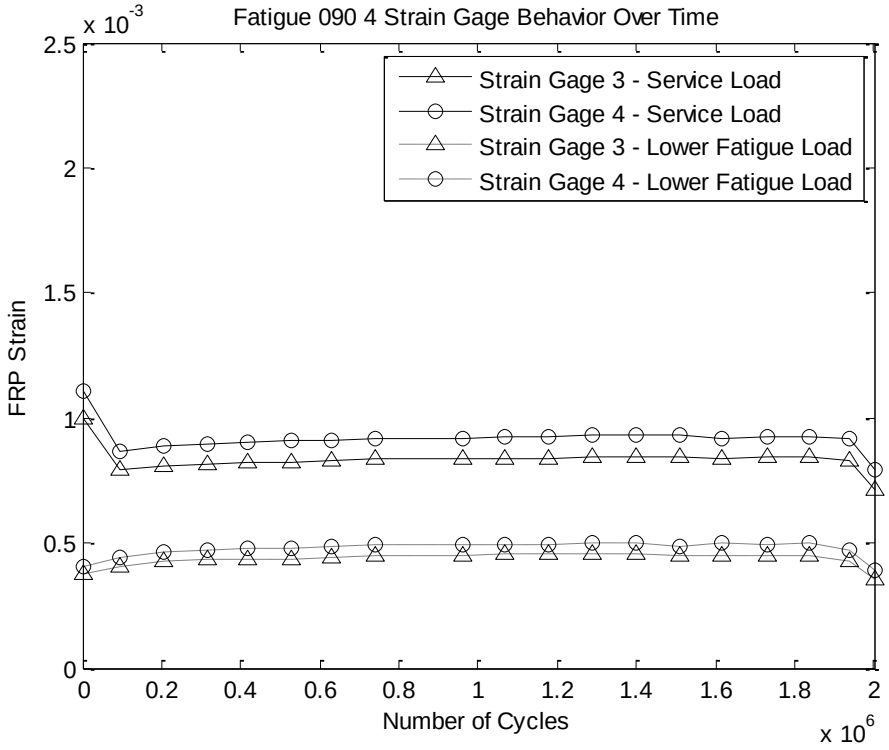

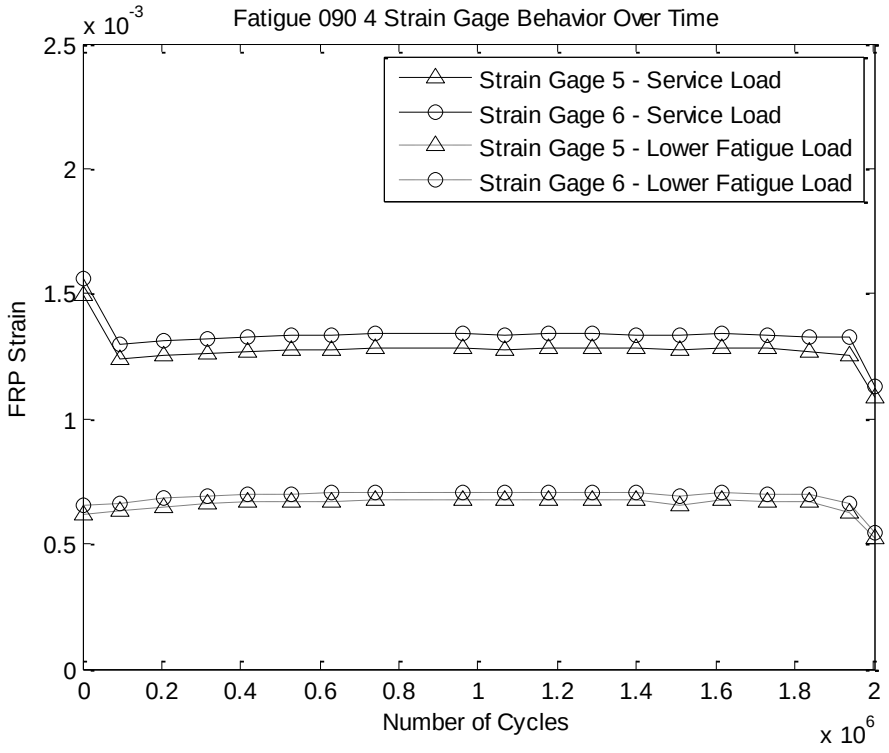
Fatigue 090 4 Strain Gage Behavior Over Time
x 10^-3
FRP Strain
Number of Cycles
x 10^6
Strain Gage 5 - Service Load
Strain Gage 6 - Service Load
Strain Gage 5 - Lower Fatigue Load
Strain Gage 6 - Lower Fatigue Load

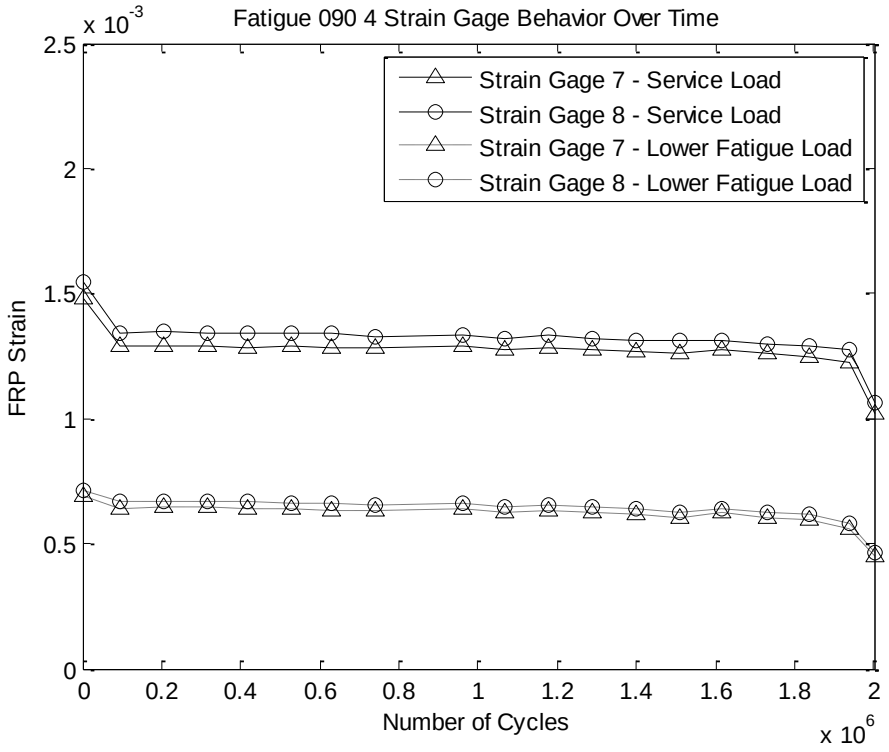
Fatigue 090 4 Strain Gage Behavior Over Time
x 10^-3
FRP Strain
Number of Cycles
x 10^6
Strain Gage 7 - Service Load
Strain Gage 8 - Service Load
Strain Gage 7 - Lower Fatigue Load
Strain Gage 8 - Lower Fatigue Load

APPENDIX E: Fatigue Test FRP Strains by Gage Location

Fatigue_045_1

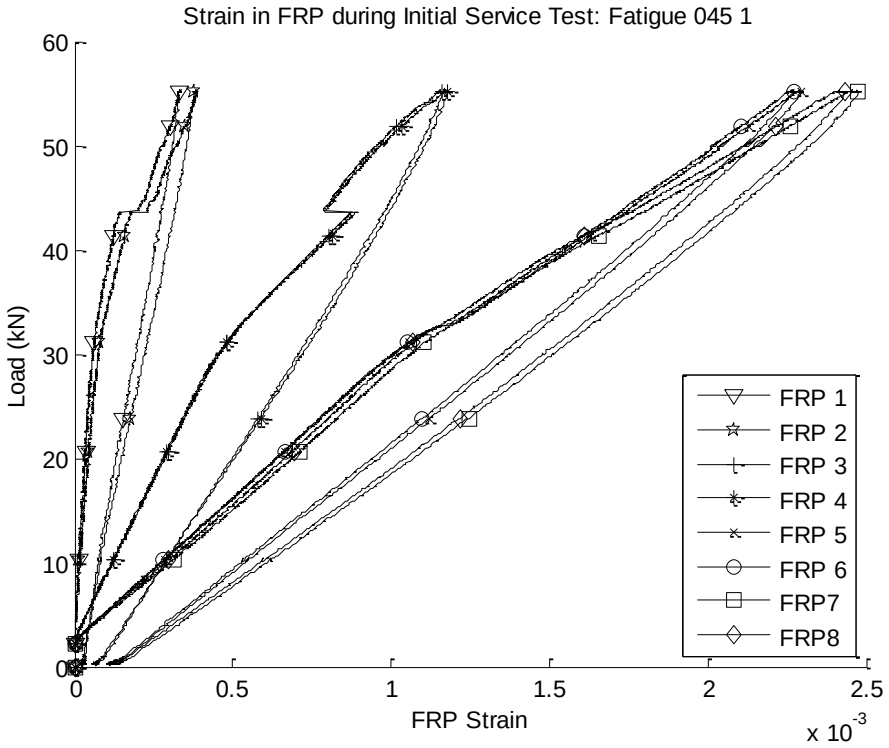

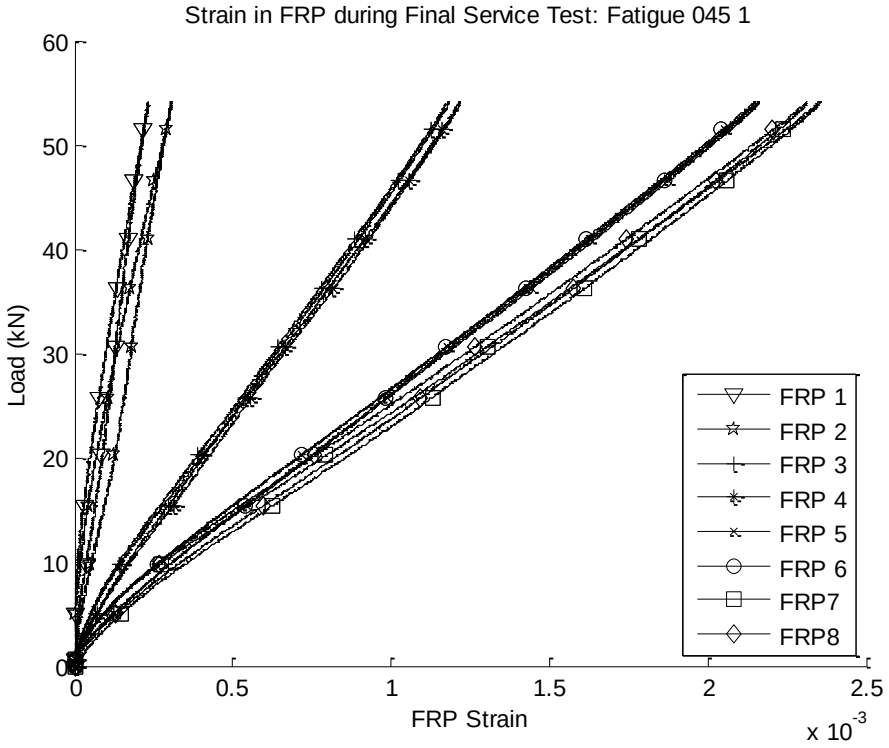

Fatigue_045_2

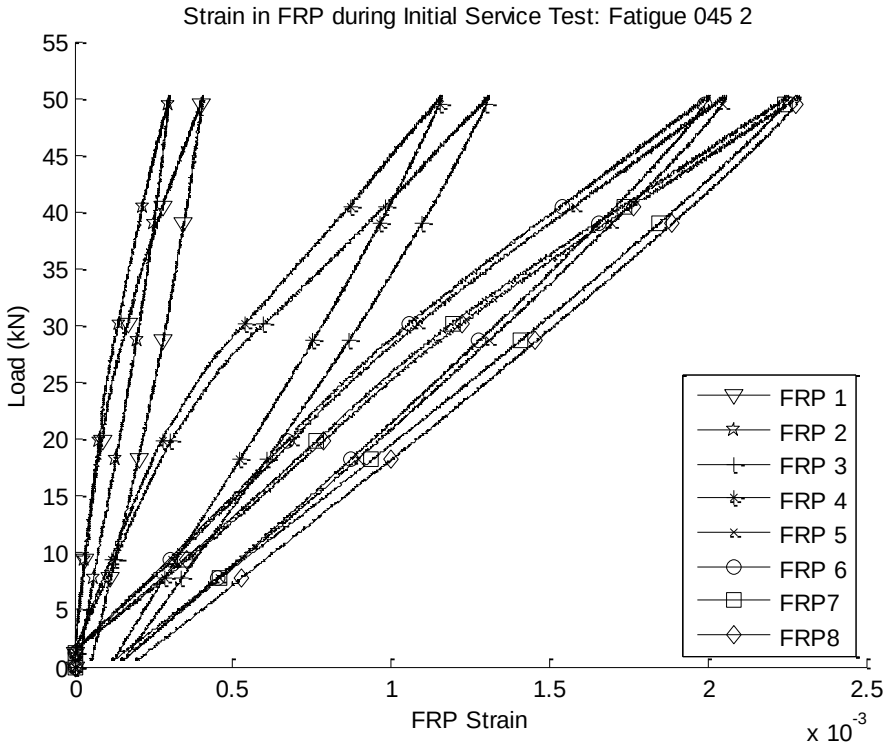

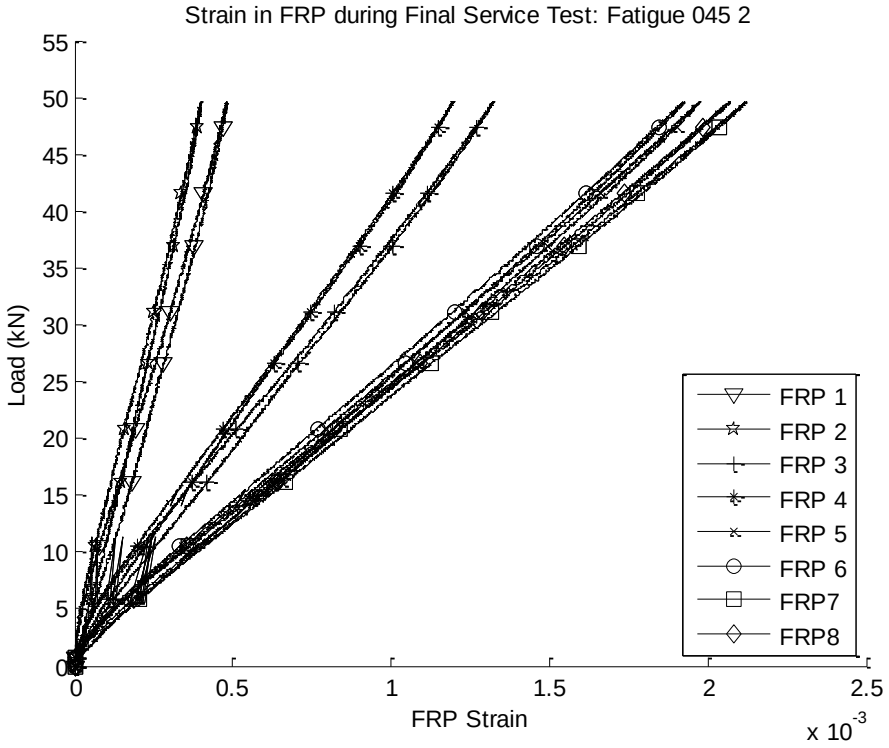

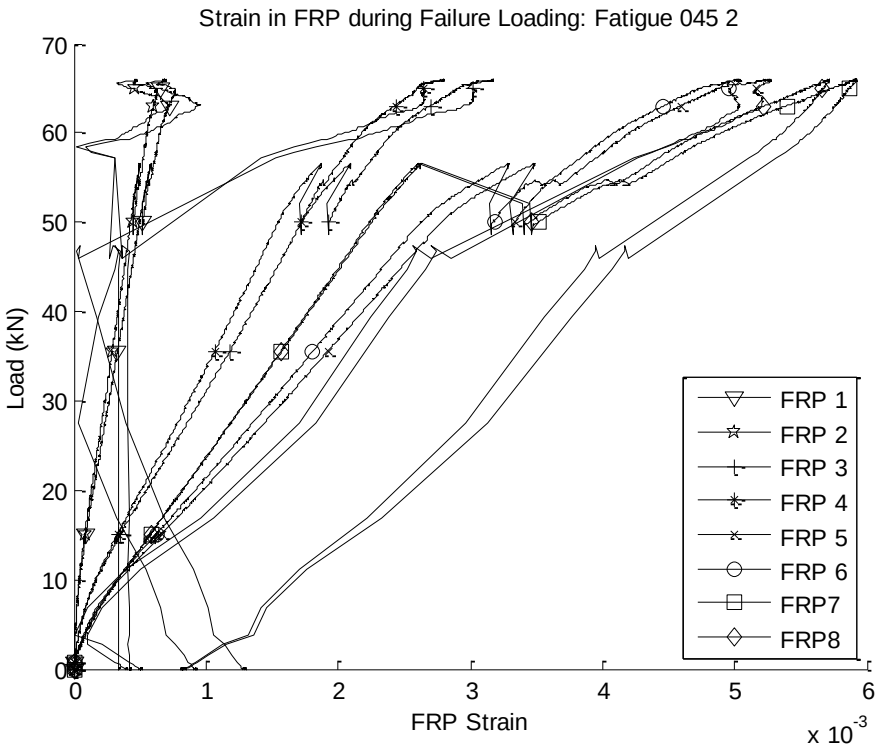
Strain in FRP during Failure Loading: Fatigue 045 2
Load (kN)
FRP Strain
x 10^-3
FRP 1
FRP 2
FRP 3
FRP 4
FRP 5
FRP 6
FRP7
FRP8

Fatigue_045_3

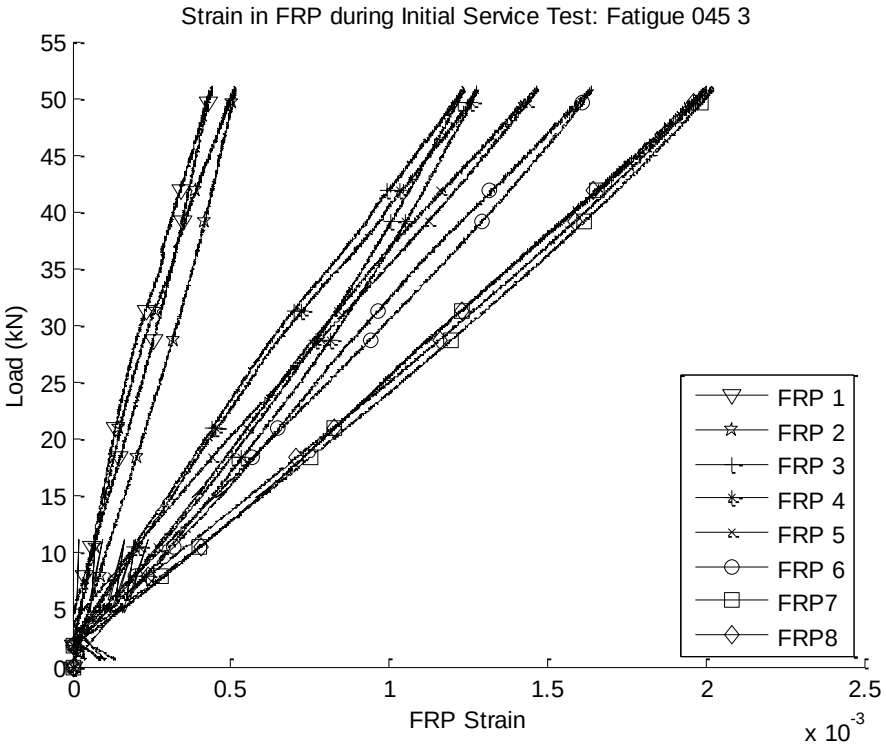

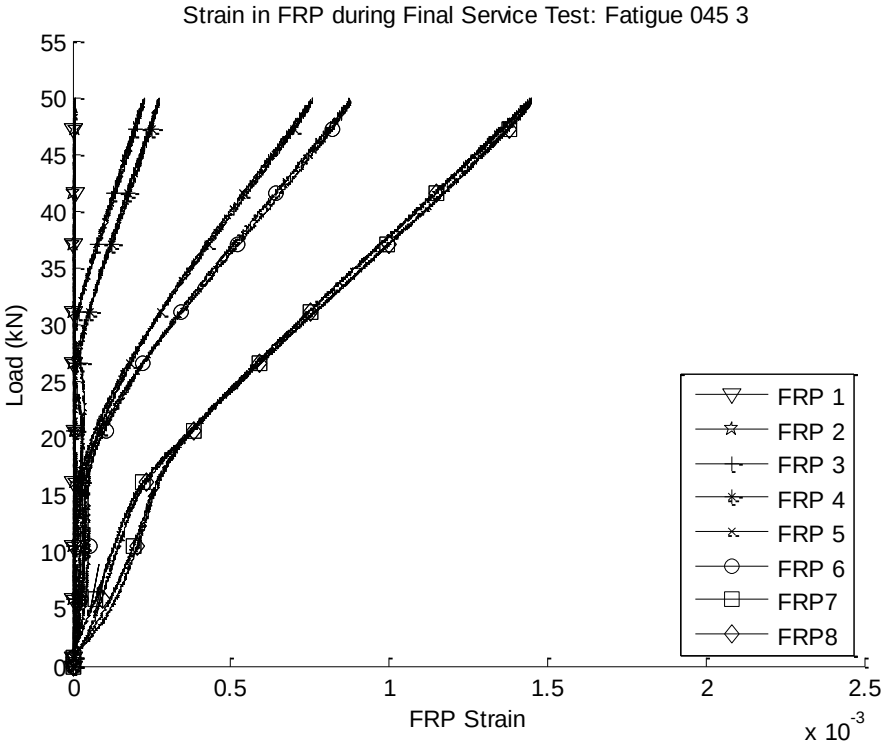

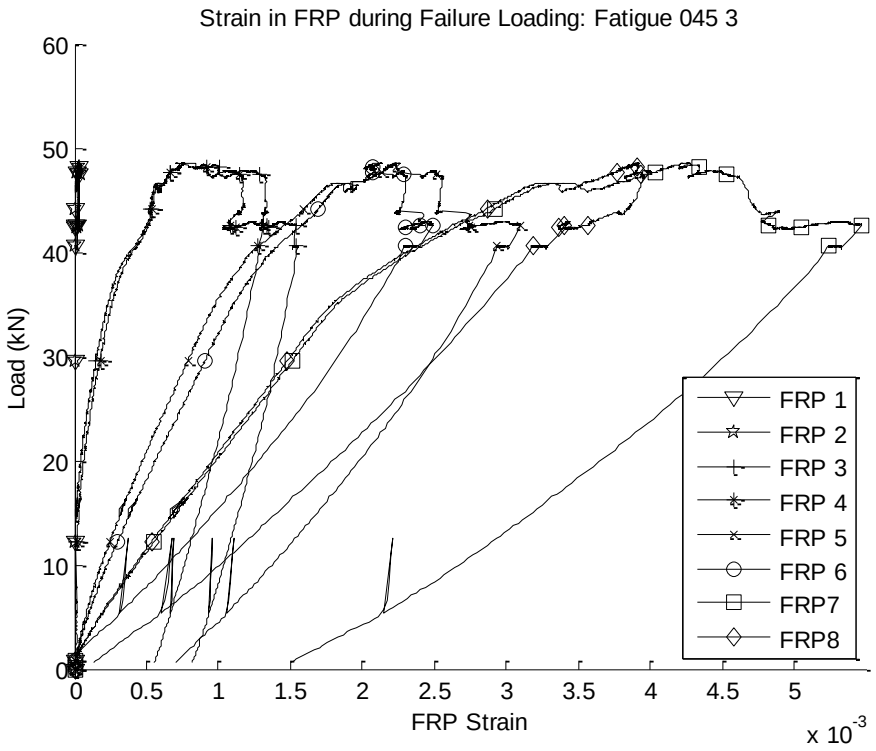
Strain in FRP during Failure Loading: Fatigue 045 3
Load (kN)
FRP Strain
x 10^-3
FRP 1
FRP 2
FRP 3
FRP 4
FRP 5
FRP 6
FRP7
FRP8

Fatigue_090_4

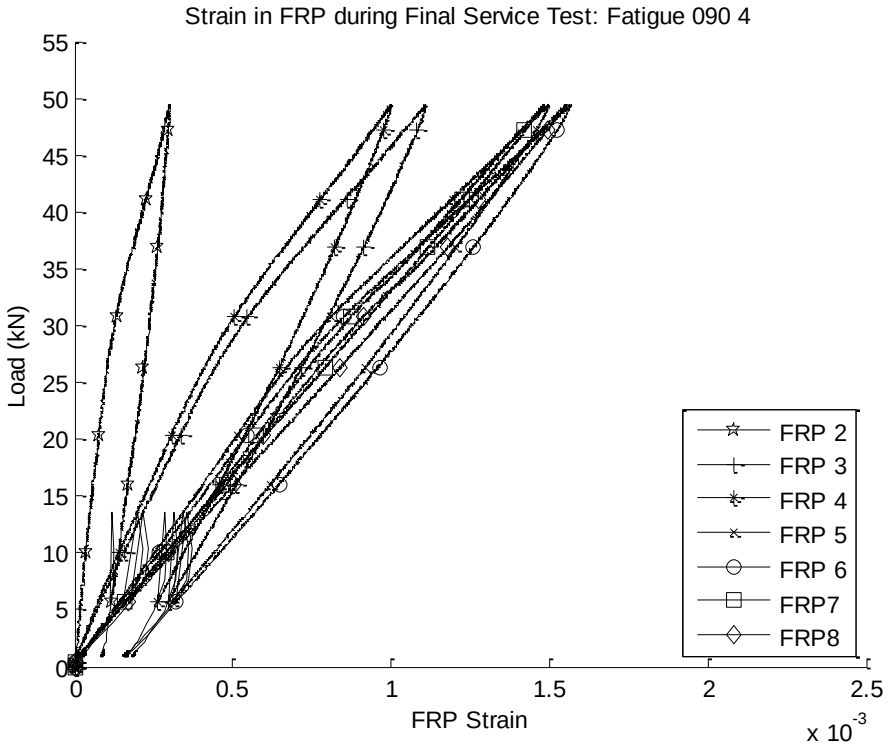

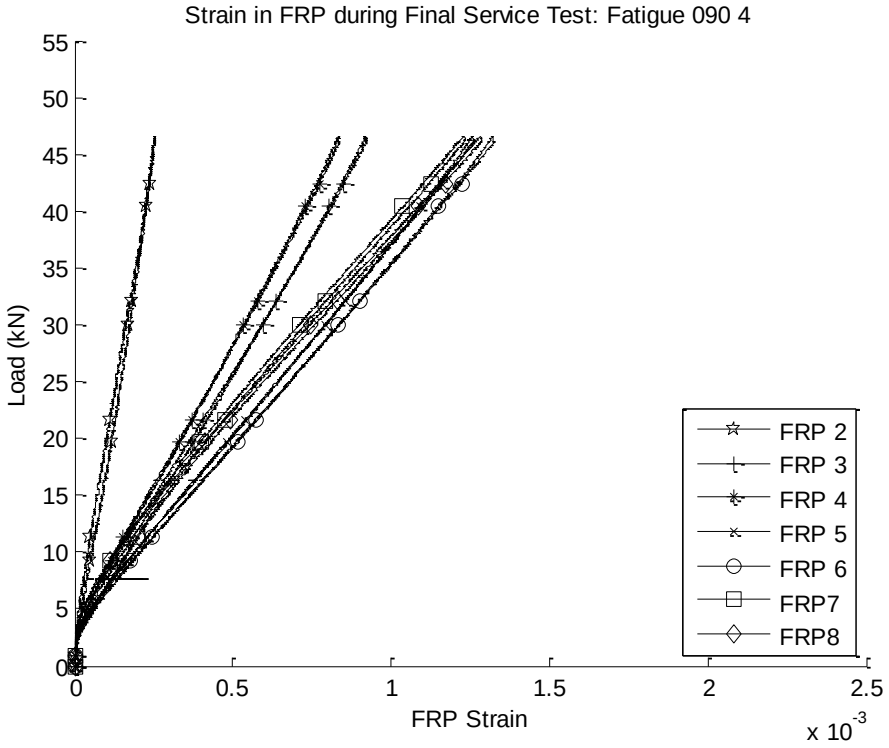

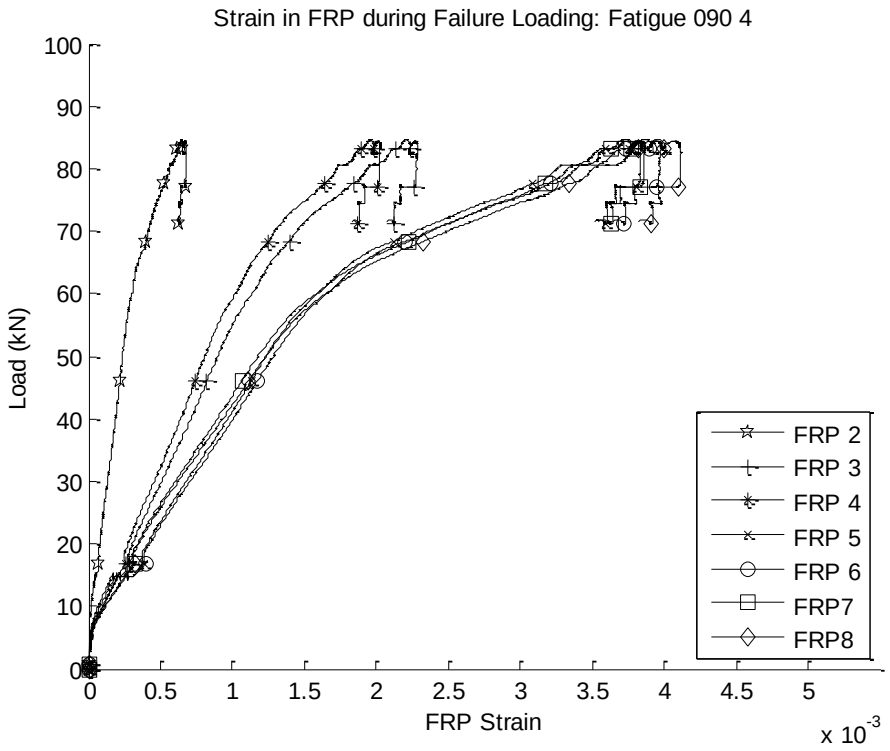
Strain in FRP during Failure Loading: Fatigue 090 4
Load (kN)
FRP Strain
x 10^-3
FRP 2
FRP 3
FRP 4
FRP 5
FRP 6
FRP7
FRP8